

GIANT MAGELLAN TELESCOPE SCIENCE BOOK 2018

**GIANT
MAGELLAN
TELESCOPE**
SCIENCE
BOOK 2018

This book was developed, edited, and designed by the GMT Science Advisory Committee and GMT Project Office; key contributors are listed below. The authors of each chapter are listed at the beginning of the chapter.

Rebecca Bernstein

GMTO Project Scientist,
Carnegie Institution for Science

Alan Dressler

Carnegie Institution for Science

Daniel Apai

University of Arizona

Martin Asplund

Australian National University

Robert Blum

NOAO

Sarah Brough

University of New South Wales

Jeff Crane

Carnegie Institution for Science

Eduardo Cypriano

University of São Paulo

Daniel Eisenstein

Harvard College Observatory,
Harvard-Smithsonian Center for Astrophysics

Joshua Eisner

University of Arizona

Daniel Fabricant

Smithsonian Astrophysical Observatory,
Harvard-Smithsonian Center for Astrophysics

Michael Gladders

University of Chicago

Jenny Greene

Princeton University

Narae Hwang

Korea Astronomy and Space Science Institute (KASI)

Adam Kraus

The University of Texas at Austin

Casey Papovich

Texas A&M University

Robert Sharp

Australian National University

Robert Simcoe

Massachusetts Institute of Technology

Dennis Zaritsky

University of Arizona

.....
Editing and design support provided by

Sarah Emery Bunn

Copy Editor, GMTO

Damien Jemison

Creative Art Director, GMTO

Amanda Kocz

Director of Communications, GMTO

Patrick McCarthy

Vice President for Operations and External Relations, GMTO

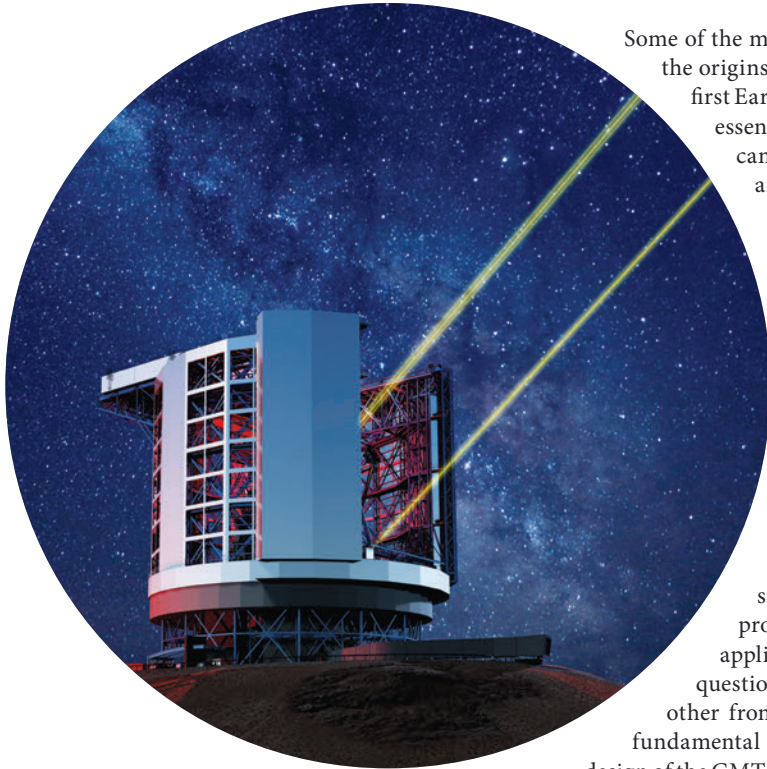
A Guide to the 2018 GMT Science Book

From the first night Galileo looked through his small telescope, to the heyday of the 100-inch Hooker telescope at Mount Wilson, to the first time the Hubble Space Telescope (HST) opened its shutter, the largest optical telescopes of their time have been humanity's crucial tools for studying the universe around us and understanding our place in it. While telescopes used today collect light across the electromagnetic spectrum, optical and infrared telescopes remain the flagships of this voyage of exploration.

Optical and infrared telescopes will always be essential tools for observing our universe because stars are brightest at optical and infrared wavelengths, and because the signatures of important atomic transitions are found at these wavelengths. Although space-based telescopes offer some unique advantages, ground-based telescopes will continue to be fundamental; they can be built with much larger mirrors than are practical for space telescopes, and they offer greater sensitivity for detection of the faint sources that define the frontier of many areas of astronomical research. In addition, adaptive optics technology allows us to overcome the angular resolution limit imposed by atmospheric turbulence, so that ground-based telescopes can now achieve the diffraction limit of their optics, giving them another advantage. Perhaps their biggest strength is that ground-based telescopes can evolve—the addition of new instruments that take advantage of new ideas and technologies ensure that they will continue to be dynamic and powerful tools for decades after their initial commissioning.

Recognizing these essential attributes, the 2000 and 2010 decadal surveys in Astronomy & Astrophysics have described and endorsed a next-generation “Giant Segmented Mirror Telescope” (GSMT) as the highest priority for ground-based astronomy, describing them as the “next great leap in the collecting power and angular resolution of optical and infrared (OIR) astronomy.”

The Giant Magellan Telescope (GMT) will provide that “next great leap” with greater collecting area and sophisticated adaptive optics, resulting in increased sensitivity by factors of tens to thousands (depending on the observing configuration) over the previous generation of telescopes. Because the GMT will come into full operation a decade from now, and because it will host many generations of instruments, the GMT’s most important discoveries will reach well beyond what we can anticipate today. While we can’t predict all the science the GMT will enable, we can envision the areas in which it will make its most important contributions, beginning with the research programs that are just beyond the grasp of contemporary telescopes.



Some of the most intriguing of those programs address the many aspects of the origins of life. For example, with the GMT we will find and study the first Earth-like planets beyond our solar system. The chemical elements essential for the formation of those planets and any life on them came from generations of star birth and death, in our own galaxy and in a hundred billion others. The GMT will provide data that helps us chart the progress of this chemical enrichment in the universe, enabling us to learn where, and perhaps when, life emerged in the universe. As the GMT peers back over cosmic time, we will also learn more about the birth and growth of galaxies and the role dark matter plays in that formation. The first episodes in this origin story will be revealed by pairing the James Webb Space Telescope’s ultra-deep images of the first fledgling galaxies with GMT spectroscopy of those sources, which are too faint for us to study today.

The 2018 GMT Science Book describes the GMT’s strengths and its potential for scientific discovery. To convey those strengths and potential, we describe (1) the facility that will provide the GMT’s unique capabilities and sensitivity, (2) the application of those capabilities to the most important unanswered questions in astrophysics today, and (3) the teaming of the GMT with other front-line facilities on the ground and in space to answer these fundamental questions in astrophysics. We begin by describing the unique design of the GMT telescope, which adapts and extrapolates from the technologies that produced the highly successful Magellan Telescopes, the MMT, and the Large Binocular Telescope. We also describe the first-generation instrument suite, which has been chosen to maximize the GMT’s scientific impact during early operations.

The discussion then moves to the science. Chapters 2 through 9 cover broad areas in astrophysical research in which the GMT will have transformative impact. Each chapter has a single page orientation followed by a several-page introduction to the subject area—written for the scientist, but not just for the specialist. Next are descriptions of scientific programs that will advance rapidly through the GMT’s unique capabilities, with specific information about instrument capabilities and observational requirements. In describing these key programs, our goal is to provide a sample of the most interesting and transformative science that the GMT will enable.

In each chapter, figures and their captions summarize the story. The figures in grey boxes support and summarize the scientific discussion. Figures and tables in orange boxes describe the instruments, technical capabilities, and specific observing programs that illustrate the GMT's unique contribution to the subject. Finally, figures and pictures in green boxes describe how the GMT will be used in synergy with other contemporary telescopes and observatories in ways that complement and leverage their capabilities to enable new discoveries in astrophysics.



Figure i-1 Figures in grey boxes support and summarize the scientific discussion.



Technical Figures

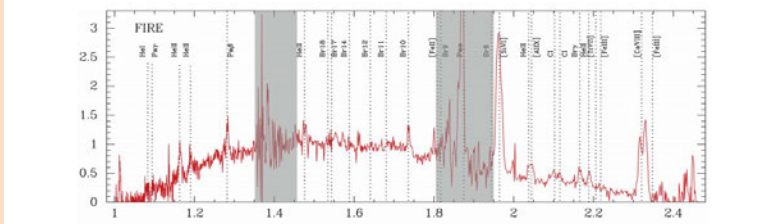


Figure i-2 Figures and tables in orange boxes describe the instruments, technical capabilities, and specific observing programs that illustrate the GMT's unique contribution to the subject.



Synergy Figures

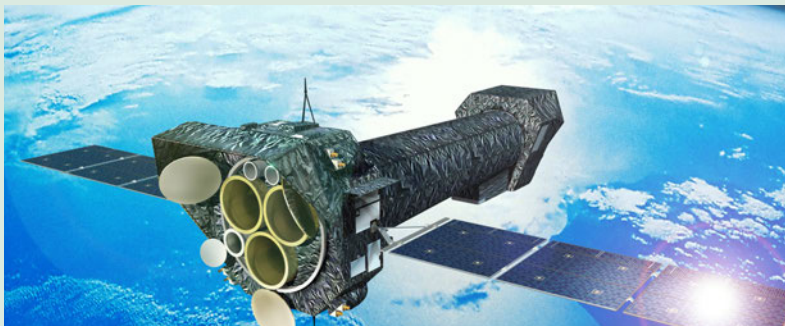


Figure i-3 Figures and pictures in green boxes describe how the GMT will be used in synergy with other contemporary telescopes and observatories in ways that complement and leverage their capabilities to enable new discoveries in astrophysics.

CHAPTER 2

Exoplanets & Planet Formation

Are we alone in the
Universe?



The chapters of this book are ordered in a way that recalls the human journey of discovery, starting in Chapter 2 with our search for other worlds. We describe how precision radial velocity measurements of stars in our corner of the Universe will detect not only large planets like Jupiter and Saturn, but even the much smaller, most common Neptune-like planets, all the way down to comparatively tiny worlds like Earth. The GMT’s search for planets orbiting the Sun’s closest neighbors will also use a unique combination of adaptive optics and high-resolution spectroscopy that will separate the ultra-faint light reflected by planets from that of the host star. Spectroscopy that detects the atmospheres of these “exoplanets” will enable us to examine the chemical compositions of diverse worlds and to search for the chemical biosignatures that are the telltales of life. Chapter 1 also describes the programs that will enable us to understand the physical environments in which planets form out of the circumstellar disks of gas and dust around young stars.

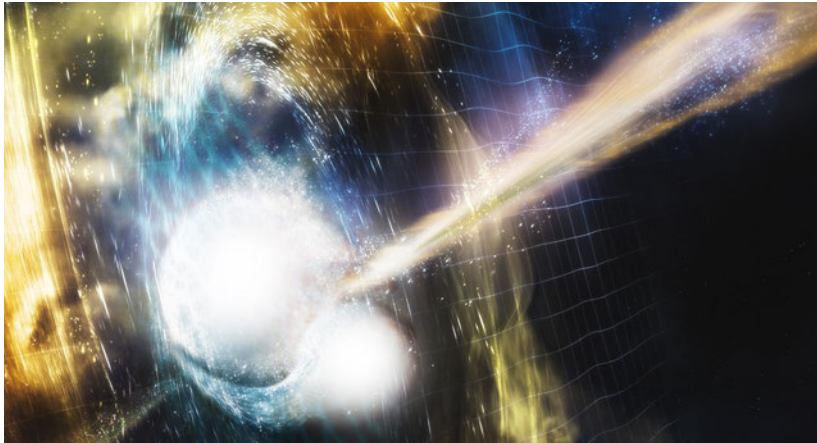
CHAPTER 3

The Birth of Stars

Where and how are
stars born?



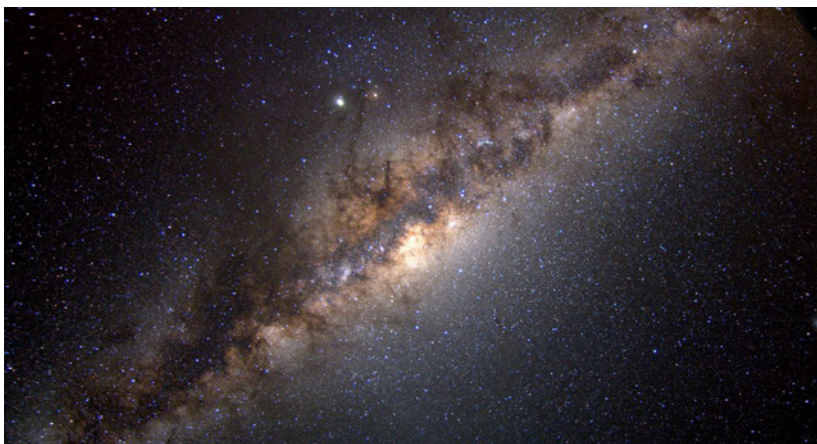
In Chapter 3 we explore how sensitive, high-resolution spectroscopy of newborn stars will enable us to answer the fundamental question of star formation: how do stars form with such a wide range of masses, temperatures, and gravities. Similarly, infrared spectroscopy of the violent, molecule-rich atmospheres of brown dwarfs — the species in between stars and planets — will help us understand the formation of these failed stars and, by extension, of giant planets, which are even harder to study. Such information is also crucial for measuring the masses of brown dwarfs, key to learning why and how stars form with the wide range of masses they do.



From the birth of stars to their death, Chapter 4 begins by describing the range of astrophysical mysteries that the GMT will address, by studying the aftermath of coalescing neutron stars. This is where the heaviest chemical elements have been made—a fact we now know because of the recent breakthrough detection of these events by the gravitational waves they emit in the final seconds before they collide. The GMT will have an unprecedented ability to study this alchemy using a rapid cadence of high-resolution spectroscopy during the hours to days following gravitational wave telescopes find these transient events. Supernovae explosions are another critical site of chemical production and are also governed by intriguing physics. The many varieties of supernovae we see beg the long-standing question of how each type comes about. The GMT's excellent spatial resolution will enable observations of recent supernovae explosions to help identify their likely progenitors. These are key issues to understanding supernovae diversity, including superluminous supernovae, GRBs (gamma-ray bursts), and the newly discovered FRBs (fast radio bursts). Moreover, the GMT will enable searches for the first supernovae to appear in the very-young universe, those that come from the first-generation stars.

CHAPTER 4 The Death of Stars

How do
stars die?



Chapter 5 explores “near field cosmology,” a name that describes the study of our galaxy’s structure and content, and that of our nearest, neighboring galaxies, to understand how galaxy formation began 13 billion years ago. With high-resolution spectrographs, the GMT will be a critical tool in measuring the chemical abundances of the earliest stars that formed in the Milky Way. Searching for those first primal

CHAPTER 5 Building the Milky Way & its Neighbors

How did galaxies
grow and evolve?

stars, which will have almost no “heavy” elements from previous generations of stars, allows us to study star and galaxy formation in the first billion years of the Universe. High resolution spectra of very metal-poor stars in the Milky Way’s outskirts and in its smallest neighboring galaxies will provide the first complete picture of how varied the process of chemical enrichment was in the building blocks of massive galaxies, and allow us to study the nature of supernovae from these first stellar generations. Faint streams of stars ring and traverse each of the giant galaxies in our neighborhood, these are the legacy of the accretion of small satellites. By associating patterns of chemical enrichment with individual streams, the process of galaxy assembly through the aggregation of smaller stellar systems will be recorded, with a fidelity well beyond the capabilities of present facilities.

CHAPTER 6

The Growth of Galaxies Over Cosmic Time

How do stars form in galaxies over cosmic time?



Chapter 6 explores galactic growth across cosmic time, emphasizing how observations with the GMT will probe cosmic noon, the period of time between 1 billion and 5 billion years after the Big Bang. During this epoch, galaxies grew from infants to adults by turning large quantities of gas into the generations of stars that produced and redistributed the chemical elements that are the building blocks of planets and life. The sheer size of the GMT will allow us to probe an unexplored regime of faint, low mass galaxies that are analogs to the first galaxies of the very young universe. Using fiber-fed spectrographs, the GMT will efficiently gather spectra of thousands of these small galaxies. Using adaptive optics, the GMT will study the substructure of galaxies over most of the history of the universe. These data will provide detailed maps of active star-formation regions, gas dynamics, gas chemistry, and the ages and orbits of different stellar populations inside non-star-forming galaxies, all of which will help us unravel the evolution and history of galaxies over time. The GMT will also allow us to find and study giant black holes inhabiting galaxy centers to understand how the black hole and its parent galaxy co-evolved. These observations together will let us watch star formation rising and falling in galaxies across cosmic time and the physics of the events and phenomena that influence it.



Chapter 7 focuses on co-evolution of galaxies and gas in the cosmic web that fueled the galaxy growth described in Chapter 5. The GMT will help us track the flow of gas along the cosmic web, into galaxies and back out again under the force of star-formation-driven winds, supernovae explosions, and supermassive black holes. Understanding the motion and chemistry of this gas is critical to understanding galaxy evolution and the star formation inside galaxies. The GMT will measure the chemistry, temperature, and density of gas at large distances from the associated galaxies (“intergalactic” gas) as well as small distances, through efficient multi-object and faint single-object spectroscopy. These are the data needed to pin down the physical drivers of outflows and to understand the cycling of gas.

CHAPTER 7 Building Galaxies from Cosmic Gas

How does the gas
that feeds star
formation get into
galaxies?



Chapter 8 discusses the GMT programs that will impact cosmology, the investigation of the universe on its largest scale. Cosmology connects (and sometimes confounds) two fields of fundamental physics: quantum mechanics and general relativity, making observations in this field particularly broad in their scientific impact. Progress on many key questions in cosmology today will require the next generation of large optical telescopes. The GMT will explore the nature of dark matter, which exists outside the otherwise successful Standard Model of particle physics, through the statistics and properties of the most dark-matter dominated halos—the ultra-faint dwarf galaxies around our own Milky Way. The GMT will also provide multiple pathways to measuring the Hubble Constant, the expansion rate of the universe, for which a conflict currently exists between the local

CHAPTER 8 Cosmology & The Dark Universe

How did the universe
form and grow?

values and the values measured on a cosmic scale (involving the cosmic microwave background). This conflict is particularly important as it suggests a confusion in our understanding of fundamental physics. These pathways involve new strategies that combine gravitational wave measurements with optical spectroscopy, as well as more traditional strategies used in the past, but pushed to fainter sources, larger distances, or greater precisions using the GMT.



CHAPTER 9 **First Light & Reionization**

What were the first sources of light and how did they transform the universe?

Chapter 9 describes GMT science in the first light epoch, when the modern universe began to take shape. Using imaging from HST and spectroscopy from large ground-based telescopes, astronomers have pushed the study of galaxy formation to distances corresponding to only 400 hundred million years after the Big Bang. Although observations of these extremely faint objects have been very difficult, we have learned that they contain gas that has already been enriched by a generation of stars, stars that are 10 million times the mass of the sun (10 million “solar masses”), and supermassive black holes that are billions of solar masses. The GMT has a historic opportunity to peer further back in space and time and detect what is truly “first light”—the primeval stars that formed devoid of heavy chemical elements, and whose deaths resulted in the supernovae that first enriched the hydrogen gas produced in the Big Bang. GMT spectra of the earliest quasars will enable us to measure the chemistry of the gas that these earliest stars enriched, helping us assemble a detailed picture of first generation stars and to understand their role in the chemical enrichment of the universe. The GMT will be uniquely capable of recording the detailed evolution of galaxies at these epochs because of its large aperture and wide-field areal coverage. Detailing the physical process of individual galaxies through diffraction-limited imaging and spectroscopy will enable a long-anticipated breakthrough in our understanding of their physical and chemical growth.

The Giant Magellan Telescope will enable a historic journey of exploration and discovery. This book skims the surface of the questions we know to ask today. The GMT will answer not only these, but also the questions we do not yet know to ask.



1 Introduction to the Giant Magellan Telescope 1

- 1.1 The GMT Partnership and Heritage..... 2
- 1.2 The Design of the GMT 4
- 1.3 Image Quality and Observing Modes 6
- 1.4 Focal Stations..... 9
- 1.5 The GMT’s First Generation Instrument Suite..... 10
- 1.6 New Capabilities, New Discoveries 23
- 1.7 Additional Reading 26



2 Exoplanets & Planet Formation.....31

- 2.1 Toward Earth: Planet Characterization..... 33
- 2.2 Toward Understanding How Planets Formed 43



3 The Birth of Stars51

- 3.1 Tracing Star Formation History via the Dynamics of Young Stellar Cluster Members 55
- 3.2 Protostellar Assembly: Accretion of Material from Circumstellar Disks 57
- 3.3 Fundamental Properties and Evolution of the Youngest Stars (and Substellar Objects) 60
- 3.4 The Most Fundamental Stellar Property: Mass 62
- 3.5 The Formation and Evolution of Substellar Objects 63



4 The Death of Stars71

- 4.1 Optical and NIR Counterparts of Gravitational Wave Sources 73
- 4.2 Supernovae..... 77
- 4.3 The First Explosions 84
- 4.4 Remnants 86
- 4.5 Tidal Disruption Events 89



5 Building the Milky Way & its Neighbors..... 95

- 5.1 The Most Metal-Poor Stars in the Galaxy 97
- 5.2 Faint Satellites and Streams 103



6 The Growth of Galaxies Over Cosmic Time..... 109

- 6.1 The Distribution of Gas, Star Formation, and Metals in Galaxies 112
- 6.2 The Evolution of Galaxy Structure and Stellar Populations.....116
- 6.3 Low Mass Galaxies Across Cosmic Time 122
- 6.4 Supermassive Black Holes and Their Co-Evolution with Galaxies 126



7 Building Galaxies from Cosmic Gas 133

- 7.1 Mapping Large-scale Cosmic Structures in Emission and in Absorption 136
- 7.2 Tracing the Movement of Gas in and out of Galaxies 137
- 7.3 Revealing Black Hole Driven Winds from Small to Largest Scales 144



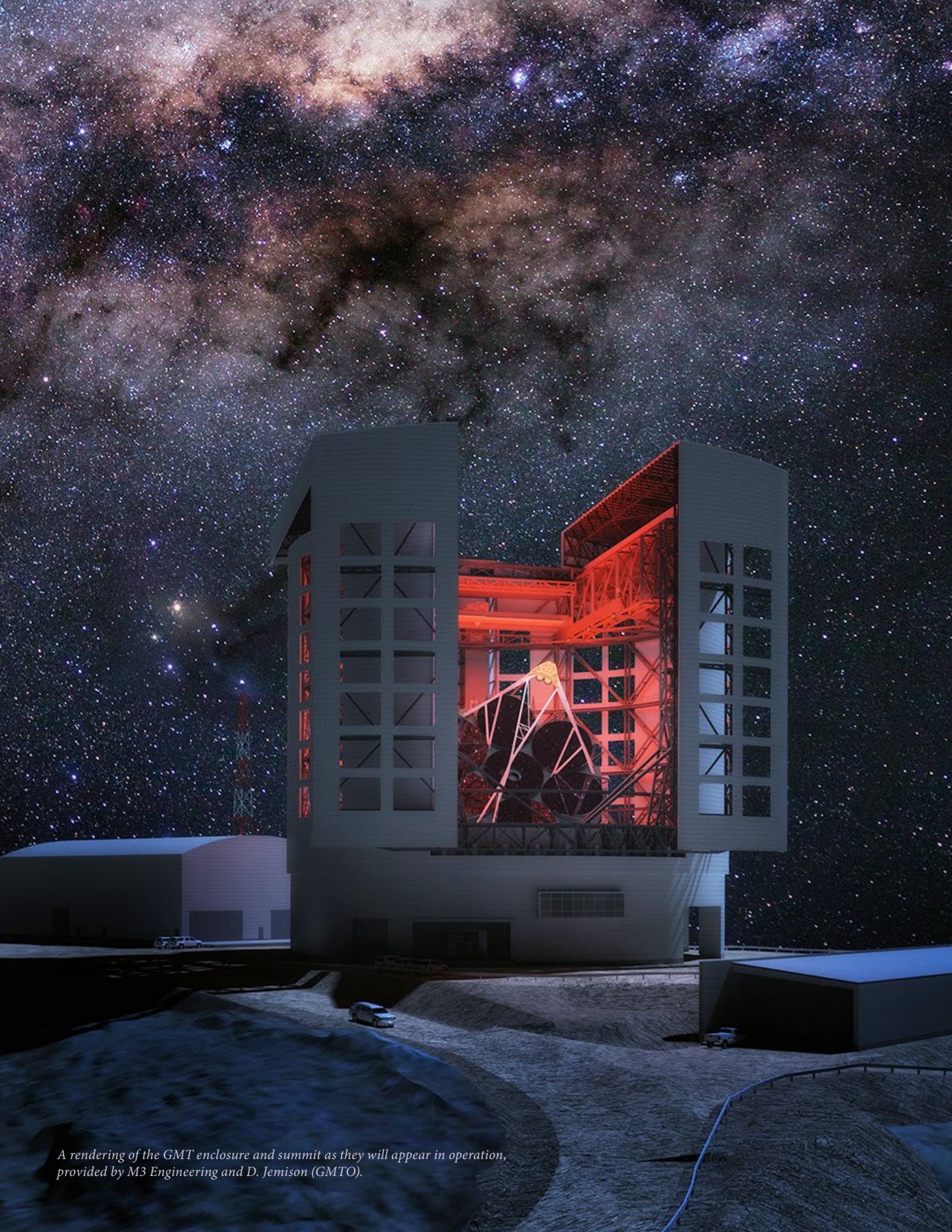
8 Cosmology & The Dark Universe 149

- 8.1 Dark Matter and Ultra-Faint Dwarf Galaxies..... 151
- 8.2 Measuring H_0 158
- 8.3 Cosmology on the Frontier: Gravitational Wave Standard Sirens..... 165



9 First Light & Reionization 169

- 9.1 Probing the First Stars and Galaxies..... 171
- 9.2 Cosmic Reionization 178
- 9.3 Observing the Formation of Supermassive Black Holes 185



A rendering of the GMT enclosure and summit as they will appear in operation, provided by M3 Engineering and D. Jemison (GMTO).



CHAPTER 1

Introduction to the Giant Magellan Telescope

The Giant Magellan Telescope (GMT) is one of a new generation of ground-based “extremely large telescopes” designed to provide unprecedented clarity and sensitivity for the observation of astrophysical phenomena.

Located at Las Campanas Observatory in the Chilean Andes, an ideal site with dark and clear skies, the GMT will explore the origins of the chemical elements, the formation of the first stars and galaxies, the mysteries of dark matter and dark energy, and the characteristics of planets orbiting other stars.

Chapter Authors

Rebecca Bernstein (GMTO Corporation)

Dan Fabricant (Harvard-Smithsonian Center for Astrophysics)

1 Introduction to the Giant Magellan Telescope

1.1 The GMT Partnership and Heritage

The GMT partnership formed in 2003 as the members of the 6.5 m Magellan Telescope consortium and interested scientists from other institutions began developing concepts for a next generation optical/infrared telescope. The conceptual telescope design, released in 2006, capitalized on the technologies and design strategies that had been demonstrated with the exceptional performance of the Magellan Telescopes.

The GMTO Corporation (GMTO) is an independent nonprofit organization formed by an international consortium of universities and research institutions to manage the development, construction, and operation of the GMT. As of 2018, the partnership includes Arizona State University, Astronomy Australia Ltd., the Australian National University, the Carnegie Institution for Science, the São Paulo Research Foundation (FAPESP), Harvard University, Korea Astronomy and Space Science Institute, Smithsonian Institution, Texas A&M University, The University of Texas at Austin, University of Arizona, and University of Chicago. GMTO is recognized by legal agreement with the Government of Chile as a special

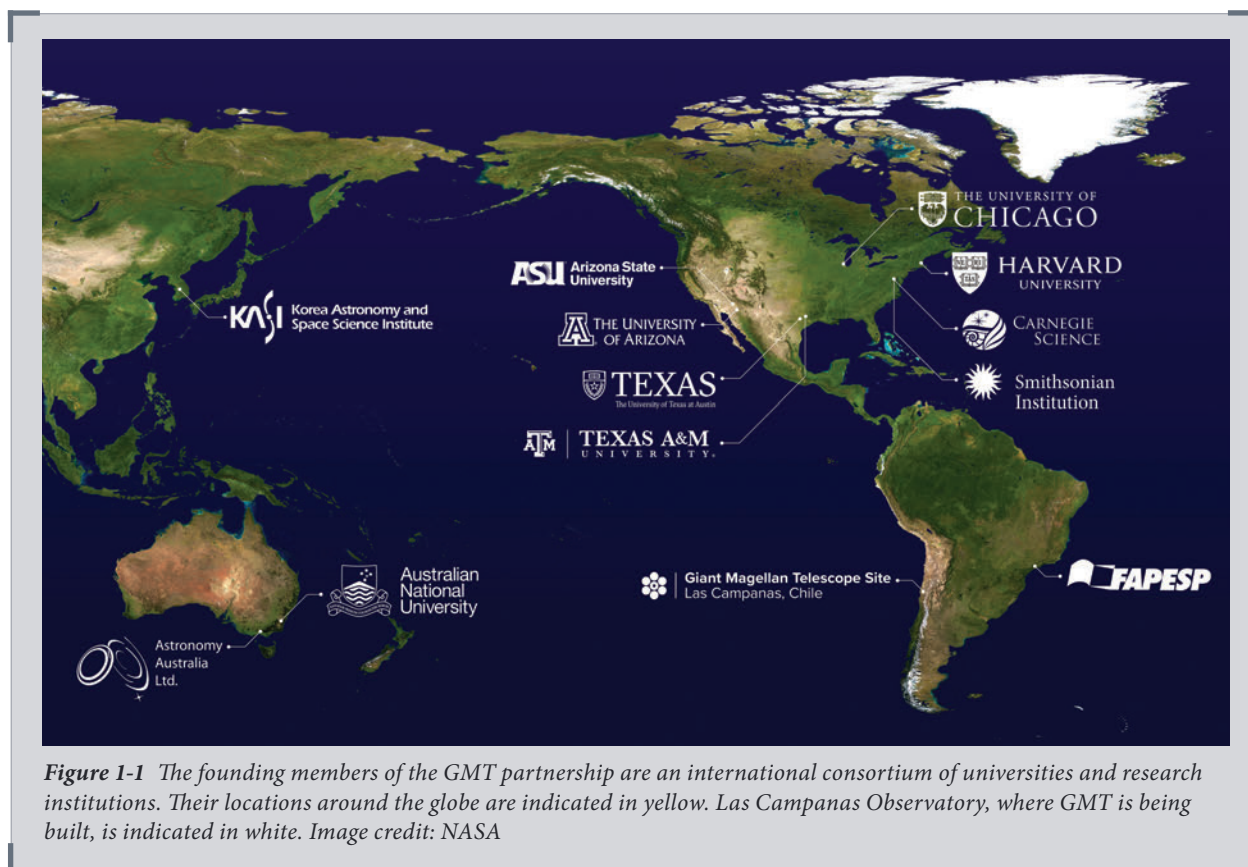


Figure 1-1 The founding members of the GMT partnership are an international consortium of universities and research institutions. Their locations around the globe are indicated in yellow. Las Campanas Observatory, where GMT is being built, is indicated in white. Image credit: NASA

international organization with permission and authority to operate within Chile. Chilean astronomers will use the GMT through a cooperative agreement with the University of Chile.

The GMT will be built at the Las Campanas Observatory (LCO) at the southern end of the Chilean Atacama Desert in the western Andes. The site is owned by the Carnegie Institution for Science and is made available to the GMTO by a long-term lease. Three candidate sites at LCO were studied while monitoring the 6.5 m Magellan site as a reference. The GMT Board selected Las Campanas Peak (Cerro Campanas) as the GMT site based on three years of new test data and review of the available historical data. Las Campanas Peak is the highest point (2,550 m) on the LCO property. The superb seeing at Las Campanas Peak (a median of 0.62 arcseconds FWHM at 550 nm) is indistinguishable from the seeing at the excellent Magellan site. LCO has outstanding weather statistics and is free from light pollution and indeed any significant threat of future light pollution.

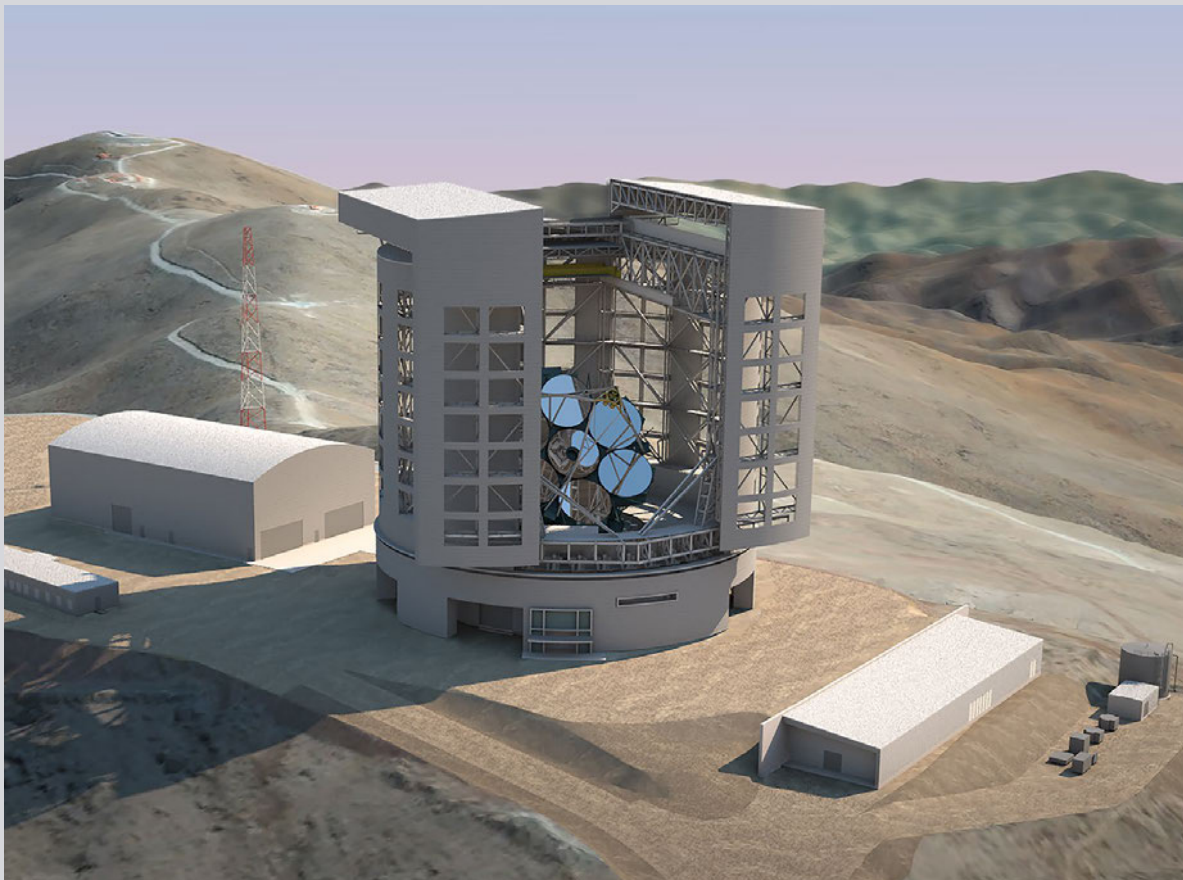


Figure 1-2 Looking North-East across the summit of Cerro Campanas with the GMT enclosure and support buildings. The road in the background leads to the rest of Las Campanas Observatory. Cerro Manque, the site of the Magellan 6.5 m telescopes, is the highest background peak near the top center of the image. The du Pont 2.5 m telescope is located at the edge of the ridge at the top left.

1.2 The Design of the GMT

Seven 8.4 m diameter segments form the GMT's primary mirror. These are being made at the Richard F. Caris Mirror Laboratory at the University of Arizona and are the largest monolithic mirrors ever made. The secondary mirror is also segmented and is composed of seven 1.05 m diameter segments. The primary and secondary segments work in conjugate pairs so that each secondary mirror reflects light from only one primary mirror segment. By using deformable mirror technology for these secondary mirror segments, the GMT will be able to correct atmospheric turbulence to form diffraction-limited images (See *Figure 1-3* and *Figure 1-4*).

The GMT optics have an aplanatic Gregorian design. In a Gregorian telescope, the light reflected from the primary mirror comes to a focus before reaching the secondary mirror. A classical Gregorian telescope (e.g. the 6.5 m Magellan Telescopes) has a parabolic primary mirror and a concave ellipsoidal secondary mirror. An aplanatic Gregorian design modifies the shape of the primary and secondary mirrors (both are concave ellipsoids) to improve the image quality across an extended field of view. Both classical and aplanatic Gregorian telescopes can add corrective lenses to extend the field of view with excellent image quality. At the edge of a 20 arcminute diameter field of view, the GMT forms images with a (RMS) diameter of 0.6 arcseconds, improving to <0.1 arcseconds with corrective lenses.

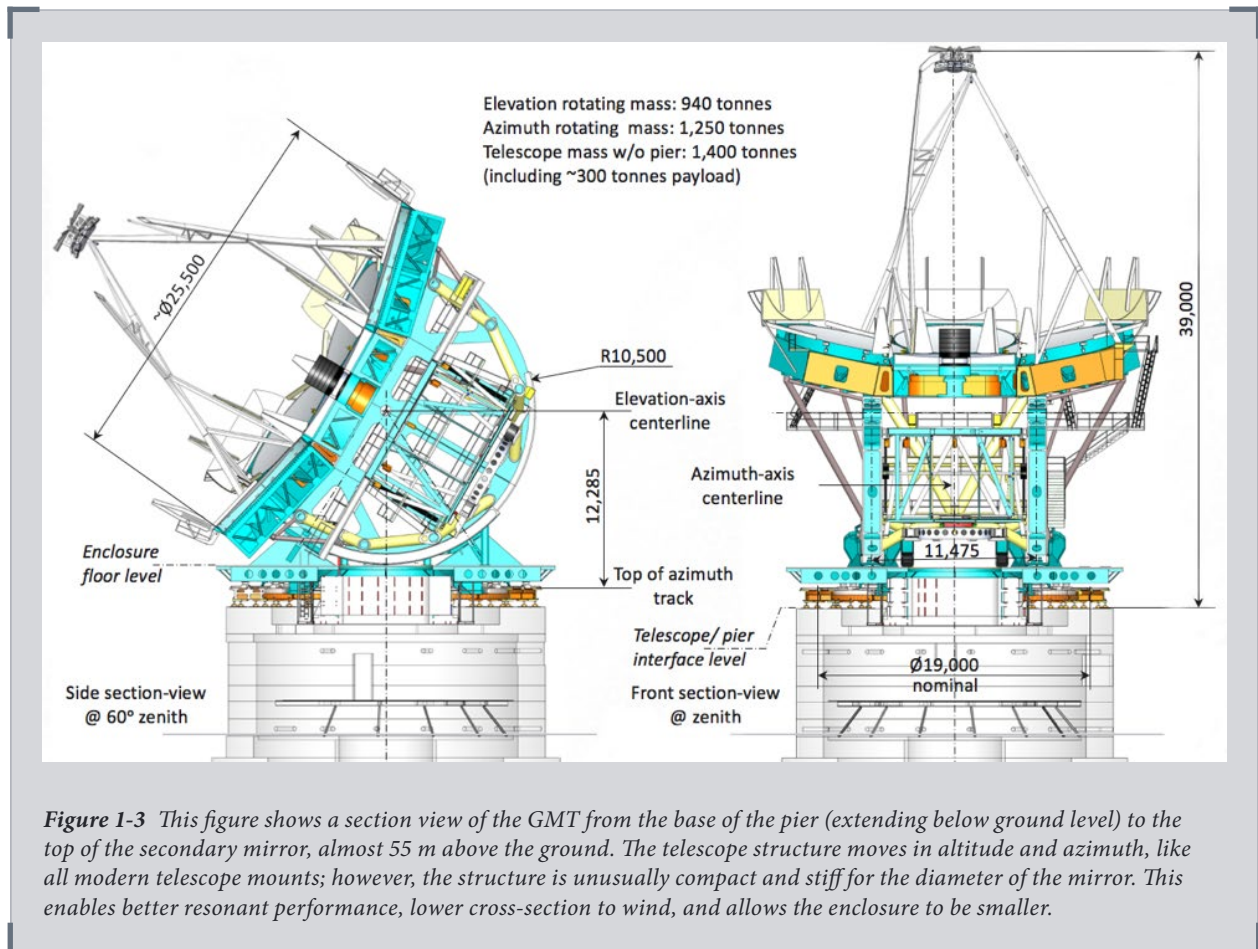


Figure 1-3 This figure shows a section view of the GMT from the base of the pier (extending below ground level) to the top of the secondary mirror, almost 55 m above the ground. The telescope structure moves in altitude and azimuth, like all modern telescope mounts; however, the structure is unusually compact and stiff for the diameter of the mirror. This enables better resonant performance, lower cross-section to wind, and allows the enclosure to be smaller.

The Gregorian design is less compact than the more widely used Cassegrain design but offers compelling advantages:

- The GMT's Gregorian secondary is optically conjugated to a position ~160 meters above the ground, enabling excellent ground layer adaptive optics correction over a large field of view, with high throughput and low thermal background
- The Gregorian design allows in-telescope calibration of the adaptive optics (AO) system with an artificial star at prime focus, which is not possible with conventional Cassegrain optics (see *Figure 1-4*)
- The telescope focal plane is curved toward the instruments, simplifying the design of the optics for a wide-field, multi-object, seeing limited spectrograph (e.g. GMACS). In addition, a very useful calibration screen can be deployed at the exit pupil of the telescope below the secondary mirror

The potentially less compact Gregorian telescope structure is mitigated in the GMT design by choosing a fast ($f/0.7$) primary focal ratio. The highly curved, off-axis primary mirror segments required to implement the GMT design are demanding to fabricate. However, these challenges were met with the 2012 completion of the first primary mirror segment. The focal ratio of the complete GMT is also fast ($f/8$), yielding a compact image scale of 1.0 mm per arcsecond, allowing us to build wide field instruments for the GMT that are not feasible for other extremely large telescope (ELT) designs. *Table 1-1* summarizes key properties of the GMT. *Section 1.4* (Focal Stations) describes the focal stations and instrument mounting locations.

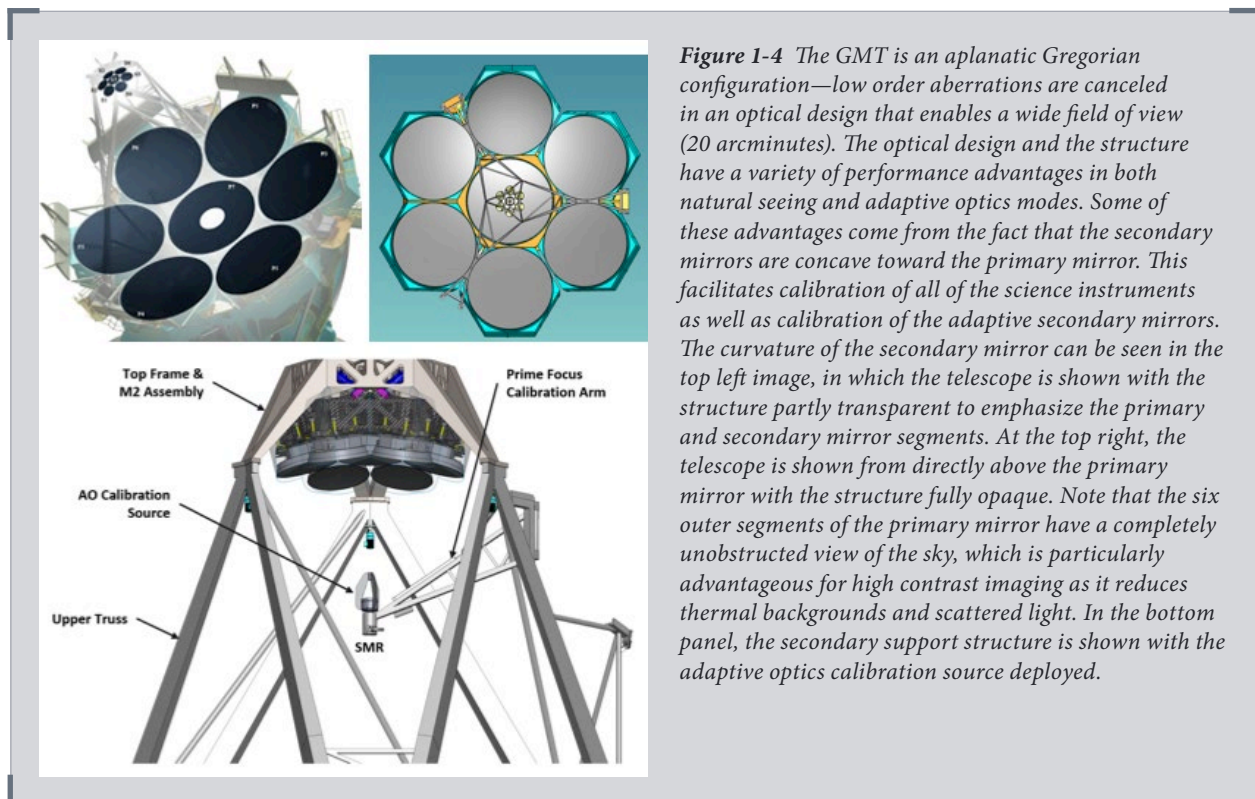


Figure 1-4 The GMT is an aplanatic Gregorian configuration—low order aberrations are canceled in an optical design that enables a wide field of view (20 arcminutes). The optical design and the structure have a variety of performance advantages in both natural seeing and adaptive optics modes. Some of these advantages come from the fact that the secondary mirrors are concave toward the primary mirror. This facilitates calibration of all of the science instruments as well as calibration of the adaptive secondary mirrors. The curvature of the secondary mirror can be seen in the top left image, in which the telescope is shown with the structure partly transparent to emphasize the primary and secondary mirror segments. At the top right, the telescope is shown from directly above the primary mirror with the structure fully opaque. Note that the six outer segments of the primary mirror have a completely unobstructed view of the sky, which is particularly advantageous for high contrast imaging as it reduces thermal backgrounds and scattered light. In the bottom panel, the secondary support structure is shown with the adaptive optics calibration source deployed.

Adaptive optics are integral to the GMT design. The adaptive secondary mirrors (ASMs) for the GMT will be the fourth generation of adaptive secondary mirrors previously used at the MMT, LBT, Magellan, and the VLT. A second, optically identical secondary mirror assembly without the adaptive optics will be used during commissioning of the GMT and during servicing of the adaptive secondary mirrors. The secondary assemblies will each have a dedicated top-end frame that will be removed completely to change between the two assemblies.

Table 1-1 Basic GMT Properties

Parameter	Value
Optical prescription	Aplanatic Gregorian
Focal plane scale	0.997 arcseconds/mm
Wavelength range	0.32 – 25 μm
Field of View	20 arcminute diameter
Primary mirror diameter & collecting area	25.4 m, 368 m^2
Primary mirror f/#	0.71
Final f/# [with Wide Field Corrector]	8.16 [8.34]
Diffraction-limited angular resolution	0.01 arcsecond at 1 μm

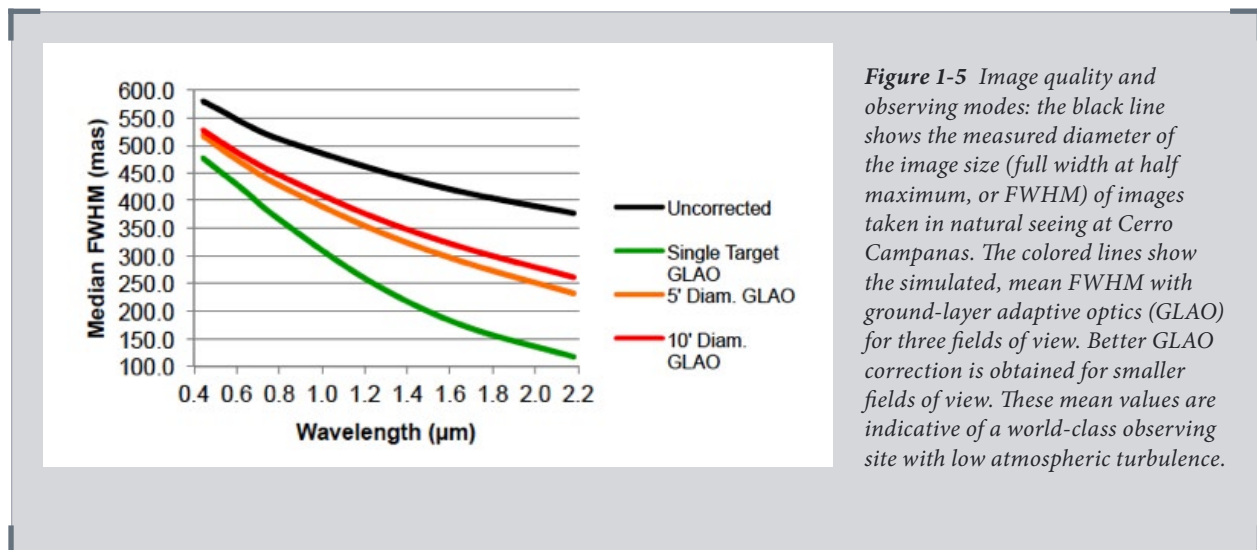
The basic parameters of the GMT configuration are listed above. The focal ratio of the telescope (roughly f/8) indicates that it comes to a focus twice as fast as the other Giant Segmented Mirror Telescopes. This enables the enclosure to be smaller than it would be with a larger focal ratio optical system, and it delivers a smaller plate scale at the focal plane, which in turn enables the instruments to remain relatively small while still capturing a wide field of view. The risk associated with fabrication of fast primary mirrors has already been retired as the first off-axis segment has been made to specification and the next four segments are already cast.

1.3 Image Quality and Observing Modes

In regular operation, the GMT will support four different adaptive optics observing modes: natural seeing, ground layer adaptive optics (GLAO), natural guide-star adaptive optics (NGAO), and laser tomography adaptive optics (LTAO).

- **Natural Seeing (NS)** – Natural seeing images are available over the full wavelength range (0.32 – 25 μm) and field of view of the GMT, with image quality limited by atmospheric wavefront distortion. Both sets of secondary mirrors support natural seeing observations. The black line in **Figure 1-5** is the median natural seeing image quality that has been measured at Cerro Campanas.
- **Ground Layer AO (GLAO)** – the GMT’s Gregorian optics allow ground-layer atmospheric turbulence to be corrected over a wide field of view (≥ 10 arcmin) by the GMT’s adaptive optics system and adaptive secondary mirrors (ASMs). GLAO will improve the natural image quality at the site (natural “seeing”) and reduce the image size by 20 – 50 % from the visible to near-IR, with the greatest improvements at red wavelengths. The GLAO mode will use wavefront sensors integral to the GMT’s active optics system, allowing any instrument to receive GLAO corrected images when the ASMs are in use. GLAO performance slowly degrades far off-axis as shown in **Figure 1-5** because very wide fields of view will travel different paths through the atmosphere.

- **Natural Guide Star AO (NGAO)** – This mode uses a single, bright, natural guide star to deliver diffraction-limited, high Strehl ratio images (>75 % Strehl in the K band) at wavelengths from 0.6 μm into the mid-infrared over a field of view a few arcseconds in diameter. This mode is provided by the ASM working with a combination of the GMT's wavefront sensors and sensors on each instrument to assure accurate correction at any instrument designed to work with diffraction-limited images.
- **Laser Tomography AO (LTAO)** – This mode uses six laser guide stars and a single, faint, natural guide star to extend diffraction-limited performance to nearly the full sky with moderate Strehl ratio (>30 % Strehl in the H band) at IR wavelengths over a field of view similar to NGAO. As with NGAO, this mode is provided by the GMT's wavefront sensors and adaptive secondary mirrors, and is available to any instrument designed to use this mode.



When the ASMs are not available, the GMT optics will deliver excellent natural seeing images thanks to *active* optical control of the primary mirror segments and tip-tilt correction in the alternate fast steering secondary mirrors (FSMs). Among the last generation of large ground-based telescopes, the MMT, Magellan, and Large Binocular Telescopes demonstrated the high performance of the stiff monolithic mirrors used in the GMT. The optical performance of these mirrors is largely determined and tested in the optical laboratory before the telescope is assembled on site. At Magellan, the intrinsic image quality of the optics and telescope is only 0.07 arcseconds FWHM, contributing negligibly to atmospheric seeing.

Figure 1-6 and **Figure 1-7** illustrate the scientific impact of adaptive optics with the GMT.

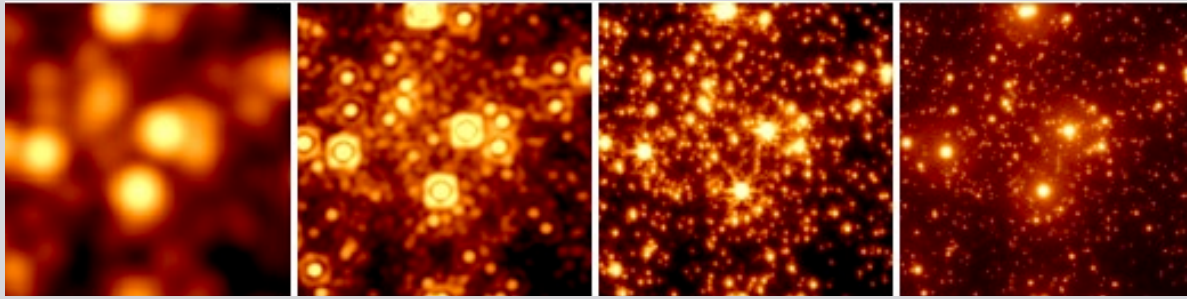
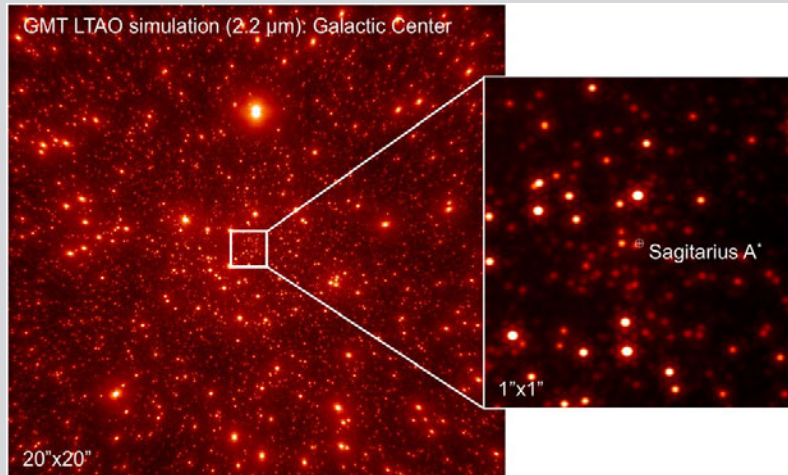


Figure 1-6 The progression of images from left to right shows the impact of adaptive optics with the GMT: (1) natural seeing at 0.5 arcsecond resolution. (2) Hubble Space Telescope with 0.2 arcsecond resolution. (3) a simulated image with James Webb Space Telescope with 0.07 arcsecond resolution, and (4) a simulation of the 0.02 arcsecond resolution images that the GMT will obtain with natural guide star adaptive optics.

Figure 1-7 A simulated image of the Milky Way’s central 2.5 light-years with the GMT and the GMTIFS Imager using laser tomography adaptive optics (LTAO). The purpose of laser guide stars is to make it possible to measure (and then correct) the turbulence in the atmosphere along the line of site to any science target in the sky. Artificial guide stars are necessary because bright stars are needed for this purpose, and sufficiently bright natural guide stars are only found over about 5–10 % of the sky. With LTAO, we can correct for atmospheric turbulence to observe targets at almost any location in the sky with diffraction-limited resolution. The simulation, a 200 second exposure in the K-band, is based on the galactic center model of Do et al. (2014), including known sources and expected fainter population.



1.4 Focal Stations

The GMT offers a versatile set of direct and folded focal stations to accommodate the needs of a wide range of instruments from large, wide-field GLAO and natural seeing spectrographs to compact adaptive optics imagers. All of these foci are located behind the primary mirror (see *Figure 1-8*). Instruments are supported within a large Gregorian Instrument Rotator (GIR) that provides four stations at the direct Gregorian focus inside the GIR, and three at the folded Gregorian focus on the top side of the GIR. The telescope beam will typically be folded with a tertiary mirror that is optimized for high reflectivity in the infrared. Visible-light instruments with small fields of view, including the high-dispersion spectrograph called G-CLEF, will be fed with tertiary mirrors optimized for their specific field of view and wavelength range.

The GMT has a station on the azimuth structure for fiber-fed instruments that require high stability, such as G-CLEF. This station rotates in azimuth but is otherwise gravity invariant. The GMT also provides two auxiliary ports located outside the elevation bearings that accommodate smaller gravity-invariant instruments fed by an optical relay, such as high-contrast adaptive optics imagers.

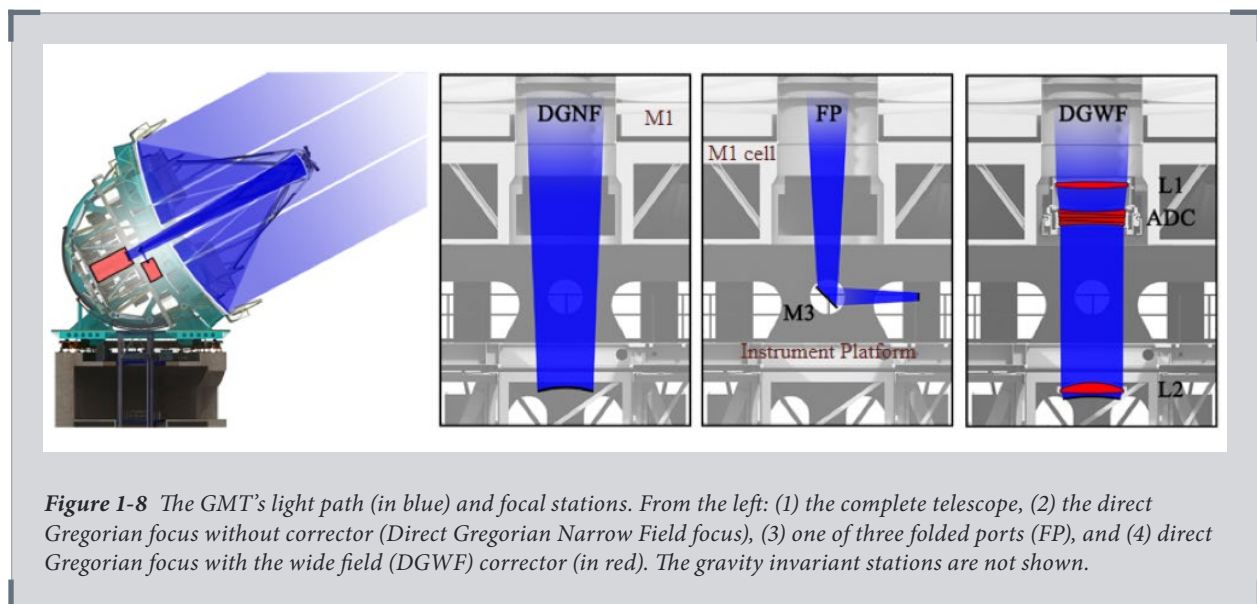


Figure 1-8 The GMT's light path (in blue) and focal stations. From the left: (1) the complete telescope, (2) the direct Gregorian focus without corrector (Direct Gregorian Narrow Field focus), (3) one of three folded ports (FP), and (4) direct Gregorian focus with the wide field (DGWF) corrector (in red). The gravity invariant stations are not shown.

In total, the GMT can support at least ten permanently mounted instruments. One direct Gregorian instrument and any of the folded-port or gravity-invariant instruments can be exchanged in 15 minutes or fewer during any observing night. Rapid switching between instruments allows agile target-of-opportunity observations of transient events, rapid response to changing environmental conditions, and optimal queue scheduling.

1.5 The GMT's First Generation Instrument Suite

Overview

The first-generation instrument suite has been chosen to maximize the GMT's scientific impact during early operations. Initial GMT instrument concepts were prepared for the telescope's Conceptual Design Review in 2006. Seven of the concepts were further developed for instrument conceptual design review in 2011. Five of those are now under development (*Table 1-2*), and the remaining two are deferred until funding is available. Two additional instruments have since been proposed that would add important early scientific capabilities of considerable interest to the GMT partnership, as recommended by the Science Advisory Committee (SAC). The two deferred and two newer instruments are listed in *Table 1-3*. All will take advantage of some mode of adaptive optics. All instruments for the GMT will be developed by teams distributed throughout the partnership, and the SAC will invite and review proposals for future generations of instruments. A final capability currently in development is the commissioning camera, which will be used to test and commission the ground-layer adaptive optics performance, and for scientific imaging.

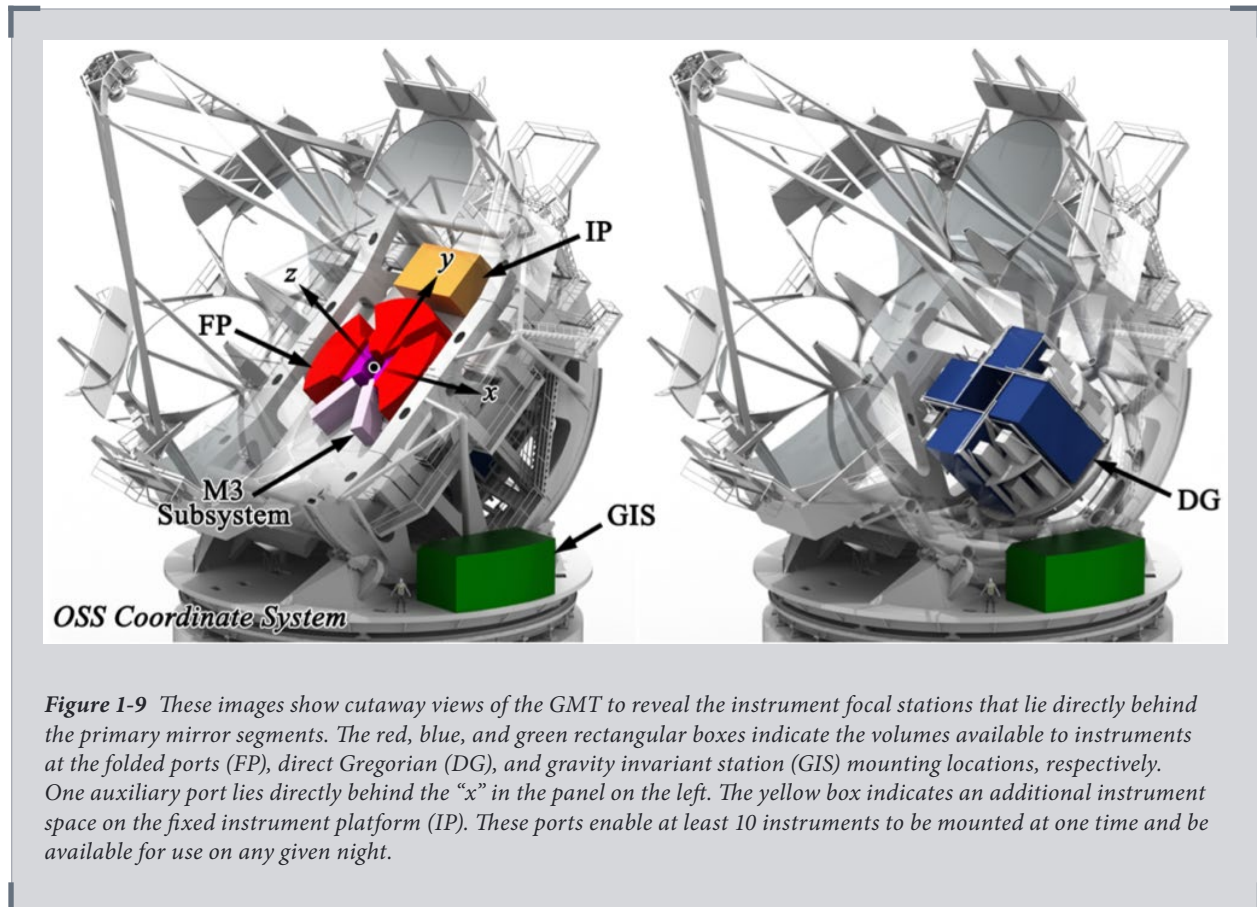


Table 1-2 The GMT's First Generation Instrument Suite

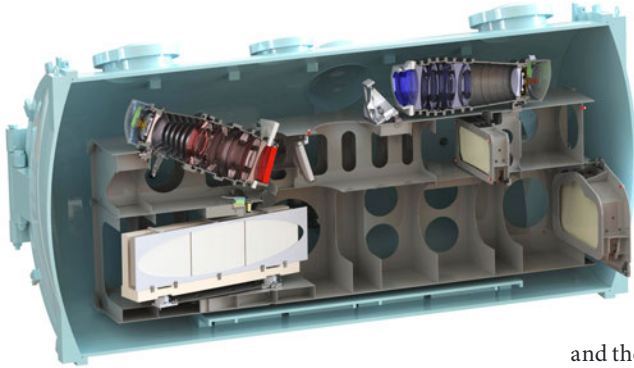
Instrument	Description	λ Range (μm)	Resolution	AO Modes	Field of View
G-CLEF	Optical High-Resolution High-Stability Spectrograph	0.36 – 1.0	20,000–100,000	NS, GLAO, NGAO	$7 \times 0.23''$ pack, or 1.2" fiber
GMACS	Wide-Field Optical Multi-Object Spectrograph	0.32 – 1.0	1,500 – 4,000	NS, GLAO	43 arcmin ²
GMTIFS	Near-IR IFU Spectrograph & Imager	1 – 2.5	5,000 – 10,000	LTAO, NGAO	10 or 400 arcsec ²
GMTNIRS	Near- to Mid-IR High-Resolution Spectrograph	1.08 – 5.4	65,000 (JHK) 85,000 (LM)	NGAO, LTAO	1.2" long-slit
MANIFEST	Facility Robotic Fiber System	0.36 – 1.0	—	NS, GLAO	20 arcmin diam.

Table 1-3 Instrument concepts for additional early-light instruments

Instrument	Description	λ Range (μm)	Resolution	AO Modes	Field of View
NIRMOS*	Wide-Field near-IR Multi-Object Spectrograph	0.8 – 2.5	1,500 – 4,000	NS, GLAO	40 – 60 arcmin ²
[Near-IR echellette]**	Single Object near-IR, near-IR, high-throughput Spectrograph	0.8 – 2.5	~6,000	NS, GLAO	Single slit (<5")
TIGER*	High Contrast IR Imager and Low Resolution Spectrograph	1.5 – 5, 8 – 25	300	NGAO	—
[High-Contrast Imager]**	NIR AO-fed IFU / Imager	1 – 5	—	NGAO	1.2" long-slit

Notes: This table lists instruments (marked by *) that were developed to the conceptual design level in 2011; further development has been deferred. New instrument concepts (marked by **) are shown that are appropriate for rapid development and could provide some of the deferred capabilities at or near first light.

G-CLEF The GMT-Consortium Large Earth Finder



G-CLEF is a visible echelle spectrograph with red and blue channels, capable of operating in natural seeing during early operations. Adaptive optics, when available, will enhance G-CLEF's power. G-CLEF has a thermally stabilized vacuum enclosure to allow precision radial velocity (PRV) measurements (accurate to at least 50 cm/s with a goal of 10 cm/s). This large instrument mounts at the gravity invariant station on the azimuth platform.

Depending on the selected fiber input size, G-CLEF provides spectral resolving powers ($\lambda/\Delta\lambda$) of 20,000, 45,000, or 100,000 (see **Table 1-4**). Scientific and technical G-CLEF requirements are summarized in **Table 1-5** and **Table 1-6**. G-CLEF can be fed by the MANIFEST multi-fiber feed to provide full spectral coverage of ~5 objects, or partial spectral coverage of up to ~40 objects if the spectral coverage is limited to two or three echelle orders. With GLAO, the throughputs of the PRV modes improve by ~25 %, and the high-throughput mode improves by ~5 % over the values in **Table 1-4**. Higher order wavefront sensors can be added to G-CLEF in the future to enable it to work with NGAO, which will improve its throughput by up to a factor of two and improve the velocity precision due to the higher stability of the input image.

G-CLEF will be the first science instrument delivered to the GMT. It will provide unique capabilities on the ELT landscape as it is the only high-resolution visible spectrograph planned for the first decade of use on the three ELTs. G-CLEF will enable observations in many areas of astrophysics. Some highly-anticipated observations include:

- Characterizing the most metal poor stars, such as the $[\text{Fe}/\text{H}] < -7.1$ star SMSS J031300.36-670839.3
- Measuring exoplanet masses, possibly as small as Mars around an M-star
- Finding O_2 in exoplanet atmospheres using transmission spectra

Table 1-4 Summary of key observing modes for G-CLEF

Observing Modes	Prioritization	Spectral Resolution	Peak Throughput
High Throughput (HT)	Throughput over resolution	20,000	16 %
Medium Throughput (MT)	Throughput and resolution	35,000	13 %
Precision Radial Velocity (PRV)	Resolution maximized	108,000	11 %
Non-scrambled PRV (NS-PRV)	Resolution maximized with higher throughput	108,000	12 %
Multi-object Spectroscopy (MOS)	Fed by MANIFEST for multi-object efficiency advantage	35,000	13 %

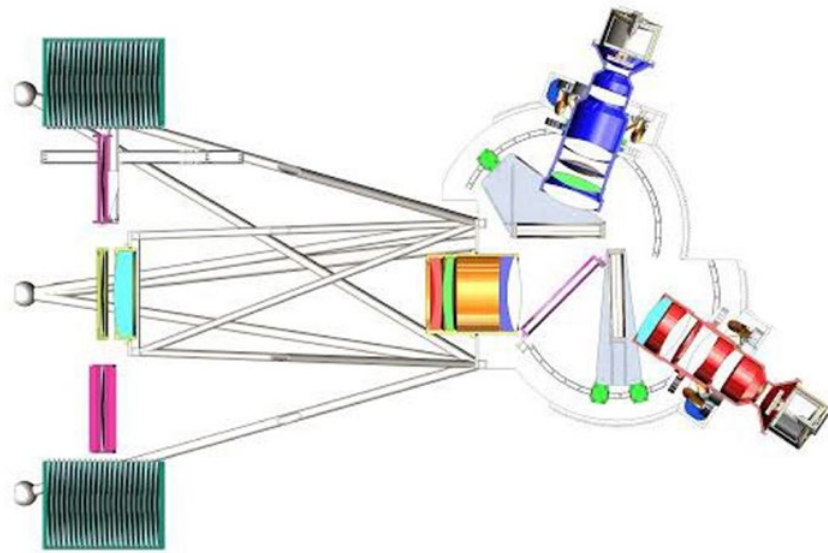
Notes: High Throughput mode is appropriate for faint sources such as quasars and low metallicity stars; Precisions Radial Velocity mode is appropriate for observations of extrasolar Earth-mass planets. Multi-object Spectroscopy mode will be ideal for situations in which high multiplexing enables efficient observation of many sources at one time. Examples include chemical abundances of metal-poor stars in the Local Group or stellar dynamics of dark-matter dominated dwarf galaxies.

Table 1-5 Scientific and technical requirements for G-CLEF in standard use

Science Application	λ range, nm	$\lambda/\Delta\lambda$	Notes
Stellar abundance studies	350 – 1,090	$\geq 35,000$	e.g., extreme metal poor stars [single object mode]
Line profile studies	350 – 1,000	$\sim 100,000$	e.g., Isotopic studies, atmospheric physics [single object mode]
Exoplanet atmospheres	380 – 650	$\sim 50,000$	Transit spectroscopy [single object mode]
IGM abundances and dynamics	450 – 1,000	30 – 50 k	Line profile studies [single object mode]
Reionization of the IGM	800 – 1,000	10 – 30 k	Gunn-Peterson effect [single object mode]
Stellar dynamics in resolved populations	400 – 950	—	Single or few orders, precision velocities [fiber feed]
IGM tomography	350 – 600	$\sim 20,000$	Faint background sources over a 20-arcminute diameter field [fiber feed]
Technical Parameter	Requirement	Goal	Notes
Wavelength range	400–950 nm	320 – 1100 nm	He I 10830 coverage desired, but not required
Spectral resolution	$R \geq 30,000$	—	Baseline resolution-slit size product for 0.7" slit width
Image quality	$< 0.25''$	$< 0.15''$	FWHM Broad-band, absent seeing
Slit length	$\geq 3''$	—	Should allow simultaneous sky sampling when observing point sources
Velocity stability	~ 40 cm/s	—	Precision radial velocity mode (per exposure)
Throughput	$\geq 20\%$, 400 – 900 nm	$\geq 30\%$, 400 – 900 nm	Exclusive of slit losses, ADC, telescope and atmosphere

Table 1-6 Scientific and technical requirements for the PRV mode of G-CLEF

Science Application	λ range, nm	$\lambda/\Delta\lambda$	Notes
Physical properties of planets	400 – 700	$\sim 100,000$	Planetary masses, internal structure
Planetary system architecture	400 – 700	$\sim 100,000$	Orbit distributions, secular evolution, stability of planetary systems
Stellar abundances	Wide as possible	$\sim 100,000$	General stellar abundance work
Variable physical constants	Wide as possible	$\sim 100,000$	Quasar absorption line spectroscopy
Technical Parameter	Requirement	Goal	Notes
Wavelength Range	400 – 700 nm	320 – 850 nm	
Spectral Resolution	100,000	—	
Velocity Stability	< 1 m/s	≤ 20 cm/s	over timescales of 3 – 12 months
Field of View	Single object	—	
Throughput	$\geq 20\%$	—	Exclusive of telescope, input losses and atmosphere



GMACS The GMT Multi-object Astronomical and Cosmological Spectrograph

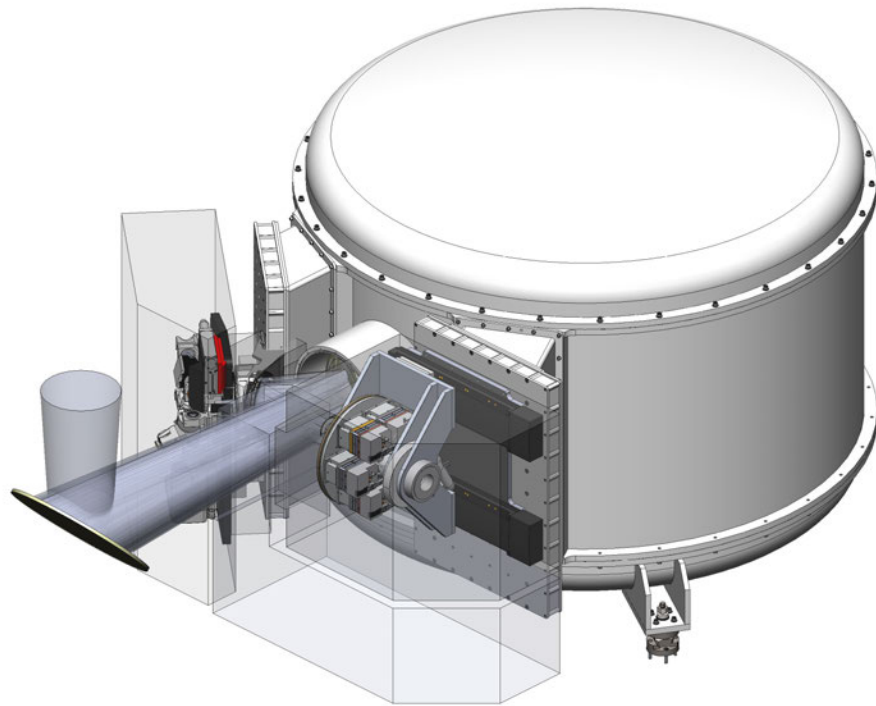
GMACS is a visible, moderate-dispersion, multi-object spectrograph with red and blue channels. It is designed to operate in natural seeing, but its sensitivity will be enhanced with GLAO correction. GMACS's field of view is 7.5 arcmin in diameter for operation with multislit masks. When fed with MANIFEST's optical fibers, objects can be observed across the GMT's full 20 arcminute field of view. MANIFEST can provide higher multiplex advantage, higher spatial and spectral resolutions using fiber-slicers, multi-fiber integral field unit (IFU) bundles, or a combination of these modes. GMACS uses VPH gratings on both the blue and red sides to achieve high throughput. GMACS's scientific and technical requirements are summarized in *Table 1-7*.

GMACS's wavelength coverage will extend from the blue atmospheric cut-off at 0.32 μm to the red limit of silicon detectors at 1 μm . GMACS is planned to be the GMT's second science instrument. Key science drivers include:

- Time domain astrophysics including gamma ray bursts (GRBs), gravitational wave counterparts, supernovae (SNe), and exoplanet transits
- Atmospheres of brown dwarfs and exoplanets
- Dynamics of dwarf and ultra-faint dwarf galaxies
- Redshift surveys
- Formation and assembly of galaxies
- Intergalactic medium (IGM) and circumgalactic medium (CGM) tomography of distant galaxies

Table 1-7 Scientific and technical requirements for GMACS

Science Application	λ range, nm	$\lambda/\Delta\lambda$	Notes
Star formation and chemical evolution in galaxies	320 – 1,000	~2,000	Abundances, stellar populations and ages, star formation rates [slit MOS]
Massive galaxy assembly	500 – 1,000	~3,000	Stellar ages, stellar populations, velocity dispersions, rotation curves [slit MOS]
Dark matter distributions	400 – 800	~5,000	Dynamics of clusters, PNe, resolved stellar populations [slit MOS]
Evolution of galaxy clustering	400 – 900	2,000	Large scale galaxy surveys [fiber MOS]
Tomography of the IGM	320 – 900	2,000, 10,000	Large galaxy surveys, IGM tomography with faint background sources [slit and fiber MOS]
Technical Parameter	Requirement	Goal	Notes
Wavelength range	320 – 980	320 – 1,000	
Spectral resolution	$\geq 1,000$ (at 600)	—	Baseline: 0.7" slit widths
Multiplex factor	>100	—	For slit fed mode
Field of view [slit fed]	35 arcmin ²	45 arcmin ²	
Field of view [fiber fed]	20' diameter	—	
Field of view [imaging]	35 arcmin ²	45 arcmin ²	Imaging capability is desired only if it does not compromise spectrograph performance
Image quality	0.24" at 10' field radius	0.16" at 10' field radius	Should not degrade images from telescope and site by more than 5 %
Velocity stability	<0.1	—	Flexure in units of spectral resolution element in one hour of observation
Throughput	≥ 25 %, 500 – 800	≥ 35 %, at blaze peak	Exclusive of atmosphere, telescope, and slit losses



GMTIFS The GMT Integral Field Spectrograph

GMTIFS is a diffraction-limited imager and integral field spectrograph operating across the YJHK bands. The spectrograph will provide spectral resolving powers of 5,000 and 10,000 over rectangular fields of view of 0.5×0.3 , 1.1×0.5 , 2.2×1.1 , and 4.5×2.2 arcsec, depending on the selection of “spaxel” size (i.e. the size of the spatial resolution element) which can be 6, 12, 25, and 50 mas. The resulting data “cube” will have 45 slits, with 88 spatial resolution elements along the slits, and 4,096 pixels in the spectral direction. The imager will accommodate ~16 filters and provide a field of view of 20.4×20.4 arcseconds at a scale of 5 mas per pixel. GMTIFS’s scientific and technical requirements are summarized in *Table 1-8*.

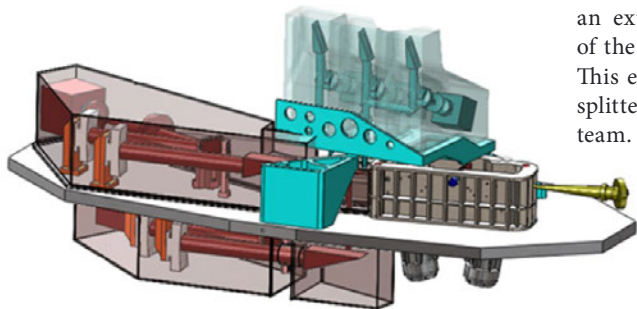
GMTIFS will be the first AO instrument at the GMT. Integral field instruments have broad applications but GMTIFS will target the physics of galaxy assembly and the evolution of galaxy chemical composition. Key observations that will be enabled by GMTIFS include:

- High spatial resolution spectroscopy of solar system objects to examine their atmospheric structure and composition
- Extending the relationship between black hole mass and galaxy velocity dispersion to greater distances and more massive black holes
- Extending the relationship between black hole mass and galaxy/cluster velocity dispersion within the local volume to the least massive black holes
- First light and reionization studies beyond the redshift range available to GMACS in Ly α , as well as observation of redder emission lines subject to dust extinction local to the source
- Studies of galaxy formation and dynamical evolution through IFU observations of galaxies in a broad redshift range

Table 1-8 Scientific and technical requirements for GMTIFS

Science Application	λ range, μm	$\lambda/\Delta\lambda$	Notes
Internal structure and dynamics of distant galaxies	1 – 2.5	5,000	Kinematics, line widths, abundances, star formation rates [LTAO coarse pitch]
Black hole masses and AGN physics	1 – 2.5	10,000	Emission line kinematics, bulge velocity dispersions, line ratios [LTAO fine pitch]
Young stellar objects	1 – 2.5	5,000	Outflows, line profiles, excitation levels [LTAO fine pitch]
IMF in dense star clusters	1 – 2.5	5,000	Line indices, velocities [LTAO fine pitch]
SNe and GRB spectroscopy	1 – 2.5	5,000	SNe and GRB redshifts, SNe physics, reionization studies [LTAO coarse pitch]
Technical Parameter	Requirement	Goal	Notes
Wavelength range	1 – 2.5 μm	0.9 – 2.5 μm	—
Spectral resolution	$R > 3,000$	$R > 5,000$	Resolving the OH airglow forest
Spatial resolution element fine pitch	≤ 10 mas	—	Nyquist sampling the short wavelength AO PSF
Spatial resolution element coarse pitch	≥ 30 mas	50 mas	Providing high sensitivity to low surface brightness regions in extended sources
Field of view fine pitch	0.15 arcsec ²	0.5" \times 0.3"	—
Field of view coarse pitch	9.9 arcsec ²	4.5" \times 2.2"	—
Image quality	Diffraction-limited	—	—
Throughput	≥ 20 %	40 %	Exclusive of atmosphere and telescope
Imaging mode	—	Full LTAO field	

GMTNIRS The GMT Near-IR Spectrograph



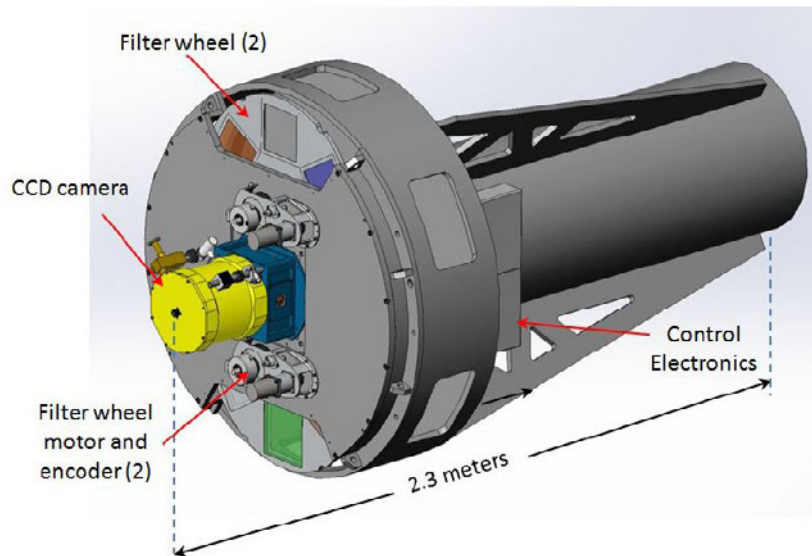
GMTNIRS is a single-object near- to mid-IR echelle spectrograph that provides an extraordinary spectral multiplex advantage through simultaneous coverage of the full JHKLM bands at resolving powers of 50,000 (JHK) and 100,000 (LM). This efficiency is enabled by the AO-feed from the GMT, multiple dichroic beam splitters, and silicon immersion echelle gratings developed by the instrument team. GMTNIRS has considerable technical heritage from IGRINS, an HK spectrograph with $R=40,000$, recently completed by the same instrument team. GMTNIRS has only one configuration and only one moving part (the rotating pupil mask), promoting reliable operations and streamlined data analysis. GMTNIRS's scientific and technical requirements are summarized in *Table 1-9*.

Key scientific objectives include:

- The formation of planetary systems and their host proto-stars
- Details of the disks surrounding young stars and planets
- Characterization of Jupiter-mass planets
- Properties of brown dwarfs

Table 1-9 Scientific and technical requirements for GMTNIRS

Science Application	λ range, μm	$\lambda/\Delta\lambda$	Notes
Pre-main-sequence stellar evolution	1 – 5	~85,000	Accretion, outflows, magnetic fields, etc.
Proto-stellar disks	1 – 5	~50,000	Dynamics, chemistry, structure
Stellar populations	1 – 2.5	~30,000	Integrated light studies, single red giant, etc.
IGM abundances	1 – 2.5	30,000 – 50,000	MgII, CIV abundances & ionization states at $z > 4$
Reionization of the IGM	1 – 2.5	10,000 – 30,000	IGM tomography
Technical Parameter	Requirement	Goal	Notes
Wavelength range	1.2 – 2.5 μm or 3 – 5 μm	1 – 5 μm	Requirement is for either 1–2.5 μm or 3 – 5 μm
Spectral resolution	$R \geq 20,000$	85,000	Goal is predicated on use of the AO corrected beam and a slit width of a few λ/D
Image quality	Diffraction-limited	—	
Slit length	$\geq 2''$	$5''$	Should allow simultaneous sky sampling when observing point sources
Velocity stability	< 0.2	< 0.1	Flexure in units of spectral resolution element in one hour of observation
Throughput	$\geq 10\%$	$\geq 25\%$	Exclusive of atmosphere, telescope, and slit losses

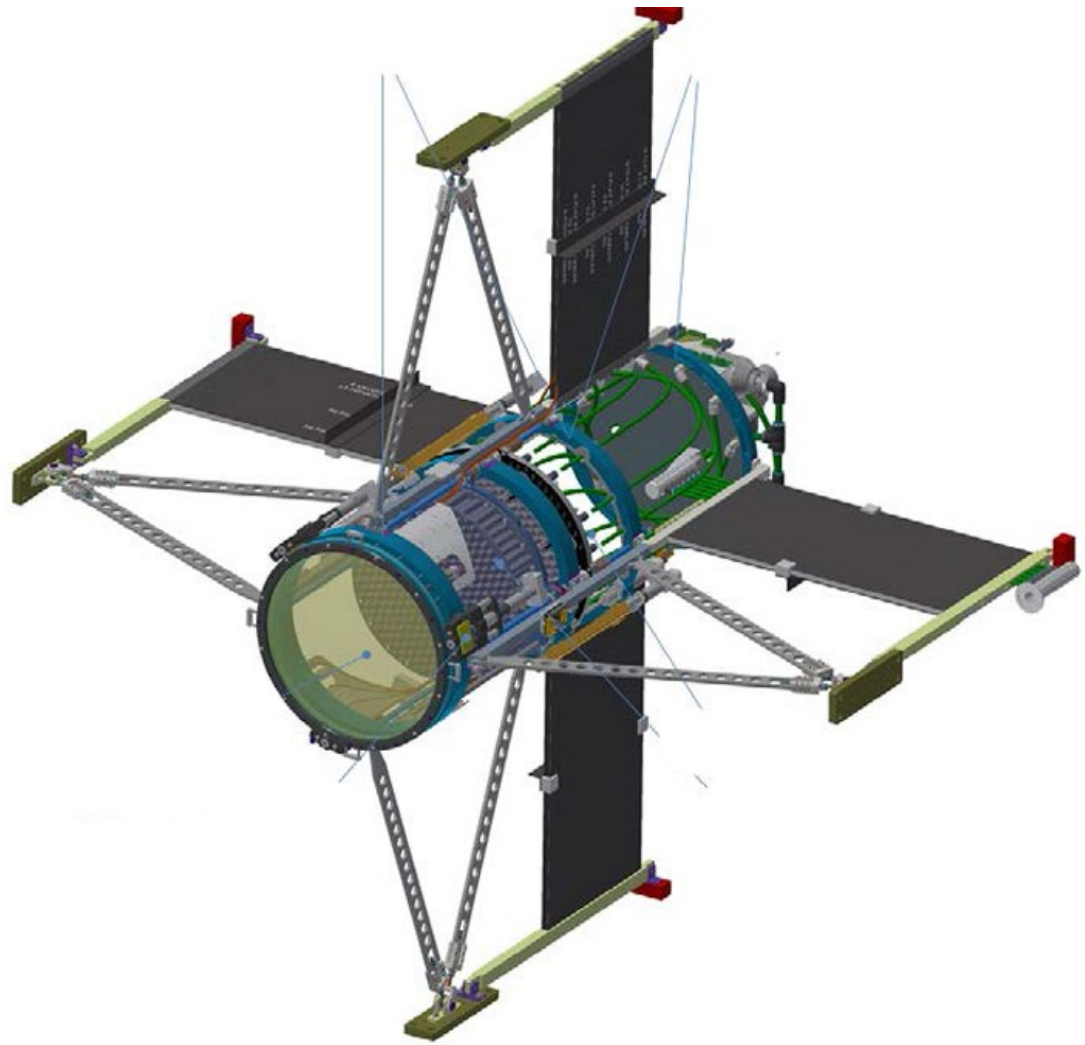


Commissioning Camera

ComCam is an alignment and image quality assessment tool that will also be a highly capable re-imaging camera for science. ComCam will have a pixel scale of 0.06 arcsec/pixel and better than 0.10 arcsecond image quality to evaluate GLAO performance across its $6' \times 6'$ field of view. With narrow- and broad-band imaging, and potentially an etalon for wide-field, slitless spectroscopy, the ComCam key scientific objectives will include:

- Stellar populations in dwarf and nearby galaxies
- Identification of planetary nebulae (Pne) at 100 Mpc and beyond, and distances measurements using the PN luminosity function
- Blind searches for high redshift Ly α sources

ComCam



MANIFEST The Many-Instrument Fiber System

MANIFEST is a facility robotic fiber positioning system that will make the GMT's full 20 arcminute field of view accessible to any visible or near-IR spectrograph. The fiber complement (single fiber, IFU bundle, or image slicer) can be defined separately for each instrument and is deployed by autonomous, mini-robots called "starbugs". The starbugs can be reconfigured over the full field of view in 2–3 minutes and positioned with a minimum center-to-center spacing of 10 arcseconds with an accuracy of 0.01 arcseconds. MANIFEST's scientific and technical requirements are summarized in *Table 1-10*.

G-CLEF and GMACS are designed for use with MANIFEST and could be operated simultaneously. With G-CLEF, MANIFEST will provide multiplexing for velocity and chemical abundance surveys (e.g., galactic clusters, nearby dwarf galaxies) that would not be practical for a single object spectrograph. With GMACS, image-slicer fiber bundles will double or triple the typical spectral resolving power of $R \sim 2,000$ to $R \sim 5,000$, thereby opening new areas of science to GMACS observers. MANIFEST will allow the GMT to be a uniquely efficient facility for observations addressing IGM tomography, galaxy assembly, chemical composition, and history of Local Group stars and galaxies.

Table 1-10 *Scientific and technical requirements for MANIFEST*

Science Application	λ range, μm	$\lambda/\Delta\lambda$	Mode	Notes
Star formation & chemical evolution in galaxies	400 – 1,000	~2,000	a, b	Abundances, stellar populations and ages, star formation rates
Massive galaxy assembly	500 – 1,000	~3,000	b	Stellar ages, stellar populations, velocity dispersions, rotation curves
Chemical tagging of Milky Way substructures	320 – 1,000	~50,000	c	Abundance and kinematic studies of tidal Streams
Dark matter distributions	400 – 800	~5,000	a	Dynamics of clusters, PNe, resolved stellar populations
Evolution of galaxy clustering	400 – 900	2,000	a	Large scale galaxy surveys
Tomography of the IGM	400 – 900	2,000, ~10,000	a, c	Large galaxy surveys, IGM tomography with faint background sources

In the “Mode” column, “a” indicates visible wavelength single fibers and IFU bundles enabling low resolution spectroscopy, “b” indicates near-IR single fibers enabling low resolution spectroscopy, and “c” indicates visible wavelength single fibers enabling high-resolution spectroscopy.

Near-IR Multi-Object Spectrograph

As studies of galaxy populations address ever higher redshifts, near-infrared multi-object spectroscopy has become increasingly important. The first suite of GMT instrument concepts included NIRMOS, a multi-object (~80), YJHK-band spectrograph and imager designed to operate both in natural seeing and with GLAO. With a 6.5 arcminute field of view, NIRMOS would be a powerful tool for characterizing galaxies near the epoch of reionization, time domain astrophysics of gamma ray bursts and other transients, revealing galaxy evolution from $z \sim 2-7$, and elucidating the nature of dark energy. In standard operation, NIRMOS would use multislit masks with 0.5 arcsecond slits, but could also be fed by MANIFEST to provide additional multiplex or resolution. After a very successful conceptual design review in 2011, further development of NIRMOS was deferred for funding reasons.

Efficient, Early Light, Single Object Near-IR Spectrograph

Because NIRMOS is not in the first generation of instruments, the SAC has considered alternative strategies for enabling high-throughput, medium resolution, near-IR spectroscopy at first light. Significant cost reductions are possible if the multi-object capability is dropped. One concept for a single object spectrograph derives from the Folded-Port IR Echellette (FIRE), a popular spectrograph at Magellan that obtains spectra from $\sim 1 \mu\text{m}$ to $2.5 \mu\text{m}$ in one exposure with spectral resolving power $\sim 6,000$. A similar instrument on GMT (a “super-FIRE”) would be designed to operate in natural seeing, before adaptive optics are enabled in standard operations, and would cover a similar wavelength range and resolution by using three spectrograph modules. Key concepts for this instrument include minimizing mechanical complexity to enable rapid development and maximizing throughput to facilitate highly efficient observations of faint targets near the redshift of reionization ($z \sim 7$).

A High Contrast Imager and Spectrograph

A concept for a high contrast, high spatial resolution infrared imager and spectrograph named “TIGER” was also reviewed at the conceptual level in 2011. The TIGER design enables high contrast imaging in two channels, $2.9-5.1 \mu\text{m}$ and $8-14 \mu\text{m}$, with the principal science goal of detecting faint planets at $2 \lambda/D$ separations from their parent stars at contrast levels as large as 10^6 . TIGER would also be ideal for spectroscopy and imaging to characterize planets and stellar disks. This design was not selected for early construction because of the rapid evolution in high-contrast techniques and the narrower range of science it would enable.

An Extreme-AO Imager for High Contrast at First Light

In the last several years, new strategies and technologies have emerged to enable very high contrast detections at inner working angles near λ/D using phase apodization coronagraphs and deformable mirrors with very high actuator density. Some of these technologies have already been demonstrated on the Magellan telescopes. Using deformable mirrors inside the instrument itself, this extreme AO imager could be deployed before the ASMs are commissioned. The SAC has endorsed development of an instrument based on these strategies that could be available soon after science operations begin if resources are available.

Future Instruments

The planned first-generation instrument suite for the GMT allows us to address the scientific questions that the partner review team gave highest priority as of 2012. These choices omitted instruments that would allow characterization of exoplanets and exploration of the highest redshift objects. In addition, new discoveries will reveal other instrument requirements.

Technology advances rapidly; we can expect to see detectors with improved performance and additional capabilities, especially in the near- and mid-infrared. There will likely be a need for specialized instruments that address very specific, but compelling questions not accommodated by the early instrument suite. The instrument plan must be augmented to respond to these challenges as resources become available. The GMT will also accept SAC-approved “PI instruments” that are intended to be used only by the instrument team. The SAC will be the nexus for initiating second generation instruments.

1.6 New Capabilities, New Discoveries

Astrophysics is an observationally driven science. The most important discoveries that will be made with the GMT over the next 50 years will come as a result of new observational capabilities, and they will likely not appear in any document written by contemporary astrophysicists. The need for greater observational capabilities has motivated the development of ever larger ground-based telescopes with greater sensitivity and hence greater reach. The development of adaptive optics, allowing us to achieve the diffraction limit of the largest telescopes, has dramatically increased the impact of large apertures. The GMT’s unprecedented spatial resolution and sensitivity will drive the next generation of discoveries.

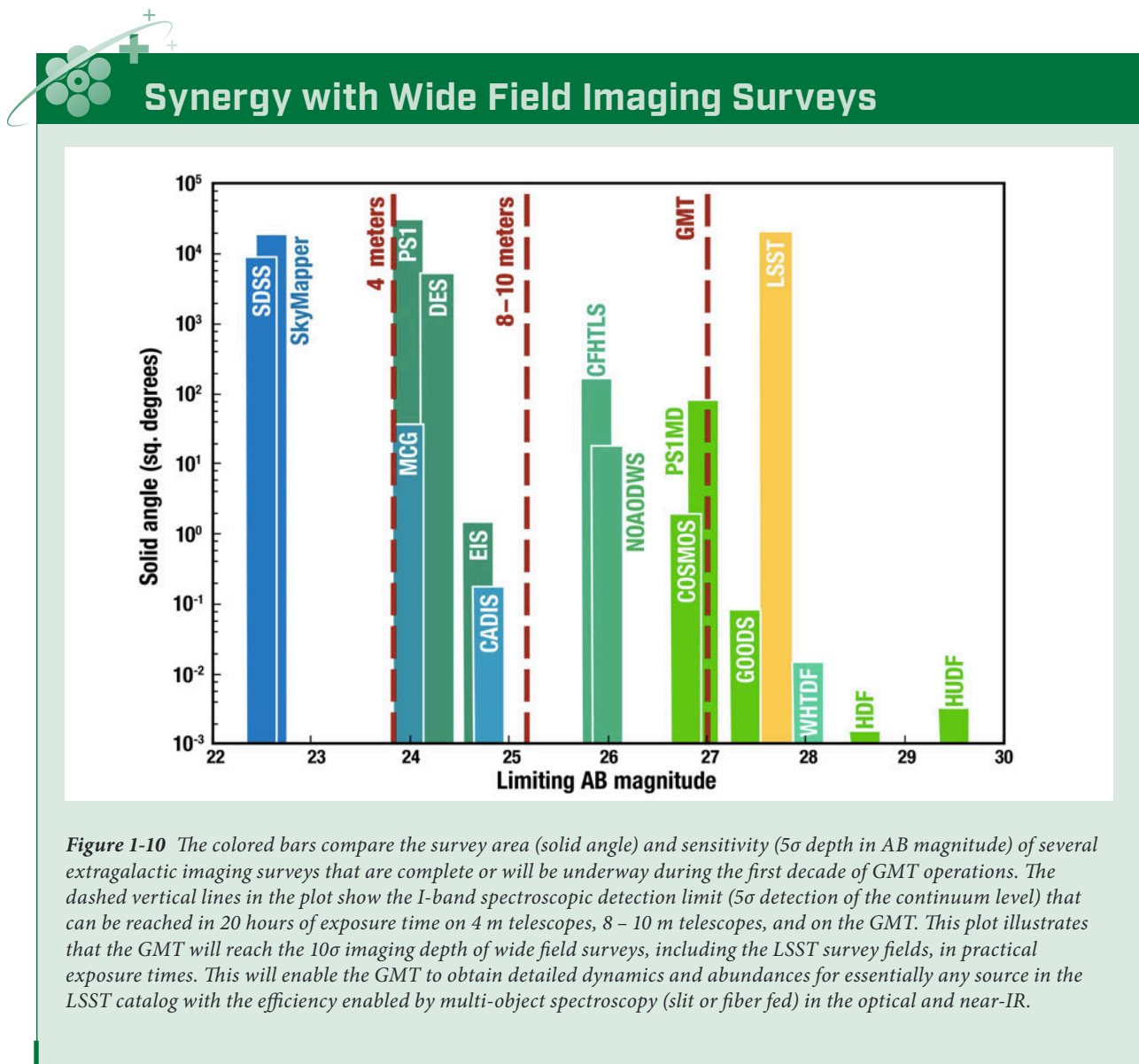
Sensitivity

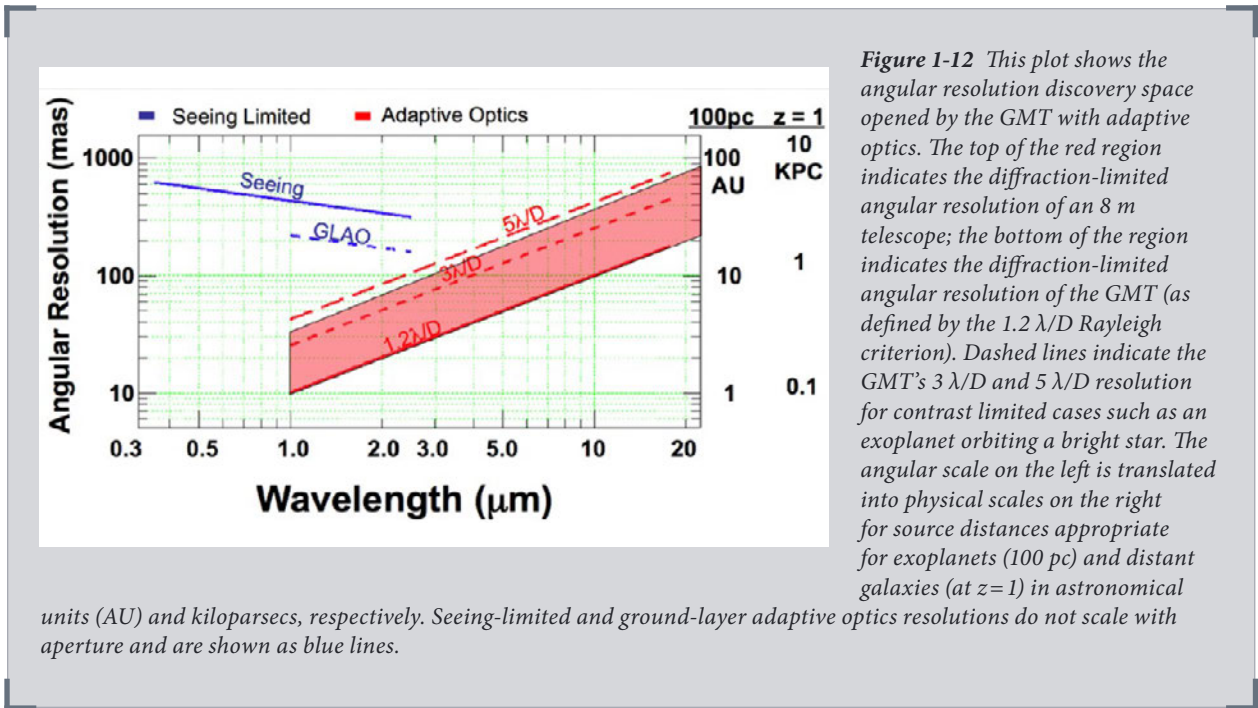
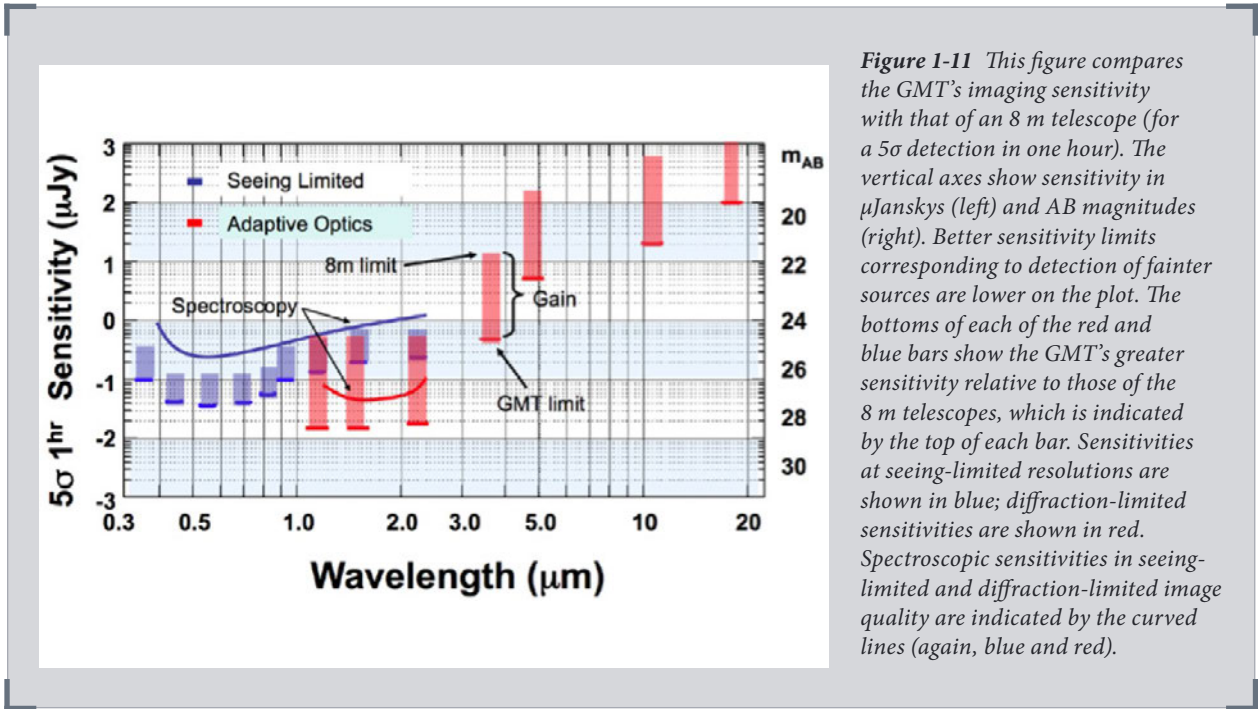
The gain from increasing aperture in seeing-limited observation is easily characterized. The number of photons collected per unit time increases with collecting area ($\propto D^2$) so that the signal to noise ratio (S/N) per unit time increases with diameter ($\propto D$) for background-limited and source count limited observations. The *time* needed to reach a given S/N then decreases as $1/D^2$. Most GMT science observations will be sky (i.e. background) limited, although high spectral resolution observations can also be detector-noise limited, a regime in which the gain is even greater.

Operating at the diffraction limit with adaptive optics concentrates the light from compact (unresolved) sources. The diffraction-limited source diameter decreases as $1/D$. The area from which background light is detected will decrease as $1/D^2$, improving the S/N by a factor of D . The *time* needed to reach a given S/N therefore goes down as $1/D^2$. The decrease in time to reach a fixed S/N with adaptive optics can be calculated by combining this factor of $1/D^2$ from the improved source concentration with the factor of $1/D^2$ from the collecting area, yielding an improvement in sensitivity that scales as D^4 . This D^4 factor is often cited as one of the primary drivers for the next generation of telescopes. Integral field spectroscopy of distant galaxies, for example, is one of the areas of greatest current interest. With significant flux in both compact and resolved structures, the gain in sensitivity when observing such sources will range between D^4 and D^2 .

There are regimes where next generation telescopes will deliver gains in sensitivity that are even greater than the powers of aperture diameter. These include crowded

fields and contrast-limited observations. Imaging of partially resolved stellar populations in crowded regions will benefit greatly from the increased image concentration for point sources and the reduced crowding and confusion noise associated with the unresolved component. Imaging of exoplanets near bright stars will also benefit from increased aperture through concentration of the faint exoplanet signal, reduced point spread function (PSF) wings from the parent star and improved stability of the PSF. Gains as significant as D^6 , or more, have been posited for these observations. *Figure 1-10* and *Figure 1-11* illustrate the discovery space opened by the GMT's gain in sensitivity.





Resolution

Adaptive optics also opens discovery space by improving spatial resolution (*Figure 1-12*). The diffraction-limited image size scales as $1/D$, so that the GMT has three times better angular resolution than an 8 m telescope. The GMT will increase the volume of space over which one can image the sphere of influence of massive black holes by nearly an order of magnitude. A factor of three reduction in the inner working angle for diffraction-limited imaging is very significant for exoplanet imaging in reflected light, where very few planets are within reach with current telescopes. The GMT's improved angular resolution will allow us to resolve stellar nurseries in the southern Milky Way and to probe terrestrial zones in nearby stars as well as protoplanetary and debris disks.

1.7 Additional Reading

Technical Background Regarding the GMT Observatory:

Bernstein, R. A. et al., "Overview and status of the Giant Magellan Telescope project," Proc. SPIE 9145, Ground-based and Airborne Telescopes V, 91451C (22 July 2014).

Bouchez, A. H. et al., "The Giant Magellan Telescope adaptive optics program," Proc. SPIE 9148, Adaptive Optics Systems IV, 91480W (21 July 2014).

Johns, M., et al., "Design of the Giant Magellan Telescope," Proc. SPIE, 9145-50, (2014).

Martin, H. M. et al., "Production of primary mirror segments for the Giant Magellan Telescope," Proc. SPIE 9151, Advances in Optical and Mechanical Technologies for Telescopes and Instrumentation, 91510J (7 August 2014).

Shectman, S.; Johns, M., "GMT overview," Proc. SPIE 7733, Ground-based and Airborne Telescopes III, 77331Y (6 August 2010).

Thomas-Osip, J. E. et al., "Giant Magellan Telescope site evaluation and characterization at Las Campanas Observatory," Proc. SPIE 7012, Ground-based and Airborne Telescopes II, 70121U (10 July 2008).

Thomas-Osip, J. E. et al., "Giant Magellan Telescope site testing: PWV statistics and calibration," Proc. SPIE 7733, Ground-based and Airborne Telescopes III, 77334N (7 August 2010).

The GMT Instrument Program & Background:

Jacoby, G. H.; Bouchez, A., Colless, M., DePoy, D., Fabricant, D., Hinz, P., Jaffe, D., Johns, M., McCarthy, P., McGregor, P., Shectman, S., Szentgyorgyi, A., "The instrument development and selection process for the Giant Magellan Telescope," Proc. SPIE 8446E-1GJ, 1 (2012).

Jacoby, G. H., et al., "Status of the instrumentation program for the Giant Magellan Telescope," Proc. SPIE 9147, Ground-based and Airborne Instrumentation for Astronomy V, 91471Y (28 July 2014).

Jacoby, G. et al., "Instrumentation progress at the Giant Magellan Telescope project," Part of SPIE Astronomical Telescopes + Instrumentation, 2016.

Morzinski, K. M. et al., “MagAO: Status and on-sky performance of the Magellan adaptive optics system,” Proc. SPIE 9148, Adaptive Optics Systems IV, 914804 (21 July 2014).

Simcoe, R. A., et al., “FIRE: A Facility Class Near-Infrared Echelle Spectrometer for the Magellan Telescopes,” PASP 125 , 270-286 (2013).

Simcoe, R., et al., “A Concept for Seeing-Limited Near-IR Spectroscopy on the Giant Magellan Telescope,” Proc SPIE 9908, 9908-382 (2016).

G-CLEF:

Furesz, G., et al., “The G-CLEF spectrograph optical design: an update to the white pupil echelle configuration”, Proc. SPIE 9147-343, (2014).

Rodler, F. and Lopez-Morales, M., “Feasibility studies for the detection of O₂ in an Earth-like exoplanet”, ApJ, 781, 12, (2014).

Szentgyorgyi, A. et al., “A preliminary design for the GMT-Consortium Large Earth Finder (G-CLEF),” Proc. SPIE 9147, Ground-based and Airborne Instrumentation for Astronomy V, 914726 (28 July 2014).

Szentgyorgyi, A, et al., “The GMT-Consortium Large Earth Finder (G-CLEF): an optical Echelle spectrograph for the Giant Magellan Telescope (GMT),” Part of SPIE Astronomical Telescopes + Instrumentation, 2016.

GMACS:

DePoy, D. L., Marshall, J. L., Prochaska, T., Behm, T. W., Smee, S. A., Barkhouser, R. H., Hammond, R. P., Shectman, S. A., Papovich, C., “The GMACS spectrograph for the Giant Magellan Telescope,” Proc. SPIE 8446-292, (2012).

DePoy, D. L. et al., “An update on the wide field, multi-object, moderate-resolution, spectrograph for the Giant Magellan Telescope,” Proc. SPIE 9147, Ground-based and Airborne Instrumentation for Astronomy V (28 July 2014).

GMTIFS:

Davies, J., et al., “GMTIFS: the adaptive optics beam steering mirror for the GMT integral-field spectrograph”, Proc. SPIE, 2016, Volume 9912, id. 991217

Hart, J. et al., “GMTIFS: challenging optical design problems and their solutions for the GMT integral-field spectrograph”, Proc. SPIE, 2016, 9908, 99089F

Hart, J., et al., “GMTIFS: cryogenic rotary mechanisms for the GMT Integral-Field Spectrograph”, Proc. SPIE, 2016, 9912, 991264

McGregor, P. J., Bloxham, G. J., Boz, R., Davies, J., Doolan, M. C., Ellis, M., Hart, J., Nielsen, J. J., Parcell, S., Sharp, R. G. and Stevanovic, D., “The GMT integral-field spectrograph (GMTIFS) conceptual design,” Proc. SPIE 8446 (2012).

Sharp, R., et al., “GMTIFS: The Giant Magellan Telescope integral fields spectrograph and imager”, Proc. SPIE, 2016, 9908, 99081Y

GMTNIRS:

Jaffe, D. T., Barnes, S. I., Brooks, C. B., Gully-Santiago, M., Pak, S., Park, C., Yuk, I.-S. “GMTNIRS (Giant Magellan telescope near-infrared spectrograph): optimizing the design for maximum science productivity and minimum risk”, Proc. SPIE, 9147-74, (2014).

Jaffe, D. T. et al., “Science instrument development for the Giant Magellan Telescope,” Author(s): Proc. SPIE 7735, Ground-based and Airborne Instrumentation for Astronomy III, 773525 (15 July 2010).

Park, C. P., et al., “Design and early performance of IGRINS (immersion grating infrared spectrometer”, Proc. SPIE, 9147-48, (2014).

MANIFEST:

Lawrence, J., et al., “The MANIFEST fibre positioning system for the Giant Magellan telescope”, Proc. SPIE, 9147-341, (2014).

The 2012 GMT Science Book:

McCarthy, P., (ed.), “Giant Magellan Telescope Scientific Promise and Opportunities,” http://www.gmto.org/Resources/GMT-SCI-REF-00482_2_GMT_Science_Book.pdf, 2012.

References

Tuan Do et al., 2014, AJ, 147, 93.



Artist's conception of daybreak on an extrasolar planet. Credit: D. Jemison, GMTO

Exoplanets & Planet Formation

Are we alone in the universe? Astronomers have discovered thousands of planets orbiting other stars. Their sheer number and amazing diversity—from lava-worlds to super-Jupiters—give us a new perspective on our place in the universe. We now know that Earth is just one rocky planet amongst billions in the galaxy, and that planets range at least from $1/10^{\text{th}}$ to 10,000 times the mass of Earth. Rocky planets that orbit their stars at just the right distance could be temperate enough to allow for the presence of seas of liquid water. Our nearest neighboring star, Proxima Centauri, likely hosts one such planet, but detecting biosignatures on exoplanets is extremely challenging because they are so much fainter than their host stars.

The GMT's sensitivity, resolution, and spectroscopic capabilities will enable us to understand the origins of the wide range of planetary systems we see in the galaxy around us. We will be able to measure the physical properties of those planets to learn if they contain life and to compare our solar system to its neighbors.

Chapter Authors

Alycia Weinberger (Carnegie Institution for Science, Department of Terrestrial Magnetism)

Jayne Birkby (University of Amsterdam)

Brendan Bowler (The University of Texas at Austin)

Mercedes López-Morales (Harvard-Smithsonian Center for Astrophysics)

Jared Males (University of Arizona)

Katie Morzinski (University of Arizona)

Sharon Wang (Carnegie Institution for Science, Department of Terrestrial Magnetism)



2 Exoplanets and Planet Formation

Perhaps the most profound and enduring question over all of human history is whether life exists elsewhere in the universe. It is only in the past two decades that we have learned for certain that there are planets orbiting other stars—thousands of them. Earth is likely one rocky planet amongst billions; every star in the galaxy could have a rocky planet (Sumi et al. 2011). Present thinking is that our best chance of finding life is on rocky planets like Earth with liquid water on their surface. Such habitable planets must orbit their stars at the correct distance to maintain a surface temperature near 300 K; remarkably, our nearest stellar neighbor, Proxima Cen, hosts one such planet (Anglada-Escudé et al. 2016).

The GMT will make revolutionary exoplanet discoveries. Radial velocity measurements, transit and direct imaging observations, and microlensing surveys have all contributed to finding these thousands of known exoplanets. These techniques will continue to be productive in the next decade, but a larger telescope is crucial to assembling a representative sample of planetary systems and measuring the surface conditions on the most intriguing planets, like those that most resemble the Earth. New space missions such as NASA's Transiting Exoplanet Survey Satellite (TESS; Ricker et al. 2016), should discover dozens of Earth-sized worlds in the habitable zones of neighboring stars, a rich sample we can probe with the GMT's unique instruments for high resolution spectroscopy and imaging in visible and infrared wavelengths.

The sheer number and diversity of the known exoplanets helps us to appreciate our place in the universe. We have discovered planets with masses as small as Mars and as large as 10,000 Earth masses, and with orbits almost as small as their parent stars to even larger than our solar system. In addition to individual planets, we have also discovered a remarkable variety of exoplanetary systems that are quite different from our own. In some, multiple rocky planets orbit their stars in a space smaller than the terrestrial planet zone of our solar system.

The challenge is to understand how this remarkable panoply of systems formed and whether planets frequently form with the inventories of elements necessary for life. Observations with the GMT will allow us to determine the densities and atmospheric compositions of these planets and to discover whether any are truly Earth-like. Earth-sized planets with Earth-like temperatures are common but we have yet to learn if they have Earth or Venus-like atmospheres or no atmospheres at all. Their atmospheres may contain water and even oxygen, key signatures for life on present-day Earth. If past exoplanet studies are any guide, we should expect to be surprised by the variety of atmospheres we discover.

Mature planets are key targets, but protoplanetary systems—where planets are born—are also critical targets if we are to understand the great variety of the worlds we see. Disks of gas and dust with sufficient mass to form a planetary system like our own surround more than 80% of young, Sun-like stars. The GMT is essential to studying these young stars because they are found farther away than mature systems. We will learn about planet formation by studying circumstellar disks that are still forming planets, a process that appears to last for a few million years, and by attempting to connect the origins of these protoplanets to the properties of mature planets orbiting older stars.

The frequency of planets and multi-planet systems derived from current surveys, particularly NASA's Kepler mission, provides insight into planet formation mechanisms. The migration of solid material during planet formation will

determine the final masses, locations, and compositions of planets, but the physics of planetesimal growth and migration is poorly understood. The origins of the planets, asteroids and comets in our own solar system are also uncertain. Neptune must have migrated into the Kuiper Belt to generate the population seen there today (Hahn & Malhotra 2005), but perhaps Jupiter and Saturn also migrated substantially from their birth locations (Gomes et al. 2005). Using the GMT to study the chemical makeup of small bodies in the solar system—the Kuiper Belt and beyond—will answer many questions about the birth of our world and its siblings.

The planet formation process must be capable of producing the wide variety of known planets; this variety will only increase with new discoveries. We estimate that 50% of Sun-like stars host a planet with a radius less than four times that of the Earth and an orbital period less than 100 days (Fressin et al. 2013; Petigura et al. 2013; Foreman-Mackey et al. 2014). Although the most common type of planet discovered so far is a mini-Neptune with a short orbital period, we do not know if such planets are common in the habitable zone and beyond. Giant planets are apparently rare, but they may provide important clues about the formation of planetary systems. Planets larger than Earth may form from condensed ices far from the star. The traditionally hypothesized mechanism of planet growth by accretion cannot form the massive planets found at large distances from solar-type and low-mass stars. Instead, self-gravitating cores may collapse to become giant planets (Boss 1997).

In the following discussion, we will explain how the GMT will contribute to our search for other worlds and other life, and how they came to be. **Section 2.1** will focus on the characterization of extrasolar planets, including measurements of mass, density, and atmospheric composition. **Section 2.2** will focus on the formation of planets and how observations of the gas and dust disks that surround young stars will answer the fundamental questions of planet formation and planet diversity.

2.1 Toward Earth: Planet Characterization

The GMT will study the demographics of mass and composition for small planets, especially Earth-sized and smaller, the occurrence rates of small planets with orbital periods longer than 100 days and, in particular, the frequency of Earth-analogs and super-Earths inside the habitable zones of stars (see **Figure 2-1**).

We know little about the nature of planets receiving stellar energy similar to what the Earth receives, i.e. at a temperature where liquid water could persist on rocky surfaces—also commonly referred to as sitting in the “habitable zone.” We have measured the densities for only three such planets. We know nothing about whether such planets typically host atmospheres like Earth or Venus, or any atmospheres at all.

The observations required to characterize such temperate planets will take a variety of forms, all described in this section. To measure the densities of transiting planets, which distinguish between water or vapor balls, iron cores, and truly rocky planets, we will need the GMT to measure masses via the radial velocity method. To go beyond density to measure light reflected off the planets’ surfaces, we will need the GMT’s combination of sensitivity and spatial resolution. Ultimately, we want to understand the composition of planetary atmospheres, and even search for gases that would suggest whether a planet is habitable. The GMT could detect molecular oxygen, whose discovery could suggest that a planet is not only habitable, but *inhabited*.

Measuring Masses of Earth-like Planets

The G-CLEF high resolution spectrograph on the GMT will make crucial and decisive measurements of the nature of Earth-sized planets. New space missions, such as NASA’s TESS (Ricker et al. 2016), and ESA’s PLATO¹, to be launched around 2024, are expected to discover dozens of Earth-sized planets in the habitable zones of nearby stars. These space missions can measure the radii of the planets they discover. However, to learn which of these planets are rocky, for example, we must measure densities, which means combining the sizes with measurements of the planets’ masses. Such density measurements provide potent insight to the structure and bulk composition of a planet, as well as information about the detectability of its atmosphere. The mass of a planet can be measured via the Doppler radial velocity (RV) technique, but with current instrumentation on the largest existing telescopes, we are sensitive only to stellar “wobbles” larger than about 1 m/s, while an Earth-like planet in the habitable zone of a star like the Sun produces a stellar wobble ten times smaller (i.e. 10 cm/s). This limitation may be mainly due to intrinsic stellar motion, or jitter, such as that produced by stellar convective motions. The GMT provides two key advantages for studying the masses of small planets, primarily

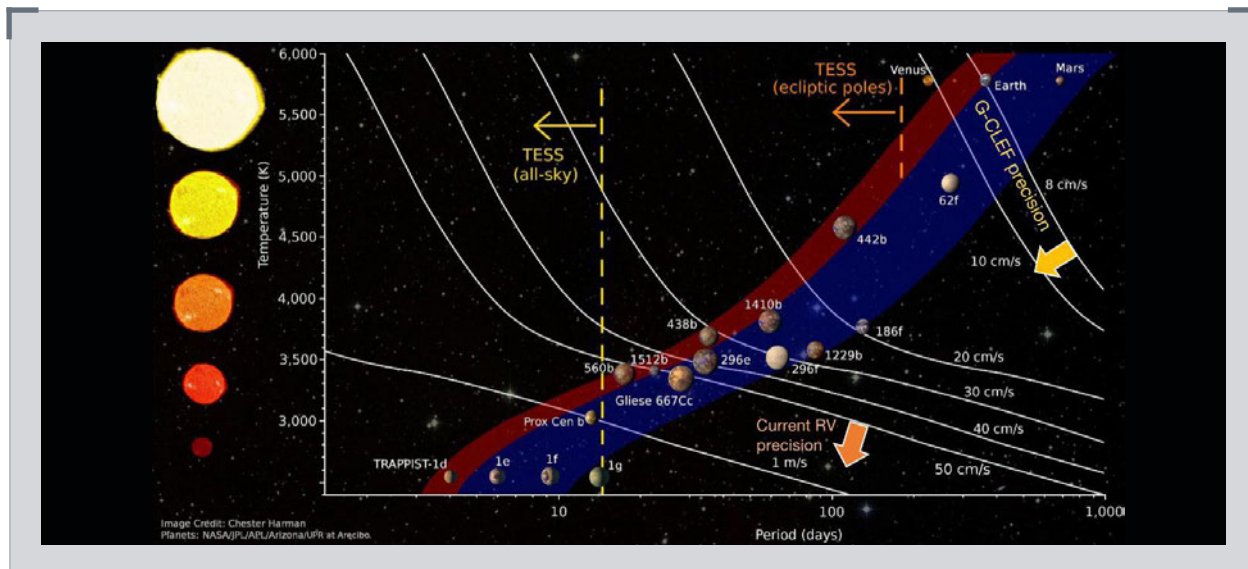


Figure 2-1 The GMT will determine the masses and characterize the atmospheres of temperate rocky planets in the habitable zone. This illustration from Chester Harman shows most of the currently known exoplanets that are smaller than 1.6 times the size of Earth (as of March 2017), around moderately bright stars, and in the “habitable zone”, along with the GMT’s radial velocity capability. It explains how precision (10 cm/s) measurements of radial velocity with the G-CLEF instrument will revolutionize the study of Earth-like worlds, through the determination of mass and density. The numbered/named planets, discovered via transit observations, orbit within the habitable zones of their stars—mapped by blue and red bands—for stars of increasing temperature (left axis; data from Kopparapu et al. 2014). White lines mark the boundaries below which planet mass can be determined from the planet’s size and the reflex velocity of the host star, due to the planet’s gravitational pull. With current telescopes and instruments, mass determinations are limited to planets in the area below the line attached to the orange arrow—planets that orbit small, cool stars. G-CLEF will determine the masses of all known Earth-like worlds in the area below the line with the yellow arrow, including, and especially, those orbiting stars like our Sun (the yellow star). Measurements of planet mass can be converted into planet density, a powerful diagnostic for each different planet that we discover—from heavy, hard rock to airy ice worlds.

¹ <http://sci.esa.int/jump.cfm?oid=59252>

through its huge collecting area that shortens the exposure time necessary to measure an RV. This means that RV time series with very high cadence will be possible, i.e. individual exposures $\lesssim 1$ min for stars brighter than $V=7$ mag. Such frequent sampling is crucial for modeling out the RV noise induced by stellar jitter (see **Figure 2-3** and Butler et al. 2004, Lopez-Morales et al. 2016, and Barnes et al. 2017). Second, short exposure times will enable efficient surveys for unknown planets and follow-up of programs that detect planet transits in front of parent stars. Typical TESS M dwarfs have V band magnitudes around 11. A one hour exposure of each star using a 10 m class telescope is limited by photon noise and achieves only about 1 m/s single measurement precision. In comparison, the GMT needs only 10 minutes to reach this precision, which is enough to detect habitable zone planets around M5-type stars and cooler.



Precision Stellar Spectroscopy

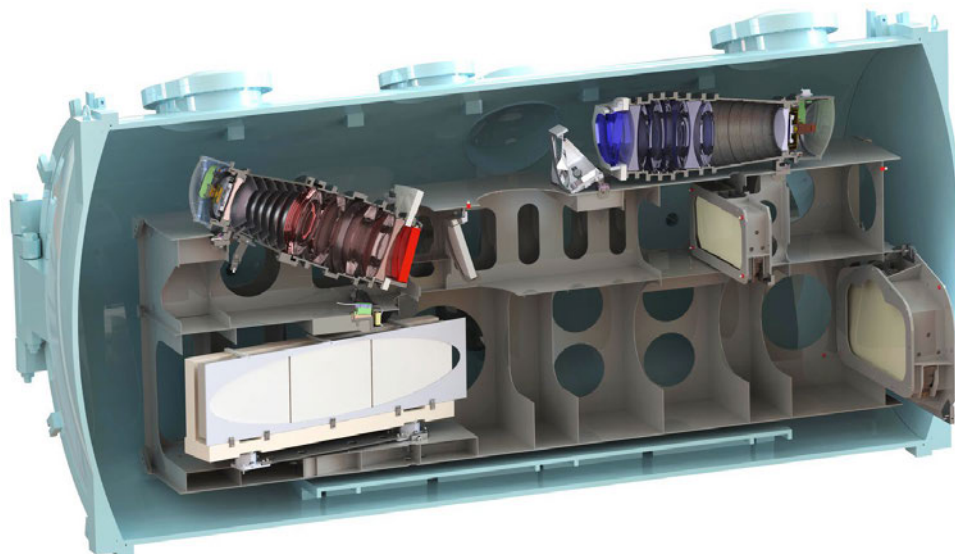


Figure 2-2 One of the first generation science instruments for the GMT is G-CLEF, the GMT–Consortium Large Earth Finder (Fzrész et al. 2014, Ben-Ami et al. 2016), which is designed to achieve the superb stability necessary to measure precise radial velocities of stars with planetary systems. To make this possible, G-CLEF will be mounted at a gravity-invariant instrument port, has a precisely controlled temperature and pressure enclosure, and has an optical fiber feed that provides the high degree of mode scrambling essential to filter out temporal variations in the light reaching the instrument (i.e., seeing stability). In keeping with its role as a first light instrument, G-CLEF will also enable a wide range of high-resolution spectroscopy science. The optical fiber feed allows G-CLEF to support a range of spectral resolutions ($R \sim 19,000, 35,000, 108,000$), input aperture sizes, and observing modes optimized for high sensitivity for faint source observations. Coupled with the MANIFEST facility, G-CLEF will enable efficient multi-object spectroscopy at the same high spectral resolutions. Credit: G-CLEF Team.

The PLATO mission is scheduled to launch around 2024 with a primary science goal of measuring the occurrence rate of Earth-like planets in the habitable zones of Sun-like stars. The GMT will play an essential role in studying these planets by measuring their fundamental properties such as mass and eccentricity, and searching their systems for additional non-transiting or long-period planets to identify solar system twins.

The GMT could observe all of the PLATO discoveries of small planets in the habitable zones of stars with $V < 11$ mag. We estimate that PLATO will detect 6–11 Earth-sized planets in habitable zones, including 1–2 around M dwarfs, 1–3 around K dwarfs, and 6–11 around G and late F dwarfs. From Las Campanas, we assume that there will be six systems on which the GMT can follow up, one with $V \sim 9$ mag and five with $V \sim 10.5$ mag. Many other candidates for Earth-like worlds will follow in the years after PLATO.

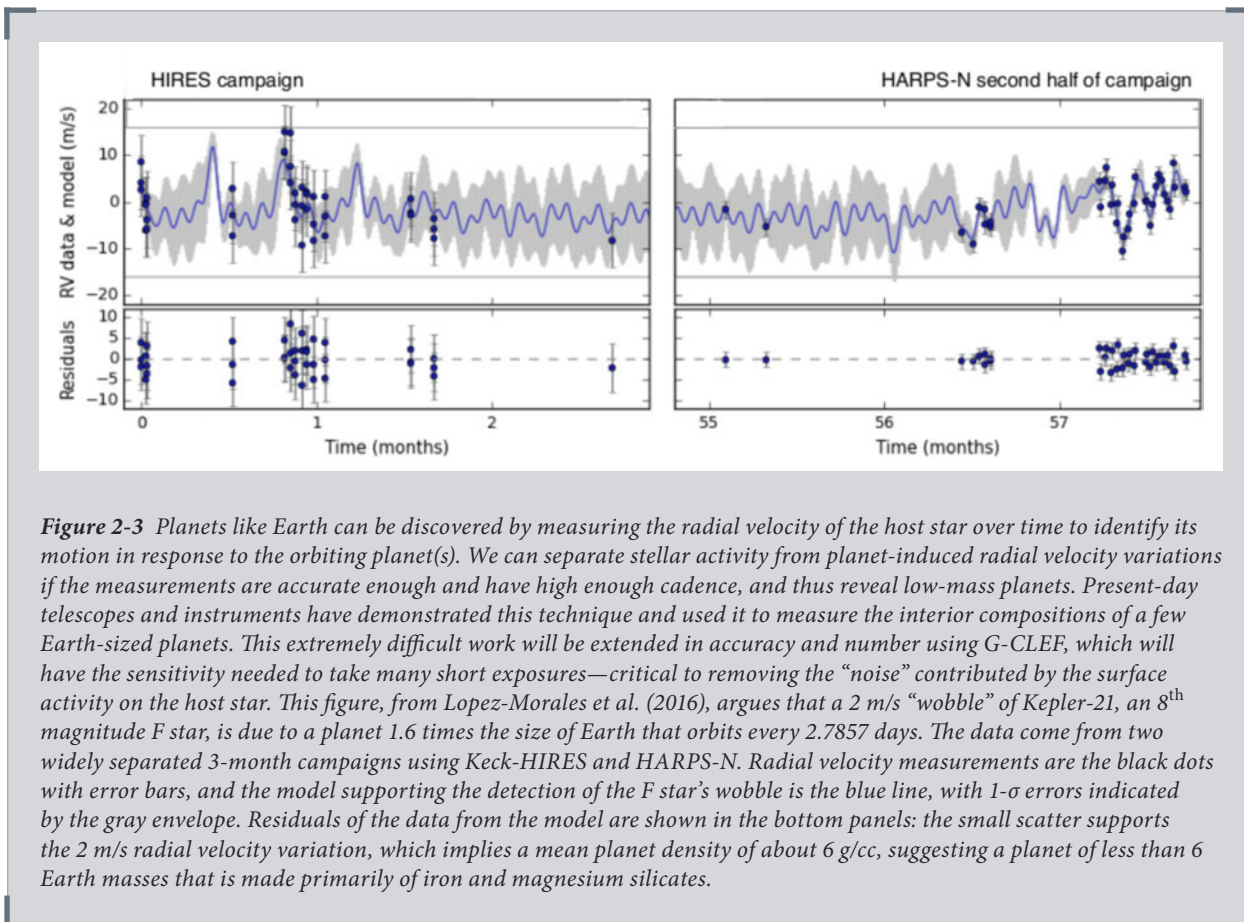
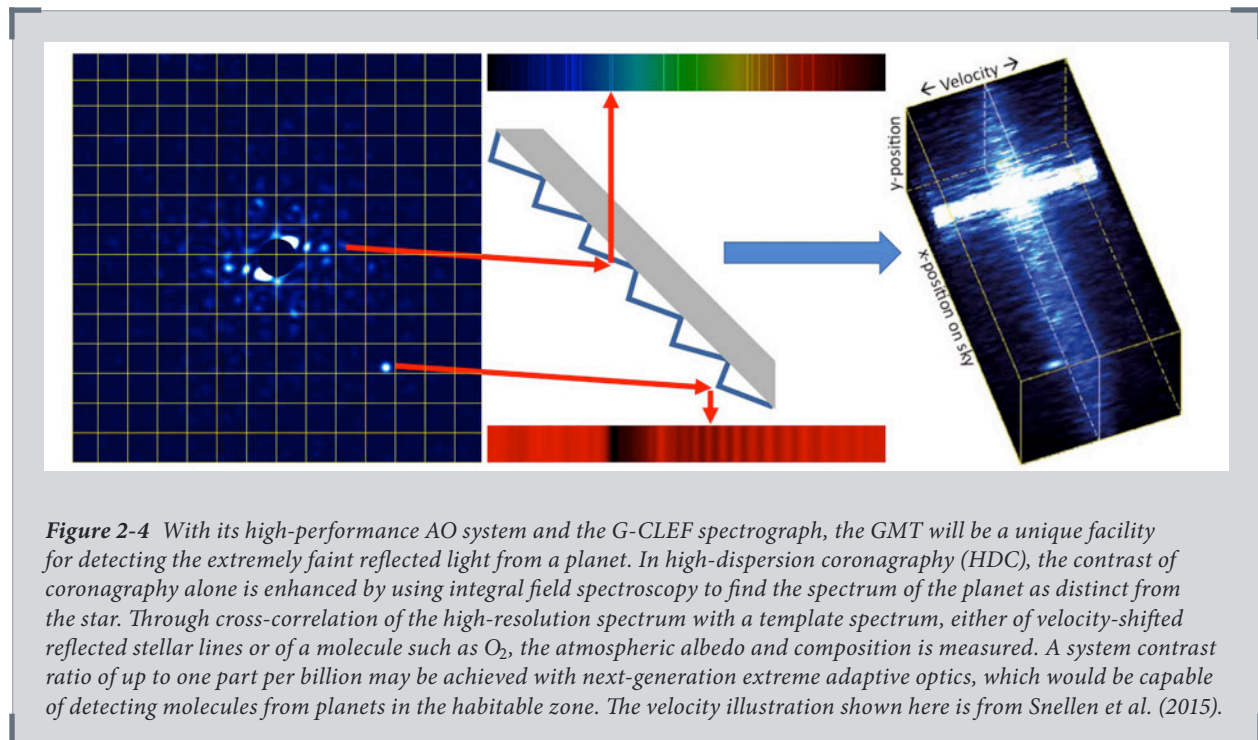


Figure 2-3 Planets like Earth can be discovered by measuring the radial velocity of the host star over time to identify its motion in response to the orbiting planet(s). We can separate stellar activity from planet-induced radial velocity variations if the measurements are accurate enough and have high enough cadence, and thus reveal low-mass planets. Present-day telescopes and instruments have demonstrated this technique and used it to measure the interior compositions of a few Earth-sized planets. This extremely difficult work will be extended in accuracy and number using G-CLEF, which will have the sensitivity needed to take many short exposures—critical to removing the “noise” contributed by the surface activity on the host star. This figure, from Lopez-Morales et al. (2016), argues that a 2 m/s “wobble” of Kepler-21, an 8th magnitude F star, is due to a planet 1.6 times the size of Earth that orbits every 2.7857 days. The data come from two widely separated 3-month campaigns using Keck-HIRES and HARPS-N. Radial velocity measurements are the black dots with error bars, and the model supporting the detection of the F star’s wobble is the blue line, with 1- σ errors indicated by the gray envelope. Residuals of the data from the model are shown in the bottom panels: the small scatter supports the 2 m/s radial velocity variation, which implies a mean planet density of about 6 g/cc, suggesting a planet of less than 6 Earth masses that is made primarily of iron and magnesium silicates.

The required observations are far beyond the capabilities of existing telescopes and instruments. For a $V \sim 9$ magnitude star, G-CLEF will reach a photon-limited single measurement RV precision of 10 cm/s in about 20 minutes (40 minutes for $V \sim 10.5$ mag, scaled using results in Plavchan et al. 2015), assuming an instrument noise floor of ~ 10 cm/s. Adopting the conventional detection criterion of $K/\sigma \times \sqrt{N} > 6$, where K is the planet’s semi-amplitude and σ is the single measurement RV precision, it will take a total of 252 hours of exposure time over their 3–5 year orbital periods to characterize all six systems down to cm/s. Progress is being made on removing stellar jitter, but 3–5 times more observations may be needed to model or average out the stellar RV signals (see the 2011 G-CLEF science book, for example).

In addition to transit mission follow-up, the GMT could conduct a survey of the

nearest, quietest stars without known large inner planets to search for non-transiting Earth-sized planets in habitable zones. These would be ideal targets for direct imaging (see the next section). Within 25 pc, and limiting $V < 7$ (for direct imaging purposes), there are 6 M dwarfs, 14 K dwarfs, and 67 G dwarfs. The chance of any of them hosting a transiting habitable zone planet is miniscule (the transit probability of a true Earth analog is 0.5 %). Once precursor studies have limited the sample to the stars exhibiting the least intrinsic RV jitter, and 8–10 m telescopes have spent ten years on a subset of the stars, there will likely be a sample of 10–20 best-case stars for the GMT, which could then be observed in a program of 25–50 nights/year for four years.



Direct detection of light from temperate extrasolar planets

The GMT will answer fundamental questions about the compositions of planets, particularly those with temperatures similar to Earth. Our solar system's architecture does not resemble that of many known exoplanetary systems; we do not have super-Earths or mini-Neptunes in our inner system. In our efforts to understand planet diversity, it is crucial to explore why and how these planets form around some stars, but not others, and whether they form with compositions like or unlike those of Earth. We also want to know whether some planets have thick atmospheres including hydrogen that were accreted during planet formation, and whether in other cases, stellar radiation might have resulted in remnant heavy atmospheres or even bare rocks. These questions are critically important for understanding exoplanets around low mass stars because these stars have long-lived, extreme magnetic activity, including flares, that may erode their planets' atmospheres. The conditions for habitability may be quite different in such systems.

A large sample of known exoplanets will be available for the GMT to study. Nearby

stars, which are most often gigayears old and of types G, K and early M, will host those planets that can be spatially resolved. The long time baselines of radial velocity searches are uncovering a rich sample of these long-period objects—more than 80 such planets with angular separations greater than 62 mas are currently known. The GMT’s resolution will enable direct imaging of a significant subset of these objects, and a much larger sample is likely to be known by the time the GMT begins operations.

Reflected Light (Albedo)

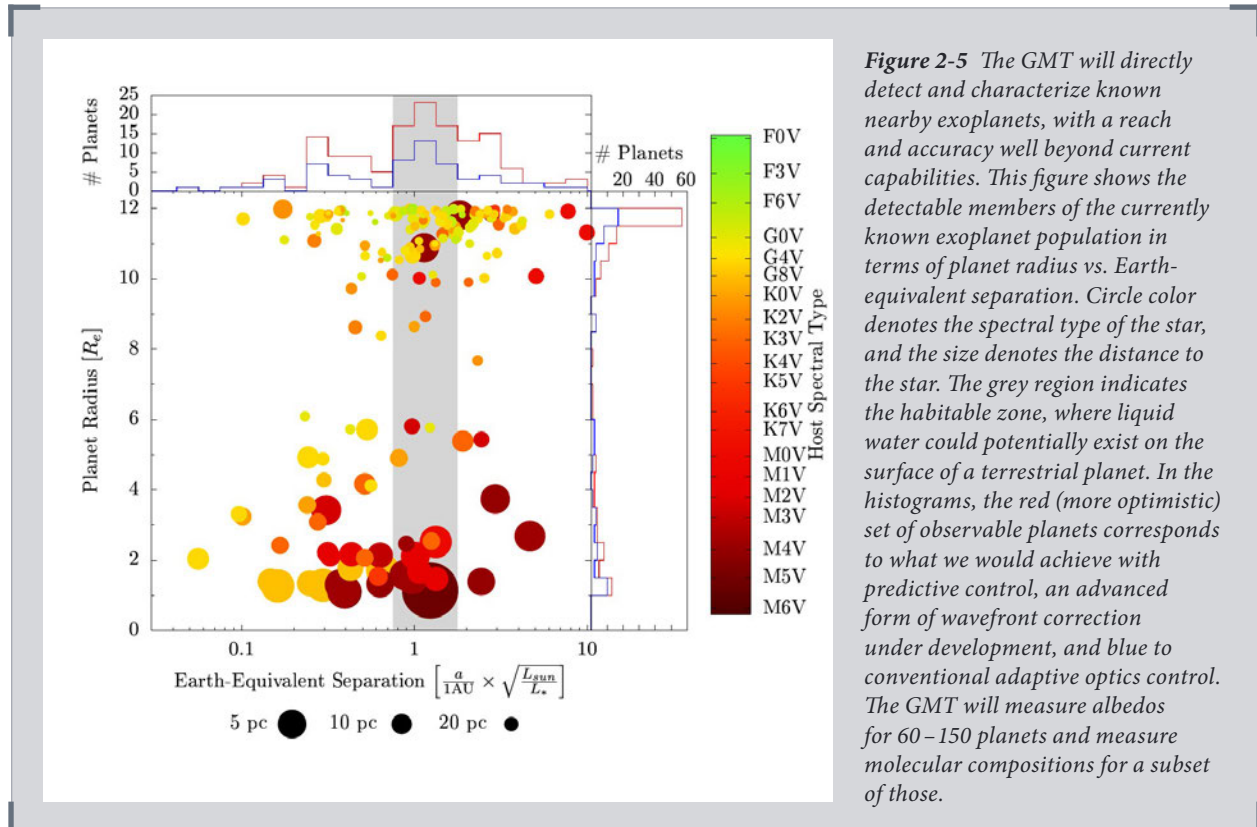
To detect starlight reflected from the surfaces or atmospheres of temperate exoplanets will require the diffraction-limited resolution of the GMT, along with a specialized instrument that can separate the light of planets that are one million to 100 million times fainter than their stars at separations of 6–60 mas. A realistic way to achieve these contrast-separation goals with a ground-based telescope is with high dispersion coronagraphy (HDC), i.e., combining a coronagraph behind an extreme adaptive optics system, which corrects for the Earth’s atmospheric turbulence, with high resolution ($R \sim 50,000 - 100,000$) spectroscopy (Snellen 2015; see *Figure 2-4*). In this method, the contrast demands on each part of the system are kept achievable, but the combined contrast is sufficient to detect a substantial number of planets.

We consider what would be required to detect the currently known exoplanets in the solar neighborhood, most of which were discovered using the radial velocity method. Their radii are not yet known and must be estimated based on planets with Kepler measurements of radii and RV masses, or Kepler “transit timing” masses. When the GMT begins operation, TESS will have measured radii for many more nearby planets, mainly around M-type stars.

In reflected light, the signal to noise (S/N) of a planet is proportional to the planet/star contrast, which is in turn a function of the planet radius and its separation from its star. High contrast is more difficult to achieve at small planet-star separations where planets reflect more light. We assume that the GMT’s extreme adaptive optics (AO) coronagraph will be modestly improved relative to current generation instruments such as SPHERE on the VLT. The residual stellar halo can be described by a Strehl ratio, or contrast curve, that depends on separation. The S/N with which we can observe a planet is proportional to the number of spectral lines that can be used and the S/N in the stellar continuum per resolution element. This is true whether we use a large bandwidth and many lines to measure the average planetary albedo as a function of phase angle, or whether we choose to use specific molecular lines to measure the atmospheric composition. M-star spectra are particularly rich in stellar lines, making much of the entire red part of the spectrum useful for measuring a broadband albedo.

We evaluated all of the known exoplanets, taking into account AO system performance on the host stars. With current levels of wavefront control/coronagraphy, and a survey time of 28 nights, the GMT will detect ~ 60 planets. With reasonable improvements in control of atmospheric turbulence, we could expect to increase this to ~ 150 planets. Fifteen of these should be $< 1.6 R_{\oplus}$ in size and thus are expected to be rocky rather than gas-rich. The full population of available planets includes ice and gas giants of a range of densities, including about 20 planets that are in the habitable zone, have radii between 1.6 and $4 R_{\oplus}$, and therefore have no analog in the solar system (see *Figure 2-5*).

Moving beyond mere detection and coarse albedo measurement, the HDC technique will allow us to search for and measure the abundances of molecules such as oxygen and water in the atmospheres of these planets. In particular, we will search for H₂O and O₂ on the known *potentially habitable terrestrial planets*: YZ Cet d, HD 85512 b, GJ 3323 b, Wolf 1061 c, GJ 273 b, Proxima b, and GJ 667C f.



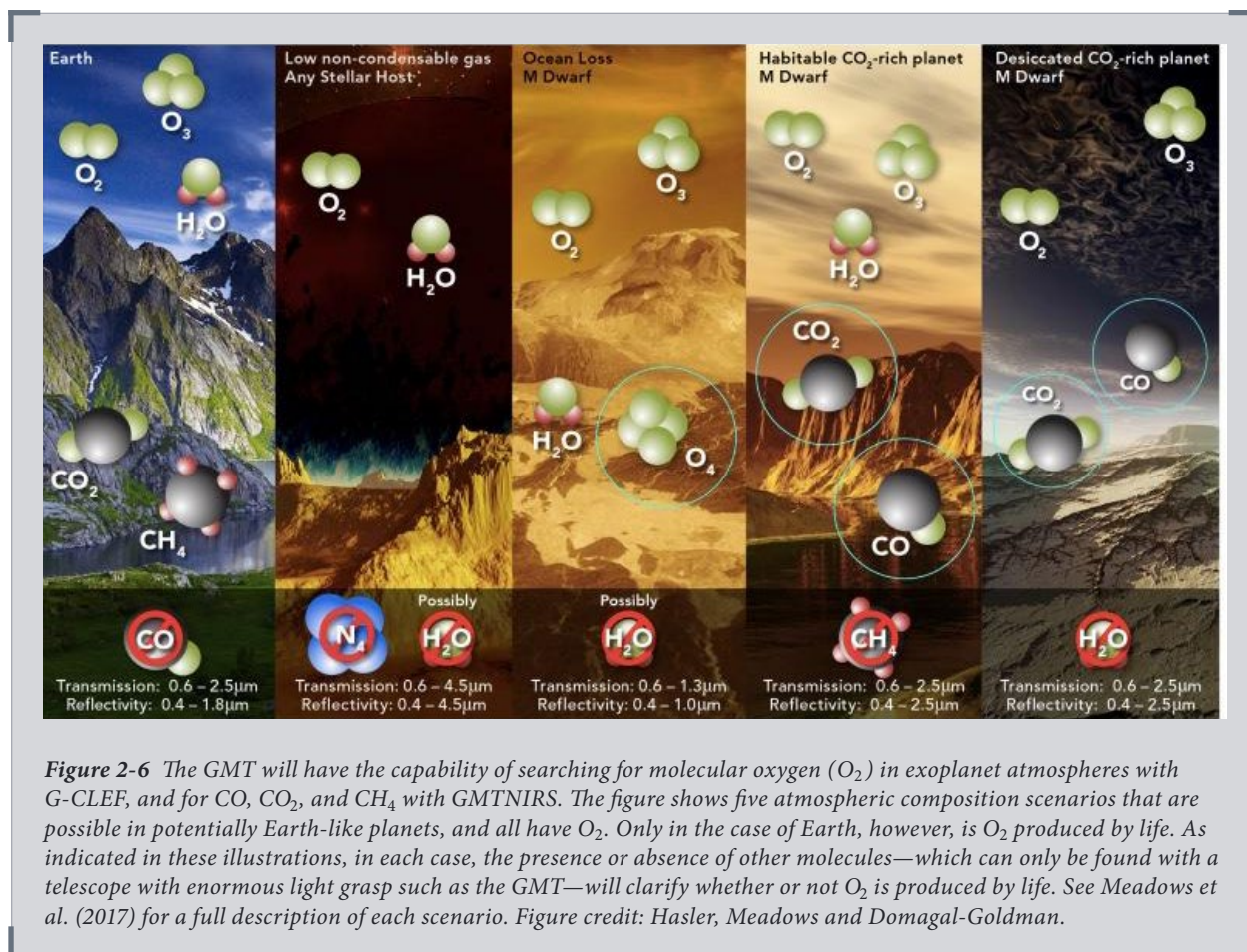
Thermal emission

Using its combination of high angular resolution and sensitivity, the GMT has the potential to detect thermal emission from ice giant (and potentially rocky) planets that Doppler, transit, and microlensing surveys suggest are relatively common. Doppler search data sets indicate that 20–30% of Sun-like stars host planets of less than 10 M_{\oplus} at periods of <50 days (Howard et al. 2010, Wittenmyer et al. 2011b). At wider separations, single-transit events of Sun-like stars from Kepler reveal an occurrence rate of about two planets per star with radii 0.1–1 R_{Jup} for orbital periods in the range of 2–25 years (Foreman-Mackey et al. 2016). The temperatures of old planets are set by their separations from their host stars. The major limitation to imaging all but the most massive and brightest has been achieving the necessary contrast and angular resolution, which will be accomplished for the first time with the GMT.

The nearest stars (i.e. $d < 10$ pc) will be prime targets for GMT direct imaging of these relatively common rocky planets in the L' (3.8 μm) or N (10 μm) bands. The expected angular separation of a rocky planet with a peak flux near 10 μm from its host star is simply a function of the apparent magnitude of the star, so the most

attractive stars to search are also the brightest ones in the sky. Planets that would maintain a “Warm Earth” temperature of 280 K (suitable for N-band detection) would lie within their systems’ habitable zones and would also be outside of the GMT’s 1.5 λ/D inner working angle threshold. The N-band brightness of a 2 R_{\oplus} planet at 5 pc is approximately 9 μJy , suggesting that super-Earths would be well above the expected noise level in a several-hour observation.

Of course, rocky planets may exist in a range of orbits around their parent stars. While planets at larger separations would be cooler and less detectable, planets closer to their stars will have equilibrium temperatures correspondingly higher, and would be even more amenable to study. An Earth-sized planet at an equilibrium temperature of 600 K would be roughly four times closer than a true Earth analog (at 280 K) and would have a peak flux in the L’-band atmospheric window. If we assume blackbody emission of the planet at its equilibrium temperature, it would have an absolute flux of 2 μJy , which compares favorably with the photometric limit



of 0.5 μJy expected for the GMT, limited by sky and telescope background in a one-hour observation. While the approximation of a 600 K blackbody for a hot Earth is almost certainly an oversimplification, spectral models for hot planets with a range of atmospheric compositions have been examined by Miller-Ricci et al. (2009). These models suggest that because the L’-band is a generally transparent window,

the detection of “hot Earths” at L' is feasible with the GMT.

The factors limiting the detectability of “warm” versus “hot” Earths are different. Photometric sensitivity in the N-band limits the number of stars around which a warm rocky planet can be detected. For L' -band “hot Earth” studies, the available photometric sensitivity will, in principle, allow detection of even sub-Earth mass planets outside $\sim 1.5 \lambda/D$ separations. The science that would come from the observation and subsequent detailed study of these classes of planets would be truly groundbreaking.

Atmospheric Characterization of Earth-like Planets: Detection of Oxygen

The GMT will search for biomarkers in the atmospheres of Earth-like planets.

Upcoming space missions TESS and PLATO will yield a large number of potentially Earth-like planets in the habitable zones of nearby stars. Once discovered, and confirmed as rocky planets by precision radial velocity spectrographs such as G-CLEF, the next task will be to search the atmospheres of those planets for signs of potential biomarkers — chemicals whose existence in our own atmosphere reveal the presence of life on Earth. Water (H_2O), carbon dioxide (CO_2), methane (CH_4), and ozone (O_3), are commonly listed in the literature as biomarkers (e.g. Kaltenecker et al. 2007). Molecular oxygen (O_2) was also identified as a biomarker after it was detected by Sagan et al. (1993) while analyzing the spectrum of Earth as observed by the Galileo probe. Even though a handful of known mechanisms can produce O_2 in planets like Earth (see, e.g., Wordsworth & Pierrehumbert 2014, Domagal-Goldman et al. 2014, Luger & Barnes 2015), the appearance of O_2 in our planet has been directly linked to the onset of oxygenic photosynthesis by cyanobacteria, and therefore to the profusion of life (see Schwieterman et al. 2017, and references therein). As a result, O_2 has gained attention as a key biomarker in the past few years.

Only an instrument like G-CLEF will be able to detect O_2 in terrestrial exoplanet atmospheres because of its high spectral resolution at optical wavelengths. The atmosphere of a planet where O_2 is being produced by biological processes similar to those on Earth should contain O_2 , O_3 , H_2O , CO_2 , and CH_4 , but no CO or O_4 . Combining optical detections of O_2 and infrared observations of other molecules will be the only way to provide a conclusive answer about whether a planet is habitable (like Earth) or not.

Figure 2-6 illustrates the five currently studied atmospheric composition scenarios that we expect to find on potentially Earth-like planets. In each of those scenarios, the JWST or the GMT could be able to detect potential biomarkers like H_2O , CO_2 , or CH_4 , but the presence of those molecules alone in the atmosphere of a planet does not ensure the presence of biological activity or even whether the planet could be habitable (for example, H_2O , CO_2 , and CH_4 have been detected in giant, gaseous exoplanets, which lack a solid surface where life could develop). The JWST or the GMT may be also be able to detect O_3 and CO . The absence of H_2O or CH_4 in a planet’s atmosphere, or the presence of CO , would hint at the absence of life, but even if we detected all of these molecules, we would still need to detect O_2 to have a full picture of which scenario we are observing. Only the first scenario of **Figure 2-6** (Earth) requires the presence of life. Therefore, the combination of visible and near-infrared observations will be key to identifying the truly Earth-like planets by revealing the presence of all necessary molecules: the atmosphere of a planet

where O_2 is being produced by biological processes similar to those on Earth should contain O_2 , O_3 , H_2O , CO_2 , and CH_4 , but not CO or O_4 .

Synergy with JWST

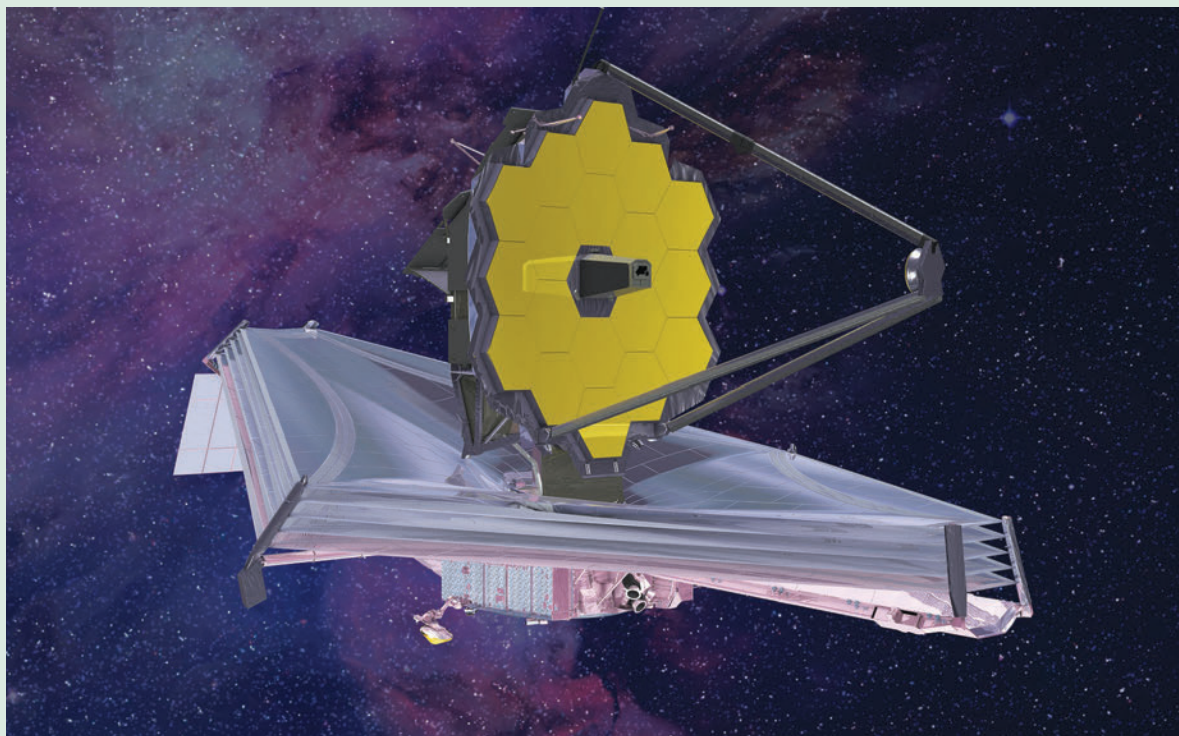


Figure 2-7 The search for biomarkers in potentially Earth-like planets will be a major science driver of the upcoming James Webb Space Telescope. The JWST, with instrumentation covering a large range of wavelengths between $0.6 \mu\text{m}$ and $28 \mu\text{m}$, may be able to detect all of the biomarkers of **Figure 2-6** in transiting planets except for O_2 (although Earth-sized planets will be very difficult to observe with JWST; Morley et al. 2017). O_2 is impossible for the JWST to detect because of 1) very low instrumental throughput at optical wavelengths ($<0.8 \mu\text{m}$) where the most prominent O_2 bands are present, and 2) low spectral resolution, which will highly dilute the depth of the O_2 features. G-CLEF observations of O_2 will thus be very complementary to the work done with JWST. The GMT with an instrument like that described in the previous section—a coronagraph plus high dispersion infrared spectrograph—will also attempt to observe molecules that absorb in the infrared (CO , CO_2 , H_2O , CH_4) in small planets. Figure credit: Northrup Grumman.

Snellen et al. (2013) provided a breakthrough method for how to detect O_2 using high-resolution spectrographs installed on large ground-based telescopes: when the potentially Earth-like planet crosses in front of its host star, O_2 molecules in that planet's atmosphere imprint an absorption signal similar to the signal of O_2 on our own Earth (telluric O_2). When observed at a resolving power $R \sim 100,000$, typical of state-of-the-art, ground-based, high-resolution spectrographs, that O_2 absorption signal will look like the model illustrated in **Figure 2-8**. Because the exoplanet system will be moving relative to us, the O_2 lines from the exoplanet will appear Doppler-shifted with respect to the telluric O_2 lines, and we can use that Doppler

shift information and cross-correlation techniques to detect the exoplanet's O₂. This same technique works in the near-infrared for H₂O, CO₂, or CH₄.

The expected amplitude (depth) of the exoplanetary O₂ signal is very small, of the order of 10⁻⁵–10⁻⁶. We will therefore need the collecting area of the next generation of ground-based extremely large telescopes to collect enough photons to, in a reasonable amount of time, reach the photon noise necessary to detect those signals. Following this idea, Rodler & López-Morales (2014) performed detailed simulations to establish the detectability of O₂ in the atmosphere of an Earth twin around a nearby star using each of the three planned extremely large telescopes, the GMT, the TMT, and the E-ELT, with high-resolution spectrographs, assuming such instruments will be available. Those simulations revealed that G-CLEF's design was optimal to pursue this science, with some of the key parameters including the availability of high resolving power ($R \sim 100,000$) at optical wavelengths, low readout noise detectors, and wavelength coverage extending from that used in many current precision radial velocity spectrographs, including the O₂ A-band.

Using the calculations in Rodler & López-Morales (2014), we expect that:

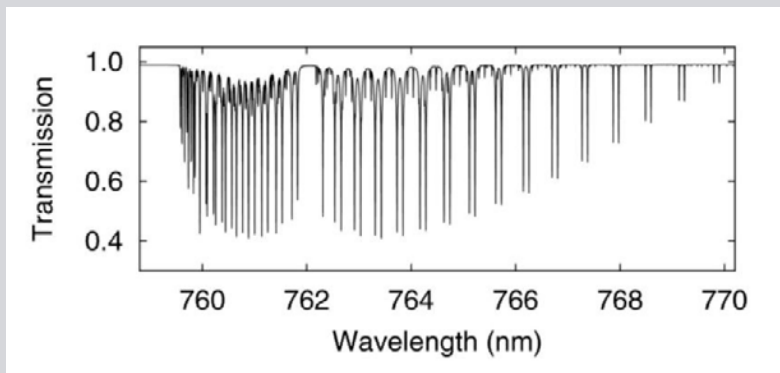
1. The detection of O₂ in an Earth-like exoplanet atmosphere will be most feasible if the planet orbits an M3V or later star. The fact that the habitable zones for those low-mass stars are at orbital periods of 30 days or less is one of the key factors; the numbers of observable transits is a factor 10 or more times larger than for a planet orbiting in the habitable zone of a solar type star.
2. Earth-like planets orbiting M4V stars will be the most favorable targets given that these are the most common types of nearby M-dwarf stars, and the planets in their habitable zones will transit every 16 days.
3. Even with a large aperture telescope such as the GMT, to be sensitive to O₂ it will be necessary to accumulate a large number of photons. In particular, for a planet orbiting an M4V star, it will take a minimum of 14 transits to detect O₂ in its atmosphere with 3 σ confidence. This means that it would take only 7–8 months if we could observe each transit, but when we factor in the number of transits observable from the ground, based on night-day cycles, and weather (i.e. only one of every 8–10 transits can be observed), we arrive at a more realistic (and conservative) timescale of 5–6 years to achieve this goal.

2.2 Toward Understanding How Planets Formed

The census of planets reveals what planet formation is possible. Ultimately, our challenge is to understand the physical processes by which planetary systems acquire their distributions of mass, locations, and compositions. Planet formation occurs in concert with the last stages of star formation: it is the process of building both rocky and gaseous bodies in a protoplanetary disk surrounding a young star (e.g., see review by Williams & Cieza 2011). Surveys have shown that disks are common around stars of age $\lesssim 2$ Myr (e.g. Haisch et al. 2001). Our goal is to connect the properties of disks over time with the planetary systems around old stars; the physical processes occurring within circumstellar disks will determine the typical properties of planets. For example, Earth formed from planetesimals that were fairly depleted in volatile compounds, particularly those containing carbon, yet enough water and carbon remained to enable life. We would like to track the inventories of

key volatiles — particularly C and O — in disks to learn whether the processes that formed Earth are universal, and to understand which systems would likely harbor habitable planets.

Figure 2-8 The GMT will have sufficient light gathering power to enable very high spectral resolution observations of the stellar hosts of planets detected via transits. When the potentially Earth-like planet crosses in front of its host star, O₂ molecules in that planet's atmosphere will imprint an absorption signal similar to the signal of O₂ on Earth (telluric O₂). The simulated G-CLEF transmission spectrum shown at a resolving power of $R \sim 100,000$ is of the atmosphere of an Earth-like planet at a wavelength of ~ 760 nm, showing the most prominent O₂ band. Because the exoplanet system will be moving relative to us, the O₂ lines from the exoplanet will appear Doppler-shifted with respect to the O₂ telluric lines, and we can use that Doppler-shift information and cross-correlation techniques to detect the exoplanet's O₂. This same technique works in the near-infrared for H₂O, CO₂, or CH₄ with the GMTNIRS instrument (Figure adapted from Rodler & López-Morales 2014).



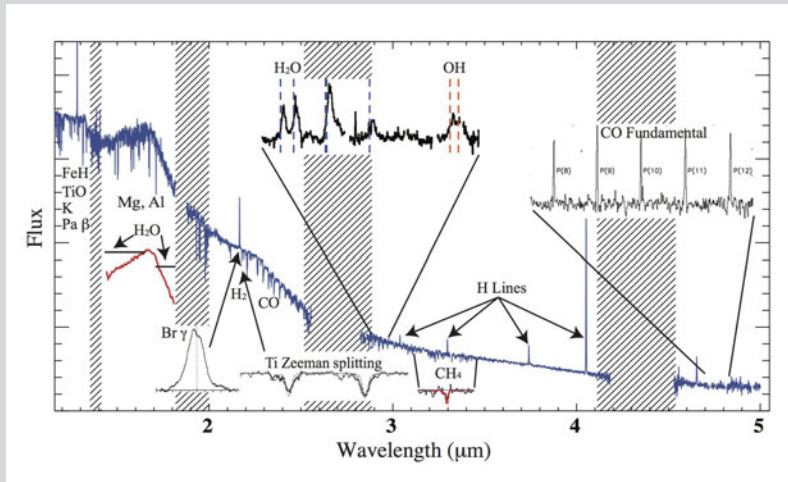
Observations of Circumstellar Disks

The GMT will be able to make two key and unique types of observations of disks: high resolution spectroscopy of molecules in inner disks (the terrestrial planet-forming region) and high spatial resolution imaging of dust in inner disks. The first is enabled by its large aperture and the uniquely sensitive and powerful GMTNIRS instrument. The second is enabled by its large aperture and high-performance adaptive optics.

Solids and gases in regions of planet formation (i.e. the inner tens of AU of circumstellar disks) are heated by the central star and reach temperatures of ~ 100 to 1000 K. They therefore emit strongly at near- and mid-infrared wavelengths. The number of protoplanetary disks within 100 pc is unfortunately small. Most disks can be found in young stellar clusters, and these are typically ~ 140 pc away and preferentially located in the southern hemisphere. Ophiuchus (ages 0.3–5 Myr), Chamaeleon I (age ~ 2 Myr), and Upper Scorpius (age ~ 10 Myr) present the closest large samples of stars in the south, though the GMT will also be able to observe Taurus (age ~ 2 Myr) in the north. In the youngest regions, extinction by remnant cloud material can be extreme. In the Ophiuchus core, for example, stars are forming within regions of high dust extinction, $A_V > 15$. The Laser Guided Adaptive Optics (LGAO) system on the GMT has an infrared wavefront sensor that will allow studies of such deeply embedded stars with disks. For $K \text{ mag} < 18$, using the target star as the tip-tilt star will allow observation of most of the known young objects. In Ophiuchus, this includes 315 stars, about half of which have been studied little because they are so heavily embedded (Wilking et al. 2008).

High resolution spectroscopy at 1–5 μm can measure the kinematics of key volatiles

Figure 2-9 This figure shows the type of spectrum GMTNIRS will obtain of circumstellar disks around young stars. The spectrum is of a classical T Tauri star with a protoplanetary disk (blue: TW Hydrae; Vacca & Sandell 2011) overlaid with a subset of the interesting spectral features available for young stars, brown dwarfs, and circumstellar disks across the broad infrared spectrum that GMTNIRS can measure simultaneously. Hydrogen emission line profiles and strengths probe disk accretion physics (Najita et al. 1996), spectral shape and atomic line widths indicate age (Allers et al. 2007), Zeeman splitting measures stellar magnetic fields (Yang et al. 2008), and molecular emission lines reveal disk kinematics, abundances, and temperature structure (Banzatti et al. 2017; Gibb & Horne 2013; Salyk et al. 2007). Regions of strong telluric absorption are shaded. Not only are the abundances of different compounds revealed with such data, but from kinematic measurements, spectra reveal the gas motions and radial locations in the disk around the star.



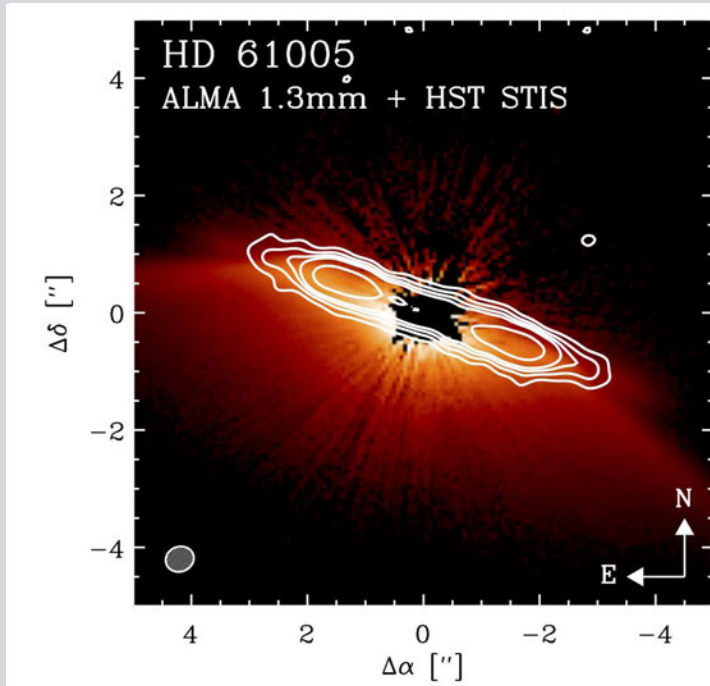
that are the main gaseous carriers of C and O: the molecules H_2O , OH, CO, CO_2 , HCN, and CH_4 as well as deuterated species of these, and lines of H_2 , Br γ , Cl, etc. While the JWST is supremely sensitive over this wavelength range, it will not have the capability to study kinematics—by resolving line profiles by velocity, we can measure the radial locations of all species as well as their abundances. Both the oxygen- and carbon-bearing species in the inner disk may participate in a rich chemical network that ultimately gives rise to the compositions of terrestrial planets. They may also act as tracers of the kinematics of the disk, including turbulence and accretion, and the excitation due to high energy photons that may drive disk dissipation. Further observations of multiple species and multiple transitions will provide constraints on the disk radii, vertical depths of the emitting locations, and structures of the molecular gas. Ultimately, we would like to know how gas species are transported and mixed, and use the gas to study the dynamics of planet formation. The C:O ratio is particularly important; it sets the oxidation state of planetesimals. The GMT will make decisive measurements of the molecular compositions of disks through the high-resolution, near-infrared, spectroscopic capabilities of GMTNIRS (see **Figure 2-9**). The $4.7 \mu\text{m}$ fundamental ro-vibrational transition of CO can trace the innermost location of the gas (Banzatti et al. 2015) and $3 \mu\text{m}$ H_2O and OH emission can be abundant in the ~ 1 AU regions of disks, interior to the snow line (Salyk et al. 2008). The sensitivity of current 8–10 m telescopes has been sufficient only to probe disks around bright, high-mass stars and those least embedded in their parent molecular clouds. A much wider range of stellar properties and evolutionary states will be enabled by GMTNIRS, including measurements of these important gases in many disks around typical young, low-mass stars. Using the technique of *spectroastrometry*, in which a slit is placed across the disk's major and minor axes and the centroid of the line emission is measured as a function of velocity at sub-pixel accuracy, we can map out the lines to resolutions of a few AU, obtaining the combination of high spatial resolution and velocity resolution to measure the distribution of emission.

One way to probe the location of the snow line is by using near-IR spectroscopy and spectroastrometry to observe both H_2O and its dissociation product, OH. A distinct change in the abundances of each should appear at the snow line.

Another important use of spectroastrometry will be to search for kinematic signatures that show the presence of giant planets. The formation of such planets should clear gaps in the disk and perhaps azimuthal asymmetries in the distribution of disk material that leave a kinematic signature. The GMT will probe the inner regions of protoplanetary disks to test for the existence of such gaps and asymmetries and provide evidence for the formation of planets on short timescales.

High spatial resolution imaging with the GMT in the near-infrared can finally reach the region where Jupiter sits in the solar system (5 AU at 150 pc is 33 mas, or $2 \lambda/D$ at $2 \mu\text{m}$). Spectroastrometry will allow observation of the gas in this location, and direct imaging of disks will be possible via light scattered or emitted from dust. Planet-disk interactions depend on the temperature, density, and turbulence structure of the disk, all of which can be influenced by the planets themselves.

Figure 2-10 This figure shows a composite image of the “moth” disk around HD61005 in two different “colors”: the HST+STIS visible light image of “scattered light” (background image) and the ALMA observation of the dust continuum (white contours). The inner working angle of HST, and of current ground-based systems, is insufficient to resolve dust structures, such as an inner dust ring, that are apparent in the ALMA images (the black pixels in the HST images are too close to the star to provide information on the disk). Such structures may be indicative of the influence of planets within the disk (MacGregor et al. in preparation). The GMT’s exceptional spatial resolution in the near-infrared will reveal the locations of planet-forming material around young stars and how planets sculpt their environments.



Models show that the density structures of disks can have a profound effect on planetary migration, from driving planets inward to become hot Jupiters to having them reverse course and migrate outward (e.g. Jang-Condell & Sasselov 2005, Walsh et al. 2012).

Ground truth on the dynamical interactions of disks and planets could be obtained by imaging both simultaneously. The GMT’s high performance AO system that will be used for high contrast imaging of young planets, as described in **Section 2.1**, can also be used to image disks to see, for example, spiral density waves launched by



Synergy with ALMA

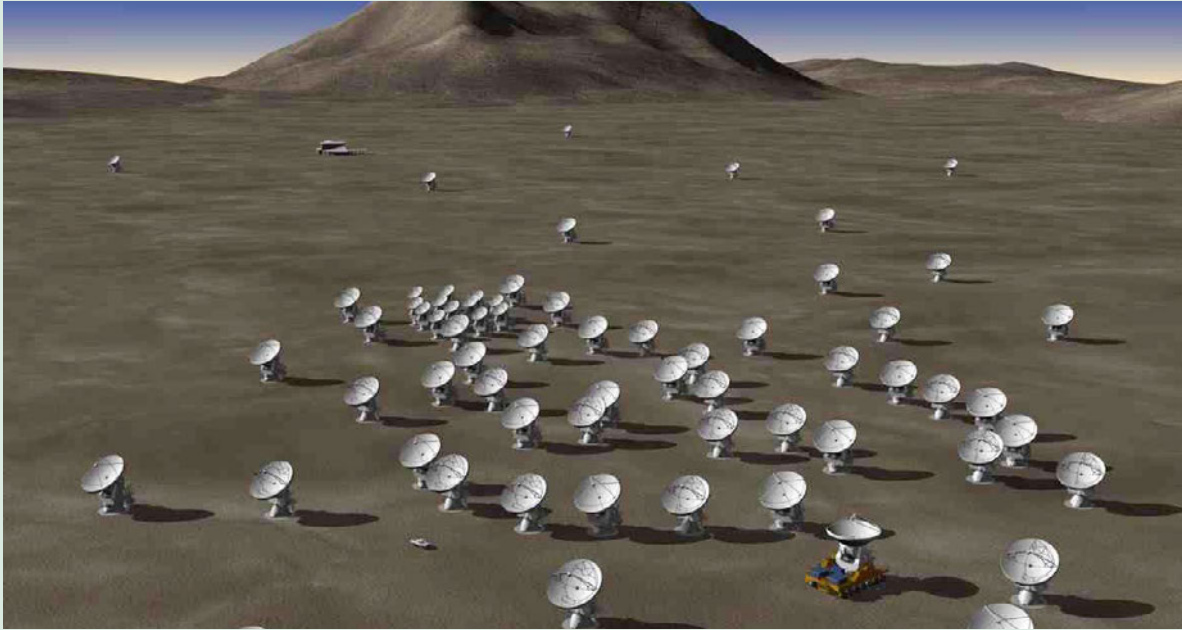


Figure 2-11 ALMA and the GMT will provide complementary images and spectroscopy of circumstellar disks at comparable spatial resolution. Spectroscopy from GMTNIRS will be sensitive to warm gas species, while ALMA will be sensitive to colder gas of the same species. We will, for example, measure the evaporation of icy grains as they migrate from the cold outer disk through the snow line into the inner disk and match the abundances of water vapor measured across that line with a combination of GMTNIRS and ALMA spectroscopy.

giant planets, offsets between the locations of small and large grains set by pressure bumps in disks, and small grains making their way into the inner disk while large grains are trapped in gas held at bay by giant planets. The current generation of extreme adaptive optics systems (SPHERE and GPI) have begun this work and revealed many disk structures, including rings and spirals, in outer disks (e.g. Maire et al. 2017, Muro-Arena et al. 2018), but they do not have the spatial resolution to probe 5–10 AU or distinguish disk features from planetary objects (e.g. Follette et al. 2017). The GMT’s contribution will be game-changing.

Observations of young planets

The combination of the GMT’s high spatial resolution and low background, from using adaptive secondary mirrors, will enable transformative observations of young planets. Observing exoplanets at a range of ages and in different environments will enable ensemble studies of the formation and evolution of planetary systems. Older planets have fully cooled to their equilibrium temperatures, but young planets still have varying luminosity based on their formation energy. The basic formation mechanism of Jupiter and Saturn as well extrasolar gas giants remains unknown. There are two possible modes of formation, variously described as core accretion

vs. disk-gravitational instability, or planet-like vs. pseudo-star-like formation, or low initial entropy vs. high initial entropy, or cold start vs. hot start. In fact, the mechanisms are not bi-modal; the initial entropy can be intermediate between the two. The mode of formation may be different in different systems and result in conditions that are more or less favorable for the formation of rocky habitable planets. With the GMT, we can make substantial progress in the difficult task of measuring key observables that may distinguish the mode of formation: cooling curves (luminosity vs. age), bulk metallicity (core accretion requires core formation out of high metallicity material), and compositional tracers of where in the disk a planet formed, such as C/O or H/D ratios (Öberg et al. 2011).

By observing the luminosity of planets via AO-assisted imaging, the GMT will create cooling curves that show the temperatures of planets over time. It is best to observe the planet at infrared wavelengths where the bulk of its energy is emitted. Young, massive exoplanets emit their peak energy at wavelengths around $1.2 \mu\text{m}$, while older and lower-mass planets shift to longer wavelengths toward $10 \mu\text{m}$. Because the GMT uses adaptive secondary mirrors, its throughput and sensitivity are optimal for these observations. The ages of stars are observed via cluster evolution, lithium burning, dynamics, and asteroseismology. Synergies with *GAIA* will be important in this case, putting tighter constraints on the masses and ages of the planet-hosting stars.

With AO-assisted spectroscopy, the GMT will determine atmospheric abundances as described in the previous sections. Higher metal content, which results from aggregations of solids, may be a signal of accretion beyond the snow line.

The statistical properties of imaged planets revealed by the GMT will provide critical tests of planet formation and migration theories. The relatively low number of exoplanets imaged with the current generation of ground-based facilities has made it challenging to answer fundamental questions about planets on wide orbits—for example, whether their occurrence rates or compositions correlate with stellar host mass (e.g., Bowler et al. 2016; Lannier et al. 2017) and whether they are more likely to be found around stars hosting debris disks (Meshkat et al. 2017). Measuring the mass-period distribution and overall frequency of giant planets beyond 5 AU, currently poorly constrained, especially below $5 M_{\text{Jup}}$, will teach us about the efficiency of planet formation and how much mass must have been present in the disk when the planets formed. We know from RV and transit surveys that occurrence rates rise steeply at lower masses, so we expect detection rates of planets much higher than currently achieved with 8–10 m class telescopes.

By probing this landscape to Saturn masses at typical separations down to a few AU, high-contrast imaging with the GMT will answer these questions for the first time by finding large numbers of planets to establish statistically sound samples, measuring planetary orbits over time, and finding planets spanning a variety of ages. With these unprecedented sensitivities, other questions will also be explored, such as whether the architectures of exoplanets vary over time—a theme that is especially difficult for RV and transit methods to address because of stellar activity at early ages. By imaging stars with a range of ages (e.g., <10 Myr, 10–300 Myr, and 300–5000 Myr), the GMT will be able to search for changes in the frequency and the period distribution of planets, which would point to signs of orbital migration similar to what is thought to have occurred in the early solar system (e.g. Gomes et al. 2005). With the GMT and its potent instrumentation, we will for the first time gain a clear picture of where and how planets form around young stars.

References

- Allers, K. N. et al. 2007, *ApJ*, 657:511
- Banzatti, A. & Pontoppidan, K. M. 2015, *ApJ*, 815, 15
- Banzatti, A. et al. 2017, *ApJ*, 834, 152
- Barnes, J. R. et al. 2017, *MNRAS*, 486, 1733
- Boss, A. P. 1997, *Science*, 276, 1836
- Bowler, B. P. 2016, *PASP*, 128j2001
- Butler, R. P. et al. 2004, *ApJ*, 600, L75
- Domagal-Goldman, S. D., Segura, A., Claire, M. W. et al. 2014, *ApJ*, 792, 90
- Follette, K. B. et al. 2017, *AJ*, 153, 264
- Foreman-Mackey, D., Hogg, D. W., & Morton, T. D. 2014, *ApJ*, 795, 64
- Foreman-Mackey, D., Morton, T. D., Hogg, D. W., Agol, E. & Scholkopf, B. 2016, *AJ*, 152, 206
- Fressin, F., Torres, G., Charbonneau, D., Bryson, S. T., Christiansen, J., Dressing, C. D., Jenkins, J. M., Walkowicz, L.M. & Batalha, N. M. 2013, *ApJ*, 766, 81
- Gibb, E. L. & Horne, D. 2013, *ApJ*, 776, L28
- Gomes, R., Levison, H. F., Tsiganis, K. & Morbidelli, A. 2005, *Nature*, 435, 466
- Hahn, J. M. & Malhotra, R. 2005, *AJ*, 130, 2392
- Haisch, K. E. Jr, Lada, E. A. & Lada, C. J. 2001, *ApJ*, 553, 153
- Jang-Condell, H. & Sasselov, D. D. 2005, *ApJ*, 619, 1123
- Howard, A. W. et al. 2010, *Science*, 330, 653
- Kaltenegger, L., Traub, W. A., & Jucks, K. W. 2007, *ApJ*, 658, 598
- Kenworthy 2016 2016SPIE.9908E..A6K
- Kopparapu, R. K., Ramirez, R. M., SchottelKotte, J., Kasting, J. F., Domagal-Goldman, S. & Eymet, V. 2014, *ApJ*, 787, 29
- Lannier, J. et al. 2017, *A&A*, 603, 54
- Lopez-Morales, M. et al. 2016, *AJ*, 152, 204
- Luger, R. & Barnes, R. 2015, *AsBio*, 15, 119
- Maire, A.-L. et al. 2017, *A&A*, 601, A134
- Meadows, V. S. Reinhard, C.T. Arney, G.N. et al. 2018, *Astrobiology* 18:630–662
- Meshkat, T. et al. 2017, *AJ*, 154, 245
- Miller-Ricci, E., Meyer, M. R., Seager, S. & Elkins-Tanton, L. 2009, *ApJ*, 704, 770
- Muro-Arena, G. A. et al. 2018, *A&A*, in press
- Najita, J., Carr, J. S. & Tokunaga, A. T. 1996, *ApJ*, 456, 292
- Öberg, K. I., Murray-Clay, R. & Bergin, E. A. 2011, *ApJ*, 743, L16
- Petigura, E., Howard, A. W. & Marcy, G. W. 2013, *PNAS*, 11019273
- Ricker, G. R. et al. 2016, *SPIE*, 9904, 2
- Rodler, F. & Lopez-Morales, M. 2014, *ApJ*, 781, 54
- Sagan, C., Thompson, W., Carlson, R., Gurnett, D. et al. 1993, *Nature*, 365, 715
- Salyk, C., Blake, G. A., Boogert, A. C. A., & Brown, J. M. 2007, *ApJ*, 655, L105
- Salyk, C. et al. 2008, *ApJ*, 676, 49
- Schwieterman, E. W., Kiang, N. Y., Parenteau, M. N. et al. 2017, arXiv:1705.05791
- Snellen, I. A. G.; de Kok, R. J.; le Poole, R.; Brogi, M. et al. 2013, *ApJ*, 764, 182
- Snellen, I.A. G., et al. 2015, *A&A*, 576, A59
- Vacca, W. D. & Sandell, G. 2011, *ApJ*, 732, 8
- Walsh, K. J., Morbidelli, A., Raymond, S. N., O'Brien, D. P., & Mandell, A. M. 2012, *M&PS*, 47, 194
- Wilking, B. A., Gagné, M. & Allen, L. E. 2008, in *Handbook of Star Forming Regions, Vol. II*, ed. B. Reipurth, ASP Monograph, 5, 351
- Williams, J. P. & Cieza, L. A. 2011, *ARAA*, 49, 67
- Wittenmyer, R. A., Tinney, C. G., Butler, R. P., O'Toole, S. J., Joes, H. R. A., Carter, B. D. Bailey, J. & Horner, J. 2011, *ApJ*, 738, 81
- Wordsworth, R. & Pierrehumbert, R. 2014, *ApJ*, 785, L20
- Yang, H., Johns-Krull, C. M., & Valenti, J. A., 2008, *AJ*, 136, 2286



A Hubble Space Telescope image of the "Mystic Mountain", a region of gas and dust that is being eroded by ultraviolet radiation from the surrounding, newly-formed, young stars. (Credit: NASA, ESA, and M. Livio and the Hubble 20th Anniversary Team (STScI).)



The Birth of Stars

Where and how are stars born? Dust-enshrouded stellar nurseries can give birth to stars over a vast range of masses, from more than 100 times the mass of our own Sun, to stars only a tenth of the mass of our Sun and as small as Jupiter. Forming stars are obscured by dust; the rich physics of star formation is hidden within dark veiling clouds that cannot be pierced by visible light. Behind this veil, the force of gravity drives cold, diffuse clouds of gas and dust to collapse inward, becoming billions of times denser and millions of times hotter, until fusion begins and stars are born.

Using infrared light, the GMT will unveil forming stars in stellar nurseries across the Milky Way, allowing us to see the complex process of star formation with new clarity. In particular, the GMT will transform our ability to study the least massive stars and even the faint, substellar objects that fail to sustain fusion and become stars.

Chapter Authors

Adam Kraus (The University of Texas at Austin)

Daniel Apai (University of Arizona)

Neal Evans (The University of Texas at Austin)

Alyssa Goodman (Harvard-Smithsonian Center for Astrophysics)

Charles Lada (Harvard-Smithsonian Center for Astrophysics)

Chris Tinney (University of New South Wales)

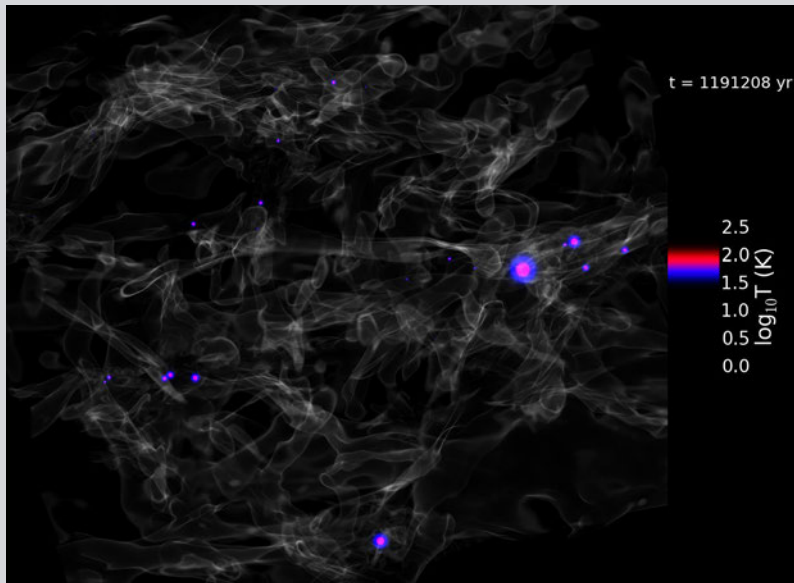


3 The Birth of Stars

The physics of star formation is central to understanding the formation and life cycle of galaxies, stars, and planets. About five new stars form each year in our Milky Way galaxy from diffuse gas between the existing stars. The gas is so diffuse and cold that it must be gravitationally compressed by 20 orders of magnitude to make a star, becoming a million times hotter and beginning nuclear fusion, the power source of stars. Star formation is integral to galaxy formation and evolution, and the great variety of planets now known condensed within disks of gas and dust surrounding protostars. The GMT will provide new insights across all stages of this process, starting from the large-scale structure and kinematics of collapsing molecular clouds, onward to the assembly of new stars at the center of individual protostellar cores, and ending with the sizes and ages of the newly-formed stars that will indicate the mass-dependence and time-evolution of star formation physics.

One of the major goals of star formation theory is to predict the large-scale formation and evolution of stellar populations (e.g., Offner et al. 2009; Bate 2009; **Figure 3-1**), for which observational constraints are badly needed. Most stars form in groups, ranging from loose unbound associations to dense clusters, during the collapse of giant molecular clouds. Star formation generally occurs in the regions within giant molecular clouds called dense clumps (Lada et al. 2010), where gravity begins to dominate over dispersive forces, such as turbulence and magnetic fields, and begins the collapse that ultimately produces a star and its planetary companions (**Figure 3-2**). While small clumps may form only a single star or binary, most star formation occurs in more massive clumps and the resulting stars have a wide range of concentrations, from loose associations to tightly bound clusters (Bressert et al. 2010). Only the most massive and dense clumps form stars of all masses, including brown dwarfs. The most massive stars form infrequently, but have an outsized influence with their radiation and winds, so studies of massive, dense clusters (most of which are at large distances) are needed to understand the origin and impact of massive stars. Most clusters must dissipate because only a small fraction of older stars are found in bound clusters (Lada & Lada 2003), but the dynamical

Figure 3-1 While existing facilities like HST, Spitzer, and ALMA allow direct tests of our understanding of star formation on large scales, the GMT will play a key role in studying the individual protostars that drive this evolution and represent the ultimate outcome of the star formation process. Here we present a simulation of a 10-pc-wide forming star cluster, including the effects of radiation generated by forming stars. Red and blue colors indicate hot gas near protostellar sources, and gray indicates regions of dense gas ($n(H) \sim 1000 \text{ cm}^{-3}$). The structure of the simulated gas is strikingly similar to real molecular clouds (as seen in the title image of this chapter). (Image courtesy of Stella Offner.)



evolution that drives this dispersal process is not well described by current observations or theory.

The extreme upper and lower mass limits of star formation, and the overall stellar mass distribution, are among the primary observable features of star formation theories and are not yet well described by theory. Within a typical dense clump, the Jeans mass is $\sim 1 M_{\odot}$, but these clumps produce objects that span 4.5 orders of magnitude in mass ($5 M_{\text{Jup}}$ to $100 M_{\odot}$). While the driving force in star formation is gravity, the process is far from simple—rotation, magnetic fields, and turbulent motions all could affect the outcome (e.g., Offner et al. 2014). To test competing theoretical models will require measurements of the masses of objects during the formation stage, when the properties of the natal cloud can still be studied. During these stages, extinction is high, so near-infrared spectroscopy is the best route to measure (sub)stellar properties. The added challenge for cluster studies is that they are more distant and the forming stars are more crowded. In the GMT era, JWST will have imaged numerous clusters in the near-infrared to find the targets, and ALMA will have probed the gas conditions. Observations with GMTNIRS, G-CLEF, and GMTIFS, which offer a wide range of spatial and spectral resolution, will provide critical new information on the stellar properties.

These mass measurements themselves are also fraught with systematic uncertainties that must be resolved. The theory of stellar structure and evolution is one of the great achievements of modern astrophysics. It explains the nature of stars as thermonuclear furnaces that forge hydrogen—the primary product of the big bang—into all of the heavier elements of the periodic table up to iron. Stellar evolution and structure theories predict the evolution of stars from shortly after their births through their entire lives, up to and including their inevitable deaths. However, stellar evolution

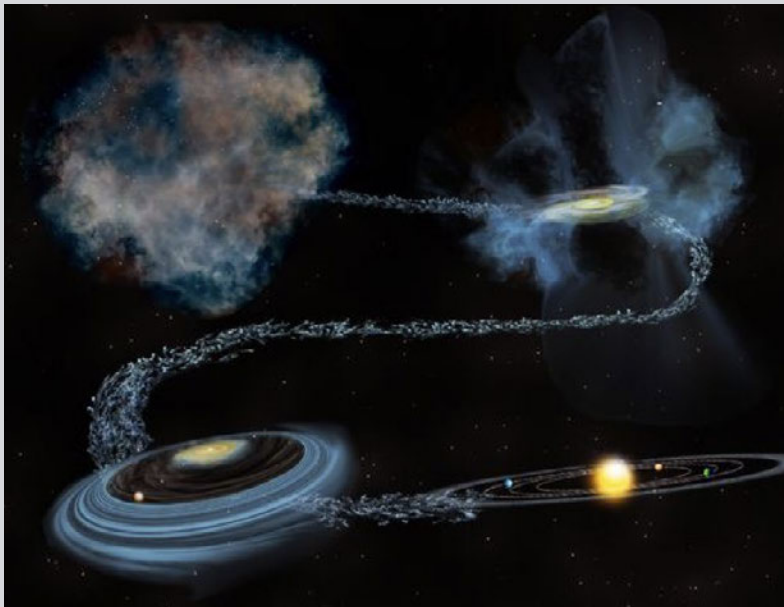


Figure 3-2 With the GMT, it will be possible to study the collapse process of star formation down to the smallest scales. This figure graphically illustrates our understanding of the full sequence of star formation; it depicts the evolution of a single star over time, from the top left to the bottom right. The process beginning with a molecular cloud containing millions of solar masses of dust and gas. It evolves into a protostar surrounded by a circumstellar disk that accretes mass from a large envelope while also forming a circumstellar disk (top right). The protostar accretes until it becomes a young star surrounded by a protoplanetary disk in the process of forming planets (lower left). Finally, a mature star remains with orbiting planetary companions.

The GMT will enable us to establish the masses and ages of central stars so that the evolution and mass dependence of this process can be understood on all scales. Credit B. Saxton.

theories do not currently encompass the earliest stages of protostellar evolution, (during which stars are assembled out of gas and dust) and cannot make accurate predictions about their physical parameters, such as temperature, luminosity, and radius, as a function of the time-dependent mass.

Brown dwarfs (defined here as objects formed in the same manner as stars, but too low in mass to maintain nuclear burning) represent a “boundary condition” for the low-mass extreme of star formation models. Observations show that star formation can make “stars” with masses below the hydrogen burning limit (~70 Jupiter masses) and even overlapping with gas giant planets (5–10 Jupiter masses). However, different star formation models predict very different mass distributions and low-mass cutoffs, and also do not agree on how environmental conditions (such as density or stellar feedback) might change these quantities. The full distribution of these objects will be characterized in terms of observable features by HST and JWST over the next decade, but there are no observational calibrations for the models used to convert those objects’ surface properties (luminosity and temperature) into the fundamental underlying parameters, their mass and age. These same calibrations will be critical for exoplanet science (see Chapter 2) because the masses, luminosities and temperatures of brown dwarfs overlap with those of gas-giant planets, but observations of isolated brown dwarfs do not require the masking of light from a host star. Brown dwarfs therefore will drive future generations of atmospheric models at the coolest temperatures, while also demonstrating the variations of atmospheric heterogeneity and cloud patterns on gas-giant-like objects outside of our solar system.

By the beginning of the GMT era, ALMA will have studied the dynamics, magnetic fields, and chemistry in star forming regions at all scales >10 AU, JWST will have provided deep images of forming star clusters that can reveal free-floating planets, and GAIA will have measured the precise distances and tangential velocities of most young stars within the nearest young stellar populations (out to 1–2 kpc). Those results will open the door to a much wider array of scientific questions for which the GMT will be an important new tool. With its large aperture and unique instrument complement, the GMT will measure stellar kinematics at the youngest ages, probe the innermost stages of protostellar assembly, characterize protostellar atmospheres (from their spectra) and interiors (from their masses and radii), and calibrate mass-dependent features for even the most extreme examples of star formation, brown dwarfs, and free-floating planets.

Near-infrared instruments on the GMT (namely GMTNIRS and GMTIFS) will be needed to push observations to the earliest stages of stellar evolution, where stars are more embedded and difficult to study, and to the very lowest masses. Stellar properties (including luminosity, temperature, surface gravity, and rotation) can indicate the mass and age dependences of observed evolutionary steps, while the assembly history also has long-lasting implications for the subsequent evolution of those properties (e.g., Koenigl 1991; Baraffe et al. 2009). Young stars are difficult to study due to extinction and reddening by circumstellar dust and veiling of spectral features by the blackbody emission of hot gas and dust, all of which combine to obscure the signatures of temperature and gravity needed to understand their early evolution. Some stars will be in binary systems or will have disks amenable to ALMA measurements of Keplerian motion, which will allow the stars’ masses to be measured dynamically. However, the measurement of most other stellar properties will require optical or infrared spectroscopy of photospheric absorption features. High-resolution spectroscopy in the near-infrared is the best way to measure these properties. Studies with IGRINS have shown that stellar absorption lines can

indicate the temperatures, surface gravities, and magnetic fields of stars even with substantial extinction and veiling (e.g., Sokal et al. 2018).

In the following sections, we describe how the GMT and its unique complement of instruments will trace the properties of natal gas clouds using stellar kinematics, reveal the innermost processes of protostellar assembly, unveil spectral diagnostics of the protostars' surface properties, calibrate the relation between those surface properties and the protostars' masses and ages, and probe the detailed atmospheric physics of even the lowest-mass objects to form from the star formation process.

3.1 Tracing Star Formation History via the Dynamics of Young Stellar Cluster Members

The GMT will offer unique measurements of stellar dynamics in the youngest regions of ongoing star formation, as measured from the radial velocities of stars and brown dwarfs. At the youngest ages, these populations are not yet virialized and the stars directly track the velocity structure of the original gas from which they formed; with sufficiently precise measurements, kinematics can therefore tie the current-day properties of stars to the dynamics of the gas that has long since dispersed. Combining radial and transverse motions, the 3D velocities of stars can be constructed. If these stars can be observed sufficiently early, they can even be traced back to their sites of original formation (as determined from the locations of minimum positional dispersion; Wright & Mamajek 2018). Kinematic tracebacks could therefore indicate whether more massive stars form in the “center” (the deepest part of the potential well), with lower-mass stars forming in the outskirts in

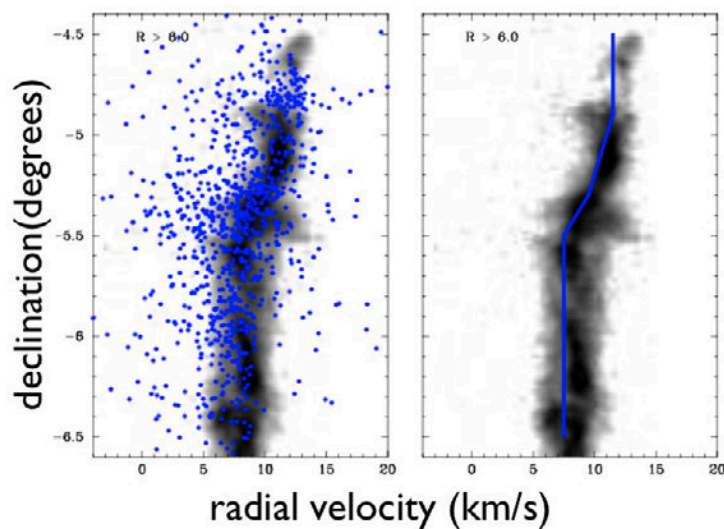


Figure 3-3 The GMT will enable us to measure accurate radial velocities of faint stars. By targeting the lowest-mass objects in nearby stellar clusters, we will be able to unravel the impact of primordial vs. dynamical mass segregation, and even extend such studies to the more distant, massive star-forming clusters in which the initial conditions are substantially warmer and more dynamic than for quiescent low-mass clusters. This figure presents a comparison of stellar and gas dynamics in the Orion Nebula cluster (from Tobin et al. 2009), showing a position-velocity plot of single stars (blue points), and of ^{13}CO gas (grayscale) in the left panel. The blue curve in the right panel shows the

peak of the stellar distribution relative to the gas. The stars clearly track the gas at km/s scales, showing that they encode large-scale kinematic information of the material from which they formed. The greater light-collecting area of the GMT, together with the stability of G-CLEF for measuring accurate radial velocities, will provide the measurements needed to study low mass structures.

a form of primordial mass segregation (e.g., Hillenbrand & Hartmann 1998). Finally, a comparison of the current rate of star formation with the census of (older) clusters indicates that the majority of star-forming clusters dissolve after dispelling the gas that gravitationally binds them together. However, it remains unclear when this occurs and why some clusters persist to ages of gigayears.

Hints of this promise can be seen in results from GAIA, which can measure the transverse motions of stars in nearby, unextincted young stellar populations (e.g., Wright & Mamajek 2018) and is revealing that star formation is often distributed and highly substructured. For stars as faint as $V \sim 20$ mag, the final GAIA catalog will resolve transverse velocities of < 10 m/s in the nearest star-forming regions ($D \sim 150$ pc) and 100 m/s in more typical dense clusters ($1 < D < 2$ kpc). GAIA will also measure radial velocities for bright stars (with $\sigma \sim 1$ km/s for $V < 12$ mag), but ground-based spectroscopy will remain an important complement to space-based astrometry.

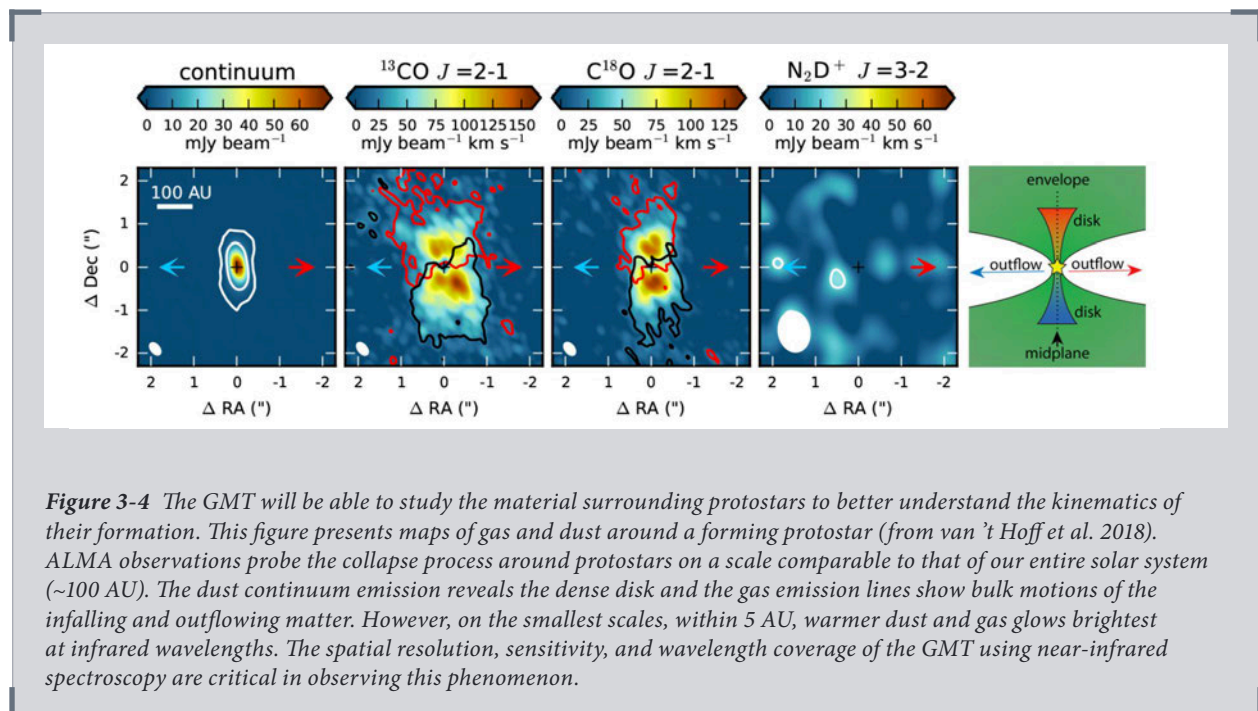
The youngest star-forming environments are typically still heavily shrouded in gas and dust, so they will remain beyond GAIA's visible-wavelength detection limits. Furthermore, massive young clusters (which are typically distant, but may form a large fraction of the Milky Way's stellar content; Lada & Lada 2003) will be subject to confusion in GAIA observations, and the modest physical velocities will translate to negligible angular velocity dispersions at such large distances. Finally, even in nearby, low-obscuration regions like Orion, GAIA will offer a limited view of the dynamics of low-mass objects that are intrinsically red, putting out too little visible light to be detectable; dynamical interactions should excite the kinematics of the lowest-mass objects first, offering a diagnostic of dynamical evolution in action.

The dynamics of the nearest, relatively unobscured/evolved clusters have already been probed with existing multi-object spectroscopic studies on modest-aperture telescopes, yielding RV precisions of < 1 km/s for hundreds of relatively bright stars (e.g., **Figure 3-3**; Tobin et al. 2009; da Rio et al. 2017). Their results show that on the largest scales, the bulk motions of the stars track those of the remaining gas, and hence the stars are not yet dynamically mixed. The scatter in stellar velocities is marginally resolved, suggesting that the clusters may be in virial equilibrium on the intermediate scales. However, the observations lack sufficient precision to probe substructure with amplitudes of $< 1-2$ km/s, and are not sufficiently sensitive to reach the peak of the Initial Mass Function (IMF) in almost any case.

The unique instruments and large aperture of the GMT will open up new regimes of kinematic characterization for young stellar populations in both single-object and multiplexed observations. G-CLEF will offer unrivaled sensitivity for faint objects, and if paired with the MANIFEST fiber system, it could measure radial velocities with precisions of < 1 km/s for dozens of faint objects in a single observation. In the red-optical regime ($\lambda = 750$ nm), G-CLEF will yield $S/N = 10$ per resolution element (suitable for RV measurements) in one hour at $i = 22.5$ mag ($M \sim 8 M_{\text{Jup}}$ for an unextincted brown dwarf in Orion; Baraffe et al. 2015). These observations will further benefit from the extensive efforts to stabilize G-CLEF for precision RV work, reducing instrumental systematics to negligible levels. GMTNIRS will also offer a window deep into the obscured centers of star-forming environments, measuring the primordial kinematics of stars immediately after their formation, even those that are undetectable at optical wavelengths. At the GMTNIRS brightness limit of $S/N = 10$ at $K \sim 18$ mag, it could detect objects as small as $4-5 M_{\text{Jup}}$ in Orion, or solar-luminosity protostars even if obscured behind $A_V > 100$.

3.2 Protostellar Assembly: Accretion of Material from Circumstellar Disks

The unparalleled spectroscopic capabilities of the GMT will provide a valuable complement to the ongoing ALMA revolution, unveiling the final stages of stellar assembly. ALMA provides exquisite spatial resolution, comparable to that of the GMT, and is resolving the kinematics and mass distribution of protostars on solar-system scales (**Figure 3-4**). However, ALMA is most sensitive to cold gas and dust ($T \sim 10\text{--}100\text{ K}$). In contrast, the inner regions of protoplanetary circumstellar disks glow brightest at infrared wavelengths. The finite spatial resolution of both the GMT and ALMA means that the inner parts of protostellar disks, and the fragmentation of proto-binaries, as well as the final accretion of mass onto the protostar(s), will remain unresolved in long-wavelength observations. To study the assembly of rare, high-mass protostars, surveys must extend to further distances with consequently even worse spatial resolution. We therefore must turn to methods that indirectly probe the innermost regions of protostars such as by detecting the spectro-kinematic signatures of hot gas in inner disks (which is best observed at optical/NIR wavelengths) or, for later stages with less obscuration, by measuring the emission of UV continuum and hydrogen emission lines from gas accreting onto the central star.

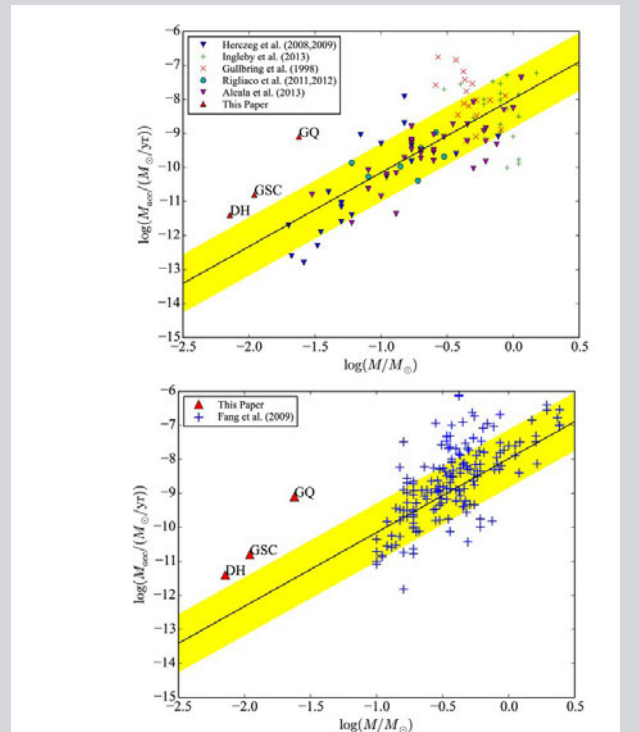


Near-infrared spectrographs can access inner solar systems by using the temperature and kinematic information encoded in spectral lines, tracing gas at temperatures of $100\text{--}1000$ K. For example, Salyk et al. (2011) showed that CO rovibrational transitions can be used to trace the inner disk edge, while Brown et al. (2013) interpreted the complicated emission line profiles from circumstellar disks in order to infer the surface density distribution of inner disks. These observations can be used to assess the degree of smoothness of the mass distribution, providing insight into the stochastic variations of mass accretion onto stars. Furthermore, the planet assembly process is likely to have already begun by the time these disks are

observable, so such observations can provide key insights into the environmental conditions at the beginning of planet formation both at and inside the snow line.

Optical spectrographs can probe the accretion of mass onto protostars by detecting the continuum emission of gas that is heated as it falls down the stellar potential well (Gullbring et al. 1998), as well as line emission from hydrogen that follows the collisional excitation of its electrons into high energy states (Muzerolle et al. 2001). Mass accretion histories and geometries are critical inputs to the star formation and stellar evolution models, as the detailed accretion process determines the amount of

Figure 3-5 The light-collecting power of the GMT will enable observations of mass accretion onto forming stars, brown dwarfs, and planets. This figure presents the mass accretion rate of a star (or planet) as a function of its mass (from Zhou et al. 2014). The mass accretion rates onto wide-orbit protoplanets (labeled points) and onto free-floating stars and brown dwarfs (remaining symbols), are inferred from the UV excess (top) or Balmer-series emission (bottom). The accretion rates onto protoplanets are inferred from UV observations with the Hubble Space Telescope, but were only detectable because they appear to be accreting much more vigorously than typical, planetary-mass, free-floating objects. It currently is not possible to study the detailed difference between companions and free-floating objects of the same mass. With the GMT, low- to moderate-resolution spectra taken with GMACS will be used to detect the continuum emission from such accretion, while G-CLEF and GMTNIRS can resolve emission lines.



entropy trapped in the central star (and hence its subsequent evolution to the main sequence). Observations of nearby pre-main-sequence stars have revealed that at late stages of assembly, accretion rates decline with decreasing stellar mass, but also broadly span over a factor of ten in magnitude (e.g., Natta et al. 2004; Herczeg et al. 2009; **Figure 3-5**). However, while those observations are critical as an input for protoplanetary disk evolution, they fall well after the peak epoch of stellar assembly.

Some accretion rates have been inferred for earlier-stage protostars based on the small fraction of scattered light that escapes (e.g., White & Hillenbrand 2004), but such observations are severely photon-limited since the vast majority of UV photons are absorbed by circumstellar material. More broadly, luminosity can be used to infer the mass accretion rate, but only once the protostellar mass and radius are known (**Section 3.4**). Even at later stages, mass accretion measurements typically are not feasible within the planetary mass regime, preventing direct comparison with (potentially anomalously high) accretion rates onto planetary-mass companions to young stars (**Figure 3-5**; Zhou et al. 2014).

The spectrographs being built for the GMT will offer an unprecedented view of inner disks and protostellar accretion. GMTNIRS will exceed the most sensitive current spectrograph (IGRINS on Gemini) by two orders of magnitude in depth, observing protostars as faint as K \sim 18 (i.e., obscured nearby solar-mass protostars behind $A_V > 100$, or less obscured proto-brown dwarfs extending into the planetary mass regime). Given its wide spectral grasp (J-M bands simultaneously), GMTNIRS will probe emission lines from a broad range of species, constraining more detailed disk chemistry than has been possible with the narrow wavelength ranges of

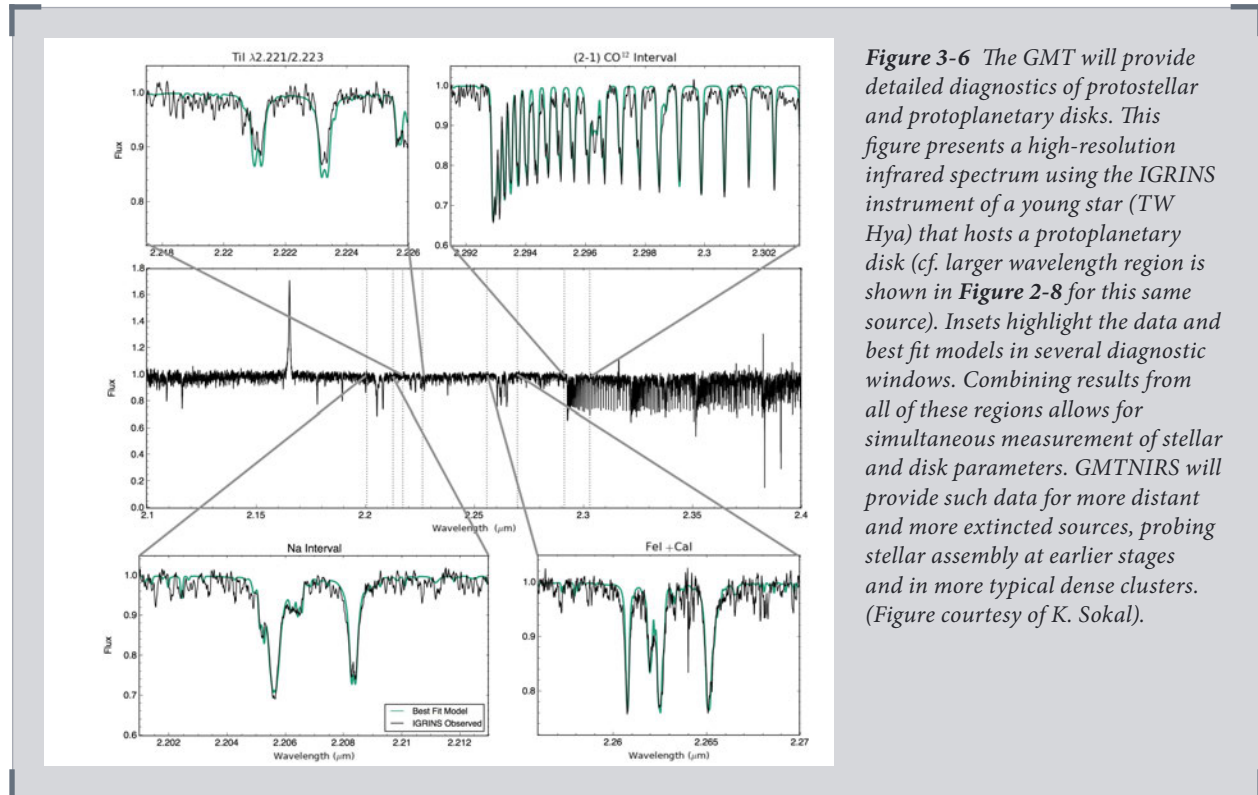


Figure 3-6 The GMT will provide detailed diagnostics of protostellar and protoplanetary disks. This figure presents a high-resolution infrared spectrum using the IGRINS instrument of a young star (TW Hya) that hosts a protoplanetary disk (cf. larger wavelength region is shown in **Figure 2-8** for this same source). Insets highlight the data and best fit models in several diagnostic windows. Combining results from all of these regions allows for simultaneous measurement of stellar and disk parameters. GMTNIRS will provide such data for more distant and more extinguished sources, probing stellar assembly at earlier stages and in more typical dense clusters. (Figure courtesy of K. Sokal).

NIRSPEC or CRIRES (see **Figure 3-6**). Similarly, G-CLEF will offer spectrally resolved observations of the gas emission lines that trace protostellar accretion, achieving S/N \sim 10 per resolution element for continuum in one hour at $r = 22.7$ mag or $F \sim 10^{-17}$ erg s $^{-1}$ cm $^{-2}$ Å $^{-1}$ (a third of the line flux from a free-floating analog to the accreting planetary-mass companion DH Tau b; Zhou et al. 2014). Finally, at later stages with less extinction, GMACS will offer multiplexed measurements of the accretion-dominated UV continuum emission down to the atmospheric cutoff ($\lambda \sim 350$ nm), detecting the UV continuum even for a DH Tau b analog ($u \sim 25$ mag; Zhou et al. 2014) with S/N \sim 5 per resolution element in one hour. This limit is ten times deeper than the corresponding limit for a current cutting-edge instrument like Keck/LRIS, and if coupled with the MANIFEST fiber system, multiplexed GMACS observations would exceed the FOV of LRIS by a factor of 10.

3.3 Fundamental Properties and Evolution of the Youngest Stars (and Substellar Objects)

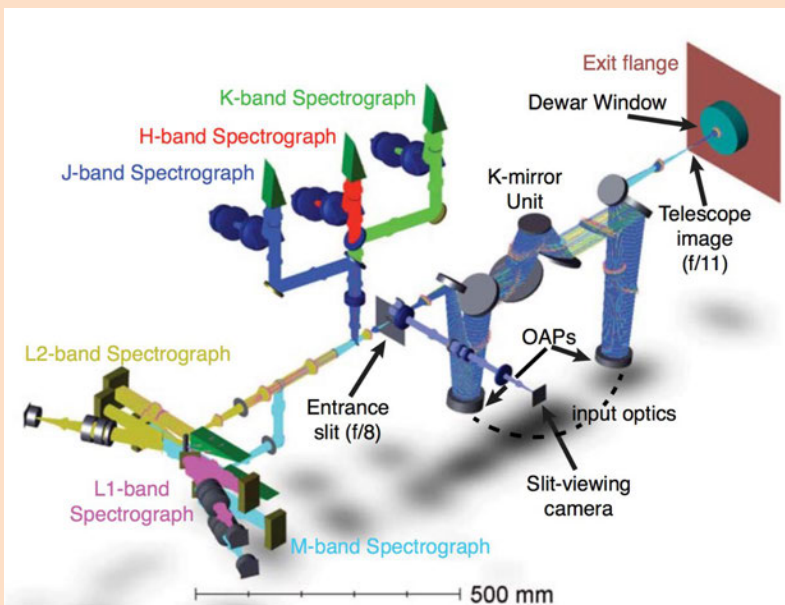
The GMT will open a new window into an unexplored frontier in stellar astrophysics, the properties of the youngest stars. The theoretical framework of stellar evolution is not currently designed to function for the earliest phases of star formation, when the stars are actually being assembled; indeed, these phases break the fundamental axiom of stellar astrophysics that mass is a fundamental constant parameter that determines all other stellar properties, since the mass of a protostar increases as it accretes material from its circumstellar disk and envelope. Stellar evolution theory therefore cannot make accurate predictions about the physical parameters (temperature, luminosity, radius) of protostars without including the complicated mass accretion history as an extra parameter.

Stellar models that include mass accretion (e.g., Baraffe et al. 2015) remain largely unconstrained by observations, since protostars are deeply embedded in surrounding gas and dust, rendering their photospheres very faint and only visible at near-infrared wavelengths. Uncertainties in the accretion history and corresponding entropy evolution of the protostar introduce large uncertainties in the subsequent evolution, potentially adding irreducible scatter to the properties of otherwise-coeval stellar populations. The observations are further complicated by the complex structure of protostars. Early-stage protostars consist of an embryonic central star that is actively growing through accretion of material from its circumstellar disk, which is in turn further embedded in a larger envelope of material, and is simultaneously generating powerful bipolar outflows and jets. The infalling envelope that obscures the central regions introduces additional absorption features.



High Resolution Infrared Spectroscopy

Figure 3-7 With high transmission efficiency and wide spectral coverage, GMTNIRS will be an ideal tool for studying young stars. GMTNIRS is a first generation, single object, high resolution spectrograph that will obtain high resolution spectra over the full near-IR to mid-IR wavelength range in a single exposure (from $\sim 1.15 \mu\text{m}$ to $5 \mu\text{m}$). GMTNIRS is also being designed to work at the best spatial resolutions enabled by GMT's adaptive optics (AO) system, which will help minimize the night sky and thermal backgrounds, resulting in even greater sensitivity for the most challenging observations of faint, dust-enshrouded, low-mass stars (Jaffe et al. 2006, 2016). Credit: GMTNIRS Team



Low resolution ($R \sim 500$) spectroscopic observations have shown protostars to be characterized by featureless continua in the near-infrared. The lack of absorption lines in these observations of the central objects is due to very high veiling (line dilution) caused by strong excess infrared continuum emission from the surrounding protostellar accretion disk and infalling envelope. Such high veiling presents a formidable challenge for probing the photospheres of the central stars, requiring high signal-to-noise, high spectral resolution ($R > 20,000$) observations to detect, resolve, and measure photospheric features. Such observations have shown that numerous photospheric absorption lines, from species such as Fe, Si, Sc, CO, Mg, Al, etc., are detectable in the brightest nearby protostars. This is true for even those that are highly veiled as long as sufficiently high signal-to-noise is achieved (i.e., $S/N \sim 100$). Such observations have already provided the first measurements of the effective temperatures, veiling, surface gravities, rotation rates and radial velocities of some of the nearest known, low mass, protostellar objects (Doppmann et al. 2005, Sokal et al. 2018; **Figure 3-6**). These results demonstrated the potential for such observations to probe protostellar photospheres in the kind of detail achieved previously only for the atmospheres of normal stars.

GMTNIRS will open a new era in protostellar studies by enabling direct near-infrared spectroscopic observations of large numbers of protostellar objects at very high spectral resolution ($R \sim 65,000$ in JHK and $R \sim 85,000$ in LM). Such observations will significantly expand the existing sample of high resolution protostellar spectra. A nearly complete census of protostars within 150 pc of the sun will be possible, doubling the ~ 50 objects with existing measurements. Since one can reach a K magnitude of 18 with a S/N of 10 in one hour of observing time, we expect that more than 200–300 protostellar objects within 500 pc of the Sun can be measured. For example, 200 protostars in the Orion A cloud alone can be detected with $S/N > 10$, and more than 50 with $S/N > 100$. Such observations will provide a statistically robust database of protostellar spectral types or temperatures. It will enable large samples of protostars to be placed on the HR diagram and provide unparalleled information about the growth and evolution of these embryonic stars.

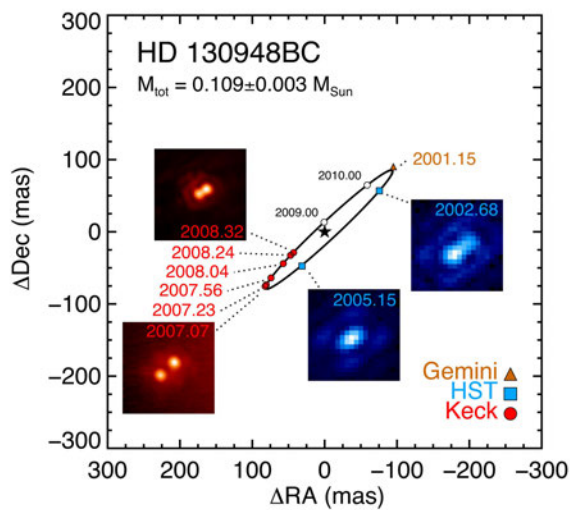


Figure 3-8 The GMT will significantly improve mass estimation techniques for stellar populations. This figure illustrates how direct stellar or sub-stellar masses are obtained using Kepler's Laws, showing the orbit of the nearby, old brown dwarf binary HD 130948BC. Keck (red), HST (blue), and Gemini (gold) relative astrometry from high-resolution imaging are shown, along with the best-fit orbit (Dupuy et al. 2009). Existing telescopes can resolve nearby old brown dwarf binaries with year long orbital periods, but younger solar-mass binaries are in more distant young star-forming regions. As such, current telescopes can only access young brown dwarf binaries, or any planetary-mass binaries, where the orbital periods are instead many decades. The GMT's higher spatial resolution is needed to access such systems with orbital periods of years, yielding direct calibrations of the luminosity and temperature measurements that are used to estimate mass functions for stellar populations.

Finally, the light-collecting power of the GMT will also enable the first detailed characterization of second-order properties (rotation, metallicity, and magnetic field strength) and their impact on stellar parameters. Indeed, these analyses can be conducted for the same objects that act as mass-luminosity-temperature calibrators; GMTIFS and GMTNIRS operate behind AO, so spectra can be obtained for binary components while their masses are also being measured. More generally, sequences of coeval objects will be within range of the GMT's sensitive spectrographs, spanning the entire mass range and at a range of ages. Magnetic field strength may be particularly important for the evolution of fully convective low-mass objects (e.g. Feiden 2016) since their interiors are hot enough to ionize hydrogen, and the charged gas convects less efficiently across magnetic field lines. Existing instruments like IGRINS are already pursuing these measurements for young stars such as TW Hya (Sokal et al. 2018), directly measuring surface magnetic field strengths. The high-dispersion NIR spectra from GMTNIRS will also yield rotation rates (from *vsini*) and the chemical composition of many individual elements (e.g., Veyette et al. 2017). The GMT will usher in a new epoch in the investigation and understanding of the earliest stages of stellar life and in doing so make significant strides toward completing the grand theory of stellar evolution.

3.4 The Most Fundamental Stellar Property: Mass

The GMT will play a central role in measuring the most fundamental property of (sub)stellar objects: mass. It is a maxim of astrophysics that after the end of assembly, the properties and lifecycle of a star, brown dwarf, or planet are largely set by its mass, and those masses are also the fundamental component encoded in the broadest testable feature of star formation models, the IMF. The vast majority of objects in our universe are not amenable to direct mass measurements, so their masses must be inferred by comparing observable properties (such as luminosity or temperature) to the predictions of (sub)stellar evolutionary models. It is therefore important to calibrate the mass predictions of theoretical models by observing stars where the mass can be directly measured, usually from binary system orbits. This need will only become more acute over the next decade. Wide-field surveys with GAIA, HST, and JWST will offer unprecedented demographic censuses of young stellar populations spanning five orders of magnitude (from $>100 M_{\odot}$ to $<1 M_{\text{Jup}}$), and theoretical models will impose systematic uncertainties that completely dominate over Poisson statistics.

The characterization of old, main-sequence field stars is now entering the regime of precision stellar astrophysics, such that models can match observations to within a few percent (e.g. Boyajian et al. 2014; Mann et al. 2015) and are probing the impact of second-order properties like rotation and metallicity. The latest observational campaigns are even enabling the first substantive tests of pre-main sequence stars (e.g., Rizzuto et al. 2015) and old brown dwarfs (Dupuy & Liu 2017; **Figure 3-8**). However, these analyses are running up against the ultimate limits of aperture size ($\lambda/D = 60$ mas for AO imaging on 8 m class telescopes) and Kepler's Law, along with a severe trend that typical binary orbits are dramatically tighter at low masses. Nearly all of the young brown dwarf binaries in the nearest star-forming regions ($D \sim 150$ pc; $M_{\text{tot}} \sim 0.1 M_{\odot}$) and planetary-mass brown dwarf binaries in the field ($D \sim 5$ pc; $M_{\text{tot}} \sim 15 M_{\text{Jup}}$) that are resolvable with current telescopes have orbital periods of many decades. Only a handful of unique measurements are available from eclipsing systems (e.g., Stassun et al. 2005) and one or two fortuitous planetary-mass binaries among our closest neighbors (e.g. Best et al. 2017).

The dramatically sharper resolution of diffraction-limited GMT imaging will

unlock entire samples of these objects. From Kepler's Law, a factor of 3 increase in resolution will open up systems with orbital periods that are 5 times shorter. After considering inclination effects, an 8 m telescope observing a pair of $5 M_{\text{Jup}}$ brown dwarfs at 15 parsecs could only measure orbits with a ~ 2 AU and $P > 25$ years, and few such systems even exist. In contrast, the GMT could resolve a 0.6 AU binary that completes its orbit in only 5 years. Such observations will be straightforward with adaptive optics and a near-infrared camera such as the guiders for GMTIFS or GMTNIRS. Even in the more distant young star-forming regions, dynamical masses will become accessible down to a few tens of Jupiter masses, enabling direct calibration of the luminosity-mass relation that underlies every IMF measurement. The GMT will revolutionize the characterization of substellar and planetary properties, unlocking the full impact of the vast number of IMF studies over the coming decades.

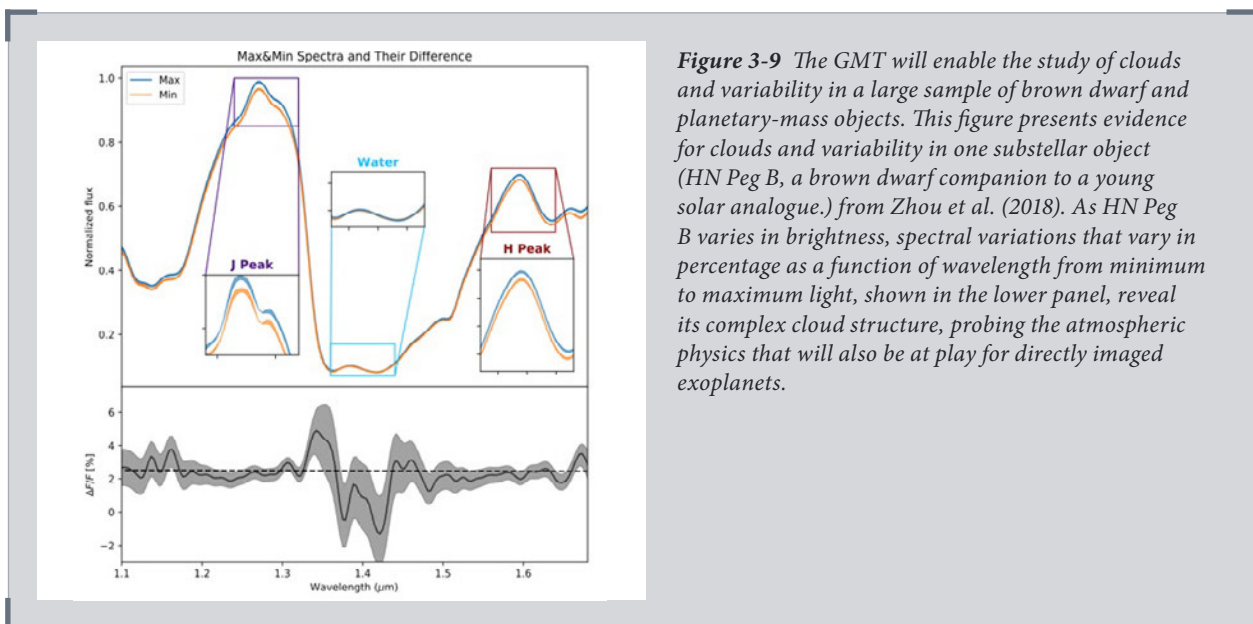


Figure 3-9 The GMT will enable the study of clouds and variability in a large sample of brown dwarf and planetary-mass objects. This figure presents evidence for clouds and variability in one substellar object (HN Peg B, a brown dwarf companion to a young solar analogue.) from Zhou et al. (2018). As HN Peg B varies in brightness, spectral variations that vary in percentage as a function of wavelength from minimum to maximum light, shown in the lower panel, reveal its complex cloud structure, probing the atmospheric physics that will also be at play for directly imaged exoplanets.

3.5 The Formation and Evolution of Substellar Objects

The GMT will cast new light on the provenance and properties of the lowest-mass objects formed via the typical star formation pathway. While such objects are typically called brown dwarfs, free-floating planetary mass objects may also form in the same way. Old, cold brown dwarfs provide a tremendous lever arm on models of both star formation and the atmospheres of substellar (and planetary) objects. Our understanding of the detailed physics has been driven very much by discovery, as models of star formation and atmospheres have proven so tremendously complex that they have had minimal predictive power. New data have been critical in driving new models and new understanding.

Development in this field has taken place through a series of ‘quantum leaps’ over the last two decades, with every leap being powered by new discoveries arising from new large surveys. Starting with the discovery of L- and T-dwarfs with $T_{\text{eff}} \sim 1,800 -$

1,000 K by large near-infrared sky surveys in the 1990's (2MASS, DENIS), along with the SDSS optical sky survey, followed by the discovery of a class of very cold T dwarfs with T_{eff} down to 600 K by the UKIDSS survey in the 2000's. The latest leap in this field has been powered by the NASA *WISE* mission which (as well as uncovering thousands of previously unknown L and T dwarfs), discovered the first examples of the next coolest class—the Y dwarfs with T_{eff} as low as 300–400 K (Cushing et al. 2011; Kirkpatrick et al. 2012). We should expect that by the time the GMT goes into service, we will have discovered—but be unable to study in detail—further examples of Y dwarfs at temperatures below 200 K at J magnitudes fainter than 24–25.

The GMT will open fundamentally new observational windows into the complex physics of brown dwarfs, driven by the quantum leap in near-infrared imaging and spectroscopy of faint objects.

Imaging and astrometry of the coldest brown dwarfs

Currently the coldest known Y dwarfs detected by WISE remain extraordinarily difficult to study at $J=23-25$, $H=24-26$ and $K>25$. The combination of diffraction-limited images and a 7 times larger aperture than an 8 m telescope, will make high quality photometric imaging of these faintest Y dwarfs possible. Moreover, it will make possible both variability searches (for the signatures of rotational

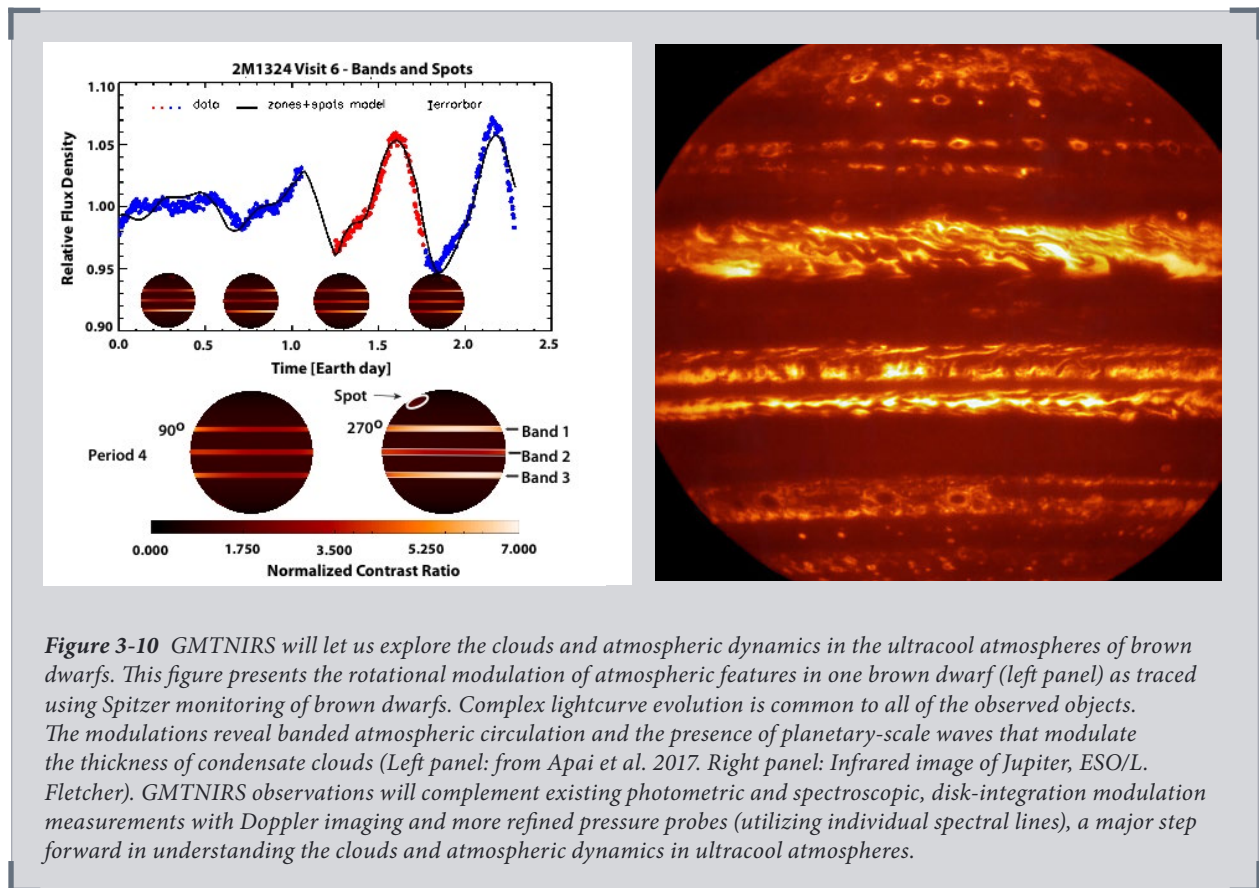


Figure 3-10 GMTNIRS will let us explore the clouds and atmospheric dynamics in the ultracool atmospheres of brown dwarfs. This figure presents the rotational modulation of atmospheric features in one brown dwarf (left panel) as traced using Spitzer monitoring of brown dwarfs. Complex lightcurve evolution is common to all of the observed objects. The modulations reveal banded atmospheric circulation and the presence of planetary-scale waves that modulate the thickness of condensate clouds (Left panel: from Apai et al. 2017. Right panel: Infrared image of Jupiter, ESO/L. Fletcher). GMTNIRS observations will complement existing photometric and spectroscopic, disk-integration modulation measurements with Doppler imaging and more refined pressure probes (utilizing individual spectral lines), a major step forward in understanding the clouds and atmospheric dynamics in ultracool atmospheres.

modulations due to heterogeneous atmospheres) and astrometry (to measure parallax measurements of the distances to these targets). Diffraction-limited images of these targets in the near-infrared will resolve the sky out to the extent that JWST will offer no significant background performance improvement, while the GMT will deliver substantially more photons due to its larger aperture.

Spectroscopy of the coldest brown dwarfs

Similarly, GMTIFS will offer a quantum leap in moderate resolution spectroscopy ($R=5,000-10,000$) for faint targets. These are the resolutions required to make the detailed studies of the molecular contents of the photospheres of the coldest ($T < 200$ K) brown dwarfs (**Figure 3-9**; Zhou et al. 2018), which will have J magnitudes fainter than 24–25. When it goes into operation GMTIFS will be unique in being able to observe these targets, and obtain spectra of the quality required to determine molecular abundances for the complex molecular soup in these atmospheres—including (among other things) CH_4 , CO , NH_3 plus H_2O ice clouds, sulfide salts and almost certainly a host of other species we have not yet predicted.

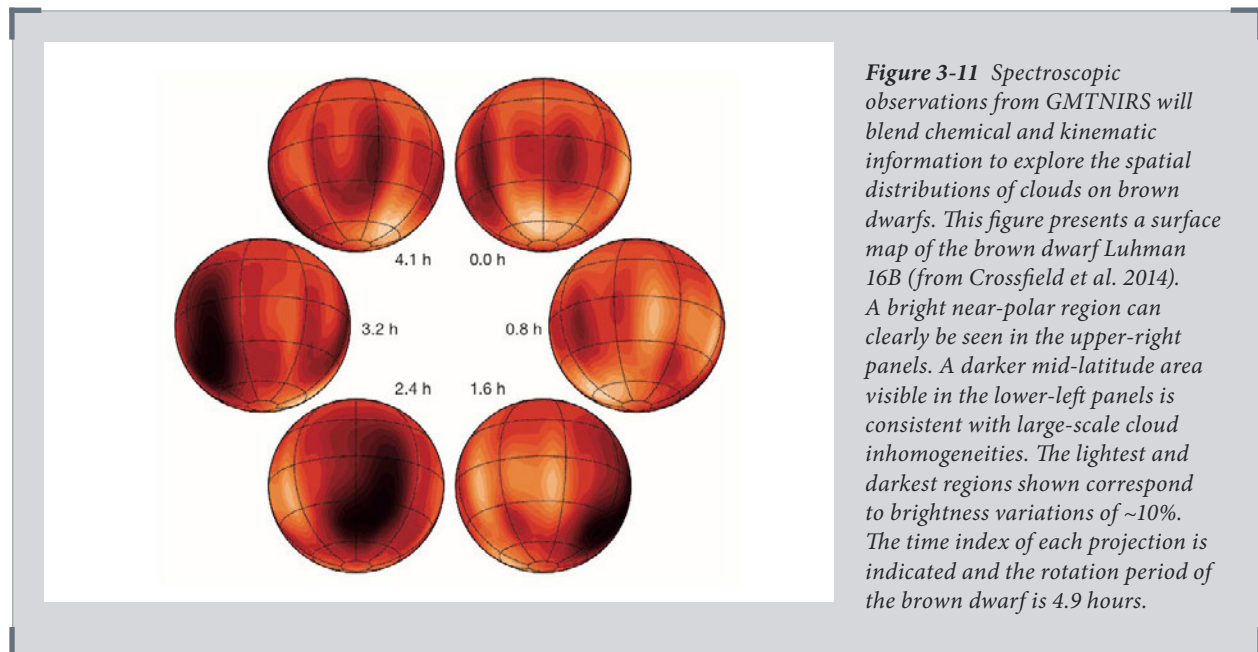


Figure 3-11 Spectroscopic observations from GMTNIRS will blend chemical and kinematic information to explore the spatial distributions of clouds on brown dwarfs. This figure presents a surface map of the brown dwarf Luhman 16B (from Crossfield et al. 2014). A bright near-polar region can clearly be seen in the upper-right panels. A darker mid-latitude area visible in the lower-left panels is consistent with large-scale cloud inhomogeneities. The lightest and darkest regions shown correspond to brightness variations of $\sim 10\%$. The time index of each projection is indicated and the rotation period of the brown dwarf is 4.9 hours.

Cloud mapping on brown dwarfs

Condensate clouds represent one of the most significant challenges to understanding the evolution and properties of exoplanets as well as brown dwarfs. The presence of condensate clouds impact the atmospheric opacity and the thermal evolution of substellar objects, significantly complicating the determination of the substellar initial mass function in star-forming regions. Time-resolved, high-precision observations (photometry and spectroscopy) of rotating heterogeneous atmospheres result in modulations of the emitted light: brightness, color, broad-band spectra and spectral line shapes all change as atmospheric patches of different composition and temperature rotate in and out of the visible hemisphere. Over the past five years, pioneering time-domain observations revealed an exciting picture of ultracool atmospheres. Multiple surveys showed that most, if not all, brown dwarfs have

heterogeneous cloud cover (Buenzli et al. 2014, Metchev et al. 2015; **Figure 3-10**); that these cloud covers are characterized by varying thickness and temperature (Radigan et al. 2012, Apai et al. 2013). Most of the cloud properties observed in these field objects should also be present in directly imaged exoplanets. This implies that simple, one-dimensional modeling of exoplanet atmospheres is missing important physics.

Current high-precision, space-born observations are limited by low spectral resolution ($R \sim 100$) and relatively small apertures, explaining why current studies focus on T2 and earlier type objects.

GMTNIRS will complement the wealth of low-resolution, high-precision, disk-integrated photometry/spectroscopy with spectrally resolved information (i.e., Doppler imaging). An exciting example of what this technique will be capable of is provided by the very-high-resolution infrared spectrograph CRIRES on the VLT, which sampled atmospheric brightness distributions on one of the components in the bright brown dwarf binary Luhman 16AB (Crossfield et al. 2014; **Figure 3-11**). These pioneering Doppler imaging observations of an ultracool atmosphere were made possible by the high near-infrared resolution of CRIRES and the brightness of the target (which is only 2 pc away from the Sun). The higher spectral resolution observations with GMTNIRS will provide more precise constraints on brown dwarf atmospheres by complementing existing disk-integrated spectroscopic modulations with line profile modulations. Bright L- and T-type brown dwarfs, for which these observations are currently impossible, will be accessible with the GMT.



Synergy with ALMA

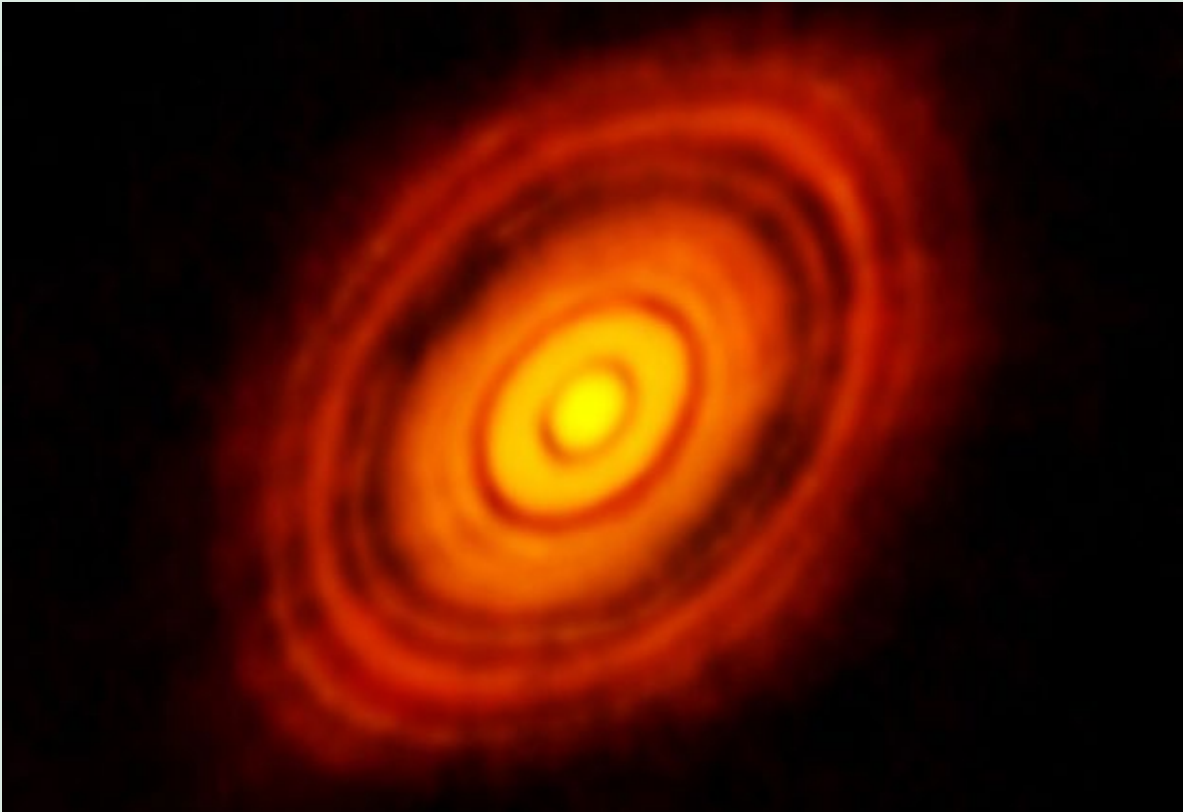
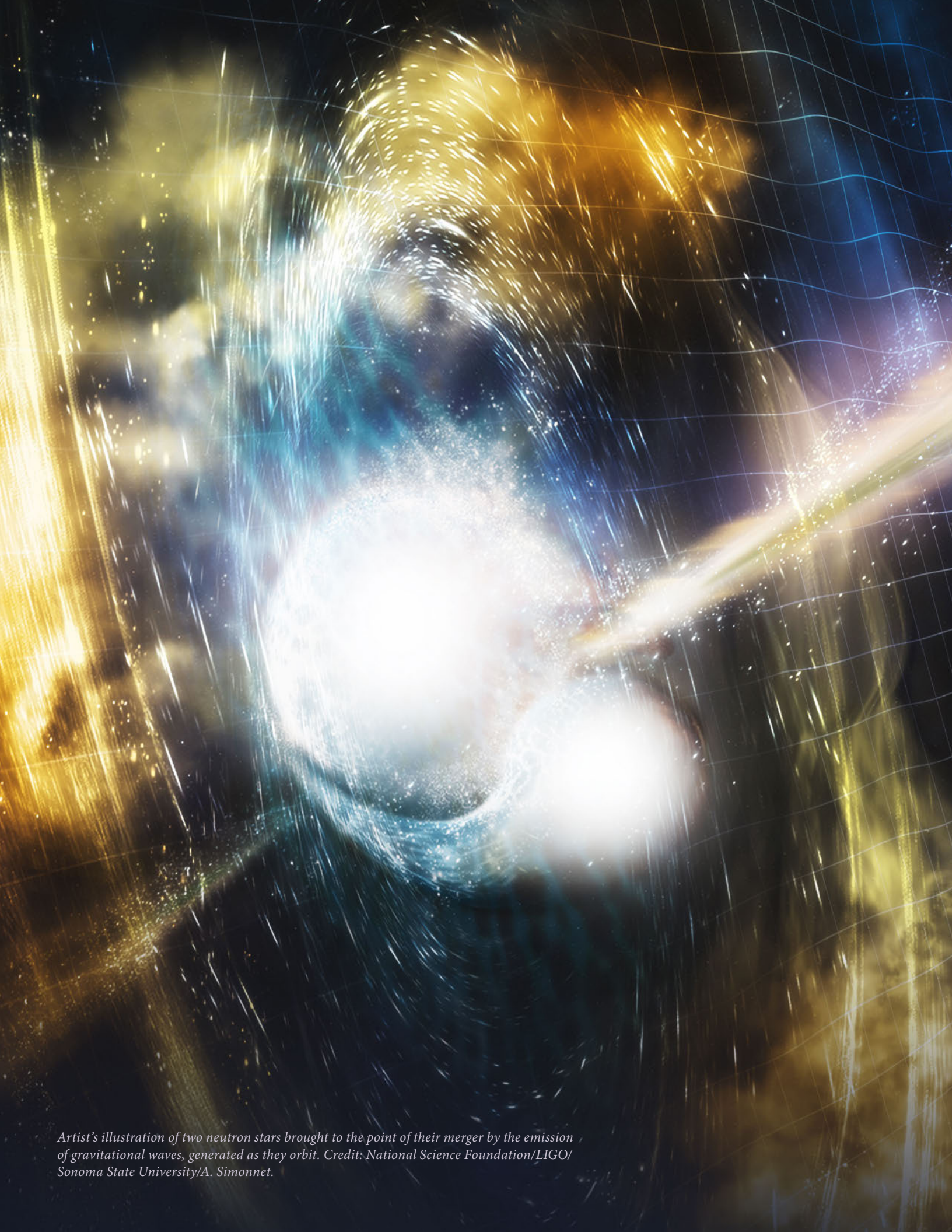


Figure 3-12 ALMA image of the disk around HL Tau, a <1 Myr old star located about 150 parsecs away. ALMA has detected its circumstellar disk and identified a complicated series of rings and gaps, while lower-resolution observatories have also seen an extended envelope of material that will eventually accrete onto the star. The gaps may reflect planet formation and the innermost gap corresponds to about 10 AU (ALMA Collaboration et al. 2015). The GMT will complement ALMA observations by probing the inner regions of disks like this one, and thus warmer dust and gas than ALMA.

Gas and dust are the input substances for stars and planets. Stars and planets are best probed by optical and near-infrared observations, while the initial conditions are best probed by long wavelengths, around a millimeter. In the GMT era, ALMA will have mapped regions of star formation in great detail, providing information on gas temperature, density, velocity, chemical abundances, and magnetic fields. Observations with the GMT will provide a large database of stellar and planetary properties. Together, these will provide deep insights into the processes involved. On the scales of star-forming regions, the motions of young stars can be compared to the motions of the gas flows to study how material reaches a star. ALMA observations of Keplerian rotation around single young stars will measure their masses. Combining these with dynamical masses of binary systems and with accurate stellar properties for all stars from the GMT will enable calibration of models of how young stars evolve. Comparison of structures and composition in disks to the nature of exoplanets will constrain models of planet formation and the availability of biogenic compounds. ALMA images of gaps and rings in disks and detection of complex organic molecules in disks (Oberg et al. 2017) will complement the studies of the star and disk in the near-infrared with the GMT.

References

- Apai, D., Karalidi, T., Marley, M.S., et al. 2017, *Science*, 357, 683
- Bate, M.R. 2009, *Monthly Notices of the RAS*, 392, 590
- Baraffe, I., Chabrier, G., & Gallardo, J. 2009, *ApJ Letters*, 702, L27
- Baraffe, I., Homeier, D., Allard, F., & Chabrier, G. 2015, *Astron & Astrophys*, 577, A42
- Best, W.M.J., Liu, M.C., Dupuy, T.J., & Magnier, E.A. 2017, *ApJ Letters*, 843, L4
- Boyajian, T.S., van Belle, G., & von Braun, K. 2014, *AJ*, 147, 47
- Bressert, E., Bastian, N., Gutermuth, R., et al. 2010, *Monthly Notices of the RAS*, 409, L54
- Brown, J.M., Pontoppidan, K.M., van Dishoeck, E.F., et al. 2013, *ApJ*, 770, 94
- Crossfield, I.J.M., Biller, B., Schlieder, J.E., et al. 2014, *Nature*, 505, 654
- Cushing, M.C., Kirkpatrick, J.D., Gelino, C.R., et al. 2011, *ApJ*, 743, 50
- Da Rio, N., Tan, J.C., Covey, K.R., et al. 2017, *ApJ*, 845, 105
- Doppmann, G.W., Greene, T.P., Covey, K.R., & Lada, C.J. 2005, *AJ*, 130, 1145
- Dupuy, T., Liu, M. & Ireland, M. 2009, *ApJ*, 692, 729
- Dupuy, T. & Liu, M. 2017, *ApJS*, 231, 15
- Feiden, G.A. 2016, *Astron & Astrophys*, 593, A99
- Gullbring, E., Hartmann, L., Briceno, C., & Calvet, N. 1998, *ApJ*, 492, 323
- Herczeg, G.J., Cruz, K.L., & Hillenbrand, L.A. 2009, *ApJ*, 696, 1589
- Hillenbrand, L.A., & Hartmann, L.W. 1998, *ApJ*, 492, 540
- Jaffe, D.T., Mar, D.J., Warren, D., Segura, P.R., 2006, *Proc. SPIE*, 6269, 4IJ
- Jaffe, D.T., Barnes, S., Brooks, C., Lee, H., Mace, G., Pak, S., Park, B.-G., Park, C., 2016, *Proc. SPIE*, 9908, 21J
- Kirkpatrick, J.D., Gelino, C.R., Cushing, M.C., et al. 2012, *ApJ*, 753, 156
- Koenigl, A. 1991, *ApJ Letters*, 370, L39
- Lada, C.J., & Lada, E.A. 2003, *Annual Reviews of Astron & Astrophys*, 41, 57
- Lada, C.J., Lombardi, M., & Alves, J.F. 2010, *ApJ*, 724, 687
- Mann, A.W., Feiden, G.A., Gaidos, E., Boyajian, T., & von Braun, K. 2015, *ApJ*, 804, 64
- Muzerolle, J., Calvet, N., & Hartmann, L. 2001, *ApJ*, 550, 944
- Natta, A., Testi, L., Muzerolle, J., et al. 2004, *Astron & Astrophys*, 424, 603
- Oberg, K.I., Guzman, V.V., Merchantz, C.J., et al. 2017, *ApJ*, 839, 43
- Offner, S.S.R., Clark, P.C., Hennebelle, P., et al. 2014, *Protostars and Planets VI*, 53
- Offner, S.S.R., Hansen, C.E., & Krumholz, M.R. 2009, *ApJ Letters*, 704, L124
- Rizzuto, A.C., Ireland, M.J., & Kraus, A.L. 2015, *Monthly Notices of the RAS*, 448, 2737
- Salyk, C., Blake, G.A., Boogert, A.C.A., & Brown, J.M. 2011, *ApJ*, 743, 112
- Stassun, K.G., Mathieu, R.D., Vaz, L.P.R., Valenti, J.A., & Gomez, Y. 2005, *Protostars and Planets V*, 1286, 8628
- Tobin, J.J., Hartmann, L., Furesz, G., Mateo, M., & Megeath, S.-T. 2009, *ApJ*, 697, 1103
- Sokal, K.R., Deen, C.P., Mace, G.N., et al. 2018, *ApJ*, 853, 120
- van 't Hoff, M.L.R., Tobin, J.J., Harsono, D., & van Dishoeck, E.F. 2018, *arXiv:1803.04515*
- Veyette, M.J., Muirhead, P.S., Mann, A.W., et al. 2017, *ApJ*, 851, 26
- White, R.J., & Hillenbrand, L.A. 2004, *ApJ*, 616, 998
- Wright, N.J., & Mamajek, E.E. 2018, *Monthly Notices of the RAS*, 476, 381
- Zhou, Y., Herczeg, G., Kraus, A., Metchev, S. & Cruz, K. 2014, *ApJ*, 783, 17
- Zhou, Y. et al. 2018, *AJ*, 155, 132



Artist's illustration of two neutron stars brought to the point of their merger by the emission of gravitational waves, generated as they orbit. Credit: National Science Foundation/LIGO/Sonoma State University/A. Simonnet.

The Death of Stars

How do stars die? For most of the life of a star, nuclear fusion deep in the star's core generates pressure and releases energy. Often, when a star has used up most of its fuel, the unrelenting force of gravity causes the star to collapse under its own weight. Paradoxically, this can lead to a supernova, a gigantic explosion, which can leave behind an exotic, small, dense central object, such as a neutron star or even a black hole. If two black holes or neutron stars end up orbiting each other, they can collide, sending gravitational ripples across the cosmos and creating a powerful explosion called a kilonova, which is also bright in visible light. Other stars explode leaving no remnants behind, but providing signposts to measure the age and fate of the universe itself.

Perhaps most importantly, the death of stars generate all the chemical elements vital for life: these elements are among the debris that is cast back into space when the dying star explodes. The GMT will probe the physics of the vast diversity of stellar explosions throughout the cosmos. With it, we will learn the detailed nature of the stars that explode, their galactic environments, and the relationships between the different types of exploding, transient sources we can see.

Chapter Authors

Rafaella Margutti (Northwestern University)

Dan Milisavljevic (Purdue University)

Maryam Modjaz (New York University)

Nathan Smith (University of Arizona)

Sung-Chul Yoon (Seoul National University)

J. Craig Wheeler (The University of Texas at Austin)

4 The Death of Stars

We see the death of stars when they explode in supernova or kilonova explosions that release enough light and energetic particles that they can be seen across the universe. The history of the star's life, the nature of its death, and its frequently flamboyant remains leave a signature in this light and energy. The GMT's great gains in sensitivity relative to the last generation of telescopes will enable us to extract a much clearer picture of stellar evolution from these signatures than has ever been possible before. The GMT will allow us to acquire detailed spectra at the onset of the stellar explosions, when only their faint outer layers are visible, and at the endpoint of the explosion, when the inner structure and composition of the star is revealed.

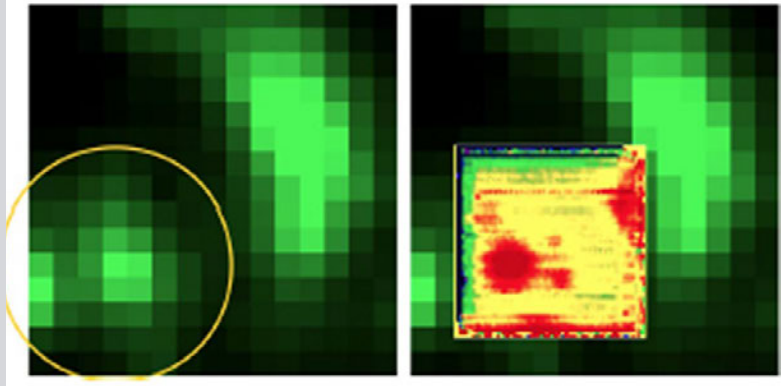
The first detailed studies of supernova explosions were made by Baade and Zwicky in the 1930's. For most of the subsequent 80 years, the study of supernovae has been gated by the pace of their discovery. Recently, searches for transient events have become increasingly efficient with the application of robotic telescopes that scan wide swaths of the sky to faint limits at a rapid cadence. These searches will generate an ample supply of candidates for study with the GMT.

Our research is driven by two fundamental questions:

1. What is the evolutionary history of the various kinds of supernovae that we observe? In general, we know that there is more than one pathway: supernovae with evidence of little or no hydrogen likely result from a white dwarf accreting matter from a companion in a binary system, while hydrogen-rich supernovae likely result from collapse of a massive star with an iron-rich core. Much more evidence is needed to support and complete this basic picture to fully understand what the supernovae progenitors are. For example, gamma-ray bursts have been detected that are likely to be associated with especially energetic, hydrogen-deficient supernovae, which may be the result of partially-exploded white dwarfs. Also, super-luminous supernovae have now been observed that push the limit of the massive-star scenario.
2. What determines the nature of the remnants (black hole or neutron star) left behind when a star goes supernovae. For example, why do some of the neutron star remnants appear as pulsars with high angular momentum, like in the Crab Nebula, while some are highly magnetic "magnetars" (neutron stars with the strongest magnetic fields known, up to 1 quadrillion Gauss).

The GMT will enable the kinds of observations that will help us understand the precursors and remnants of supernovae. Because the material in stellar explosions moves at high velocities, broadening the spectral lines that reveal the chemical composition of this material, diagnostic observations depend on high sensitivity, rapid acquisition, and broad spectral coverage. Infrared observations in particular will allow us to detect additional spectral features associated with hydrogen, helium, iron-peak elements, and molecules. The GMT's greatly enhanced angular resolution will also help separate the light of the dying star and its local environment from the complex background light of the star's parent galaxy (see *Figure 4-1*). With up to 0.01 arcsecond resolution at 1 μm , infrared observations on the GMT would allow us to probe the host galaxies of transients at high spatial resolution (~ 50 pc) when the Universe was only 600 million years old.

Figure 4-1 The GMT's extraordinary spatial resolution will bring into view the galactic environments of distant supernovae that will enable us to understand the precursors and remnants of supernovae. The left panel contains the optical light image of a supernova site. The supernova position is indicated inside the 2 arcsecond radius circle. The image spans 220 parsecs on a side. The right panel shows the same region observed with a higher resolution infrared image superposed obtained on the 8 m VLT telescope in Chile (Kuncharayakti et al. 2015). The single cluster in the lower resolution optical image is resolved into multiple clusters. The GMT will offer nearly 20 times the spatial resolution of this optical image (and 4 times that of the VLT image).



In this chapter, we survey the range of topics in this area that are likely to be at the forefront during the first decade of GMT observations. We explore the exciting new window into astrophysics and cosmology brought by the advent of gravitational wave astronomy and survey progenitors and remnants of a variety of transients, including thermonuclear explosions, core-collapse supernovae, and rare types of transients. We also discuss the transient events that may appear among the first stars after the end of the cosmic Dark Ages, and describe the compact and extended remnants left behind in the death of stars. Finally, we examine tidal disruption events in which stars are tidally destroyed but reveal the presence of supermassive black holes that would otherwise remain undetected, and provide a summary of the capabilities of the GMT to explore these topics, summarizing the key GMT capabilities, proposed observations, and the challenging open questions.

4.1 Optical and NIR Counterparts of Gravitational Wave Sources

The GMT will make major contributions to particle and gravitational wave multi-messenger¹ astronomy with its large aperture and sensitive optical (GMACS) and near infrared (NIRMOS, GMTIFS) spectrographs.

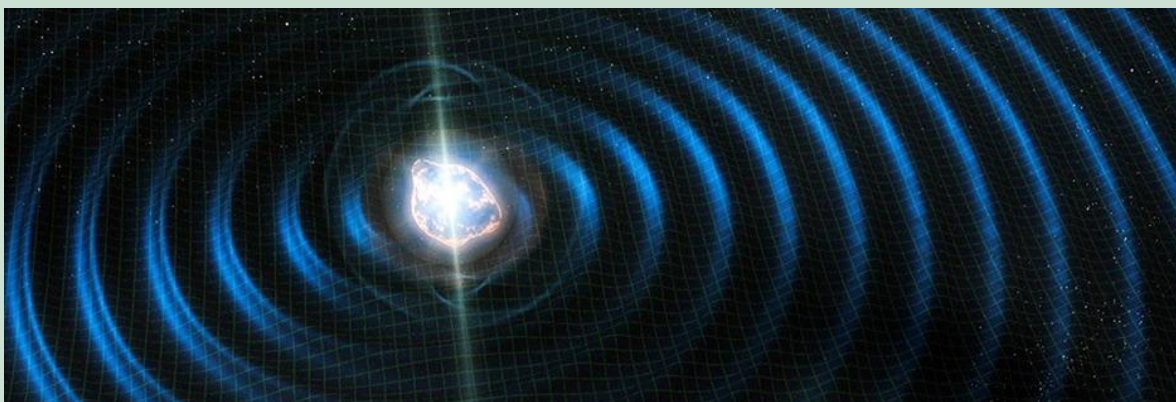
Gravitational wave astronomy became a reality with the recent detections of gravitational waves (GW) from merging stellar mass black holes (Abbott et al. 2016) and neutron stars (Abbott et al. 2017). While the observations of high-mass black hole mergers seriously challenge stellar evolution theory in a manner that may be explored by the GMT, these mergers give no transient electromagnetic event to which the GMT could contribute observations. BH-BH mergers are not expected to produce electromagnetic emission under standard circumstances, and the BH-BH mergers

¹ One of NSF's Ten Big Ideas, "Windows on the Universe: The Era of Multi-Messenger Astrophysics" speaks to the synthesis of observations, datasets, and techniques across disciplines to make progress on astrophysical questions. https://www.nsf.gov/news/special_reports/big_ideas/universe.jsp

found so far from their GW emission have not been detected in the electromagnetic spectrum. Neutron star mergers, on the other hand, were predicted to produce optical and IR events. This prediction was fulfilled on August 17, 2017, with the first detection of electromagnetic signals from a binary neutron star merger detected first by GW. The study of the emission of light from binary neutron star mergers and neutron star black hole mergers will undoubtedly be a major topic of research for decades to come, and one for which the GMT is ideally suited (see *Figure 4-2*).

Synergy with Gravitational Wave Telescopes—LIGO

Figure 4-2 *The LIGO Observatory (top) and artists' impressions of gravitational wave events. With spectrographs providing high throughput, high spectral resolution, and high spatial resolution across the optical to mid-IR spectrum (G-CLEF, GMTNIRS, and GMTIFS), the GMT will play a leading role in the follow-up of gravitational wave sources. The first detection of the infinitesimal "vibrations" of space itself that come from the merger of two neutron stars (lower left) was a monumental achievement in 2017, long ago predicted by the General Theory of Relativity. To reach the full potential of gravitational astronomy—to study how the heavy elements are born in the hugely energetic merger—observations of electromagnetic counterparts are indispensable (lower right). In the GMT era when LIGO (US and India), Virgo (Italy), and KAGRA (Japan) become fully operational, the positions of gravitational wave events in the sky will be determined with an accuracy of 10–100 square degrees. Precise localization of gravitational wave sources will still be made only with their electromagnetic radiation. The GMT will be key to identifying and studying these powerful, exotic events in visible and infrared light. (Image credits: LIGO—Caltech/MIT/LIGO Lab, Neutron stars colliding—Robin Dienel/Carnegie Institution for Science, Gravitational Waves—Fermilab).*



The GW “chirp” that heralded the binary neutron star merger event GW170817 was followed 1.7 seconds later by a flare of gamma-rays attributed to the outward propagation within the binary neutron star ejecta of a magnetic jet that was launched in the merger event. The optical/IR counterpart was first detected 10.9 hours later and followed by a host of ground-based and space-based observatories for the following days and months, which detected the electromagnetic counterpart to GW170817 across the spectrum from X-rays to radio (Abbott et al. 2017).

The GMT Can Address the Variation of NS-NS and BH-NS with Larger Samples: Most of the major properties of GW170817 were predicted by models and extrapolated from the properties of short, hard gamma-ray bursts (see Berger 2014 for a review) or inferred from theoretical studies (Metzger 2017). The merger of two neutron stars or a neutron star with a black hole was expected to be accompanied by the ejection of a small amount of mass ($M_{\text{ej}} = 10^{-4} - 10^{-2} M_{\odot}$) at high velocity ($v_{\text{ej}} = 0.1 c - 0.3 c$) that would in turn produce optical or NIR transients of relatively low bolometric luminosity ($L_{\text{bol}} \sim 10^{41}$ erg/s) and short characteristic time ($\sim 1 - 8$ d) compared to a typical supernovae. These events have been labeled kilonovae or macronovae. While the inferred mass of the binary neutron star ejecta was larger than expected and the inferred velocities are on the high end of the theoretical predictions, GW170817 fulfilled these expectations reasonably well.

The ejecta of neutron star mergers were expected to be major sources of r-process elements, the decay of which is the power source of kilonovae. Numerical simulations indicated that the matter ejected along the equator should contain neutron-rich lanthanide elements ($A > 130$) that make the opacity very high ($\kappa \approx 10 \text{ cm}^2 \text{ g}^{-1}$; Kasen et al. 2017). The high opacity was expected to make kilonovae intrinsically red (red kilonovae), with a characteristic time of a week. Given the very high ejecta velocity, the expected extremely large number of spectral lines would be highly broadened and blended and the spectrum nearly featureless without any prominent absorption lines. If the ejecta were lanthanide-free, the corresponding emission would be blue (blue kilonovae), with a duration of only about a day. GW170817 showed an early blue continuum followed by a later red continuum, suggesting that outer material was rather lanthanide poor, and that inner material was lanthanide rich (*Figure 4-4*).

Winds, Jets, and What the GMT Could Help Us Learn with Super-Fast Follow-up: Another important component of a kilonova is the expected mass outflow from the disk around the central remnant. The mass of the wind ejecta would be comparable to that of the dynamical ejecta, but the average velocity is expected to be much lower ($v = 0.01 c - 0.1 c$). The chemical composition of this disk wind may be lanthanide-free if the merged neutron star lifetime is sufficiently long (> 300 ms) in case of a neutron star merger or if a black hole produced in the merger is rapidly spinning. The corresponding wind emission with $L \sim 10^{41}$ erg/s would be blue and optically bright compared to that of the merger-ejected matter. Given the relatively low ejecta velocity, many absorption lines may be discernible in the spectra. The wind emission may be obscured by the lanthanide-rich dynamical ejecta that is expanding ahead with a higher velocity, unless the viewing angle is toward the polar region of the ejecta.

Other possible features of kilonovae that could be explored with the GMT include a re-brightening due to late-time injection of energy from the long-lived central engine (a magnetar or fallback accretion onto a black hole) and a UV-bright and blue precursor ($L \sim 10^{41}$ erg/s) of a few hours due to free neutron decay in the rapidly expanding outermost layers ($M \sim 10^{-5} M_{\odot}$, and $v \gtrsim 0.4c$) of the merger ejecta along the polar direction. This will require very fast response and that will challenge even the GMT.

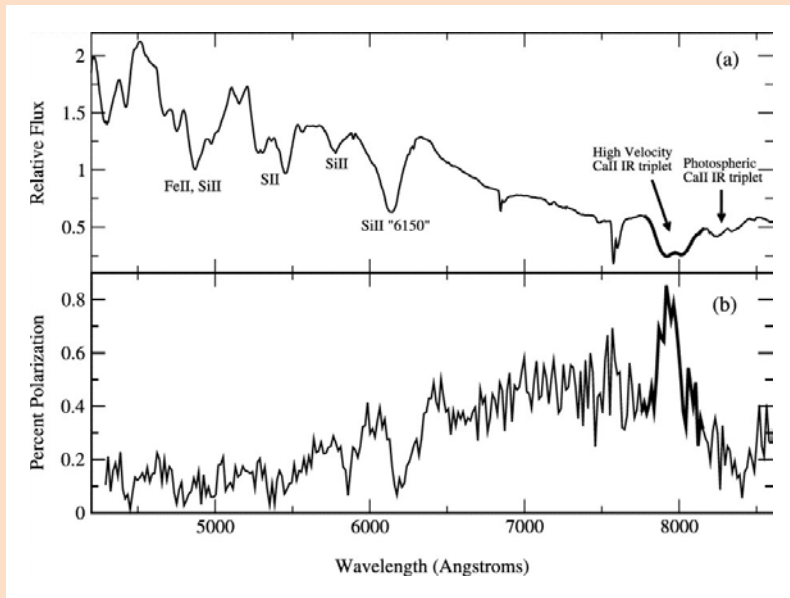
Multi-Messenger Astrophysics and the GMT: The joint detection of GW and light from the binary neutron star merger GW170817 opened the era of multi-messenger GW astronomy. After GW170817, the remaining major open questions are deeply connected to the *diversity* of transients from NS-NS mergers, whether neutron stars or black holes survive the merger, how the properties of BH-NS mergers differ, and how these properties relate to the properties of the progenitor systems.

The very large collecting area and spectral coverage of the GMT will allow us to follow up the much larger population of kilonova transients at larger distances. In addition, the GMT will enable us to map the later-time spectral evolution of the kilonova emission into the nebular phase. Spectroscopy during this late, optically-thin phase can reveal the interior, as it does for supernovae (see *Section 4.2*).



Aspirational Technique—Spectropolarimetry

Figure 4-3 Spectropolarimetry, measuring the polarization of light as a function of wavelength, such as in this figure from Kasen, et.al. (2003) of the Type Ia Supernova 2001el, is a technique which allows the inference of three dimensional information from angularly unresolved objects by using not only the flux of the object at each wavelength, but also the amount of polarization as well. Reflected light is polarized, and if it is observed from objects or surfaces that are not circularly symmetric, will provide information that can be reconstructed into a three dimensional geometry as inferred from detailed computational models. In the case above the absorption feature of Ca II at high velocity is inferred to be produced by a dense clump in the ejecta moving rapidly toward the observer.



The ability to explore an explosion in three dimensions (not just projected in the plane of the sky from our perspective) gives powerful constraints on the physics of stellar explosions. With standard techniques of photometry and spectroscopy, we can study the 3D structure of explosions only in the case of nearby young supernovae remnants. For more distant events, the vast majority of the targets of this enterprise, the only practical way to glean any information about geometrical structure is through spectropolarimetry. Combined with line-of-sight Doppler shifts, spectropolarimetry yields information on the 3D structure of an explosion for which the direct aspect is only a point of light. Only spectropolarimetry can resolve different chemical structures blown off at different angles, a critical clue to the nature of the underlying explosion or perhaps the interaction with a neighboring star. All the transients discussed here would benefit from high-cadence spectropolarimetry. In the next generation of telescopes, the GMT may be the only one with this capability because its optical design facilitates the use of wide-field spectrographs fed directly by the telescope's secondary mirror. A low-resolution spectrograph like GMACS can readily be designed to include this spectropolarimetry, which is critical not only for exploding stars but a host of other areas of modern astrophysics.

At this phase, the emitting material is moving more slowly, and the resulting emission lines will suffer less line blending. Rather than “normal” supernova composition, however, these observations will allow us to probe the composition and velocity structure of material that once resided in neutron stars.

More distant NS mergers and the nebular spectra of events like GW170817 are out of the reach of current facilities. Spectral studies of future kilonovae with the GMT, more distant and deeper, will thus be important to probe the diversity of nucleosynthesis of binary NS and NS-BH mergers. Future detections of GWs from NS-NS and NS-BH mergers would also provide strong constraints on the equation of state of neutron stars and on massive binary star evolution.

4.2 Supernovae

With its large aperture and sensitive optical and near infrared imager spectrographs, the GMT will be a powerful tool for understanding supernovae. GMACS and NIRMOS will be especially powerful both shortly after and long after the explosion, when supernovae are dim and traditionally hard to observe on current 8 – 10 m class telescopes. Their spectra in these faint, late time phases are particularly important for

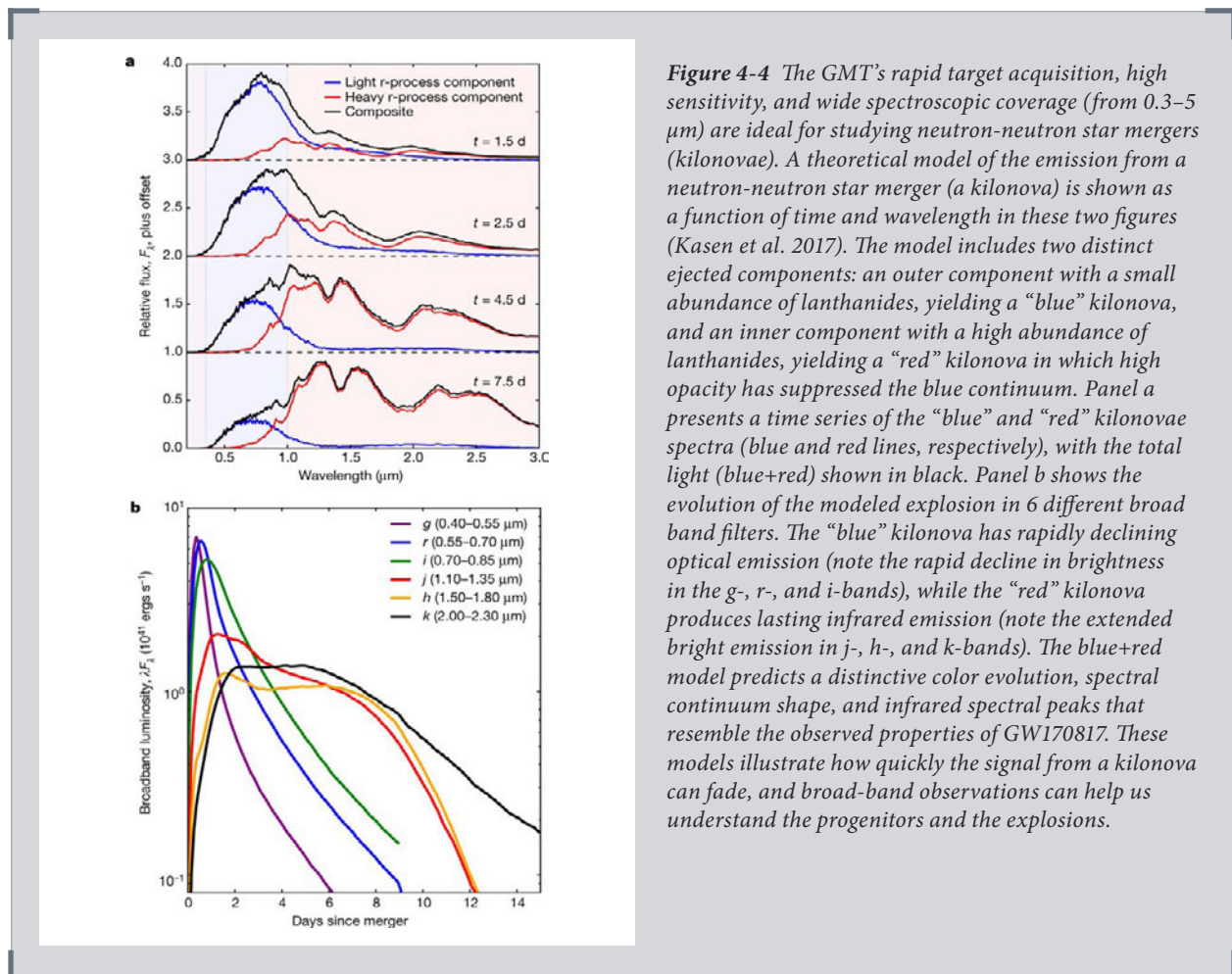
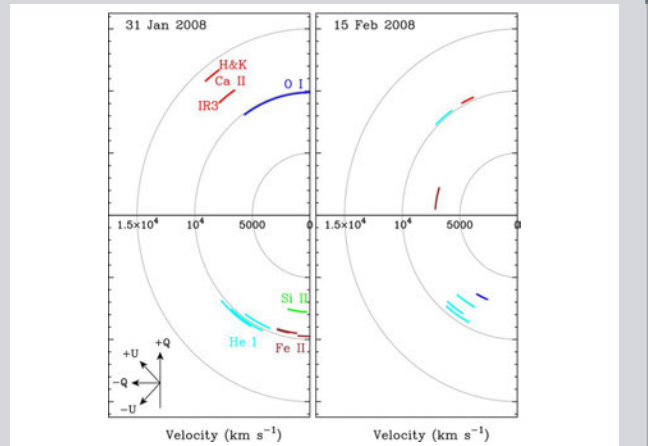


Figure 4-4 The GMT’s rapid target acquisition, high sensitivity, and wide spectroscopic coverage (from 0.3–5 μm) are ideal for studying neutron-neutron star mergers (kilonovae). A theoretical model of the emission from a neutron-neutron star merger (a kilonova) is shown as a function of time and wavelength in these two figures (Kasen et al. 2017). The model includes two distinct ejected components: an outer component with a small abundance of lanthanides, yielding a “blue” kilonova, and an inner component with a high abundance of lanthanides, yielding a “red” kilonova in which high opacity has suppressed the blue continuum. Panel a presents a time series of the “blue” and “red” kilonovae spectra (blue and red lines, respectively), with the total light (blue+red) shown in black. Panel b shows the evolution of the modeled explosion in 6 different broad band filters. The “blue” kilonova has rapidly declining optical emission (note the rapid decline in brightness in the g-, r-, and i-bands), while the “red” kilonova produces lasting infrared emission (note the extended bright emission in j-, h-, and k-bands). The blue+red model predicts a distinctive color evolution, spectral continuum shape, and infrared spectral peaks that resemble the observed properties of GW170817. These models illustrate how quickly the signal from a kilonova can fade, and broad-band observations can help us understand the progenitors and the explosions.

constraining physical models. The high spatial resolution of GMTIFS with AO will reduce source confusion and be critical for the study of the galactic environments of distant supernovae, which provide some of the best clues to SNe progenitors. G-CLEF and GMTNIRS will allow a high-dispersion study of the material along the line of sight that will enable probing circumstellar, interstellar, and intergalactic matter.

The death of stars as supernovae will continue to be a dominant topic in the era of the GMT. Some supernovae arise in white dwarfs, themselves the product of moderate-mass stars. Other stellar explosions arise in massive stars. Some come from single stars, others may require evolution in a binary system. Some produce rather dim explosions, others among the most dramatically bright events in the universe. Key questions involve the stellar progenitors, the explosion mechanisms, the environment in the host galaxy from which the explosions arise, and the compact and extended remnants they leave behind (Branch & Wheeler 2017).

Figure 4-5 The GMT optical design is well suited to spectropolarimetry, which can provide unique constraints on models of explosions. For example, it can reveal that different components of the composition of the ejecta are expelled at different angles and with different velocities. These polar plots present measurements of the velocity and polarization angle at absorption minimum for Ca II H & K, He I 15015, 15876, 16678, and 17065, Fe II, Si II 16355, O I 17774, and the Ca II near-IR triplet for the observations of SN 2008D near maximum and 15 days after maximum, corresponding to 21 and 36 days after the explosion (Maund et al. 2009). The angle of each arc corresponds to the observed polarization angle on the sky and the radius of the arc corresponds to the velocity.



Using the GMT Large Aperture to Understand the Explosion Geometry: Supernovae are complex, three-dimensional structures. Evidence for this comes from a variety of observations: the shape of young supernova remnants, asymmetries reflected in nebular lines and, especially, from spectropolarimetry (see **Figure 4-3** and **Figure 4-5**). Knowledge of the geometry and its origin promises important clues to the nature of progenitor stars and of the explosion mechanism. Of the three techniques, only spectropolarimetry can yield a time-resolved history of the ejecta structure and even of individual elements that comprise the ejecta (Wang & Wheeler 2008). Current data from 8–10 m class telescopes has given a framework to understand the basic spectropolarimetric behavior of various classes of supernovae, but the field remains photon starved and rich for exploration by the GMT.

Using the GMT’s High Angular Resolution to Discover the Nature of Supernovae Progenitors: An outstanding question for many transients is which stellar systems give rise to them; i.e. what is the nature of their progenitors? A key tool in this study is to conduct “stellar forensics.” While the outcome of stellar death is easily visible across the universe, astronomers are challenged to deduce which star(s) exploded and how. Answering the progenitor question impacts many fields of astrophysics.

Synergy with Transient Survey Telescopes

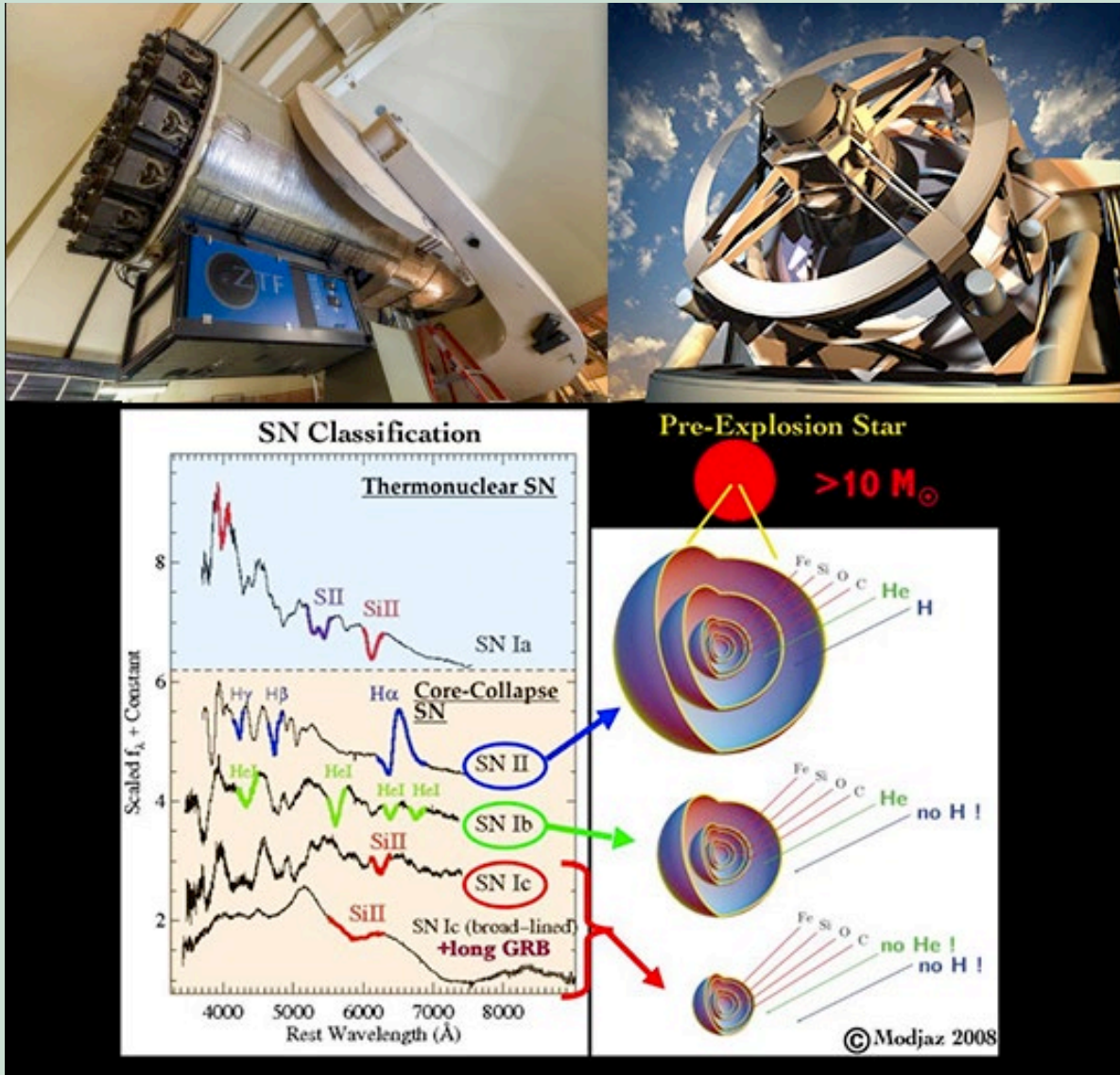


Figure 4-6 The GMT will be a key tool in a “new” kind of astronomy: transient events that include erupting and exploding stars, stars falling into black holes, and the spectacular mergers of neutron stars. For the first time, we are monitoring the full sky every night for such “transient events.” The Zwicky Transient Facility (top left) and the future LSST (top right) will patrol the sky each night for common and rare exotic supernovae (bottom panel), along with TDEs (tidal disruption events), GRBs (gamma-ray bursts), and FRBs (fast radio bursts). The GMT’s capability for high resolution spectroscopy of extremely faint sources over the full optical to mid-IR spectrum is essential to understand their exotic physics. For example, in fading supernovae explosions, the radioactive glow of chemical elements and their velocities allow us to model the progenitor star and the birth of chemical elements needed for planets and life. Image credits: Caltech Optical Observatories (top left), LSST/NSF/AURA (top right), Modjaz (2011; bottom).

The method of direct detection of pre-explosion stars has either not been successful for many kinds of transients or cannot be used for rarer transients discovered at large distances. Thus, there is strong need for a complementary method to conduct stellar forensics. Probing the habitats of the explosions (i.e., the host galaxy environments) is a very promising and rapidly expanding field (e.g., Modjaz 2011, Anderson et al. 2015) in which the GMT with its new capabilities will have great impact. The combination of the GMT's spatial resolution, light-gathering power, and the near infrared integral field unit capabilities will enable the unprecedented ability to zoom into the explosions' habitats to scrutinize crucial stellar parameters such as metallicity and star formation rate, as well as age of the stellar population amongst which the progenitor star lived.

Supernovae are historically classified by the features in their spectra near peak light that identify the elements that make up the composition of the ejected material (see discussion below). Supernovae that show distinct evidence for hydrogen in their spectra are called Type II. Most arise in *massive stars* with extended red giant envelopes and explode by core collapse in regions of active star formation. Type Ia show no hydrogen or helium in their spectra, but evidence for other elements such as silicon, sulfur, calcium, and iron. They are produced by lower mass stars, exploding white dwarfs, leave no compact remnant and tend to explode far from regions of new star formation. There are still many open issues regarding the progenitor evolution and explosion mechanisms of low mass and high mass stars that are ripe for new revelations from the GMT.

Type Ia supernovae (SN Ia)

In the currently favored scenario, a SN Ia is a thermonuclear explosion of a carbon-oxygen white dwarf that reaches the Chandrasekhar limit by mass accretion from a non-degenerate companion star or by a merger with another carbon-oxygen white dwarf (e.g., Branch & Wheeler 2017). Attempts to directly identify SN Ia progenitors have mostly been futile. For ordinary SN Ia, the non-degenerate companions of white dwarf progenitors, if any, are predicted to be faint ($M_v > 0$) for most cases, and very deep searches in pre-SN images or in SN Ia remnants of nearby galaxies would be needed for their unambiguous identifications. Indirect tests for the progenitor scenario include:

- Investigation of the impact of SN Ia progenitors as super-soft X-ray sources on the ionization of the circumstellar matter (CSM)
- Search for the signature of shock-heating of the companion by the SN Ia ejecta
- Search for hydrogen lines in late-time spectra of SN Ia
- Probe of the asymmetry and nucleosynthesis of SN Ia using spectropolarimetry, the nebular phase spectra, and supernova remnants
- Looking for evidence of interactions with circumstellar matter
- Inferring the delay time distribution of SN Ia progenitors from the properties of their host galaxies and SN remnants

There are a variety of reasons why Type Ia supernovae could be asymmetric. The progenitor, especially in the case of a white dwarf merger, could be rotating and

aspherical. The explosion could be asymmetric. The ejecta could strike and immerse a companion. Careful monitoring of any asymmetry with spectropolarimetry could yield information on any or all of these aspects. Small effects of asymmetry could also affect the use of SN Ia for precision cosmology.

The current sparse data on SN Ia suggest that the continuum polarization is typically small, suggesting that the ejecta are not strongly distorted near maximum light. This statement already rules out certain models of violently merging white dwarfs, but is consistent with standard thermonuclear combustion models. An important exception are the relatively dim SN 1991bg-like events that show appreciable continuum polarization rising to the red. This is one clue among several that this sub-class of SN Ia arise in a different manner than typical SN Ia.

On the other hand, individual spectral lines of SN Ia show substantial polarization $\sim 1\%$. Of special interest in this regard are the high-velocity features that are strongest before maximum light and have characteristic velocities ~ 8000 km/s higher than the photospheric velocity. Although nearly ubiquitous in typical SN Ia (and absent in SN 1991bg-like events), these remarkable features are unexplained. Suggestions include some aspect of the explosion physics or interaction with a very nearby circumstellar medium.

All these aspects of SN Ia—progenitor evolution and explosion physics—would be enhanced by high-cadence spectropolarimetry from the optical through the NIR. The large aperture of the GMT is crucial to progress in this field, as is the GMT's ability to acquire new targets rapidly with quick switching between instruments.

Core-collapse supernovae (CCSN)

CCSN are induced by gravitational collapse of the iron or oxygen-neon-magnesium cores in massive stars ($M > 8 M_{\odot}$) at the final evolutionary stage. A large fraction of massive stars ($> 50\%$) end their lives as red supergiants to produce SN IIP with distinct features of hydrogen in their spectra (Smartt 2009). Stripping of the hydrogen envelope via stellar winds and/or binary interactions can lead to other subtypes of CCSN, including SN Ib, and Ic. Some massive stars undergo mass-loss enhancements or mass eruptions shortly before the core collapse (< 100 yr), producing supernovae powered by interactions with circumstellar material. Some SN Ic, including those associated with long GRBs and superluminous SN Ic (**Section 4.2**), are unusually energetic and luminous (Woosley & Bloom 2006; Quimby et al. 2011). Theories suggest that they are powered by a central engine like a magnetar or accretion onto a black hole, both of which require rapid rotation of the cores of the progenitors.

Many outstanding questions concerning CCSN progenitors remain to be addressed:

- Why are all the observed supernovae that are associated with long GRBs and superluminous Type I SN Type Ic, instead of Type Ib?
- Do the majority of stripped envelope supernovae (i.e., SN I Ib, Ib, and Ic) originate from binary systems?
- What causes strong mass loss from supernova imposters and SN IIn/Ibn progenitors?

- How do the evolution and final fates of supernova progenitors depend on metallicity, and why do long GRBs and superluminous Type I SN occur preferentially in metal poor environments?
- Is there a mass limit of progenitor stars for the formation of black holes? What would be the observable signatures of black hole formation in massive stars?
- Do peculiar SN-like events such as fast luminous blue transients (Drout et al. 2014) have a massive star origin? Observations with GMACS would be game-changing by illuminating the habitats of these mysterious transients.

These questions can be addressed by studies of the environments with early and late time observations of supernovae. Another important approach in the GMT era would be to study individual massive stars and their populations of the local group galaxies with a deeper spectroscopic survey than currently possible. This would allow better constraint of stellar evolution models as a function of metallicity and direct identification of progenitors of supernovae that will occur in the local group in the near future.

Virtually all core-collapse supernovae reveal evidence of strong asymmetry (Wang & Wheeler 2008). The general trend is that the line and continuum polarization tend to get stronger with time as inner layers are revealed. The data suggest that the large asymmetries are connected with the explosion process itself.

Time-resolved spectropolarimetry of core-collapse supernovae has been shown to be remarkably powerful in disentangling the asymmetries in individual components of the ejecta; calcium has been seen ejected at different angles and with different velocities than hydrogen, helium, oxygen, or iron (*Figure 4-5*). Such studies are in their infancy, and will become much more sophisticated with the increased sensitivity of the GMT. The GMT will change the study of spectropolarimetry from one of sparse data on a few events to one with a substantial statistical sample. In this way, spectropolarimetry of core-collapse supernovae can lead to deep insights into the progenitor evolution (differences between single star and binary star evolution and among the many varieties of supernovae) and the explosion mechanism.

Long-duration gamma-ray bursts (GRB) and broad-lined SN Ic are the most powerful explosions in the universe. GRBs can be seen out to redshifts of 8–10; however their progenitors are not known in detail. As for superluminous supernovae, the debate is about low-metallicity vs. high-mass stars as their progenitors (e.g. Modjaz 2011). The outcome of this debate will profoundly affect their use as star formation indicators over cosmological distances, even out to the epoch of reionization.

Superluminous Supernovae

Superluminous supernovae (SLSN) are rare but fantastically bright supernovae that give us a new window into the evolution and explosion of massive stars.

SLSN (Quimby et al. 2011) are characterized as having an absolute magnitude exceeding -20.5 . Many SLSN are of a factor 10 brighter than SN Ia and nearly a hundred times brighter than typical core-collapse supernovae. These events produce as much energy in radiation alone as more normal supernovae do in kinetic energy, about 10^{51} ergs. Hydrogen-rich SLSN II clearly derive their large luminosity from the collision of the exploding ejecta with circumstellar matter (CSM)

under conditions where kinetic energy is efficiently converted to radiation. Some discussions discriminate between SLSN II that show distinct narrow emission lines and others that show broad hydrogen lines. The nature of the underlying explosion is less clear since it is shrouded by the substantial CSM. Hydrogen-deficient SLSN I lack any obvious evidence for CSM near maximum light (but may show evidence for later collision with CSM), and their explosion mechanism and the origin of their substantial luminosity are both uncertain.

Many mysteries still surround the nature of SLSN, including the origin of the differences between hydrogen-rich events that do or do not show narrow lines (SLSN II), and the fundamental cause of the great luminosity of the hydrogen-deficient events (SLSN I). Spectropolarimetry promises to reveal critical information. SLSN are especially challenging mysteries to unravel because they are rare and thus rarely observed nearby, making them very faint events despite their intrinsic brightness. Once again, the GMT can substantially add to the sample of SLSN and thus reveal the nature of these spectacular events.

The GMT may provide observations that are key to identifying the progenitors of SLSN I—a hotly debated mystery today. Recent work shows a nearby SLSN I exploding in a high-metallicity, massive galaxy nominally violating the pattern of explosion in low-metallicity environments; however, detailed spatially-resolved maps showed that the environment at the exact position of the event was in fact low metallicity. This finding underscores the crucial importance of spatially-resolved studies to zoom into the actual natal supernova habitat as closely as possible, as the GMT will be able to do.

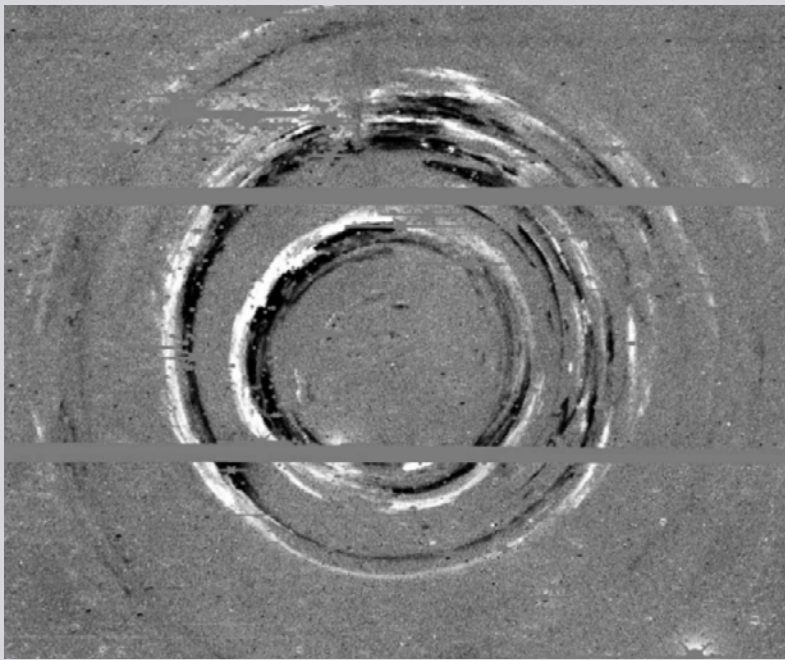


Figure 4-7 The GMT will take spectra of the light echoes from ancient supernovae. These spectra will be used to infer the supernova types and 3-D structure (in some cases) of the explosion. This figure shows the light echoes from the supernova 1987A in the Large Magellanic Cloud (Rest et al. 2005). The image is constructed by taking the difference between images taken approximately 15 years and 18 years after the supernova. The bright and dark rings are reflections of light from the supernova reflecting off successively more distant dust clouds surrounding the supernova. Because the image is a difference, starlight is cancelled out and only light which is due to changes between the images remains.

Light Echoes

Light that was emitted at the time of a supernova can reflect off surrounding dust before arriving at the Earth centuries after light that came directly from the original explosion. Study of these “light echoes” can provide a deeper understanding of both the supernova explosion and the nature of the circumstellar and interstellar dust itself (Yang et al. 2017). This reflected light can also be polarized, revealing properties of the dust. The acuity of the GMT will allow a significant increase in the range of light echoes that can be studied.

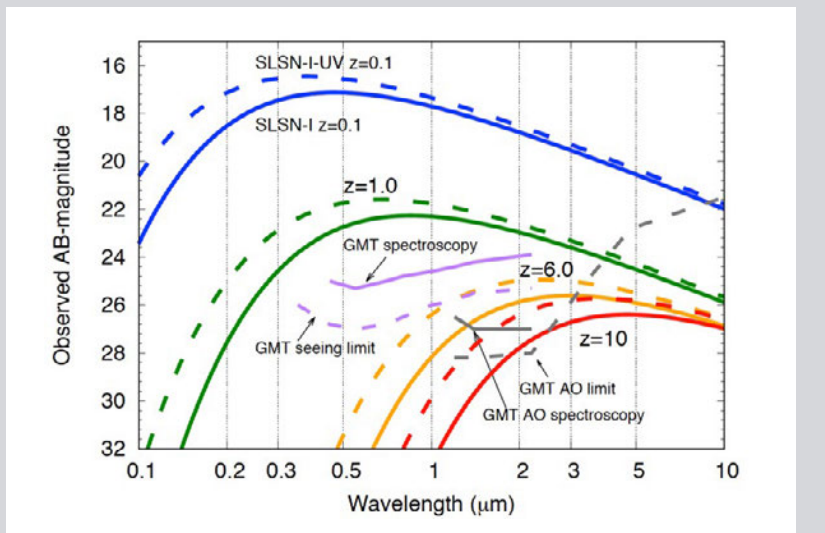
The GMT will also enable an extension of the dramatic new technique to determine the spectral type of old supernova from observations of the light echo of the original supernova (see *Figure 4-7*). Spectra obtained with this technique showed that Cas A was specifically from a Type IIb supernova, a category of massive star explosion from which most of the outer envelope of hydrogen has been stripped away, leaving only a shred of hydrogen and the underlying helium layer (Krause et al. 2008). A similar technique was employed to definitively prove that Tycho’s supernova of 1572 was a classic SN Ia replete with high-velocity spectral features that had only recently been determined to be a common characteristic of contemporary supernovae (Rest et al. 2008). Spectra of light echoes from different patches of dust reveal the spectrum emitted in different directions in the original explosion, a complement to spectropolarimetry in determining the 3D structure of the explosion.

4.3 The First Explosions

The large aperture and sensitive optical and near infrared imager spectrographs will enable the GMT to observe some supernovae at large distances, deep into cosmological history when supernovae first began to occur. GMTIFS with AO will be especially powerful in this regard.

After the Big Bang, the universe became dark. The cosmic dark ages ended with the formation of the first stars at $z \sim 20$, only ~ 200 Myr after the Big Bang. These stars started cosmic reionization, created the first heavy elements, and illuminated the first galaxies. Some of these early stars may have created the first black holes. No

Figure 4-8 The GMT is expected to detect superluminous supernovae (SLSN), among the first stars that are born and explode at the end of the cosmic dark ages. The figure presents the predicted AB magnitude of SLSN I as a function of wavelength at a variety of redshifts (image courtesy of J. Vinko). Solid lines correspond to a photospheric temperature of 12,000 K, dashed lines to 15,000 K. With AO at 2 mm, spectra could be obtained at redshift 10 and imaging could reach to even higher redshifts. GMACS can get spectra of SLSN to redshift 3 at 0.5 mm. Seeing-limited imaging could extend to redshift 6.



foreseeable facility will be able to directly detect those first stars, but some of them will explode to produce bright, detectable sources that will yield insight into the rate of production and nature of those first stars. The first explosions will also point the way to deep studies of the host environment. As we discuss below, a wide range of different kinds of supernovae may be visible in the first generations of stars.

It has long been recognized that long, soft gamma-ray bursts should be detectable at very high redshifts. Because their continua rise to the blue, redshifting brings more flux into the observer frame and compensates for the increased distance. If the first stars produced GRBs, then their study can provide information on the nature of the explosion to complement the burgeoning body of evidence from relatively nearby events at redshifts less than 6 to 8. GRBs could be seen in principle at redshifts of 30 or more and track the literal onset of the end of the dark ages. The line-of-sight spectra of these events will probe the intergalactic media through which their flux propagates.

Another potentially critical probe of the first stars are SLSN. SLSN I, in particular, are commonly observed in low-metallicity, star-forming galaxies. This makes them especially promising events to track the rate of star formation at high redshift and to seek any evolution of the intrinsic properties of the explosion at the earliest era. SLSN I are especially bright in the UV, a property that will aid their detectability at high redshift. Their observed rate per unit volume increases at least to $z \sim 4$, beyond the peak in the star formation rate at $z \sim 2$ to 3 (Cooke et al. 2012). The large UV luminosity can last for months in the rest frame and correspondingly longer by $1+z$ at higher redshift. LSST will have detection limits fainter than $m_{ab} \sim 24$ mag; in principle LSST can see SLSN up to $z \sim 3$ (Figure 4-8). The redshift evolution of SLSN can provide evidence for the physical origin of SLSN and for how the stellar initial mass function changes with redshift.

The GMT could produce a 5σ seeing-limited spectrum in an hour at $0.5 \mu\text{m}$ at $m_{ab} = 25$. (GMACS will achieve a S/N ratio of about 10 in an hour-long exposure at a resolution of $R=2000$ down to about 24th magnitude. The performance of NIRMOS is expected to be comparable). For an SLSN I with $M \sim -22$ this corresponds to $z \sim 3$

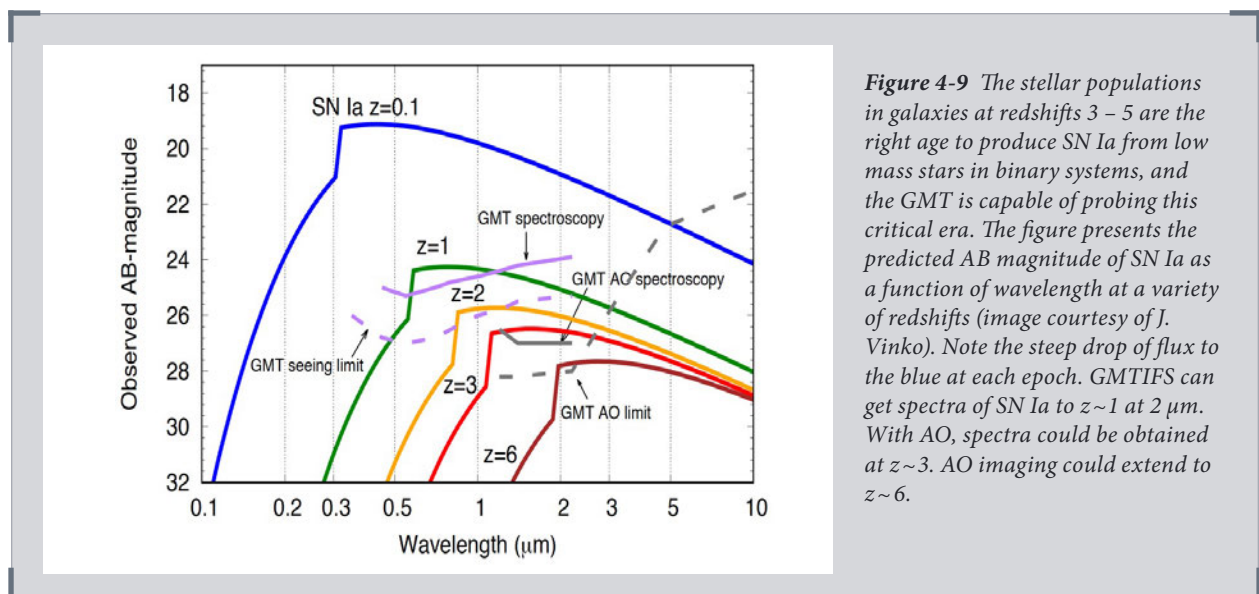


Figure 4-9 The stellar populations in galaxies at redshifts 3 – 5 are the right age to produce SN Ia from low mass stars in binary systems, and the GMT is capable of probing this critical era. The figure presents the predicted AB magnitude of SN Ia as a function of wavelength at a variety of redshifts (image courtesy of J. Vinko). Note the steep drop of flux to the blue at each epoch. GMTIFS can get spectra of SN Ia to $z \sim 1$ at $2 \mu\text{m}$. With AO, spectra could be obtained at $z \sim 3$. AO imaging could extend to $z \sim 6$.

(within LSST's detection limits, as discussed above). For imaging, the limit at $0.5 \mu\text{m}$ drops to $m_{\text{ab}} = 27$ at a redshift of $z \sim 4$. For observations at $2 \mu\text{m}$, the seeing-limited spectroscopic limit is $m_{\text{ab}} \sim 24$ at $z \sim 2$. With AO at $2 \mu\text{m}$, the spectroscopic limit is $m_{\text{ab}} \sim 27$ corresponding to $z \sim 10$. With AO at $2 \mu\text{m}$, the imaging limit of $m_{\text{ab}} \sim 28$ substantially exceeds $z = 10$. SLSN will be sparse at these redshifts. Special techniques utilizing the deep imaging capabilities of the GMT may be required to detect them. SLSN clearly represent a powerful probe of the early Universe, and the GMT can see them.

Theoretical models suggest the possibility of pair-instability supernovae (PISN) arising in massive stars that are hot enough to create destabilizing electron/positron pairs (Barkat et al. 1967). These could also be visible at high redshifts. Such models predict thermonuclear explosion of their oxygen cores and total disruption of the star. Models predict that some PISN may produce a large amount of radioactive ^{56}Ni that could yield exceptionally bright events, depending on the mass and whether a hydrogen envelope were retained. Some of these could be seen at large redshift, if rarely (Hummel et al. 2012). Due to time dilation, PISN are expected to be detectable for about 10 years in the observer frame.

The first Type Ia supernovae (SN Ia) must await the sedate processes of lower mass stars in binary systems. The first SN Ia are expected at $z \sim 3$ to 5. At that redshift, SN Ia will be within 1 mag of peak light for about 100 days in the local frame. At $0.5 \mu\text{m}$, SN Ia will drop out at $z \sim 1$ because of the strong UV deficit (**Figure 4-9**). For an SN Ia with $M \sim -19$, the GMT could produce a 5σ seeing-limited spectrum in an hour at $2 \mu\text{m}$ to somewhat less than $z = 1$. With AO at $2 \mu\text{m}$, the spectroscopic limit is $m_{\text{ab}} \sim 27$ corresponding to $z \sim 3$. With AO at $2 \mu\text{m}$, the imaging limit of $m_{\text{ab}} \sim 28$ extends to $z \sim 6$. Beyond $z \sim 6$, SN Ia would again drop out because of their UV deficiency. In principle, the GMT could directly observe the epoch of turn-on of SN Ia. This would bring a revolution in our understanding of galaxy evolution, star formation history, stellar evolution in both single and binary systems and the progenitors and explosion mechanism of SN Ia. A critical question is whether the first SN Ia resemble "typical" SN Ia on which supernova cosmology is based, or are biased in some way.

4.4 Remnants

The GMT, with its large aperture and sensitive optical (GMACS) and near infrared (NIRMOS, GMTIFS) imager spectrographs, will make major contributions to the study of young supernova remnants in the Milky Way and beyond.

Following supernovae many months to years after explosion during the SN-to-SN remnant (S/N) transition via *late-time observations* has enabled many exciting fundamental connections to be made between supernovae, their progenitor stars, their products (both compact and ejected debris), and resolved S/N analogs from which three dimensional kinematic and chemical information can be extracted (Milisavljevic & Fesen 2016). **Figure 4-10** shows a prime candidate for such studies, Cassiopeia A. The power of late-time observations comes from their ability to simultaneously probe 1) inner regions of the debris cloud that are normally hidden when the SN is brightest, and 2) nearby environments sculpted by the progenitor system's mass loss in the terminal stages that prelude an explosion.

There are many challenges associated with observing supernovae during extremely late epochs and only with the GMT can the full potential of SN-SNR investigations be realized. The primary difficulty is simply light gathering power: The majority of supernovae fade at least eight magnitudes below peak brightness in their first 2

years (often even more rapidly), limiting observations to 1 year or so after maximum light when they are at apparent magnitudes <22 . Thus, the enormous aperture of the GMT in combination with the high efficiency of its instruments both in the optical and NIR will revolutionize late-time investigations of supernovae both in the volume of space that can be sampled (and hence the number of objects to study) and the quality of data to be obtained (see **Figure 4-11**). Using conservative estimates for rates of objects of interest, the GMT will dramatically increase the data yield from ~ 10 events per year that are scattered in observed cadence, to ~ 100 events per year uniformly sampled through synergistic support from LSST. This marks a giant leap in capability that will enable transformative progress in time-domain astrophysics.

There are three sources of late-time emission that each provide rich information about the explosion, products, and the progenitor system that we briefly describe here:

Radioactivity: During phases when supernova emission is powered by radioactive material, the evolution of their bolometric light curves constrains the ejecta mass and energy and is sensitive to the efficiency of gamma-ray trapping and asymmetries in the distribution of material. The relatively few cases of well-sampled late-time



Figure 4-10 The GMT will allow ever-deeper studies of supernova remnants. One example is illustrated by this false color image of the remnant of the Type IIb supernova Cassiopeia A. Infrared data from the Spitzer Space Telescope (red), optical from The Hubble Space Telescope (orange), and X-ray data from the Chandra X-ray Observatory (green) show a complex structure with a jet toward the upper left, a counter jet to the lower right, and rings denoting boundaries of “bubbles” of radioactive ^{56}Ni . X-ray data from NuSTAR have revealed the distribution of radioactive ^{44}Ti . The faint cyan dot just off-center, and difficult to see, is the subluminal neutron star remnant. Credit: NASA/JPL/Caltech/Oliver Krause, University of Arizona.

light curves extending beyond 1 yr that exist are heterogeneous and inadequate to properly characterize the many diverse supernova classifications. Relative line strengths can be modeled to estimate chemical abundances, and then compared to predictions of nucleosynthesis yields from supernovae of different progenitor masses and metallicity. Emission line profiles provide information about ejecta kinematics, clumping, and large-scale asymmetry. Late-time monitoring of supernovae at “nebular” stages of ~ 1 yr have made key contributions to our understanding of various transients, including SN II, SN Ib/c, SN Ia, Ca-rich transients (Perets et al. 2010), and SLSN. The GMT will enable statistically significant samples of these objects to be observed and pushed into unexplored epochs > 2 yr post explosion. This will be particularly illuminating for rapidly evolving and luminous transients that have not been observed > 50 days post-explosion (Drout et al. 2014).

Compact objects: Late-time optical+NIR observations can also probe for the formation of compact objects formed in core-collapse explosions. The presence of a central magnetically active neutron star can be inferred by looking for changes in optical emission line widths. Decreasing widths are associated with the reverse shock sampling slower moving ejecta as it progresses inward, whereas increasing line width is anticipated from a pulsar wind nebula that heats and ionizes surrounding ejecta. There are few objects for which this technique has been applied robustly because of insufficient high quality late-time data. The GMT, however, will enable distant supernovae to be investigated in this manner with exquisite signal-to-noise. This is a critical test for broad oxygen lines observed in some SLSN. By following multiple systems through many years of evolution, the debated origin (interaction with an O-rich CSM environment versus heating from a pulsar wind nebula powered by a rapidly spinning neutron star) may be resolved.

SN-CSM interaction: Because the SN blast wave travels orders of magnitude faster than the progenitor stellar wind, one can use interaction between the supernova and the surrounding circumstellar matter (CSM) to probe thousands of years of massive star evolution and mass loss preceding core collapse in only a few years. Many examples of supernovae undergoing late-time rebrightening due to interaction with CSM enhancements encountered by the forward shock have been observed, implying that mass loss can be eruptive on irregular timescales. Interestingly, precursor activity is not limited to H-rich stars and has been observed in explosions of stripped-envelope progenitors where SN Ib/c interact with H- or even He-rich circumstellar shells. This is significant because it runs contrary to the smooth wind hypotheses commonly assumed in stellar evolution and in widely adopted models of synchrotron emission from SN-CSM interaction. Eruptive mass loss has serious ramifications in many areas of astronomy that depend on accurate mass loss estimates and detailed knowledge of supernova explosion products (see discussion in Smith 2014). Leveraging from systematic monitoring provided by LSST that can provide alerts for rebrightenings and follow up spectroscopy with the GMT will enable a broad characterization of SN-CSM interaction across supernova types, luminosities, and ages. The resulting rich data set will be used to constrain progenitor star structure and composition, and provide powerful tests of next-generation end-to-end supernova explosion simulations seeking to model emissions across the electromagnetic spectrum and neutrino, cosmic ray, and gravitational wave signatures.



Aspirational Technique – Continuous, Wide-band IR Spectroscopy of Faint Sources

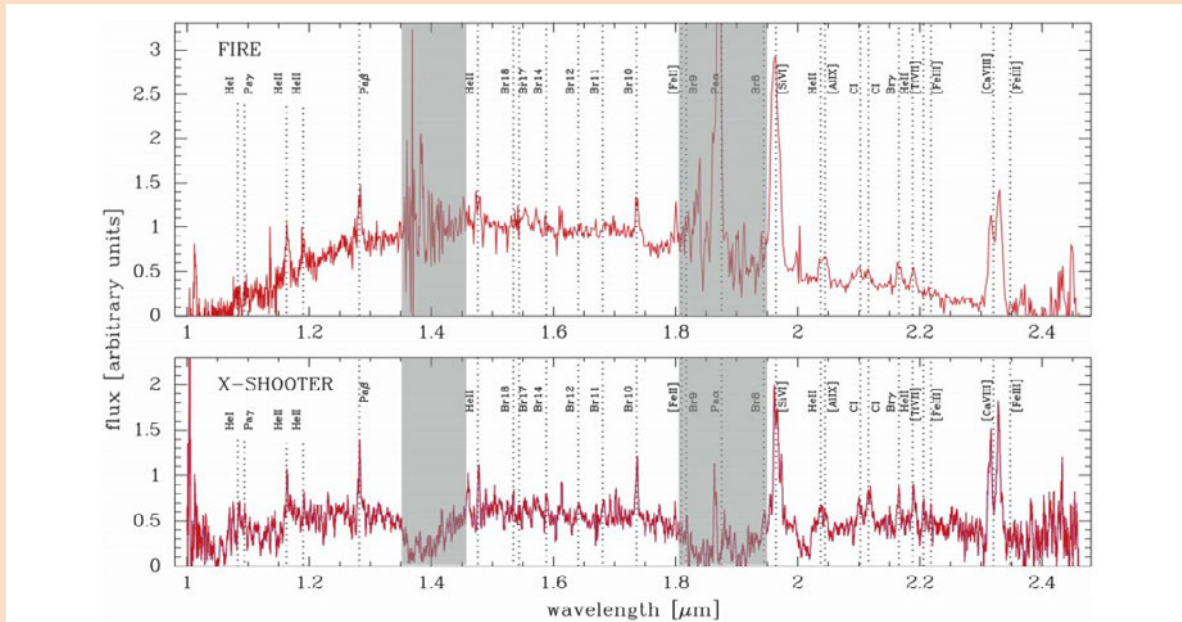


Figure 4-11 The transients discussed here are compact object mergers, supernovae, tidal disruption events and hence they are single objects spread sparsely on the sky. They require broad wavelength coverage in a one-dimensional spectrum and would benefit from a low-resolution, high-throughput, single-object spectrograph coupled to the large light gathering aperture of the GMT. Study of the death of stars would strongly benefit from access to a high throughput “Super-FIRE” instrument with an $R \sim 6000$ Echellette.

The figure shows spectra from FIRE on the 6.5 m Magellan telescope and XSHOOTER on the European Southern Observatory 8 m VLT from an explosive transient at 1300 and 1350 days after the transient was discovered, respectively, and whose nature is not yet known, but is possibly a supernova or stellar merger event (see Minniti et al. 2017). Note the clear changes in the strength of the emission lines over this range in time. The spectral range depicted covers near infrared wavelengths from approximately 1 to 2.5 μm and includes terrestrial absorption bands with poor transmission (the grey regions) due to earth’s atmospheric water vapor. Coupled with the large aperture of the GMT, an instrument like FIRE or XSHOOTER would have very high sensitivity: the ability to gather observations of faint objects quickly or obtain precise observations of explosions at very late times when they have faded to very faint levels. Such late time observations on the GMT would open up a parameter space unavailable for discovery on current 8 m class telescopes for more distant transients.

4.5 Tidal Disruption Events

The GMT with its large aperture and sensitive optical and near infrared imager spectrographs will make major contributions to the study of stars ripped apart by supermassive black holes. GMACS will be especially powerful to determine the composition and flow of disrupted material. The high spatial resolution of GMTIFS will allow critical study in the near infrared, including the formation and distribution of dust.

Stars that pass too close to supermassive black-holes (SMBHs) at the cores of their host galaxies can encounter death and be completely ripped apart by the SMBH tidal forces (*Figure 4-12*). The result of the tidal encounter is a flare of luminous radiation across the electromagnetic spectrum (X-ray to radio) powered by partial accretion of the stellar material onto the SMBH. Theoretically predicted in the seventies (e.g. Hills 1975, Frank & Rees 1976), these flares of radiation are now routinely observed and are known as Tidal Disruption Events (TDEs).

TDEs are interesting for several reasons. First, TDEs can be used as a marker for SMBHs that otherwise lie dormant and undetected in the centers of distant galaxies (>100 Mpc away), where they are too far away for the orbits of gas and stars around them to be resolved. Furthermore, TDEs are excellent probes of relativistic effects in regimes of strong gravity and provide a new means to measure SMBH masses *and* spins. Finally, TDEs are signposts of intermediate-mass BHs, binary BHs and recoiling BHs.

The first TDE candidates were detected in the nineties at X-ray wavelengths (by *ROSAT*), and later in UV (mainly by *GALEX*). TDEs are now routinely detected by current optical transient surveys (e.g. *PanSTARRS*, *ASAS-SN*, *PTF*; see Komossa 2015 for a review). Only a few TDEs have an associated radio counterpart so far. At the time of writing, only ~70 TDE candidates have been identified². Even this small sample of events has greatly expanded our understanding of these transients.

- TDEs show a diverse phenomenology, with at least two broad classes identified so far. The first class includes high-energy TDEs associated with collimated relativistic outflows. A second class includes optical/UV TDEs with no signature of collimated outflows. At the time of writing, it is not clear what the key physical properties are that enable some SMBHs to launch relativistic jets at the time of stellar disruption.
- TDEs seem to show a preference for post-starburst galaxies. The reason for the overabundance of TDEs in post-starburst galaxies is unclear.
- The theoretically-predicted light-curve decay $\sim t^{-5/3}$ is only observed in a few TDEs. All TDEs with good data quality show deviations from this prediction.
- The spectral signatures of TDEs are also a puzzle. Some TDEs display He II emission lines, with no sign of H. Other TDEs instead do display H emission. The spectral properties of TDEs are the focus of intense theoretical modeling.

The limited understanding of the optical properties of TDEs, and the lack of a clear picture of how these map into the SMBH properties is significant, as it impairs our capabilities to realize the full potential of TDEs as probes of extreme gravity.

The limitations of current investigations can be traced to two key factors: statistics, and the limited range of redshift probed (i.e. limited volume). TDEs are intrinsically rare ($\sim 10^{-4}$ - 10^{-5} events per galaxy per year). Like SN Ia, TDEs typically reach mag ~ -19 at maximum light. Different from SN however, TDEs show a much longer-lived optical/UV emission, which can last for months. The much longer time scales of evolution make TDEs the perfect targets for LSST. Indeed, the LSST contribution to TDE studies will be substantial, with ~4000 TDEs discovered per year. More than 1000 TDE will be discovered per year above 24th magnitude, well within the reach of

²<https://tde.space/>

GMT optical/NIR spectroscopic capabilities.

GMT spectroscopic follow-up of LSST-discovered TDEs will enable the following *new science*:

1. accurate census of dormant SMBH in the local Universe, with the potential to identify correlations of SMBH properties with host-galaxy properties (mass, bulge, type);
2. demographics of dormant SMBH out to $z \sim 0.7$, a redshift range currently not accessible;
3. identification of intermediate-mass BHs in dwarf galaxies; and
4. through spectropolarimetry, the GMT will reveal the geometry of the emitting material.

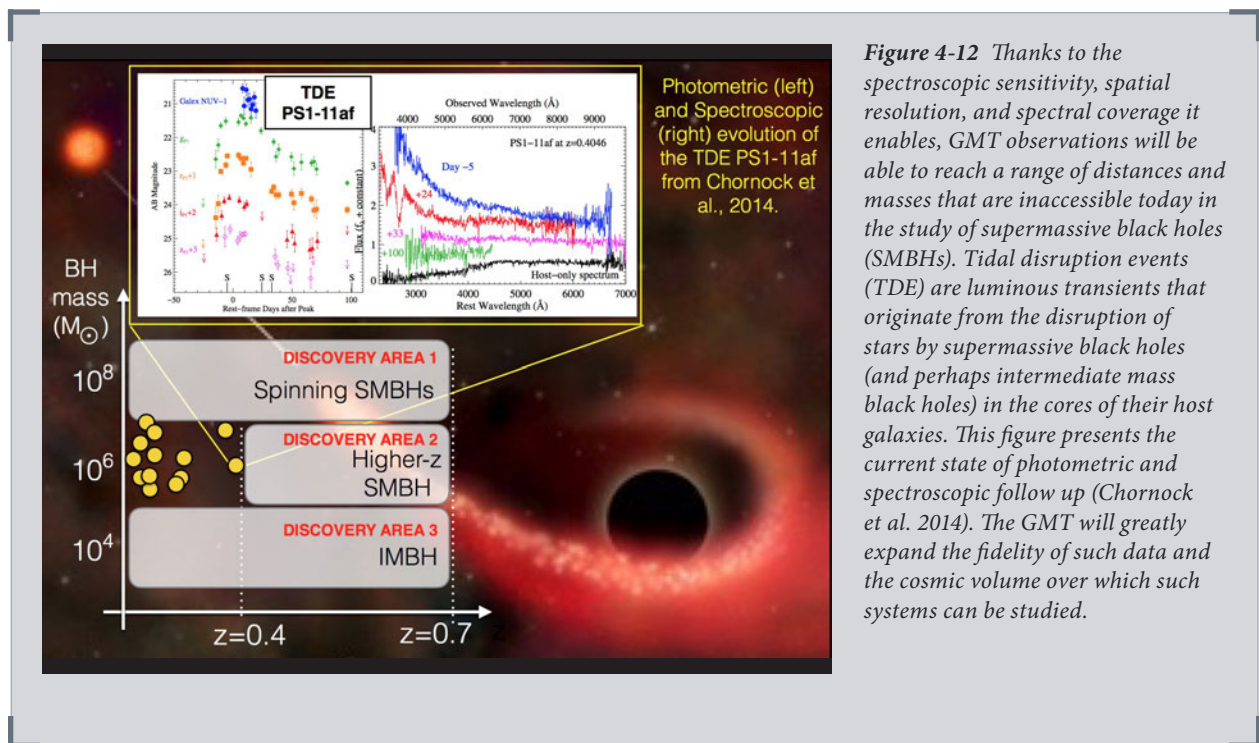


Figure 4-12 Thanks to the spectroscopic sensitivity, spatial resolution, and spectral coverage it enables, GMT observations will be able to reach a range of distances and masses that are inaccessible today in the study of supermassive black holes (SMBHs). Tidal disruption events (TDE) are luminous transients that originate from the disruption of stars by supermassive black holes (and perhaps intermediate mass black holes) in the cores of their host galaxies. This figure presents the current state of photometric and spectroscopic follow up (Chornock et al. 2014). The GMT will greatly expand the fidelity of such data and the cosmic volume over which such systems can be studied.

References

- Abbott, B. P., Abbott, R., Abbott, T.D., et al. 2016, Physical Review Letters, 116, 061102
- Abbott, B. P., Abbott, R., Abbott, T. D., et al. 2017, ApJL, 848, L12
- Abellán, F. J., Indebetouw, R. Marcaide, J. M., et al. 2017, ApJL, 824, L24
- Anderson et al. 2015, PASA, 32, 19
- Barkat, Z., Rakavy, G., & Sack, N. 1967, Physical Review Letters, 18, 379
- Berger, E. 2014, ARAA, 52, 43
- Branch, D. & Wheeler, J. C. Supernova Explosions (Springer).
- Chornock et al., 2014, ApJ, 780, 44.
- Cooke, J., Sullivan, M., Gal-Yam, A., et al. 2012, Nature, 491, 228
- Drout, M.R. 2014, ApJ, 794, 23
- Frank & Rees 1976, MNRAS, 176, 633
- Hills, J.G. 1975, Nature, 254, 295
- Hummel, J. A., Pawlik, A. H., Milosavljević, M., & Bromm, V. 2012, ApJ, 755, 72
- Daniel Kasen ,1 Peter Nugent ,1 Lifan Wang ,1 D. A. Howell ,1 J. Craig Wheeler ,2 Peter Höflich ,2 Dietrich Baade ,3E. Baron ,4 and P. H. Hauschildt, 2003, ApJ, 593, 788
- Kasen, D., Metzger, B., Barnes, J., Quataert, E., & Ramirez-Ruiz, E. 2017, Nature, 551, 80
- Komossa 2015, Journal of High Energy Astrophysics, Volume 7, p. 148-157
- Krause, O., Birkmann, S. M., Usuda, T., et al. 2008, Science, 320, 1195
- Kruehler et al. 2017, A&A, 602, 85
- Kuncarayakti et al. 2015, PKAS, 30, 139
- Maund, J.R. et al. 2009, ApJ, 705, 1139
- Metzger, B. D. 2017, Living Reviews in Relativity, 20, 3
- Milisavljevic, D., Fesen, R. 2016, Chapter in Supernova Handbook, eds. A. Alsabti and P.
- Minniti, D, et al. 2017, “The Emergence of the Infrared Transient VVV-WIT-06,” ApJ, 849, L23
- Murdin (Springer)
- Modjaz 2011, AN, 332, 434
- Perets, H., et al. 2010, Nature, 465, 322
- Quimby et al., 2011, Nature, 474, 487
- Rest, A., et al. 2005, Nature, Volume 438, Issue 7071, pp. 1132-1134
- Rest, A., Welch, D. L., Suntzeff, N. B., et al. 2008, ApJL, 681, L81
- Siebert, M. R., Foley, R. J., Drout, M. R., et al. 2017, ApJL, 848, L26
- Smartt, S. 2009, ARAA, 47, 63
- Smartt, S. 2015, PASA, 32, e016
- Woosley, S.E., & Bloom, J.S. 2006, ARAA, 44, 507
- Maund, J.R., Gal-Yam, A., et al. 2017, ApJL, 837, L14
- Maund, J. R., Wheeler, J. C., Baade, D., et al. 2009, ApJ, 705, 1139
- Wang, L., & Wheeler, J. C. 2008, ARAA, 46, 433
- Yang, Y., Wang, L., Baade, D., et al. 2017, ApJ, 834, 60



A photograph of the Milky Way. Credit: Serge Brunier

Building the Milky Way & its Neighbors

How did galaxies grow and evolve? When and where do their stars form? How do the heavy elements forged in supernovae find their way into the next generations of stars? These are among the basic questions about galaxies that remain unanswered because existing telescopes do not have sufficient sensitivity and resolution to obtain the necessary observations—detailed observations of stellar populations in range of different galaxies.

The GMT will be able to collect high-resolution spectra of very faint stars in the local group of galaxies. These spectra will allow us to study stars that formed from primordial gas in the earliest epoch of star formation and explore the complex formation and evolution of galaxies like our own.

Chapter Authors

Mike Boylan-Kolchin (The University of Texas at Austin)

Sarah Brough (University of New South Wales)

Narae Hwang (Korea Astronomy and Space Science Institute)

Sarah Martell (University of New South Wales)

David Yong (Australian National University)

Dennis Zaritsky (University of Arizona)

5 Building the Milky Way & its Neighbors

Our cosmic neighborhood of galaxies includes the Milky Way, Andromeda (M31), and a host of smaller systems, collectively known as the Local Group. In these nearby galaxies we can see a wealth of detail that reveals how these galaxies formed and evolved. We can study recently born stars as well as stars that formed when the universe was young. We can resolve the gas clouds that will become stars and trace the disrupted remnants of galaxies that have fallen into larger systems. In the Local Group we have a rich view of how galaxy formation might proceed throughout the universe. Reconstructing the appearance of the Local Group at earlier cosmic times constitutes near-field cosmology. In this chapter, we describe how the GMT will transform our understanding of galaxy formation.

The Local Group contains two giant spiral galaxies (the Milky Way and Andromeda), separated by approximately 800 kpc (10 billion billion miles), but falling towards each other. A host of satellite galaxies surround these two central galaxies. Many of these faint satellites, some with stellar masses of only a few hundred Suns, remain to be discovered.

The proto-Milky-Way (and proto-M31) formed in the deepest potential wells present at early times growing via mergers and gas accretion to form the magnificent spiral galaxies of the present day. The Milky Way and Andromeda galaxies therefore have long and messy assembly histories and harbor many merger remnants within the bulge and halo as well as ongoing disruption events in the form of tidal streams (Bullock & Johnston 2005; Belokurov et al. 2006).

Thousands of sites of star formation from the earliest epochs (over 13 billion years ago) are found in the present-day Local Group. Many stellar systems have evolved in isolation, with little to no star formation, since the first billion years of the Universe's history (Ricotti & Gnedin 2005, Brown et al. 2014, Weisz et al. 2014). Other galactic fragments grew more rapidly, retained their gas, and continued to form stars until falling into the gravitational potential of the Milky Way or M31 at later times. The descendants of such objects constitute the “classical” dwarf satellites of the Local Group.

The primary goal of near-field cosmology is to extract the formation history of all of the components of the Local Group, and to understand the physical conditions and processes operating at earlier cosmic epochs (Freeman & Bland-Hawthorn 2002). We can begin by answering some fundamental questions. How resilient are galactic disks to merger events? How are the stellar halos surrounding galaxies built? The GMT's wide field-of-view, coupled with multi-object spectroscopy, will enable efficient characterization of the metallicities and velocities of large numbers of stars in and around Local Group streams. Chemical fingerprints may link individual stars to their birth cluster and enable reconstructions of disrupted galaxies. These disrupted galaxies can then be compared directly to surviving systems to reconstruct the assembly process.

Galactic archaeology focuses on the Milky Way, where we can collect highly detailed information for large numbers of individual stars. This research aims to follow the universal processes of galaxy formation and evolution at a close-up level. With these fine-grained data, we will determine the initial mass function for stars and star clusters across Galactic history, track the progress of chemical evolution through a high-dimensional abundance space, and quantify the effects of the various processes

responsible for radial migration. These developments will be critical to our understanding of nucleosynthesis and stellar evolution in individual stars, and to our ability to interpret the integrated measurements and semi-analytic model predictions used in galaxy evolution studies. The GMT, as the only ELT offering low- and high-resolution spectroscopy across the optical waveband in its first-light instrument suite, is well placed to take a leading role in this field. These opportunities include divining the origins of the extremely metal-poor stars in the Milky Way, and full membership identification and self-enrichment histories for newly discovered low-mass satellites of the Milky Way.

Synergy with GAIA and Spectroscopic Surveys



Figure 5-1 Artist's image of the ESA GAIA Space Telescope with a photograph of the Milky Way in the background. The ESA GAIA Space telescope, which is planned to be in operation through 2020, will provide 6-dimensional phase-space positions, spectrophotometry, stellar parameters and many different abundances for several million stars within 10 kpc of the Sun, and radial velocities, stellar parameters and a few abundances for several million stars out to a few hundred kpc across the Local Group (Prusti et al. 2016). The final catalogue of all GAIA data products is currently planned for 2023. Significant coordinated follow-up efforts are already underway

(e.g., APOGEE; Holtzmann et al. 2015, GALAH; De Silva et al. 2015, the GAIA-ESO Survey; Gilmore & Randich 2012, LAMOST; Luo et al. 2015, and FunnelWeb; <https://funnel-web.wikispaces.com>), but high-resolution follow-up of the faintest, most distant stars will only be possible with the GMT. G-CLEF and GMACS will play a key role in probing deep into the formation history of the Milky Way and Local Group galaxies using candidate stars selected based on their spectroscopic properties from current large surveys as well as multi-dimensional phase space information from GAIA. Image Credit: ESA/ATG medialab; background: ESO/S. Brunier

The landscape for Galactic archaeology in the mid-2020s will present many exciting opportunities for extremely large telescopes. These science goals capitalize on unique GMT capabilities to develop new insights on fundamental aspects of Galactic archaeology, with major ramifications for subfields from nuclear astrophysics to galaxy formation.

5.1 The Most Metal-Poor Stars in the Galaxy

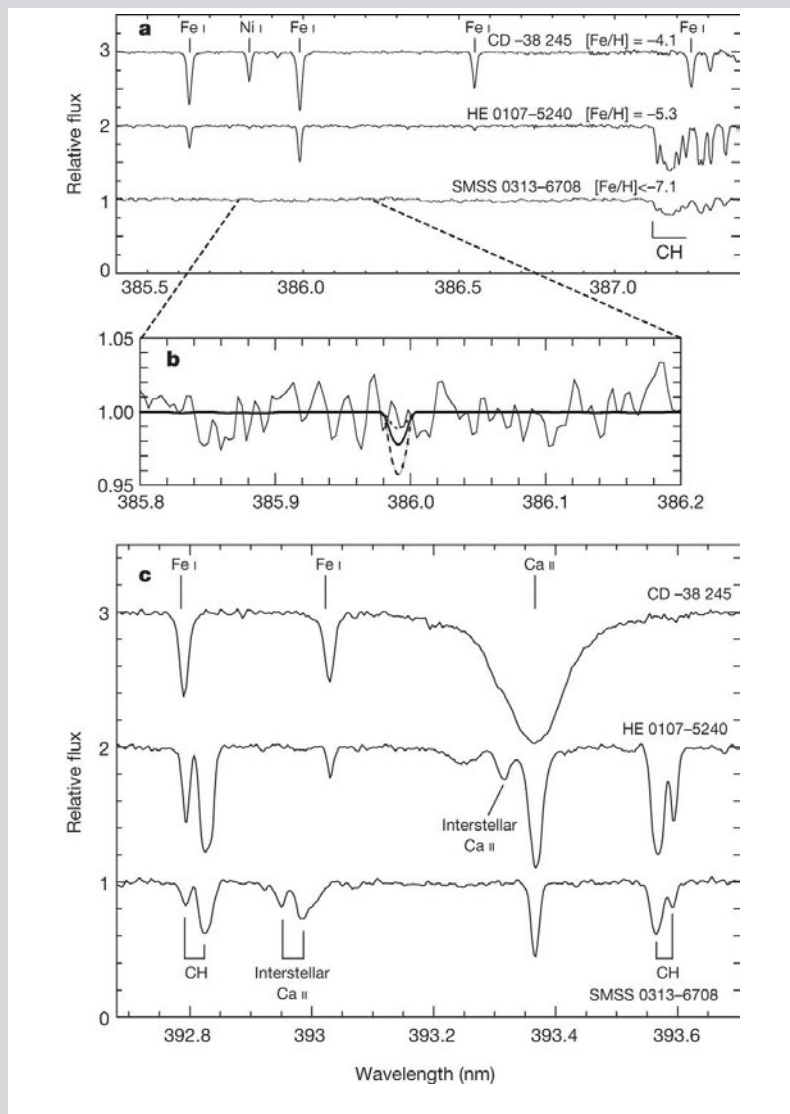
The universe was produced from the Big Bang some 13.8 billion years ago. Hydrogen, helium and then lithium were created by nuclear fusion reactions in the first 10–1,000 seconds. The universe then cooled and expanded in darkness for 100,000

years before light from the first stars illuminated the cosmos. The nature of that first generation of stars, however, remains a mystery.

How energetic were the first stars? What was their mass distribution? By what mechanisms did they explode and return the elements back to the interstellar and intergalactic medium that fused in their cores? Which chemical elements did they produce and return to the gas, and in what quantities? These questions are fundamental to astrophysics and the oldest, most metal-poor stars in the Milky Way galaxy hold the clues to answering them.

Low-mass stars (<1 solar mass) have lifetimes of billions of years, and in principle can survive as long as the universe has existed. Because fusion only occurs in the cores of stars, the atmospheres of these low-mass stars retain the chemical

Figure 5-2 The GMT will help us determine the formation environments of the first stars and the chemical production of the first supernovae. This figure shows a spectrum of SMSS J0313-6708, the most iron-poor star known so far, in comparison with other metal-poor stars of similar temperature and surface gravity (from Keller et al. 2014). All of these absorption features are created as light passes through the atmosphere of the star from the core, where the nuclear fusion is ongoing throughout the stable life of the star. Only stars less massive than 1 solar mass can exist for the lifetime of the universe (>13 billion years) in a state of stable, core fusion. Because fusion only occurs in a star's core for these low mass stars, their atmospheres retain the chemical composition of the interstellar gas at the time and place of their formation. These stars are faint and the GMT will extend the volume over which we can identify and study these stars at the required level of detail. Studying chemical abundances in the oldest, most metal-poor stars with G-CLEF will provide a unique opportunity to study the formation environments of the first stars and the chemical production of the first supernovae.



composition of the interstellar gas at the time and place of their birth. Studying chemical abundances in the oldest, most metal-poor stars provides a unique window through which we can probe the early universe and infer the properties and details of the first supernovae. Indeed, in the inner region of the Milky Way Galaxy, some 15% of stars with less than 1/1,000th the solar iron-to-hydrogen ratio, $[Fe/H] < -3$, are predicted to have formed at redshifts $z > 15$ (Tumlinson 2010, Howes et al. 2015). Ancient metal-poor stars can thus be considered local analogues of the high redshift universe and provide constraints on the conditions in the first ~100 Myr of the Milky Way.

There is fierce international competition for the discovery and detailed chemical abundance analysis of metal-poor stars, as they provide a unique opportunity to understand the physical conditions of the earliest star-forming environments in the universe. The GMT and G-CLEF will be the most powerful tools for the analysis of these incredibly rare objects.



Science Campaign to Observe the First Stars

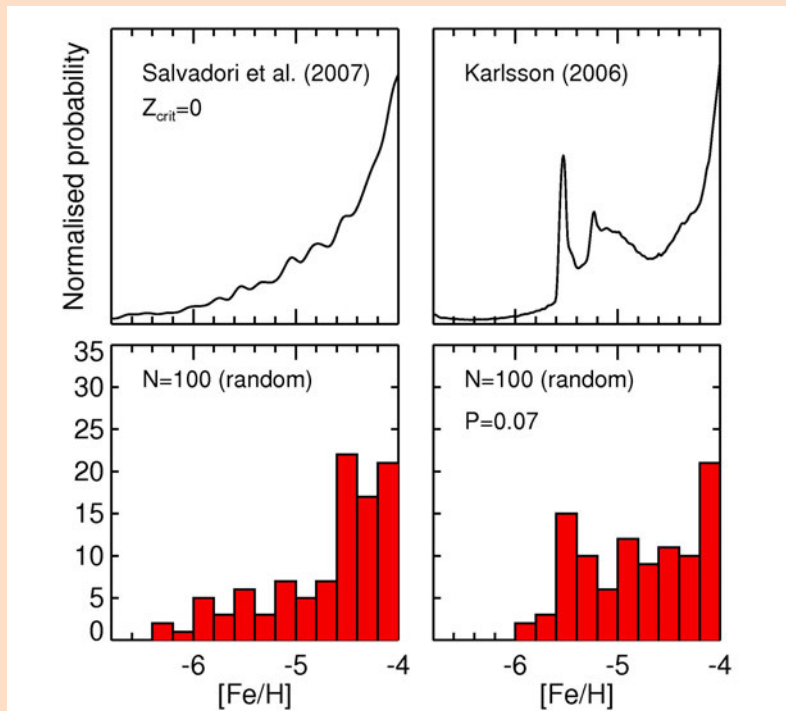


Figure 5-3 A sample of 100 stars is sufficient to gain crucial constraints on the nature of the first stars and the early evolution of the Milky Way. Depending on the nature of the first stars and early evolution of the galaxy, very metal poor stars appear with different frequency relative to more metal rich stars. The upper panels in this figure show theoretical iron distribution functions from Salvadori et al. (2007, left) and Karlsson (2006, right). The lower panels show mock samples of 100 stars randomly drawn from the upper distributions along with the significantly low probability that the two samples are drawn from the same distribution

A 50-night multi-semester observing campaign using G-CLEF would obtain high-resolution spectra of ~100 of the most promising metal-poor star candidates with $[Fe/H] < -4$ in the magnitude range

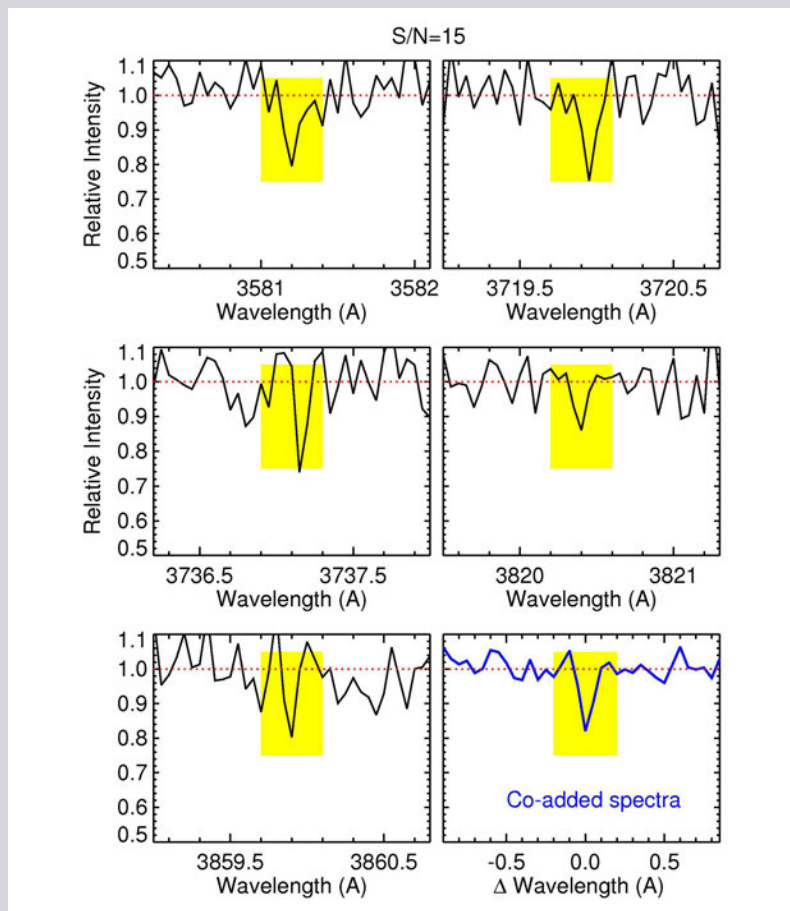
$18.7 < V(\text{mag}) < 19.7$. $S/N=15$ at 385 nm can be achieved in ~2 hours ($V=18.7$ mag) to ~8 hours ($V=19.7$ mag) in either the MT (medium throughput, $R=35,000$) or HT (high resolution, $R=19,000$) modes. As seen in **Figure 5-2**, $S/N=15$ at 385 nm will enable metallicity measurements down to $[Fe/H] = -5.5$ as well as measurements of (or limits on) C, N, O, Na, Mg, Ca, Ni, Sr, and Ba. The interpretation of those abundance signatures in metal-poor stars will constrain the nature and nucleosynthesis of the first stars and thereby the early evolution of the Milky Way.

Progress to Date

Iron is the canonical measure of stellar “metallicity”—the number density of chemical elements heavier than helium. Only *five* stars have ever been found that have less than $1/100,000^{\text{th}}$ the solar iron-to-hydrogen ratio, $[\text{Fe}/\text{H}] < -5$, (Frebel & Norris 2015). These five so-called *hyper-metal-poor* stars are of particular interest as they are the most chemically ancient objects known. These and other metal-poor stars exhibit an enormous range in their relative chemical abundance ratios, which implies that there was a wide variety in the properties (mass, explosion energy, rotation, mass cut, explosion mechanism) of the first supernovae (Nomoto et al. 2013). To better constrain the diversity of properties and their relative frequency amongst the first supernovae, a qualitatively different sample of stars needs to be assembled.

However, stars with less than $1/100,000^{\text{th}}$ the solar iron-to-hydrogen ratio, $[\text{Fe}/\text{H}] < -5$ are incredibly rare. If we were randomly selecting stars, we would need to observe 10,000,000 in order to find one such star. To increase the probability of finding these rare objects, astronomers have devised a raft of ingenious techniques to identify candidate metal-poor stars (Beers & Christlieb 2005). At present, the most promising efforts involve wide-field, deep photometric surveys with narrow-

Figure 5-4 The GMT will enable us to study ~100 of the most promising metal-poor star candidates in the Local Group. The blue part of the spectrum is critical for determining the overall chemical abundance of stars because the strongest, unblended iron lines in the spectrum of stars are all at blue wavelengths (344.06 nm, 358.12 nm, 371.99 nm, 373.71 nm, 382.04 nm and 385.99 nm). This figure shows a simulated G-CLEF spectrum with signal to noise ratio (S/N) of 15 at wavelengths around the five strongest iron lines in a hyper metal-poor star. The stellar parameters for this simulation are $T_{\text{eff}}=5150$ K, $\log(g)=2.2$, $[\text{Fe}/\text{H}]=-5.5$. In the lower right panel, the five spectral regions are stacked and co-added. This S/N pushes the limit for abundance analysis, but illustrates that G-CLEF could study ~100 of the most promising metal-poor star candidates in the Local Group in 2 (for $V=18.7$) to 8 (for $V=19.7$) hours each.



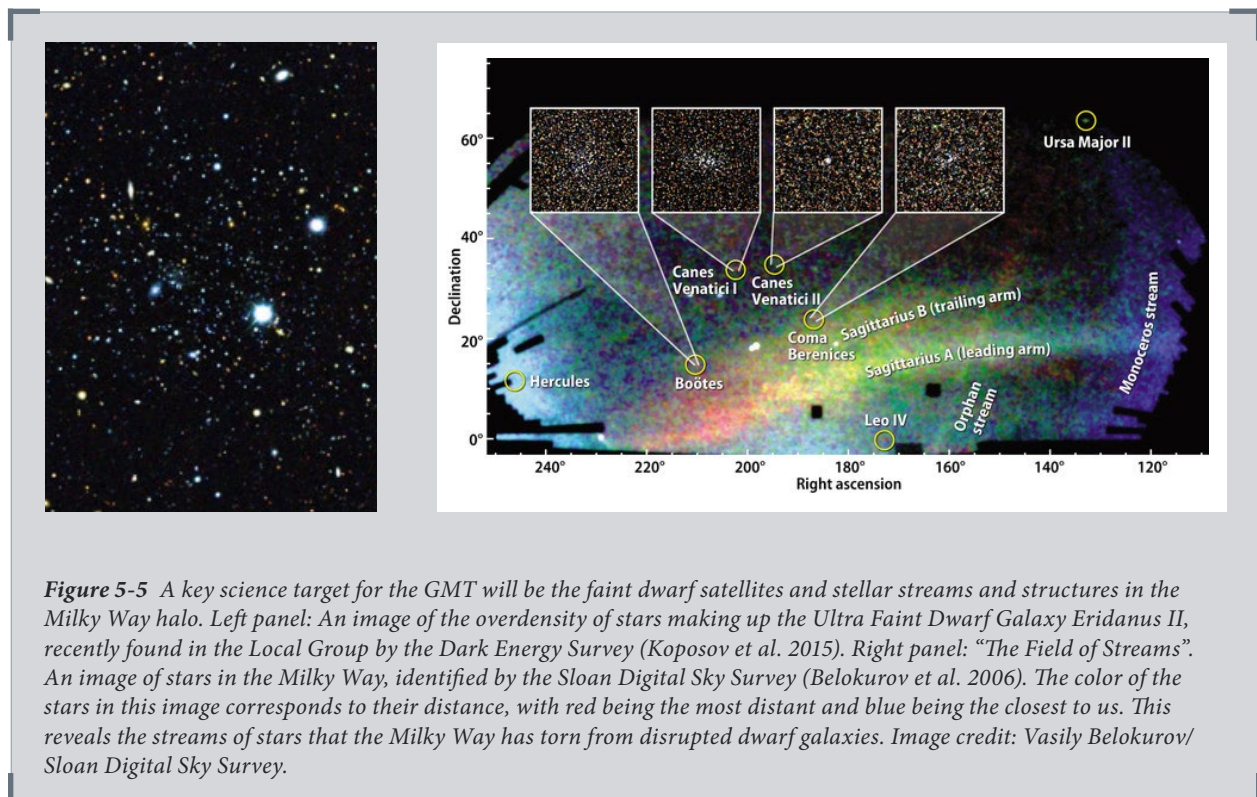
band metallicity-sensitive filters such as SkyMapper (Keller et al. 2007) and Pristine (Starkenburg et al. 2017).

The most iron-poor star currently known, SMSS J031300.36–670839.3 with $[\text{Fe}/\text{H}] < -6.5$ ($< 1/3,000,000^{\text{th}}$ the solar iron-to-hydrogen ratio) and $V=14.7$ mag, was discovered in the SkyMapper survey (Keller et al. 2014; Nordlander et al. 2017), see **Figure 5-2**. The abundances of key elements relative to iron (“relative abundances”) could only be measured for Li, C, O, Mg, and Ca (upper limits were obtained for the remaining elements). Those abundances are the signature of the first-generation star(s) that enriched the gas before SMSS J031300.36–670839.3 formed. The best fitting models to the abundance pattern of this star indicate that the progenitor was a zero-metallicity, low-energy, 10–60 solar mass supernova. More examples of similar objects are needed to better constrain the properties of those first supernovae.

High-Resolution Spectroscopic Landscape: Now and in the GMT Era

Surveys such as SkyMapper and Pristine are expected to increase the numbers of candidate metal-poor stars with $[\text{Fe}/\text{H}] < -5$ by an order of magnitude. Those candidates will require high-resolution spectroscopy to confirm their low iron abundance and to characterize their chemical abundance patterns. Many of those objects, however, will be too faint for high-resolution spectroscopy using current facilities. Among the ELTs, the only first-light, high-resolution spectrograph will be G-CLEF on the GMT.

At present, the most efficient high-resolution spectrograph on a >6 m class



telescope is MIKE (the Magellan Inamori Kyocera Echelle) on the 6.5 m Magellan Clay Telescope at Las Campanas Observatory in Chile. It has a remarkable ~40 % maximum efficiency in the blue (~450 nm), which is at least a factor of two higher than UVES on the 8 m VLT and HIRES on the 10 m Keck Telescope.

ESPRESSO (Echelle SPectrograph for Rocky Exoplanet and Stable Spectroscopic Observations) at ESO's Paranal Observatory in Chile achieved first light in late 2017. While ESPRESSO can be fed by all four 8 m VLTs through long fibers, the light-collecting power of the GMT and the efficiency with which light can be fed to G-CLEF will likely be more than a factor of two greater, which corresponds to a factor of ~7 increase in volume over which stars can be studied. That increase in volume is of enormous benefit when searching for and studying these exceptionally rare metal-poor stars. However, the amount of time available to simultaneously use all four VLTs will limit the contribution ESPRESSO can make compared to the GMT and G-CLEF.

Even more crucially, G-CLEF has a bluer wavelength cut-off than ESPRESSO (350 nm vs. 380 nm). This difference is critical for the discovery and characterization of metal-poor stars; as the strongest, unblended iron lines in the optical spectrum are all at blue wavelengths (344.06 nm, 358.12 nm, 371.99 nm, 373.71 nm, 382.04 nm and 385.99 nm; see *Figure 5-4*). These lines were stacked and co-added in Nordlander et al. (2017) to obtain the upper limit of $[Fe/H] < -6.5$ for SMSS J031300.36 – 670839.3. While five of these lines will be accessible to G-CLEF, only two can be reached when using ESPRESSO.

With more data, we can begin to answer the following questions and explore their implications:

Are there any zero-metallicity stars observable today?

If so, this would be the ultimate confirmation of the Big Bang and would reveal that low-mass star formation is possible at zero metallicity (Bromm & Larsen 2004, Stacy & Bromm 2014). G-CLEF will provide an unsurpassed capability for the confirmation of any zero-metallicity stars via the non-detection of the strongest iron lines shown in *Figure 5-4*. Any such discovery would provide invaluable insights into the formation of the infant Milky Way Galaxy.

What is the shape of the metallicity distribution function at lowest metallicity?

A cut-off in the metallicity distribution function would indicate the critical value below which low-mass star formation cannot occur and thereby constrain the star formation modes of the first stars (Salvadori et al. 2007). Such information would constrain the initial mass function of zero-metallicity stars and provide crucial details about the formation and early evolution of the Milky Way. While medium-resolution spectroscopy enables metallicity measurements down to $[Fe/H] = -4$, accurate iron abundance measurements at lower metallicity require high-resolution spectroscopy, and G-CLEF will be the world's premier facility.

What is the fraction of stars enriched in CNO elements?

At lowest metallicity, the fraction of objects with large overabundances of CNO elements approaches 100%, and more data are needed to reveal the physical properties and relative numbers of the progenitor “mixing and fallback” supernovae or rapidly rotating massive stars (Nomoto et al. 2013). High-resolution spectroscopy using G-CLEF is essential for measuring C (CH molecular lines near 4300 Å), N (CN molecular lines near 3883 Å and 4215 Å), and O (atomic lines near 6300 Å and 7770 Å). In some circumstances (e.g., high reddening, large CNO values) CNO abundances could also be measured from molecular lines in the near-IR (H- and K-bandpasses) using GMTNIRS. Quantifying the fraction of stars with enhanced CNO abundances at low metallicity would constrain the properties of the zero-metallicity stars that drove the early evolution of the Milky Way.

5.2 Faint Satellites and Streams

Low-mass satellite galaxies and stellar streams surrounding the Milky Way are significant to many fields in astronomy for a number of reasons:

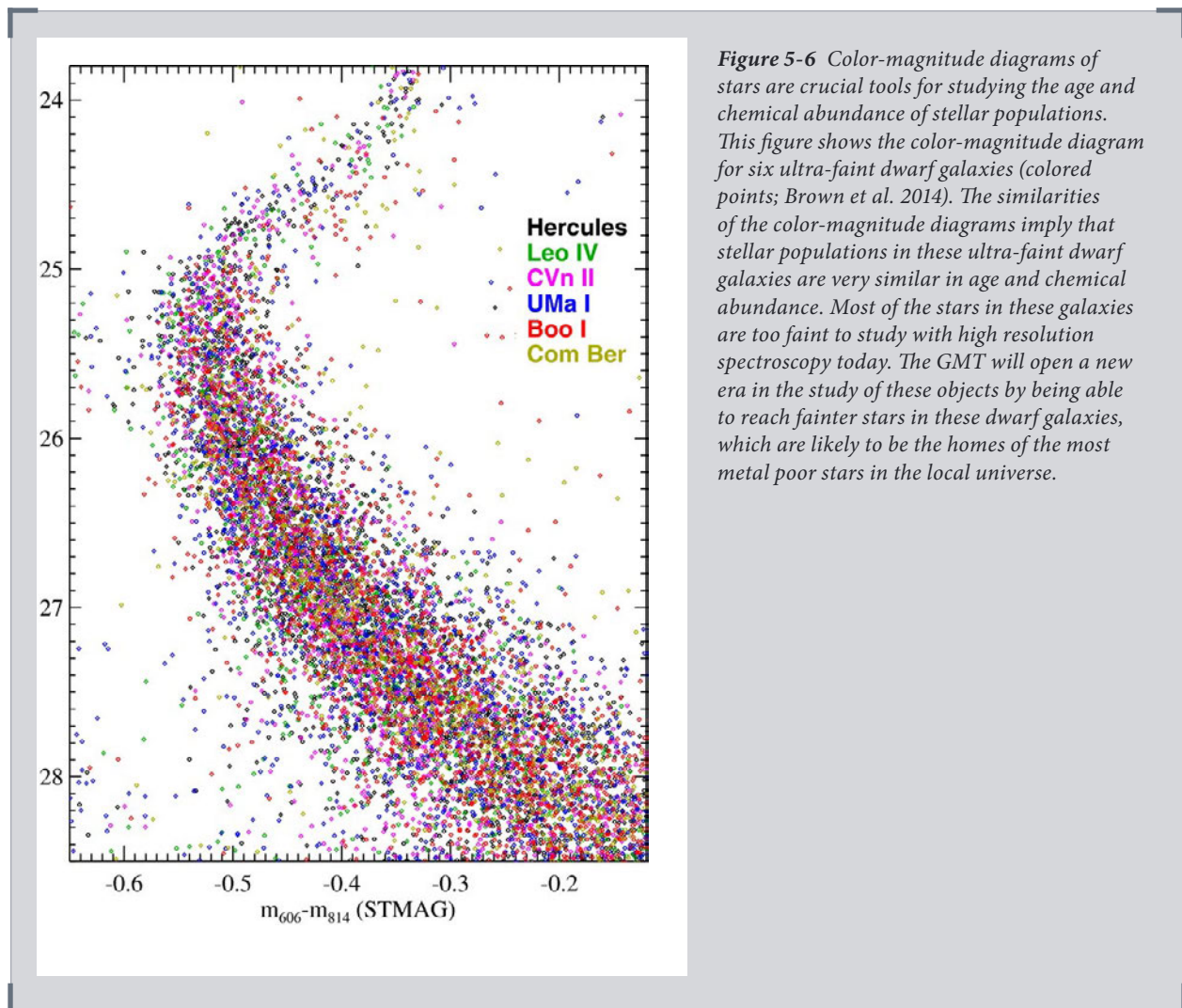


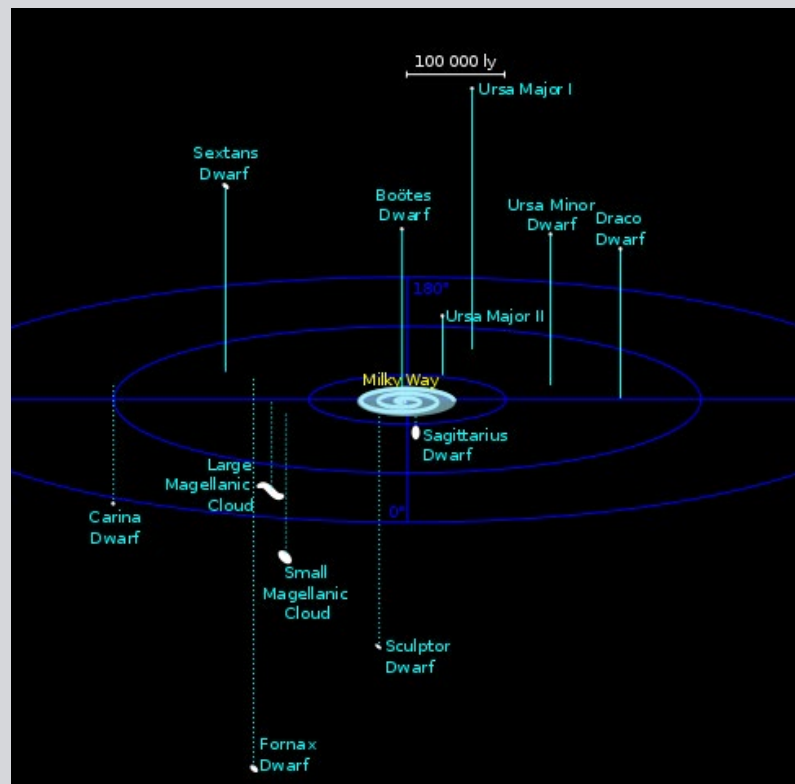
Figure 5-6 Color-magnitude diagrams of stars are crucial tools for studying the age and chemical abundance of stellar populations. This figure shows the color-magnitude diagram for six ultra-faint dwarf galaxies (colored points; Brown et al. 2014). The similarities of the color-magnitude diagrams imply that stellar populations in these ultra-faint dwarf galaxies are very similar in age and chemical abundance. Most of the stars in these galaxies are too faint to study with high resolution spectroscopy today. The GMT will open a new era in the study of these objects by being able to reach fainter stars in these dwarf galaxies, which are likely to be the homes of the most metal poor stars in the local universe.

- they represent galaxy formation and evolution in the lowest-mass regime and in the lowest-density environments;
- they contain proportionally more very metal-poor stars, making them crucial for exploring the early universe;
- they may solve the Missing Satellite Problem (Moore et al. 1999) or their spatial distribution may challenge the standard Λ CDM cosmology (Pawlowski et al. 2012); and
- they are the present and future of accretion into the Milky Way halo. (See *Figure 5-5*, *Figure 5-6* and *Figure 5-8*.)

The GMT will enable a rich inventory of the chemical and dynamical properties of the faint but numerous galaxies that were prevalent in the cosmic dawn era (but are too faint to be observed directly even with the GMT or JWST) through the study of their fossilized remains in the Local Group. The faintest known galaxies in the Local Group are all gas-poor and have uniformly old stellar populations (Brown et al. 2014; Weisz et al. 2014). They therefore reflect the physical conditions present in the early universe, and studies of these systems in the near field with the GMT will reveal how these earliest galaxies formed.

New low-mass satellite galaxies and stellar streams surrounding the Milky Way have been found by large-scale imaging projects like DES and Pan-STARRS (e.g., Drlica-Wagner et al. 2015; Kim et al. 2015, Koposov et al. 2015), and many more will be

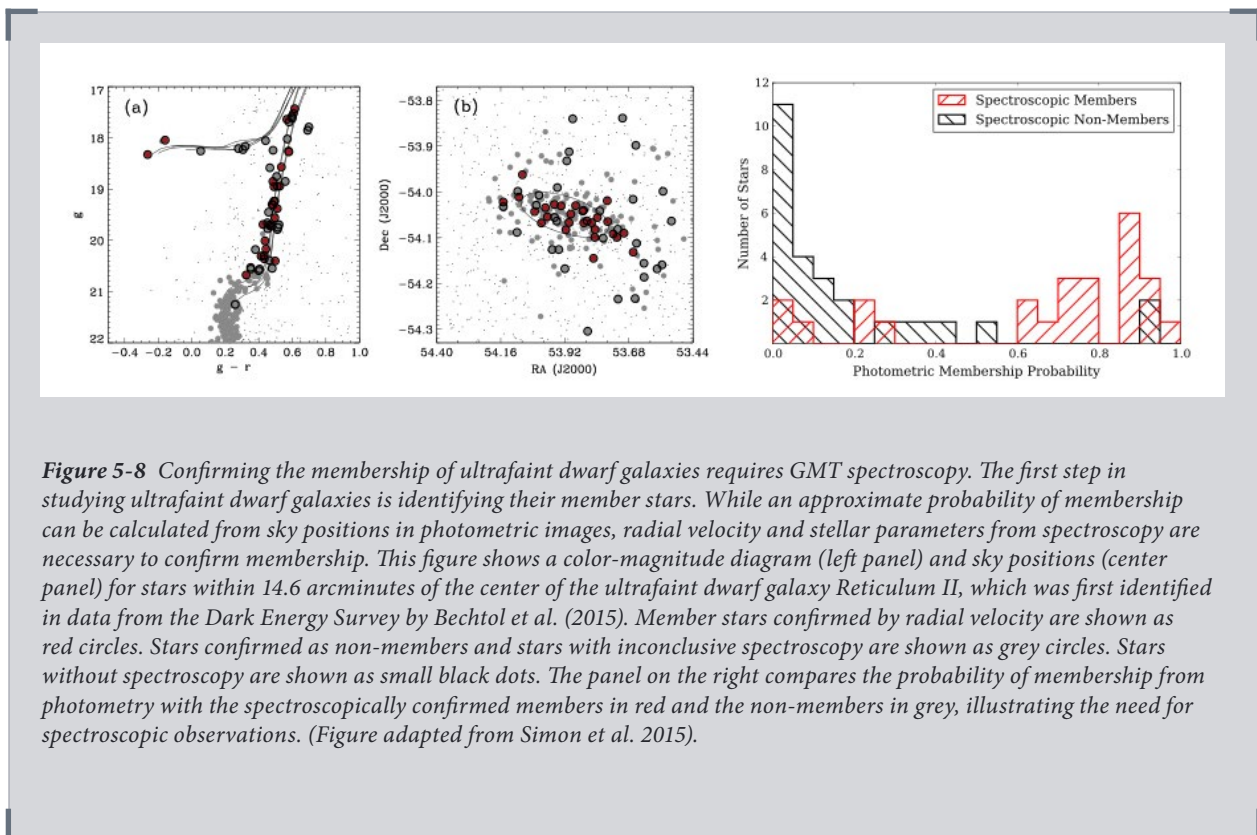
Figure 5-7 The GMT will be in a unique position to study the dwarf galaxy satellites of the Milky Way, spectroscopically, star by star, in the first decade of its operation. This 3D map shows some of the dwarf galaxies that surround the Milky Way. Newly discovered ultrafaint dwarf galaxies also inhabit this volume, typically falling within 50 kpc of the Milky Way. The largest blue circle has a radius of 150 kpc. The satellites mapped here hold interest for a wide range of astronomy fields as they hold clues to the formation of the first stars, the distribution of dark matter in galaxies, and the formation of structure in the universe. (Figure adapted from Wikimedia Commons)



identified by LSST, which is scheduled to start operations in the mid-2020's. But in order to use the newly identified ultra-faint dwarf (UFD) galaxies and streams for science, we must obtain detailed abundance information for as many of their member stars as possible. Because of the extremely low masses of these galaxies, low on-sky densities of member stars, and significant foreground contamination by Galactic sources (in some cases), it is challenging to positively identify the members of a newly discovered UFD without making *a priori* assumptions about the age, metallicity, or spatial distribution of the stars.

Spectroscopic follow-up observations are crucial for membership confirmation, but they are extremely time-consuming, even when target stars are restricted within a few tens of kpc. Current spectroscopic facilities are only able to reach the brighter stars in these objects at high resolution (e.g., Ji et al. 2016b), and fall back to lower resolution (with proportionally less information per star) in order to collect a more comprehensive data set (e.g., Simon et al. 2011).

The GMT is at a significant advantage for analyzing these satellites and streams relative to other ELTs, because its first-light capabilities include both high-resolution optical spectroscopy of individual stars and low-resolution, multi-object spectroscopy across a wide field of view with the high configurability of a fiber positioner, MANIFEST. When GMACS is fed by MANIFEST, the combination will be able to obtain low-resolution spectra for several hundred stars simultaneously within a 20' field of view. It will acquire high-quality (S/N \sim 80) spectra for stars brighter than the main-sequence turnoff in any UFD galaxy out to 100 kpc in two hours, and in ten minutes for dwarf galaxies at 40 kpc, where roughly half of new UFDs have been



found. This enables a quick and confident assessment of membership and kinematics in these tiny systems, and also permits repeat observations to check for both binary and variable stars. Further, advanced analysis techniques being developed for current large spectroscopic surveys (e.g., Ting et al. 2017) will allow fundamental stellar parameters, a subset of elemental abundances, and potentially ages to be determined from the low-spectral-resolution GMACS data.

G-CLEF will then be able to collect targeted high-resolution spectroscopy, providing a comprehensive chemical inventory of the member stars identified by GMACS work. Recent studies of the abundances in UFD galaxies have found that they can be quite heterogeneous in metallicity, and that the minimum metallicity is lower in less massive galaxies (Kirby et al. 2013). G-CLEF spectra will provide abundances for the elements that carry the most information about the history of star formation and chemical evolution in these galaxies. These include alpha elements Ca (4434, 4454) and Ti (4337, 4563), which are typically lower in dwarf galaxies (e.g., Venn et al. 2004). The abundances of Mn (4030), Zn (4722), Na (5889, 5895) and Cu (5105) are also typically low in dwarf galaxy stars, which may be a result of supernova winds escaping from the relatively weak gravitational potential of such small galaxies (Venn et al. 2012). Elements produced through neutron-capture processes are particularly informative: the ratio of Ba (4934) to Y (3950), Sr (4077) and Zr (3998) is typically high, which is thought to reflect the metallicity distribution of the stars that produced those elements (Herwig 2005). These chemical signatures are unique to stars that formed in dwarf galaxies.

GMACS and G-CLEF together are well suited to the two questions at the center of studies of ultrafaint dwarf galaxies. First, to understand the bulk properties of the galaxies it is crucial to be certain about which stars belong to them. Second, to map their histories of star formation and self-enrichment, it is necessary to have high-quality abundances across a range of elements. Together, these data will show us how these low-mass systems evolve (e.g., Frebel et al. 2016), and provide key insights into the properties of the population of stars accreted into galaxy halos.

References

- Bechtol, K. et al. 2015, ApJ 807:50
- Beers & Christlieb 2005, ARA&A, 43, 531
- Belokurov et al. 2006, ApJ, 642, 137
- Bromm & Larsen 2004, ARA&A, 42, 79
- Brown, T. et al. 2014, ApJ, 796:91
- Bullock & Johnston 2005, ApJ, 635, 931
- Cirasuolo, M. et al. 2014, Proc. SPIE 9147:91470N
- Dalton, G. et al. 2016, Proc. SPIE, 9908:99081G
- de Jong, R. et al. 2016, Proc. SPIE, 9908:99081O
- De Silva, G. et al. 2015, MNRAS 449:2604
- Drlica-Wagner, A. et al. 2015, ApJ 813:109
- Frebel, A. et al. 2016, ApJ 826:110
- Frebel, A. & Norris, J. 2015, ARA&A 53:631
- Freeman & Bland-Hawthorn 2002, ARA&A, 40, 487
- Gilmore, G. & Randich, S. 2012, ESO Messenger 147:25
- Herwig, F. 2005, ARA&A 43:435
- Holtzman, J. et al. 2015, AJ 150:148
- Howes et al. 2015, Nature, 527, 484
- Karlssohn 2006, ApJ, 641, L41
- Keller et al. 2007, PASA, 24, 1
- Keller et al. 2014, Nature, 506, 463
- Kim, D. et al. 2015, ApJL 804:44
- Kirby, E. et al. 2013, ApJ 779:102
- Koposov, S.E. et al. 2015, ApJ, 805, 130
- Luo, A. et al. 2015, RAA 15:1095
- Moore, B et al. 1999, ApJL 524:19
- Nomoto et al. 2013, ARA&A, 51, 457
- Nordlander et al. 2017, A&A, 597, A6
- Pawlowski, M.S., et al. 2012, MNRAS 423:1109
- Prusti, T. et al. 2016, A&A 595:A1 T
- Ricotti & Gnedin 2005, ApJ, 629, 259
- Salvadori et al. 2007, MNRAS, 381, 647
- Simon, J.D. et al. 2011, ApJ 733:46
- Simon, J.D. et al. 2015, ApJ 808:95
- Stacy & Bromm 2014, ApJ, 785, 73
- Starkenburger, E. et al. 2017, MNRAS 471:2587
- Ting, Y.-S. et al. 2017, ApJL 849:9
- Tumlinson 2010, ApJ, 708, 1398
- Venn, K. et al. 2004, AJ 128:1177
- Venn, K. et al. 2012, ApJ 751:102
- Voggel, K. et al. 2016, MNRAS 460:3384
- Weisz, D. et al. 2014, ApJ 789: 147



*The Hubble Space Telescope "Frontier Field," containing the rich cluster of galaxies
MACSJ0717.5+3745. Credit: NASA*



CHAPTER 6

The Growth of Galaxies Over Cosmic Time

How do stars form in galaxies over cosmic time? The diversity of galaxies we see around us today is the product of more than ten billion years of galaxy evolution over the history of the universe. As we move outward from local galaxies, we are looking back in time; the light we see left the galaxies that produced it billions of years ago. This fact means that we can observe the history of galaxy populations directly, although these observations are challenging because distant galaxies are small and extraordinarily faint.

The tremendous light-gathering power of the GMT and the sharp images that it will produce will transform our understanding of the evolution of galaxy populations. The GMT will reveal the internal workings of galaxies across the entirety of cosmic history, and will enable us to measure the smallest and faintest galaxies ever observed.

Chapter Authors

Guillermo A. Blanc (Carnegie Institution for Science, The Observatories)

Alan Dressler (Carnegie Institution for Science, The Observatories)

Valentino Gonzalez (University of Chile)

Brent Groves (Australian National University)

Andrew Newman (Carnegie Institution for Science, The Observatories)

Jonelle Walsh (Texas A&M University)

6 The Growth of Galaxies Over Cosmic Time

In the 1920s Edwin Hubble succeeded in measuring the distance to the Andromeda “spiral nebula” and proved that it lay far beyond the bounds of the Milky Way. This discovery was profoundly important: we learned that the universe was much larger than the Milky Way and that Andromeda was a giant structure, made of hundreds of billions of stars like the Milky Way. The word *galaxy* could no longer be reserved for the Milky Way, because galaxies fill the observable Universe.

One hundred years later, the challenge remains of understanding how these galaxies formed and grew over cosmic time. We have a powerful advantage in this quest: at any instant we can observe galaxies at all stages in their development. The light from Andromeda takes 2.5 million years to reach us, so we observe that galaxy as it was 2.5 million years ago. This is a huge span of time in human terms, but is a tiny fraction of the 13 billion-year age of the universe. With powerful telescopes such as the GMT we will be able to observe faint light from the most distant galaxies, allowing us to see these galaxies as they were forming 13 billion years ago. Our challenge translates into piecing together the complex history of any one galaxy from snapshots of different galaxies over the age of the Universe.

We now understand that galaxies form within gravitational potential wells of dark matter at the densest parts of the universe’s large scale matter distribution,

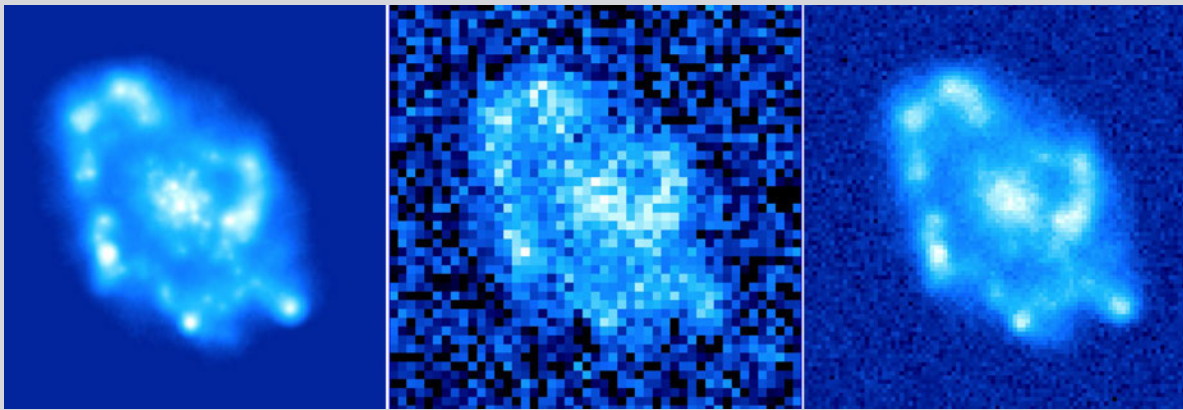


Figure 6-1 GMT imaging with adaptive optics will test ideas and models of how galaxies grew in the era of intense star formation. This figure shows a single galaxy extracted from a “N-body” computer simulation of a large volume of the universe. On the left, the galaxy is shown as it appears, in full resolution, in the computation (Illustris, Torrey et al. 2015). The middle and right panels show how well the details of such a galaxy would be recovered using an 8 m class telescope (middle) and the GMT (right). The middle panel shows that, even when assisted by adaptive optics, existing telescopes are barely capable of resolving the galaxy’s detailed structure. The GMT’s formidable light collecting capability and high spatial resolution will provide a much clearer picture that retains all the major characteristics of the galaxy’s true appearance. This is essential information for studying of how galaxies change and grow across most of cosmic time and particularly during key epochs in the formation history of the universe.

commonly called the “cosmic web.” Gas, the raw material from which stars form, falls into these dense regions. Star formation begins, giving rise to galaxies. Galaxies grow as successive generations of stars are born from gas that includes hydrogen and helium formed in the Big Bang, enriched by heavier chemical elements forged in previous generations of stars. These heavy elements are essential for building planets and the development of life.

While this general picture has been confirmed, important physics regarding the formation of galaxies is far from understood. We know, for example, that stars did not form at a constant rate over the lifetime of galaxies and, indeed, galaxies show wide variation in the star formation histories. Our observations indicate that, on average, the star formation rate (SFR) in galaxies peaked about 10 billion years ago (at a redshift $z \sim 2$, e.g. Madau & Dickinson 2014). Since that time, galaxies have grown significantly in size, stellar mass, and abundance of heavy elements (metallicity). Among the most massive galaxies the fraction of quiescent (not actively forming stars) galaxies has increased by almost a factor of five.

The size of the gas reservoir from which stars may form is regulated by the balance between gas accretion onto galaxies, the rate at which stars form from this gas, and gas loss from galaxies. Gas may be driven out of galaxies by stellar winds, supernova explosions (called stellar feedback), and the energetic radiation from hot gas falling into the supermassive black holes found at the center of galaxies, called active galactic nucleus feedback (Davé et al. 2011a,b, 2012, Forbes et al. 2013). We do not understand how these processes interact to produce the overall, substantial decline of star formation since $z=2$, and how these processes depend on basic galaxy properties, including their mass.

Measuring the fractional abundance of the heavy chemical elements in the gas (the *metallicity*) provides insight into these processes of gas loss and accretion. Star formation produces heavy elements through the nuclear reactions that power star *nucleosynthesis*. These heavy elements mix with the surrounding medium and may be expelled from the galaxy via stellar feedback. The accretion of unenriched gas onto the galaxy will dilute the enriched gas and decrease the metallicity. The growths of galaxy and central black hole masses over time are also important tracers of the star formation history.

Dynamical processes within galaxies and between galaxies are also expected to have a strong impact on star formation. These include gravitational instabilities, the formation of disks and spheroids within galaxies, and tidal interactions and mergers between galaxies. A diverse array of theoretical models and detailed numerical simulations have been developed to describe the physics behind the formation and evolution of galaxies. Many of these models do not agree, and the necessary observations to discriminate among the models is often beyond the reach of current telescopes (see *Figure 6-1*).

The limited spatial resolution achievable with current telescopes prevents us from resolving individual regions of star forming, whose typical dimensions are less than 100 pc, beyond the local universe. The limited sensitivity of current telescopes precludes observing the full range of stellar masses to learn about stellar populations, star formation histories, and stellar dynamics.

In this chapter we explore the leap forward in galaxy evolution studies enabled by the GMT’s extraordinary spatial resolution (up to 0.01 arcsecond resolution) and enormous sensitivity.

- We will learn how rapidly the largest black holes were formed, revealing if supermassive black holes and galaxies grew together, or if black holes led the way
- We will resolve very distant galaxies, allowing us to get a clearer picture of the structure of these very young galaxies
- The GMT's huge light grasp will allow us to isolate individual sites of star formation across cosmic time
- GMT measurements of the birth rate of stars at discrete sites and for entire galaxies will reveal how galaxies grow and evolve
- GMT spectroscopy will chemically assay the gas that fuels star factories. Measurements of the chemical composition of outflowing gas will reveal how primeval gas clouds are transformed over billions of years to the splendor and variety of galaxies we see today
- The GMT will open a window into the very abundant faint galaxies that may be close analogs of the first generations of galaxies that formed in the very young universe

6.1 The Distribution of Gas, Star Formation, and Metals in Galaxies

What drove the star formation process at $z \sim 2$ —so-called “cosmic noon”—when star formation rates of galaxies were fifty times higher than today? At this epoch, ten billion years ago, the star-formation-rate density of the universe peaked (Madau & Dickinson 2014), presumably driven by larger gas supplies in galaxies (Tacconi et al., 2013). Star-forming galaxies in this epoch appear as unsettled disks, with star formation occurring in a more clumpy manner, and in star-forming regions with much higher velocity dispersions in their gas, than is observed today in local galaxies (Genzel et al. 2006; Förster Schreiber et al. 2006, 2009, Elmegreen et al. 2009, Newman et al., 2013, Wisnioski et al., 2015).

From cosmic noon to today, the star formation rate and gas fraction of galaxies have declined and the star formation activity within them appears smoother, and possibly less efficient. The heavy elements produced by evolved stars have been distributed across the galaxies. Yet the processes that lead to this decline in star formation rates and gas are uncertain, as is how the elements have been distributed. Unlike with the current generation of telescopes, the sensitivity, spatial resolution, spectral resolution, and wavelength coverage of the GMT and its instruments will provide definitive answers to the question of what drives the star formation processes in galaxies during cosmic noon and the decline since then. Below we discuss GMT observations that will map how gas drives star formation and the production and dispersal of heavy elements across cosmic time.

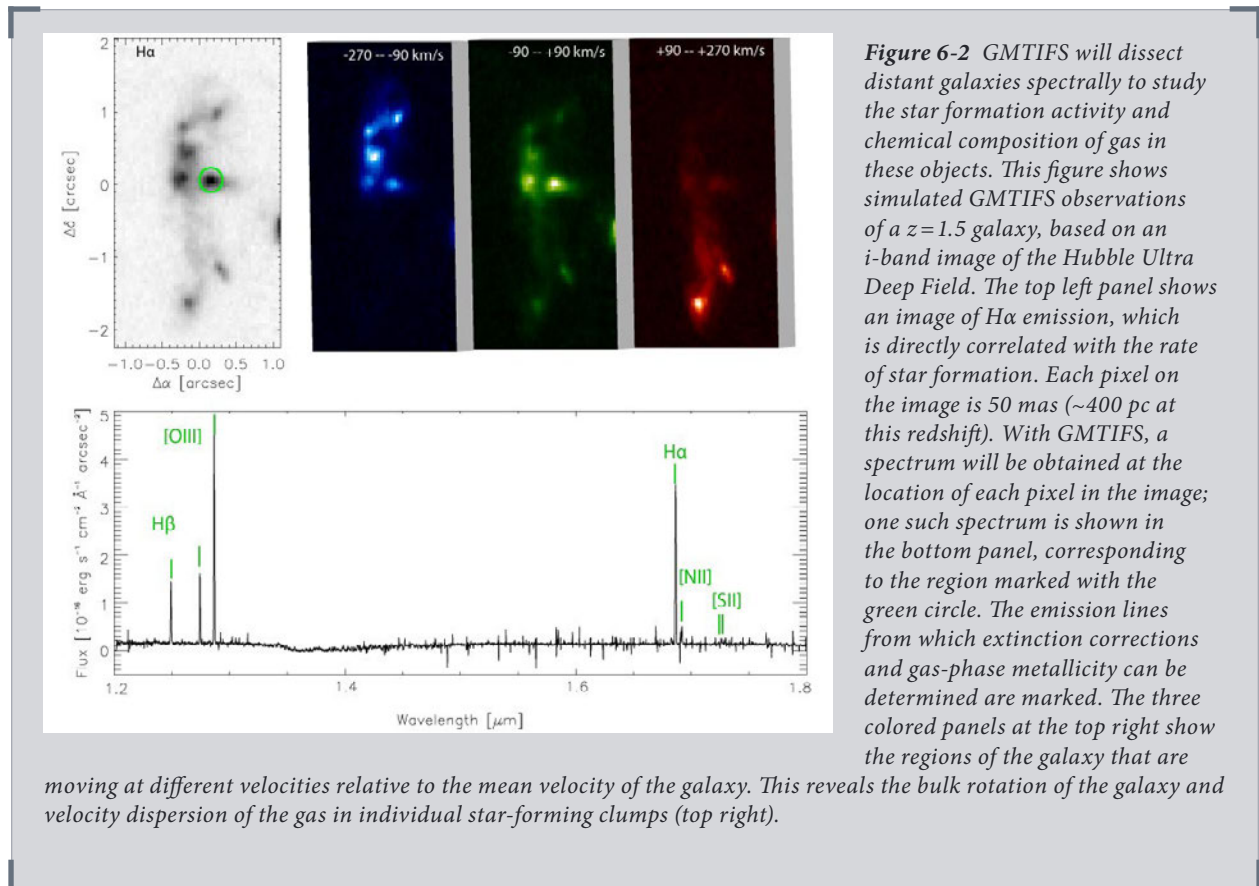
Mapping the star-formation rate across galaxies

The vigorous star formation rates observed at cosmic noon must be supported by rapid rates of accretion of gas onto young galaxies (e.g. Concelice et al., 2013). Yet such star formation rates will also prodigiously produce heavy elements and drive strong winds and outflows from these systems. Both the gas accretion and outflows

could lead to the higher gas velocity dispersion we observe at cosmic noon, but current observations cannot distinguish between these processes (Johnson et al. 2017). To understand the drivers for the distribution and rates of star formation at these epochs and the high gas velocity dispersions observed, we need high spatial resolution maps of star formation, with the highest spectral resolution possible.

At $R = 10,000$, GMTIFS has a much higher spectral resolution than any current or planned NIR Integral Field Spectrographs (cf. KMOS with $R \sim 4000$, Keck OSIRIS with $R \sim 4000$, Gemini/NIFS with $R \sim 5000$, and JWST NIRSpec with $R \sim 3000$). This higher instrumental spectral resolution translates into a velocity resolution of $\sigma \sim 15$ km/s and access to a much greater spectral window ($\sim 80\%$ clear of atmospheric emission). The sensitivity of the GMT means that the H α line can be measured down to a flux of 5×10^{-17} erg s $^{-1}$ cm $^{-2}$ arcsec $^{-2}$ ($S/N \lesssim 5$ in all bands) with only 2 hrs integration, assuming 25 mas spatial resolution elements (or “spaxels”), and line widths of 100 km/s.

With this capability GMTIFS will map H α and gas velocity structure out to 1–1.5 effective radii (R_e) in $>0.1 L_{\text{H}\alpha}^*$ galaxies ($M_{\star} > 10^{9.5} M_{\odot}$), out to redshifts of $z \sim 2.5$ (based on typical radii and fluxes for $z \sim 2$ galaxies; van der Wel et al. 2014, Genzel et al. 2014). With the addition of H β line maps, dust extinction can be determined for producing extinction-corrected star-formation-rate surface densities. Star forming galaxies can be mapped at ~ 400 pc (0.05”) resolution from redshifts $z \sim 2.3$ until today (see **Figure 6-2**). Furthermore, using the highest angular resolution of



GMTIFS with LTAO (6 mas spaxels) allows the brightest clumps at these redshifts to be resolved into individual star-forming regions at ~ 100 pc scales.

The hydrogen Balmer emission lines H α and H β (6563 Å and 4861 Å rest-frame, respectively) and nearby strong emission lines such as [OIII]5007, [NII]6548,6584, and [SII]6716,6731, are key to estimate dust extinction-corrected star formation rates, along with other measures of the ISM such as dust attenuation, ionization mechanisms, and gas-phase elemental abundances. The NIR atmospheric transmission windows mean that the hydrogen lines are available in 3 redshift ranges: $z \sim 0.8-1.0$, $1.4-1.7$, and $2.1-2.6$, using a combination of the *ZJ*, *JH*, and *HK* bands, respectively, enabling a direct measurement of how star formation proceeds from cosmic noon until today.

Based on the H α Luminosity function (Sobral et al. 2013), we expect to observe 6.6 (0.29), 11.4 (0.5), 6.2 (0.27) galaxies more luminous than $0.1 L_{\text{H}\alpha}^*$ ($1.0 L_{\text{H}\alpha}^*$) per arcmin², at $z=0.85, 1.5, 2.25$ (*ZJ*, *JH*, *HK*). Such number densities point to a strong synergy with JWST: a $2.2' \times 2.2'$ JWST NIRCcam deep field would find 30–40 $0.1 L_{\text{H}\alpha}^*$ ($1-2 L_{\text{H}\alpha}^*$) galaxies per field, providing sufficient targets for detailed mapping with GMTIFS of the H α surface brightness (star formation rate surface density) and gas kinematics (turbulence, outflows), the H α /H β line ratio (dust extinction), and diagnostic lines for the gas-phase metallicity ([NII], [SII], and H α) and ISM conditions ([OIII]/H β).

Such maps would give unprecedented insights into how the distribution of star formation in galaxies evolves from cosmic noon until today. The spectral resolution of GMTIFS means that the velocity profiles of the star-forming regions would be resolved to ~ 15 km/s, allowing us to answer the question of whether the gas velocity dispersion at these epochs is from turbulent motions as is expected from gas accretion, or if non-gaussian structures are predominate, indicating shocks and bulk motions of gas such as winds. Dust extinction maps will give insights into how the gas and metals are distributed.

The distribution of heavy elements in star-forming galaxies across redshift

As galaxies evolve, new generations of stars produce and release heavy elements or “metals” into the ISM. The chemical balance of the interstellar gas in galaxies is regulated by this metal production, the accretion of low metallicity material, and the ejection of enriched gas via galactic outflows. How these processes proceed determines the overall chemical composition and internal chemical structure of galaxies. The high velocity dispersions of the star forming clumps in high-redshift galaxies may be indicative of such outflows. By resolving the velocity structure of individual clumps using the high spectral resolution mode of GMTIFS, such outflows will be detected through asymmetries in the H α line. Furthermore, the high spatial sampling of GMTIFS (approximately 20 spatial resolution elements 0.05 arcsec, ~ 400 pc in size across a L_{\star} disk—where metal-sensitive spectral features from oxygen, nitrogen, and sulfur will be strongest) will enable unambiguous measurements of the internal distribution of metals inside distant galaxies.

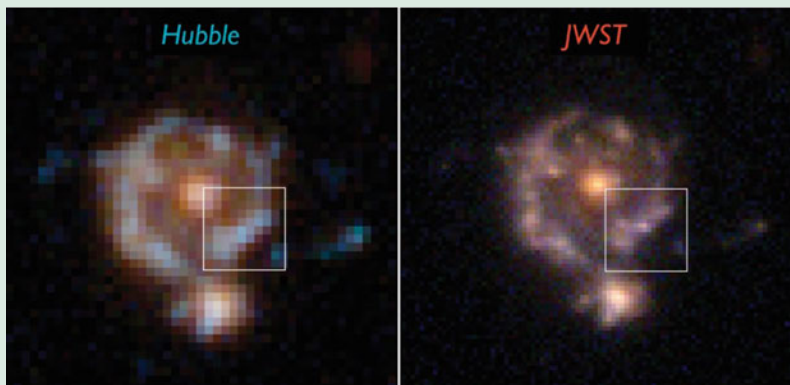
In the local universe, a tight correlation is observed between the stellar mass and metallicity of galaxies, with the metallicity increasing for more massive systems (Garnett, 2002; Tremonti et al., 2004). At higher redshifts this correlation is also observed, but offset to lower overall metallicities (e.g. Erb et al. 2006, Zahid et



Synergy with JWST Deep-Field Data



Figure 6-3 The GMT will significantly increase the scientific value of the deep-field data taken by NASA's James Webb Space Telescope (JWST; top). The NIRC*am* instrument on JWST will produce samples of a few dozen galaxies at redshifts right before and close to the epoch of "cosmic noon" ($1 < z < 2$). The GMTIFS integral field spectrograph will provide crucial follow-up to study these JWST targets in detail, as it will provide "data cubes" of high signal-to-noise ratio spectra of even low mass galaxies, with ten times better spatial resolution than can be achieved with JWST. Image credits: Northrup Grumman (top). A simulated galaxy at redshift of two as viewed by HST (left) and JWST (right). JWST will resolve star-forming regions on 250 pc scales (Ceverino, Moody, and Snyder).



al. 2014, Kashino et al. 2017). When resolved, the metallicity maps of local star forming galaxies show consistently declining radial gradients ($\Delta Z/\Delta R = -0.1 \text{ dex}/R_{\odot}$; Sanchez et al. 2014, Ho et al. 2015). At higher redshift, the slopes appear flatter ($\Delta Z/\Delta R \sim 0 \text{ dex}/R_{\odot}$; Leethochawalit et al. 2016, Wuyts et al. 2016), but current

observations have barely the angular resolution to measure the metallicity gradients at these epochs, except in a few gravitationally lensed cases. GMTIFS, assisted by adaptive optics, will answer the question of how consistent is the slope of the metallicity gradients across galaxies, and if current stellar feedback is sufficient to drive such gradients. Star forming regions tend to be centrally concentrated at both low and high redshifts, and star formation induced outflows are thought to be essential to redistribute the heavy elements and transport them to the galaxy outskirts (e.g. Schaefer et al. 2017, Genzel et al. 2013). The spatial sampling of GMTIFS is sufficient to distinguish individual star-forming complexes (~ 800 pc or $0.1''$ in size at $z \sim 1.5$; see **Figure 6-2**), to determine whether they are driving outflows, and if their metallicity differs from the surrounding gas. Lower metallicities could also be a “smoking gun” of recently accreted gas, as suggested for some local galaxies (Richards et al. 2014).

Such work builds upon the pioneering IFS work of SINS (Förster-Schreiber et al. 2009), KMOS3D (Wisnioski et al. 2015) and KROSS (Magdis et al. 2016) on high redshift star formation, and answers the questions posed by these surveys by using the unprecedented spatial and spectral resolution of GMTIFS with the sensitivity provided by the GMT’s collecting area of 368 m^2 . The maps of star formation, dust extinction, gas-phase metallicity, and velocity structure provided by GMTIFS at $0.05\text{--}0.1''$ spatial resolution for $\sim L_\star$ galaxies will prove revolutionary in understanding how star formation proceeds at cosmic noon, and help understand how galaxies have grown and evolved from this epoch to the galaxies we observe locally.

6.2 The Evolution of Galaxy Structure and Stellar Populations

When and where did the stars in galaxies form, and how do their assembly histories vary within galaxies and with fundamental galaxy properties such as mass and environment (for example, membership in groups or clusters)? What processes cause star formation to die off in progressively smaller galaxies over time? When and how did galaxy structure and stellar populations become linked? Lookback studies that connect galaxy populations over cosmic time are the main tool for answering these questions. Further progress requires more detailed information on the kinematics, ages, and chemical abundances of stars in distant galaxies. The stellar continuum in a galaxy’s spectrum is much fainter and harder to detect than the bright emission lines that arise from gaseous components; as a result, current facilities are severely limited in their ability to study the stellar components of these systems. The GMT will enable major advances over current facilities through its improved angular resolution and sensitivity.

The Kinematics of Star-Forming Galaxies and the Emergence of Mature Disks

Even when studying the kinematics of their gas components via bright emission lines, the limitations of current observations have left many key questions regarding the formation of stellar structures in galaxies unanswered. First, the fraction of galaxies at a given mass and redshift that show ordered rotation is not well known. Since the galaxies that appear to be the most dispersion-dominated are also among the smallest in size (Newman et al. 2013), it may be that current observations simply cannot resolve an underlying disk, or that they lack the sensitivity needed to detect

rotation at larger radii. Second, the relation between the galaxies currently under study and their descendants is unclear. High velocity dispersions in the gas suggest that we are observing the thick components of present-day disks being formed *in situ*, rather than being dynamically scattered out of a thin disk. However, with only a handful of exceptions, progenitors of Milky Way-like galaxies are too small and faint to be found in current samples, which are made up of larger, more massive systems that may instead become early-type galaxies (Glazebrook 2013). Systematic observations of ionized gas kinematics of lower-mass galaxies are needed to unveil the early history of Milky Way analogs. The sensitivity and angular resolution of GMTIFS will enable these observations for the first time.

For the more massive galaxies ($M^* > \sim 10^{10} M_{\odot}$) at $z \sim 2 - 3$ that are currently under study, GMTIFS will improve on existing data via its superior spatial sampling of the velocity fields. Another key advantage will be increased sensitivity to reach the faint outer disk, possibly probing into the dark matter-dominated regime that is currently beyond reach (Genzel et al. 2017). The sensitivity and spectral resolution of GMTIFS will enable mapping of kinematic asymmetries and non-circular motions indicative of inflowing or outflowing gas or mergers, which can then be correlated with the signatures of galaxy-scale outflows seen in rest-frame UV spectra to provide a comprehensive picture of baryon flows. GMTIFS also has the resolution and sensitivity required to map lower-mass galaxies that are nearly unexplored at present. Consider a typical Milky Way progenitor at $z = 2.5$ (stellar mass $\sim 3 \times 10^9 M_{\odot}$, $R_e \sim 1.5$ kpc, SFR $\sim 4 M_{\odot}/\text{yr}$): Such a galaxy is at the very limit of present facilities, but GMT with AO can resolve it into 340 independent resolution elements, whereas JWST will provide only 24. A 4-hour observation with GMTIFS will be sufficient to produce a detailed velocity map in a galaxy analogous to the young Milky Way, providing a new window into the formation history of the Galaxy that complements stellar archaeology.

Quantifying the level of rotational vs dispersion (V/σ) support in massive galaxies will also provide insight into how galaxies migrate from star-forming to quiescent. Theoretical work is beginning to link merging (major and minor, dry and wet) with the evolution in spin parameter for galaxies over cosmic time (e.g., Naab et al. 2014, Choi & Yi 2017, Penoyre et al. 2017, Lagos et al. 2017), so that we can start to use the evolution of galaxies in V/σ with mass and cosmic time to understand the relative roles that merging and gas accretion play in creating quiescent galaxies.

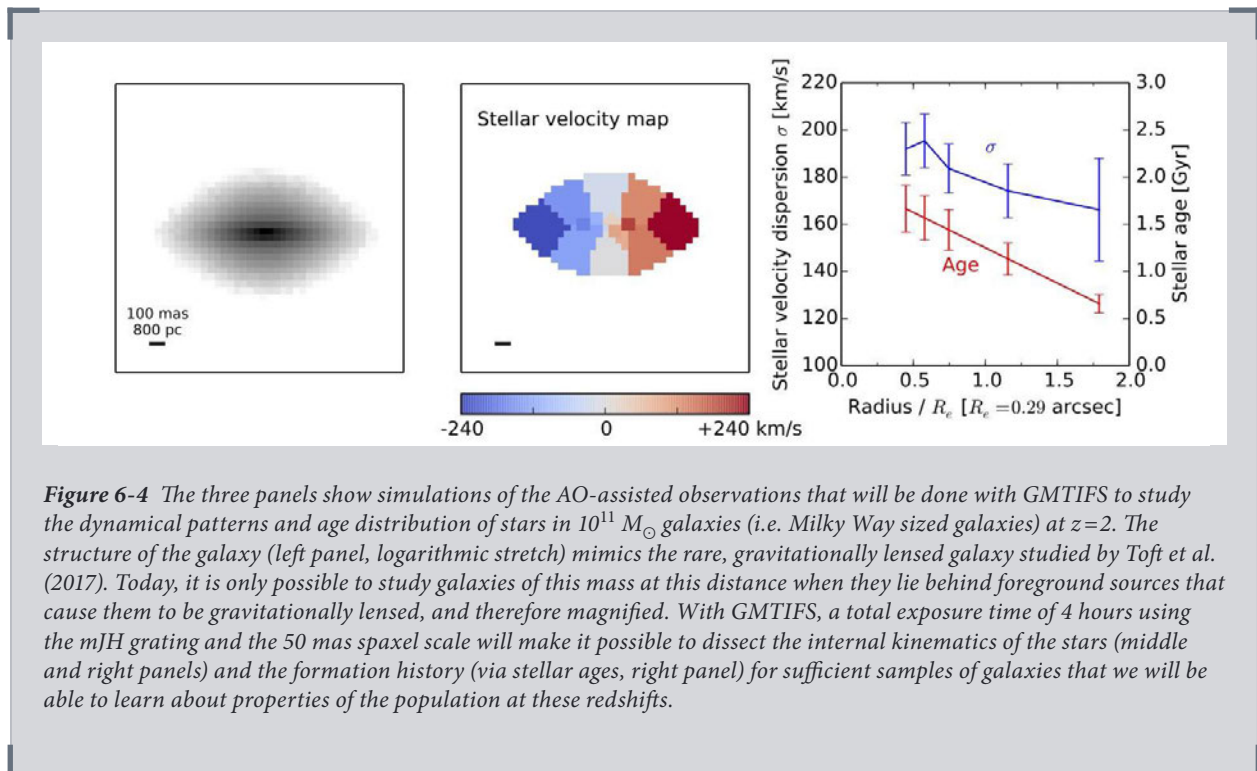
The Kinematics and Stellar Populations of Quiescent Galaxies

Even with the current suite of sensitive instrumentation, spectroscopy of $z > 1.5$ galaxies has been almost entirely of gas in emission or absorption, rather than of stellar absorption features. This is particularly problematic for quiescent galaxies, which lack bright gas emission lines. These galaxies are a non-negligible part of the galaxy population by $z \sim 2$ (about one-third of galaxies exceeding $10^{11} M_{\odot}$), and the physical causes of the cessation of star formation in these galaxies (so-called “quenching”) remain a major open question. These systems are essential for understanding the star formation histories of the early generations of stars that form the older stellar components of galaxies. The GMT will prove critical in the study of quiescent galaxies at high redshifts, overcoming the enormous difficulties currently faced to study these systems with present day instrumentation.

Given the long exposures required with current facilities, only a handful of $z > 2$ galaxies have yet been observed with adequate depth to measure stellar absorption lines in any detail. These observations have provided the first stellar velocity

dispersions and dynamical masses for quiescent galaxies at $2 < z < 2.8$ (e.g., van de Sande et al. 2013, Belli et al. 2017). Even more desirable are *spatially resolved* observations of the stellar continuum. So far this has been possible only for two gravitationally lensed galaxies (Newman et al. 2015; Toft et al. 2017). The lensed cases revealed massive and compact disk galaxies seen ~ 1 Gyr after quenching that are rotating extremely rapidly, perhaps up to ~ 500 km/s. Such galaxies are very rare or absent in the local universe, implying that structural transformation into elliptical galaxies followed the quenching of star formation. This may be related to the surprisingly large growth in size seen in quiescent galaxies over the same period (e.g., van Dokkum et al. 2010), and the transition from rapidly rotating disks to slow rotators with significant dispersion dominated components (Choi & Yi 2017). The GMT will enable major progress in the study of stellar populations and dynamics across cosmic time via the NIRMOS and GMTIFS instruments. For brighter systems, GMTIFS will be able to spatially resolve the stellar continuum. For fainter systems, NIRMOS will obtain high S/N integrated measurements of the stellar continuum.

Theoretical simulations predict there are multiple pathways to produce quiescent galaxies in the early universe (Wellons et al. 2015). A key discriminating observation is whether massive galaxies were quenched uniformly or “inside out.” Spatially resolved GMTIFS observations will test these ideas by mapping the star formation history of stellar populations for representative samples near the epoch of quenching for massive galaxies. Measuring their kinematics, including rotational support, will provide an additional way to connect these galaxies to their immediate star-forming progenitors at $z > 3$. A simulated observation of a $z=2$ galaxy with a stellar mass of $10^{11} M_{\odot}$ is shown in **Figure 6-4**. The simulation reveals a remarkable stellar velocity field with detail that is currently unobtainable beyond the local universe. Besides



kinematics, this observation yields detailed information on the ages, chemical abundances, and abundance ratios of the stars as a function of galactocentric radius, using the age-sensitive Balmer lines and metallic transitions (e.g., Mg b, Fe lines). A 15-night program could cover ~ 30 similarly massive quiescent galaxies at $z \sim 2-3$, enough to provide a census of their resolved star formation histories and kinematics. In addition to sensitivity, the angular resolution of the GMT is critical: quiescent galaxies at $z > 2$ have effective radii $< \sim 0.2''$, which will barely be resolved with JWST.

Since quiescence is strongly mass-dependent, understanding the emergence of quiescent galaxies demands observations over a wide range of masses. Quiescent systems at $z > 1.5$ and $< 10^8 M_{\odot}$ are virtually unexplored with current spectroscopic facilities and will be studied systematically with the GMT. For faint low mass galaxies, seeing-limited (or GLAO-assisted) observations with NIRMOS will probe the stellar continuum down to $K_s = 23.5$ AB, corresponding to a $1 \times 10^{10} M_{\odot}$ quiescent galaxy at $z = 2$, with adequate quality (S/N ~ 10 per resolution element in H-band) to



A GMTIFS Survey of High Redshift Galaxies

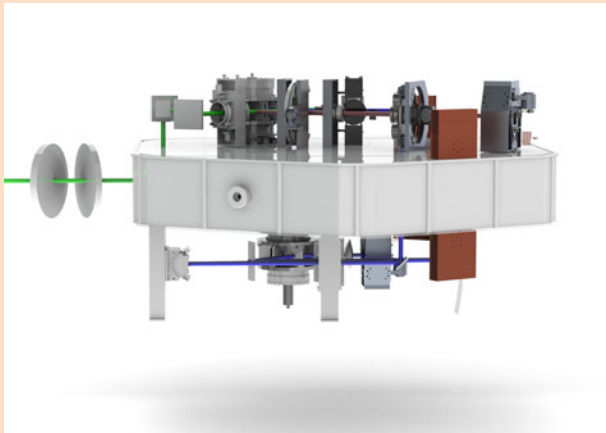


Figure 6-5 A multi-semester 30-night program with GMTIFS could target ~ 60 star forming galaxies and ~ 30 quiescent galaxies across the $z = 0.8-1.0$, $1.4-1.7$, and $2.1-2.6$ redshift windows. In these windows, several rest-frame optical diagnostic spectral features tracing the extinction corrected star formation rate, the chemical abundances of both gas and stars, and the stellar and ionized gas kinematics can be measured. Total exposure times of only 2 hrs will be sufficient to map ionized gas emission lines in star forming systems (S/N = 5 per $0.05''$ spaxel for a $10^{-17} \text{ erg s}^{-1} \text{ cm}^{-2}$ emission line). Exposure times of 4 hrs in quiescent systems will enable spectral mapping of the stellar continuum (S/N = 5 per 1 \AA for an average $\sim 1 \text{ kpc}$ sized Voronoi spaxel for a $K_{AB} = 22 \text{ mag}$ system). Image credit: GMTIFS Team

measure stellar kinematics and ages in a 4 hour observation. Approximately 90 galaxies at $z = 2-2.6$ down to this K_s limit are present within a NIRMOS field of view, enabling efficient multiplexing. Understanding the first quiescent galaxies that emerge at $z > 3$ (e.g., Glazebrook et al. 2017) will also be a premier area for NIRMOS; given their lower surface density, the integrated stellar continuum of these galaxies can be efficiently observed with a single-object near-infrared spectrograph.

The Properties of Massive Stars in High-redshift Galaxies

Massive stars play a key role in galaxy evolution: they produce metals, ionizing radiation, and the winds and radiation pressure thought to regulate star formation. The GMACS optical spectrograph on the GMT, coupled with the wide-field MANIFEST multi-fiber system, will observe rest frame UV spectra of high redshift galaxies, where emission is dominated by massive stars, with unprecedented

sensitivity. Observations indicate that the massive stars that dominate the light of star-forming galaxies at $z \sim 2$ have ionizing spectra and/or chemical abundances that differ from local galaxies (Steidel et al. 2014, Shapley et al. 2015). Recent stellar models imply that binary star evolution effects at low metallicity could lead to important differences in the properties of such stars (Stanway et al. 2016).

The rest-frame UV spectrum contains a wealth of photospheric and wind features (e.g., He II 1640, N V 1240, C IV, blends at 1415-1435 Å and 1935-2050 Å; Rix et al. 2004) that can be used to infer critical parameters of the massive star population that remain highly uncertain, including stellar metallicity, ionizing flux, the initial mass function, and the physics of binary evolution. These UV features are redshifted to optical wavelengths at $z > 2$ and so become accessible from the ground. A moderate resolution optical spectrum ($R \sim 1500$) with $S/N \sim 15$ is sufficient to study these features and has so far been obtained for a stack of 30 Lyman break galaxies at $z = 2.4$ with $R \sim 24.4$ using Keck/LRIS (Steidel et al. 2016, see also Rigby et al. 2017). GMACS, coupled with MANIFEST, will enable a major advance. In an 8-hour exposure, GMACS will reach $S/N \sim 15$ for individual $>L^*$ galaxies at $z = 2$ (see *Figure 6-7*), and given an on-sky target density of ~ 1 per arcmin² could observe a few hundred targets simultaneously in a single MANIFEST configuration. A modest program would quickly enable a first measurement of how the properties of massive stars vary with bulk galaxy properties (e.g., stellar mass, specific star formation rate, metallicity), providing novel constraints on stellar evolution and feedback-driven models of galaxy evolution.

The JWST deep fields and existing deep optical and near-IR fields from HST will provide the ideal surveys for selecting the higher redshift targets needed for the projects described in *Figure 6-5* as well. For the high redshift samples identified in those fields, the GMT will be able to obtain integral field spectra, resolving them into dozens to hundreds of independent elements $0.05'' - 0.10''$ in size. Such detailed mapping of galaxies sampling a wide range in the parameter space of galaxy properties and epochs will provide an unprecedented view of the growth and evolution of galaxies. In addition, GMACS on the GMT will be able to obtain spectra in the rest-frame UV for galaxies at redshifts $2 < z < 4$ for comparison to the redder wavelength coverage of JWST, making it possible to study the same rest-frame wavelengths of galaxies at similar masses out to $z > 5$. This complementary extended baseline will provide a direct window into how the basic properties of low mass galaxies evolve through the first third of the history of the universe.



Synergy with ALMA

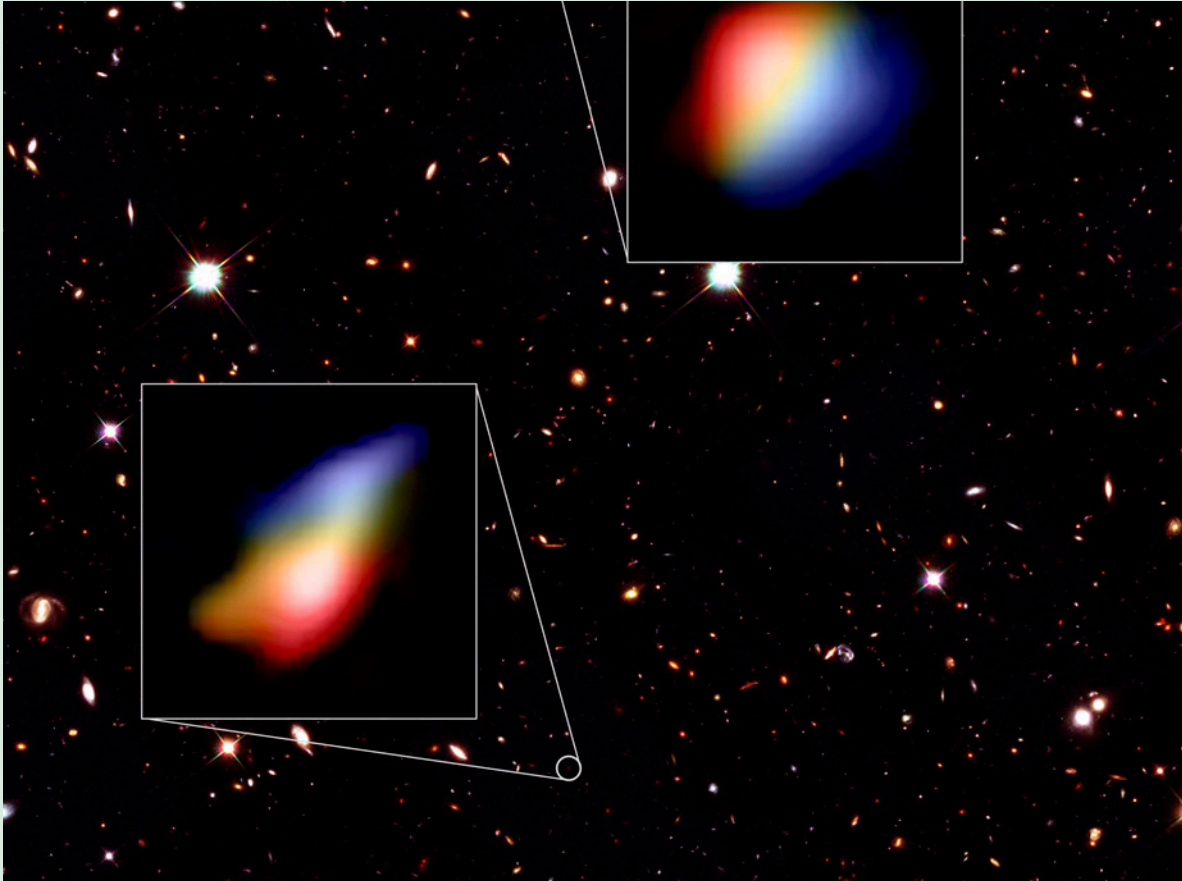
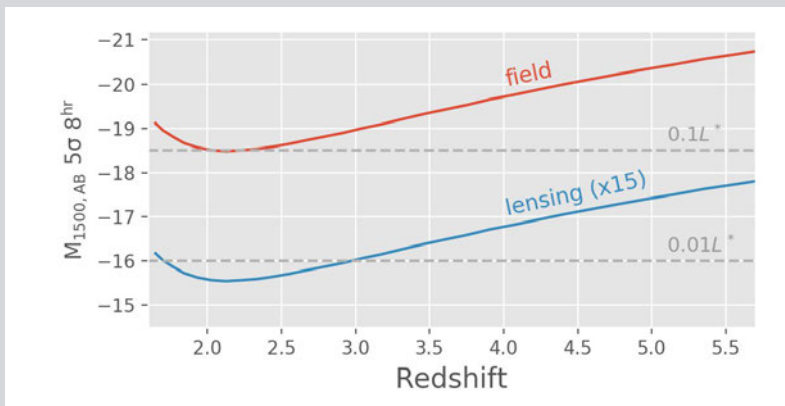


Figure 6-6 GMT and ALMA, both operating in the southern hemisphere, will have common sky access and be able to observe the same objects. While the GMT will produce detailed star formation maps of distant galaxies, ALMA will map the cold molecular gas reservoirs out of which stars form and the thermal emission from interstellar dust being heated by young massive stars. Together, these facilities will provide a complete view of how gas is turned into stars, and how star formation self-regulates by injecting energy and turbulence into the surrounding interstellar gas. The unprecedented spatial resolution of the GMT at optical and near-IR wavelengths can be well matched by ALMA at mm and sub-mm wavelengths. Image Credit: Rotation curves for redshift two galaxies as observed in molecular gas by ALMA (Smit et al. 2018).

6.3 Low Mass Galaxies Across Cosmic Time

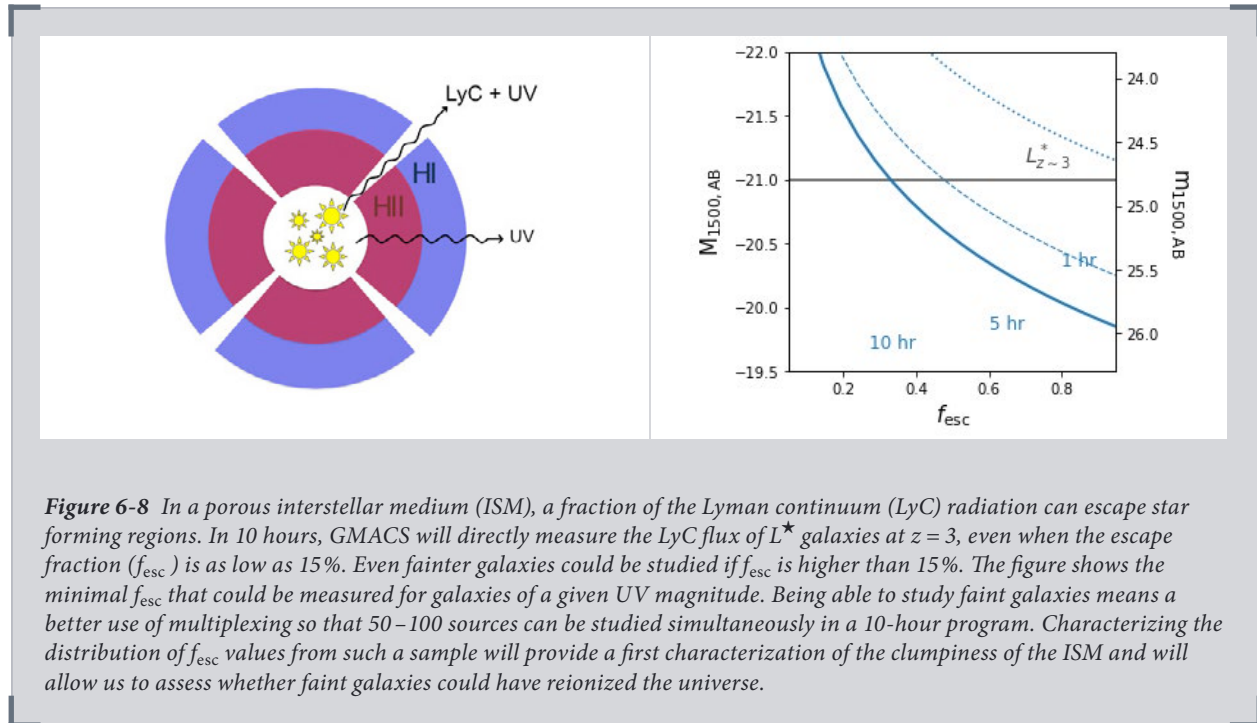
With a photon collecting area of 368 m², the GMT will be a transformational facility for the study of faint low mass galaxies. GMACS on the GMT will take integrated spectra of galaxies as faint as 0.1L^{*} at z~2 and will probe even fainter when combined with gravitational lensing (see **Figure 6-7**). Distant low-mass galaxies are the building blocks of the more typical massive systems that we observe in the local universe. Understanding their physical properties and the process through which they grow and combine to form larger galaxies is one of the main objectives of extragalactic astronomy. Due to their intrinsically faint nature, however, spectroscopic studies of their properties are very limited. The GMT will open the exploration of these galaxy building blocks and allow us to learn, for example, about their stellar metallicities, ISM dynamics, and ionization state, among other things. GMT observations will be particularly important for the rest-frame UV spectra of z~2–4 sources as the main competing facility in space, JWST, is optimized to work at longer wavelengths/higher redshifts.

Figure 6-7 GMACS will allow us to obtain medium resolution, rest-frame UV spectra of sub-L^{*} galaxies at 1.5 < z < 5.6. When combined with gravitational lensing, we will be able to study the UV spectra of galaxies as faint as ~0.01L^{*} at z~2. The figure shows the faintest absolute magnitude, in fractions of a typical luminosity galaxy L^{*}, reached at 5 sigma per pixel in 8 hours as a function of redshift. Even for this early time in the history of the universe, the GMT will be able to observe galaxies that are only 10% as bright as typical galaxies, and only 1% as bright when the GMT is assisted by lensing from foreground galaxies. Including observations of galaxies much fainter than the brightest at that epoch is essential for understanding how the general population of galaxies evolved in the early universe.



Can low-mass galaxies at high-z reionize the universe and keep it ionized?

At z > 3.5 GMACS on the GMT can directly observe Lyman continuum (LyC) photons escaping from low-mass galaxies, analogous to the first generation of galaxies that ionized the universe. Hydrogen in the universe became almost completely ionized sometime around 750–1,000 Myr after the Big Bang (z~6–7). The sources that produced the necessary ionizing radiation are still unknown but our best candidates so far are the abundant low-mass galaxies that likely dominate the net production of ionizing photons. To accomplish this, the ionizing photons must actually escape from these low-mass galaxies. Measuring the fraction of ionizing photons that make it out of a galaxy (the escape fraction, f_{esc}) directly at z~6–7 is impractical due to the high opacity of the IGM to LyC photons, but at lower redshifts accessible to GMACS, these low mass analogs will provide the best proxy to determine how and how much of the ionizing emission can escape from galaxies in the early universe.



The GMT will push the sensitivity of LyC observations to a new regime where the escape fraction will be measured directly, at high S/N, for single objects. Except for few contentious claims (e.g. De-Barros et al. 2016, Nestor et al. 2013), all attempts to measure f_{esc} directly at intermediate redshifts have failed. The primary reason for the lack of success is the expected faintness of the Lyman continuum radiation. For a typical $z \sim 3.5$ galaxy, for example, the LyC luminosity at 900 \AA can be 3.7 mags fainter than the UV continuum flux at $1,500 \text{ \AA}$ (assuming a fiducial galaxy spectral energy distribution with $(L_{\text{UV}}/L_{\text{LyC}})_{\text{intrinsic}} \sim 3$, line of sight IGM opacity of ~ 0.5 , and $f_{\text{esc}} \sim 20\%$). This is precisely the kind of issue that will be overcome with the large collecting area of the GMT. De-Barros et al. (2016) report on a source, *Ion2*, for which they estimate a rather high $f_{\text{esc}} \sim 65\%$ measured from a deep 14 h VLT spectrum. The GMT will measure the LyC for a source like this in under 3 hours ($S/N > 10\sigma$ in the range $880\text{--}910 \text{ \AA}$). The leakage of LyC photons is likely very dependent on geometry due to the clumpiness of the ISM. Consequently, we expect f_{esc} to vary significantly from source to source. Importantly, the GMT will measure the LyC for sources like *Ion2* even if f_{esc} was only $\sim 20\%$ (in 10 h, $> 5\sigma$, see *Figure 6-8*).

The UV spectra of low-mass, low-metallicity galaxies at intermediate redshifts.

GMACS will sample the rest-frame UV spectral region at intermediate redshifts, $1.5 < z < 5.5$ (while other complementary missions like JWST will sample the same wavelength range at higher redshifts), allowing us to study how the properties of low-mass galaxies changed from ~ 1 Gyr after the Big Bang to well after the global peak of the cosmic star formation. The rest-frame UV spectrum of galaxies is rich with information about the metallicity of the ISM, its dynamical state (outflowing

winds, for example), and the massive end of the stellar population. Recent pioneering works have found that the UV spectrum of a few rare galaxies at $z \sim 3$ show a variety of spectral features that are quite uncommon in local galaxies, but that could be the norm at $z > 7$ (e.g. Stark et al. 2015, 2017). For example, Amorin et al. 2017 (VUDS survey; Le Fèvre et al. 2015) has measured weak rest-frame UV emission lines (CIII] $\lambda\lambda 1906, 1909$, OIII] $\lambda\lambda 1661, 1666$, HeII $\lambda 1640$ and CIV $\lambda\lambda 1549, 1551$) that only arise in extreme metallicity and ionization conditions. If these galaxies represent the dominant population at $z > 7$, during reionization, it would be quite important to understand their properties.

Local galaxies with very high SFR and blue colors are rare, and their UV spectra are inaccessible from ground-based telescopes, so they are of little use for comparison with their high- z counterparts. A sample of high- z analogs at intermediate redshifts $z > \sim 2-4$, however, is much more amenable to the study of their UV spectrum and they are also more common. Existing imaging surveys such as COSMOS and CANDELS will provide the targets. With GMACS we could study in detail the UV spectrum of these galaxies and provide valuable insight about the physical properties of $z > 7$ galaxies.

These UV emission lines are rich with information about the physical conditions of the ISM of these galaxies, but the current data quality is inadequate to extract this information due to low S/N and spectral resolution (e.g., $R \sim 200$ in VUDS). With a resolving power up to $R \sim 6,000$, GMACS will allow us to study the CGM winds in regions of high ionization down to velocities of 20 km/s. Beyond teaching us about the dynamical properties of the ISM, such resolution will allow us to distinguish between different possible origins for some of the lines. Problematically, the HeII $\lambda 1640$ line can be produced both in nebular regions with high ionization and in the atmospheres of Wolf-Rayet stars. In the latter case, they are characterized by large wind speeds (> 300 km/s). Characterizing the Wolf-Rayet population in these galaxies will allow us to explore the bright end of the IMF in faint galaxies and test for possible variations with redshift or other properties. Alternatively, the origin of this line can be traced to regions of high ionization which can arise from extreme SF densities or possibly binary star interaction. This would also have a significant impact on the estimates of f_{esc} (because the intrinsic ratio would change depending on the binary fraction of the stellar population).



A Seeing-Limited GMACS+MANIFEST Survey of Low-Mass, High-Redshift Galaxies

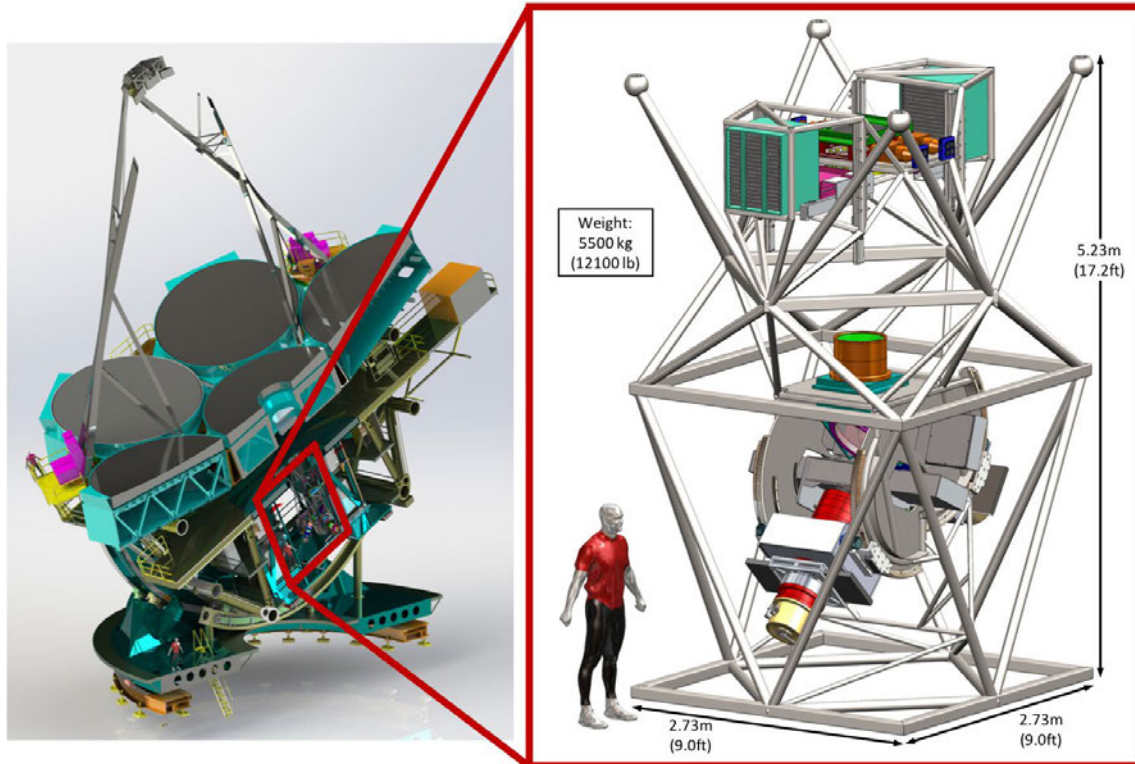


Figure 6-9 The GMACS spectrograph (shown above, right) fed by the MANIFEST fiber positioner will enable the simultaneous acquisition of optical spectra for ~1,000 targets over a 20' diameter field of view. This field of view and multiplexing power is perfectly matched to the source density (a few galaxies per arcmin²) of high redshift, low mass, low luminosity ($< L^*$) galaxies. As shown in Figure 6.7, an 8-hour exposure with GMACS+MANIFEST in natural seeing conditions will provide a $S/N=5$ detection of the rest-frame UV continuum for 0.1 ($0.5 L^*$) galaxies at $z=2$ ($z=5.5$).

In a 10-night program, the GMT could survey more than 10,000 low mass galaxies across the $2 < z < 5$ redshift range. Mapping the physical properties of the ISM and stellar components of young galaxies over a long baseline in cosmic time will tell us about the evolution of star formation activity from the early universe to its peak. Such unprecedented statistics will allow us to conduct similar statistical studies to those that today can only be pursued in the local universe. Observing the early universe and statistically mapping the distribution of galaxy properties for the majority of the galaxy population as a function of galaxy mass, epoch, and environment cannot be achieved without the GMT. Image credit: GMACS Team

6.4 Supermassive Black Holes and Their Co-Evolution with Galaxies

Supermassive black holes (SMBHs) are essential components of galaxies—they regulate galaxy properties and star formation via feedback processes, (e.g., Fabian 2012), dynamically influence the shape of galaxies (e.g., Milosavljević & Merritt 2001), and give rise to exotic phenomena such as high-velocity stars (e.g., Brown 2015) and tidal disruption events. Basic questions about SMBHs remain unanswered: How and when were SMBHs formed? Did they grow before or after their host galaxies? Are these growth processes coordinated, and if so, why? The GMT will play a crucial role in answering these questions.

SMBHs reside at the centers of virtually every massive galaxy (e.g., Richstone et al. 1998), with our own Milky Way providing the “gold standard” of SMBH detections, as we are able to resolve individual stars orbiting the Galactic center and place very tight constraints on the enclosed mass. Beyond the Galaxy, SMBHs have been dynamically measured in ~ 100 galaxies (see Kormendy & Ho 2013, Saglia et al. 2016), most often by modeling the integrated kinematics of stars or the rotation of nuclear gas disks, and, in some cases, by using pc-scale megamaser disks in active galaxies. From these measurements, clear connections between SMBHs and galaxies have emerged, such as those between the SMBH mass (M_{SMBH}) and the bulge luminosity (e.g., Dressler 1989, Kormendy & Richstone 1995) or mass (e.g., Häring & Rix 2004), and the stellar velocity dispersion (σ_* ; e.g., Ferrarese & Merritt 2000, Gebhardt et al. 2000). These relations are unexpected given the drastically different scales involved: the large-scale galaxy bulge properties are far beyond the gravitational influence of the SMBH. For this reason, such relations imply that SMBHs and galaxies have somehow *co-evolved*.

Despite research on SMBHs over the past two decades, the exact role SMBHs play in galaxy evolution and the primary physical mechanisms that drive the empirical correlations between SMBHs and galaxies are far from understood. In addition, the local SMBH mass census is highly incomplete, with sparsely populated low ($\lesssim 10^7 M_\odot$) and high ($\gtrsim 10^9 M_\odot$) ends, and is biased, with existing MBH measurements being made in galaxies that are not representative of the global galaxy population (e.g., van den Bosch et al. 2015, Shankar et al. 2016). Moreover, basic questions remain unanswered. Do SMBHs and galaxies grow in lockstep with one another over time, or does the growth of the SMBH precede that of the galaxy, or vice-versa? Are there SMBHs in low-mass galaxies (with masses less than the Milky Way) and in globular clusters? How do SMBHs form, what are their initial seed masses, and how can they acquire enough mass (several billion solar masses) so quickly (~ 800 million years) after the Big Bang?

Gaining insight into the interplay between SMBHs and their hosts, and ultimately a deeper understanding of galaxy formation and evolution, requires the combination of the GMT’s unparalleled angular resolution and impressive light collecting area. The GMT will enable SMBH science that includes:

- The tracking of the SMBH scaling relations as a function of redshift
- The detailed study of the SMBH–galaxy connection over a much more diverse and representative sample
- The search for intermediate-mass SMBHs ($10^2 \lesssim M_{\text{BH}} \lesssim 10^6 M_\odot$), a missing link between stellar-mass black holes and SMBHs and whose mergers or in-

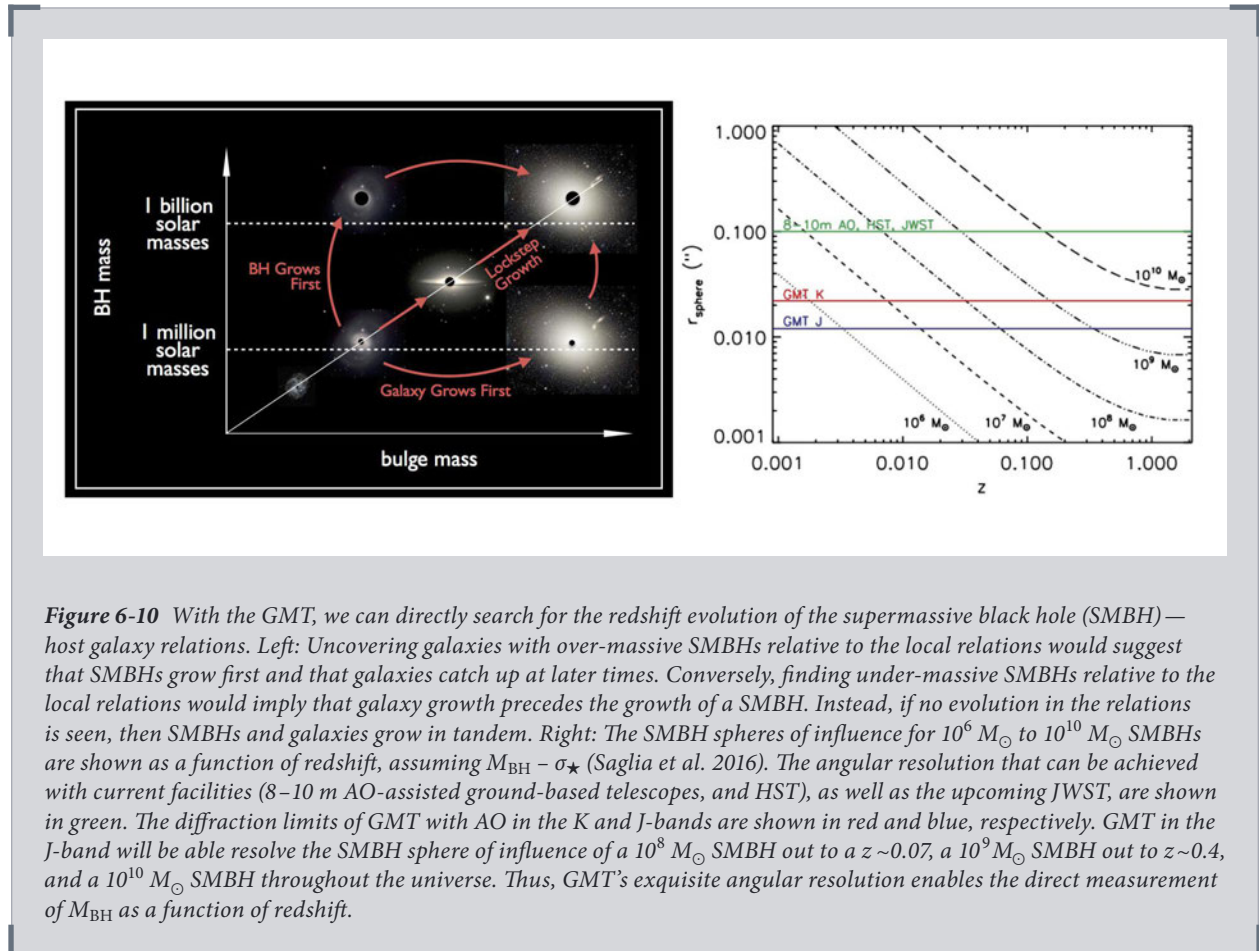
spiral events are hyper-powerful sources of gravitational waves

- The unprecedented detection of faint, short-period stars orbiting close the Galactic Center SMBH, which will enable the first precision tests of General Relativity
- The investigation of SMBH feeding and feedback through the spatial and kinematic mapping of coronal emission lines, such that outflows and ionization from the AGN in the innermost cores of galaxies can be identified and their properties quantified

Below, we focus on one of the science cases above as an example of the GMT's groundbreaking potential.

Which grows first?

One fundamental question regarding SMBH–galaxy co-evolution is whether SMBHs grow in symbiosis with their hosts over time. There are hints that SMBHs at higher redshift are over-massive at fixed galaxy mass compared to the local scaling relations, suggesting that SMBH growth predominantly occurs prior to galaxy growth (e.g., Woo et al. 2006, Bennert et al. 2011). However, there are



also studies that find no change in the SMBH relations as a function of redshift (e.g., Salviander & Shields 2013), and selection bias can lead to the false identification of evolution in the relations (e.g., Lauer 2007, Schulze & Wisotzki 2014). The above results are highly controversial and rely on indirect estimates of M_{BH} in AGN; the more reliable dynamical M_{BH} measurements have thus far been limited to galaxies within ~ 150 Mpc.

The GMT will facilitate the first direct search for evolution of the SMBH scaling relations. We will dynamically measure M_{SMBH} in redshift bins and compare to the local SMBH – galaxy relations (**Figure 6-10**). The GMT and its AO system will provide a nearly order of magnitude improvement in angular resolution over HST, AO on 8–10 m ground-based telescopes, and even JWST. High angular resolution is necessary for resolving the SMBH sphere of influence ($r_{\text{sphere}} = G M_{\text{BH}} / \sigma_{\star}^2$), and is a key ingredient for robust dynamical M_{SMBH} measurements. GMT using AO in the *J*-band will allow for r_{sphere} of a $10^6 M_{\odot}$ SMBH to be resolved out to the distance of the Virgo cluster (16 Mpc), whereas currently this can only be done out to a few Mpc. Likewise, a $10^8 M_{\odot}$ SMBH can be resolved out to a $z \sim 0.07$, a $10^9 M_{\odot}$ SMBH can be resolved out to $z \sim 0.4$, and remarkably a $10^{10} M_{\odot}$ SMBH can be resolved at *any* redshift. Therefore, searching for possible redshift evolution of the relations of SMBH and galaxy properties is best accomplished using the highest mass SMBHs.

Measuring the mass of a SMBH requires the combination of several datasets. We will use the GMTIFS imager with a broadband NIR filter to determine the luminous mass distribution, and GMTIFS in integral-field spectrograph mode to map out the stellar kinematics in the central regions of galaxies. For $z < 0.1$, the $2.22 \mu\text{m}$ CO band-heads are ideal features for measuring stellar kinematics (**Figure 6-10**), while for $0.1 < z < 0.5$, the $1.6 \mu\text{m}$ CO bandheads will be shifted into the *K*-band and the Ca II triplet lines will be shifted into the *J*-band. Pushing past $z \sim 0.5$ requires the exclusive use of the Ca II triplet lines. Once the measurement of absorption features becomes too challenging due to strong surface brightness dimming, dynamical M_{SMBH} measurements can be made at higher redshifts using narrow emission-lines, such as H α , provided the gas traces out regular rotation that is not dominated by turbulent motion. Given the focus on high-mass SMBHs, the $R \sim 5000$ setting of GMTIFS provides sufficient velocity resolution. We expect that ~ 1 hour on-source (8 hours total exposure time) is sufficient for reaching the S/N needed to measure the line-of-sight velocity distribution of stars at the center of a $z \sim 0$ ($z \sim 0.5$) massive early-type galaxy. This utilizes the 12 mas pixel scale, which will Nyquist sample the *K*-band PSF. Spaxels can be binned together as needed in the outer regions of the IFU to reach the desired S/N. Including time for offset sky exposures, a survey targeting a handful galaxies in each of $z \sim 0.2$, $z \sim 0.4$, and $z \sim 0.8$ bins would require about 40 nights spread out over multiple years. While such a program is ambitious, the GMT will make a profound and lasting impact on our understanding of how SMBHs and galaxies grow and evolve together over time.

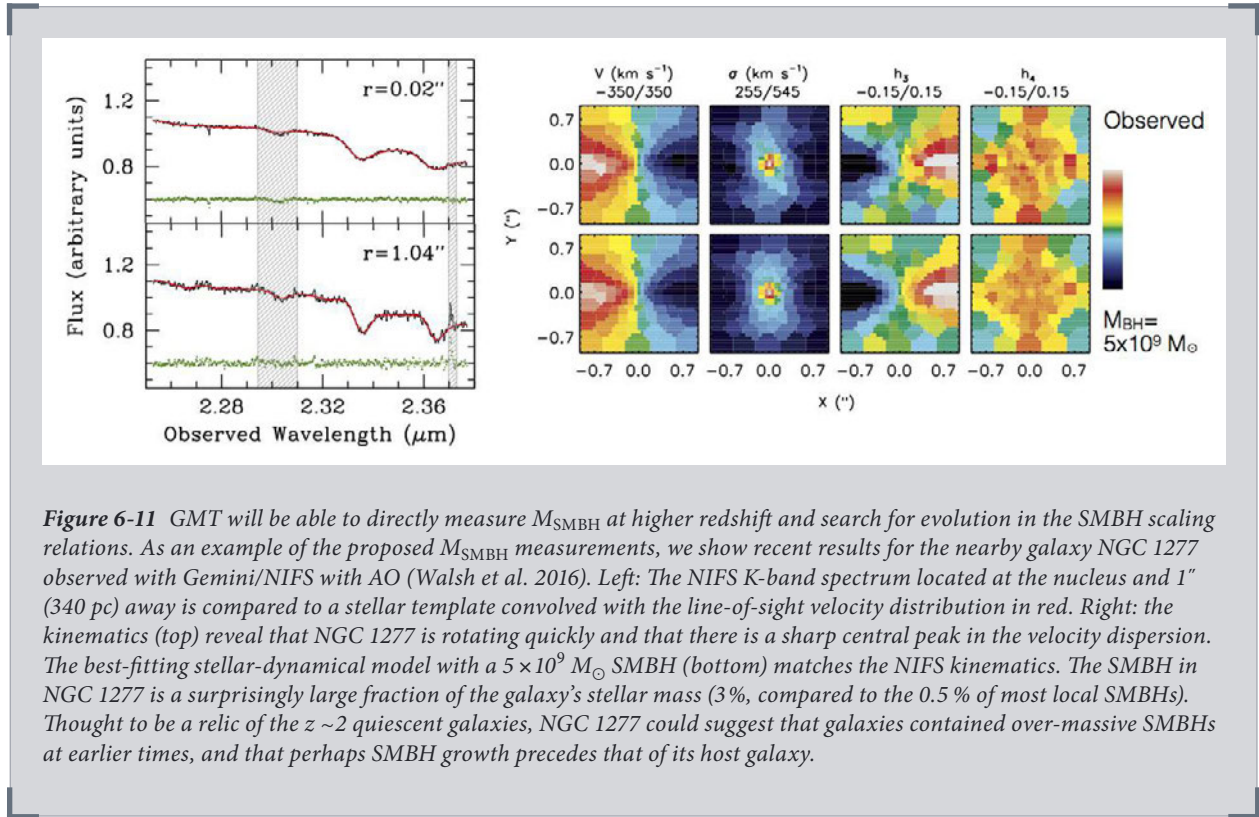


Figure 6-11 GMT will be able to directly measure M_{SMBH} at higher redshift and search for evolution in the SMBH scaling relations. As an example of the proposed M_{SMBH} measurements, we show recent results for the nearby galaxy NGC 1277 observed with Gemini/NIFS with AO (Walsh et al. 2016). Left: The NIFS K-band spectrum located at the nucleus and $1''$ (340 pc) away is compared to a stellar template convolved with the line-of-sight velocity distribution in red. Right: the kinematics (top) reveal that NGC 1277 is rotating quickly and that there is a sharp central peak in the velocity dispersion. The best-fitting stellar-dynamical model with a $5 \times 10^9 M_{\odot}$ SMBH (bottom) matches the NIFS kinematics. The SMBH in NGC 1277 is a surprisingly large fraction of the galaxy’s stellar mass (3%, compared to the 0.5% of most local SMBHs). Thought to be a relic of the $z \sim 2$ quiescent galaxies, NGC 1277 could suggest that galaxies contained over-massive SMBHs at earlier times, and that perhaps SMBH growth precedes that of its host galaxy.

References

- Amorin, R., Fontana, A., Pérez-Montero, E., et al. 2017, *Nature Astronomy*, 1, 52
- Belli, S., Newman, A. B., & Ellis, R. S. 2017, *ApJ* 834, 18
- Bennert, V. N., Auger, M. W., Treu, T., Woo, J.-H., & Malkan, M. A. 2011, *ApJ*, 742, 107
- Brown, W. R. 2015, *ARA&A*, 53, 15
- Choi, H. & Yi, S. K. 2017, *ApJ* 837, 68
- de Barros, S., Vanzella, E., Amorin, R., et al. 2016, *A&A*, 585, 13.
- Dressler, A. 1989, in *IAU Symposium 134, Active Galactic Nuclei*, ed. D. E. Erb, D. K., Steidel, C. C., Shapley, A. E., et al. 2006, *ApJ*, 647, 128
- Fabian, A. C. 2012, *ARA&A*, 50, 455
- Ferrarese, L., & Merritt, D. 2000, *ApJL*, 539, L9
- Garnett, D. R. 2002, *ApJ*, 581, 1019
- Gebhardt, K., Bender, R., Bower, G., et al. 2000, *ApJL*, 539, L13
- Genzel, R., Förster Schreiber, N. M., Lang, P., et al. 2014, *ApJ*, 785, 75
- Genzel, R., Förster Schreiber, N. M., Übler, H., et al. 2017, *Nat* 543, 397
- Genzel, R., Tacconi, L. J., Kurk, J., et al. 2013, *ApJ*, 773, 68
- G.F. Snyder, et al. 2015, *MNRAS*, 451, 4290.
- Glazebrook, K. 2013, *PASA* 30, 56
- Ho, I.-T., Kudritzki, R.-P., Kewley, L. J., et al. 2015, *MNRAS*, 448, 2030
- Häring, N., & Rix, H.-W. 2004, *ApJ*, 604, 89
- Kashino, D., Silverman, J. D., Sanders, D., et al. 2017, *ApJ*, 835, 88
- Kormendy, J., & Richstone, D. 1995, *ARA&A*, 33, 581
- Kormendy, J., & Ho, L. C. 2013, *ARA&A*, 51, 511
- Lauer, T. R., Tremaine, S., Richstone, D., & Faber, S. M. 2007, *ApJ*, 670, 249
- Le Fèvre, O., Tasca, L. A. M., Cassata, P., et al. 2015, *A&A*, 576, 79
- Magdis, G. E., Bureau, M., Stott, J. P., et al. 2016, *MNRAS*, 456, 4533
- Milosavljević, M., & Merritt, D. 2001, *ApJ*, 563, 34
- Nestor, D. B., Shapley, A. E., Kornei, K. A., et al. 2013, *ApJ*, 765, 47
- Newman, S. F., Genzel, R., Förster Schreiber, N. M., et al. 2013, *ApJ* 767, 104
- Newman, A. B., Belli, S., & Ellis, R. S., 2015, *ApJL* 813, 7
- Osterbrock \& J. S. Miller, 217
- Richards, S. N., Schaefer, A. L., López-Sánchez, Á. R., et al. 2014, *MNRAS*, 445, 1104
- Richstone, D., Ajhar, E. A., Bender, R., et al. 1998, *Natur*, 385, 14
- Rigby, J. R., Bayliss, M. B., Chisholm, J., et al. 2017, arXiv:1710.07294
- Rix, S. A., Pettini, M., Leitherer, C., et al. 2004, *ApJ* 615, 98
- Saglia, R. P., Opitsch, M., Erwin, P., et al. 2016, *ApJ*, 818, 47
- Salviander, S., & Shields, G. A. 2013, *ApJ*, 764, 80
- Schaefer, A. L., Croom, S. M., Allen, J. T., et al. 2017, *MNRAS*, 464, 121
- Schulze, A., & Wisotzki, L. 2014, *MNRAS*, 438, 3422
- Shankar, F., Bernardi, M., Sheth, R. K., et al. 2016, *MNRAS*, 460, 3119
- Shapley, A., E., Reddy, N. A., Kriek, M., et al. 2015, *ApJ* 801, 88
- Smit et al, 2018, *Nature*, 553, 178–181
- Sobral, D., Smail, I., Best, P. N., et al. 2013, *MNRAS*, 428, 1128
- Stanway, E. R., Eldridge, J. J., & Becker, G. D. 2016, *MNRAS* 456, 485
- Stark, D. P., Richard, J., Charlot, S., et al. 2015, *MNRAS*, 450, 1846
- Stark, D., P., Ellis, R. S., Charlot, S., et al. 2017, *MNRAS*, 464, 469
- Steidel, C. C., Rudie, G. C., Strom, A. L., et al. 2014, *ApJ* 795, 165
- Steidel, C. C., Strom, A. L., Pettini, M., et al. 2016, *ApJ* 826, 159f
- Sánchez, S. F., Rosales-Ortega, F. F., Iglesias-Páramo, J., et al. 2014, *A&A*, 563, A49
- Toft, S., Zabl, J., Richard, J., et al. 2017, *Nat* 546, 510
- Torrey, P et al. 2015, *MNRAS*, 447, 2753
- Tremonti, C. A., Heckman, T. M., Kauffmann, G., et al. 2004, *ApJ*, 613, 898
- Walsh, J. L., van den Bosch, R. C. E., Gebhardt, K., et al. 2016, *ApJ*, 817, 2
- van Dokkum, P. G., Whitaker, K. E., Brammer, G., et al. 2010, *ApJ* 709, 1018
- van de Sande, J., Kriek, M., Franx, M., et al. 2013, *ApJ* 771, 85
- van den Bosch, R. C. E., Gebhardt, K., Gültekin, et al. 2015, *ApJS*, 218, 10
- Wellons, S., Torrey, P., Ma, C.-P., et al. 2015, *MNRAS* 449, 361
- Woo, J.-H., Treu, T., Malkan, et al. 2006, *ApJ*, 645, 900
- Zahid, H. J., Kashino, D., Silverman, J. D., et al. 2014, *ApJ*, 792, 75



This image shows a large-scale projection (15 Mpc/h deep) through the Illustris simulation at $z=0$, centered on the most massive cluster in the simulation. The density of dark matter is shown in pink to blue, with the gas velocity field overlaid in orange. Credit: Illustris Collaboration.



Building Galaxies from Cosmic Gas

How does the gas that feeds star formation get into galaxies?

The content of our universe is much richer and more complex than the structures we can see in starlight alone. Galaxies, and the stars and gas within them, make up a tiny fraction of the ordinary matter in the universe. Most of the remaining material resides in the vast volume of space that lies between galaxies—the intergalactic medium. This reservoir contains both the raw materials for building galaxies and a fossil record of feedback from previous generations of galaxies and supermassive black holes.

With the GMT, astronomers will be able to study galaxies and their surroundings with greater resolution and sensitivity than ever before. That resolution will enable us to peer into the hearts of galaxies to understand how their stars and central black holes process gas. That sensitivity will enable us to study the light directly emitted by the diffuse gas, as well as study its detailed structure in absorption.

Chapter Authors

Hsiao-Wen Chen (University of Chicago)

Sean Johnson (Princeton University)

Gwen Rudie (Carnegie Institution for Science, The Observatories)

Robert Simcoe (Massachusetts Institute of Technology)

Emma Ryan-Weber (Swinburne University of Technology)



7 Building Galaxies from Cosmic Gas

Our cosmological world-view is based on a century of observing starlight from galaxies with the largest available telescopes. However, we have learned that only a tiny fraction of the matter in galaxies is found in stars. For every unit of mass in stars, galaxies contain twelve units of mass in diffuse gas. We detect another 65 units of dark matter from the effects of its gravity on the 13 units of ordinary matter in gas and stars. The distribution of these components of the universe is illustrated in *Figure 7-1*.

We use numerical simulations on supercomputers to help us understand the variety and complexity of galaxy assembly. We simulate pristine gas accreting onto dark matter agglomerations and forming stars (e.g., *Figure 7-2a*). Simple computer simulations suggest that most of the gas falling into galactic halos should turn directly into stars, contrary to observations of the real universe. Somehow star formation is regulated, yielding the rich taxonomy of galaxies we observe today.

Two energy sources are thought to provide this regulation by heating the gas: supernovae associated with bursts of star formation and accretion onto the black holes in galactic nuclei. These processes could episodically heat interstellar gas, preventing its condensation to the high densities required for star formation. Heated gas could be ejected into a gas halo ten times larger than the galaxies' stellar disks. This gas would not form stars until it cooled and re-condensed into the disk.

More sophisticated simulations incorporating these two feedback loops have been remarkably successful at producing realistic galaxies. However, current computing

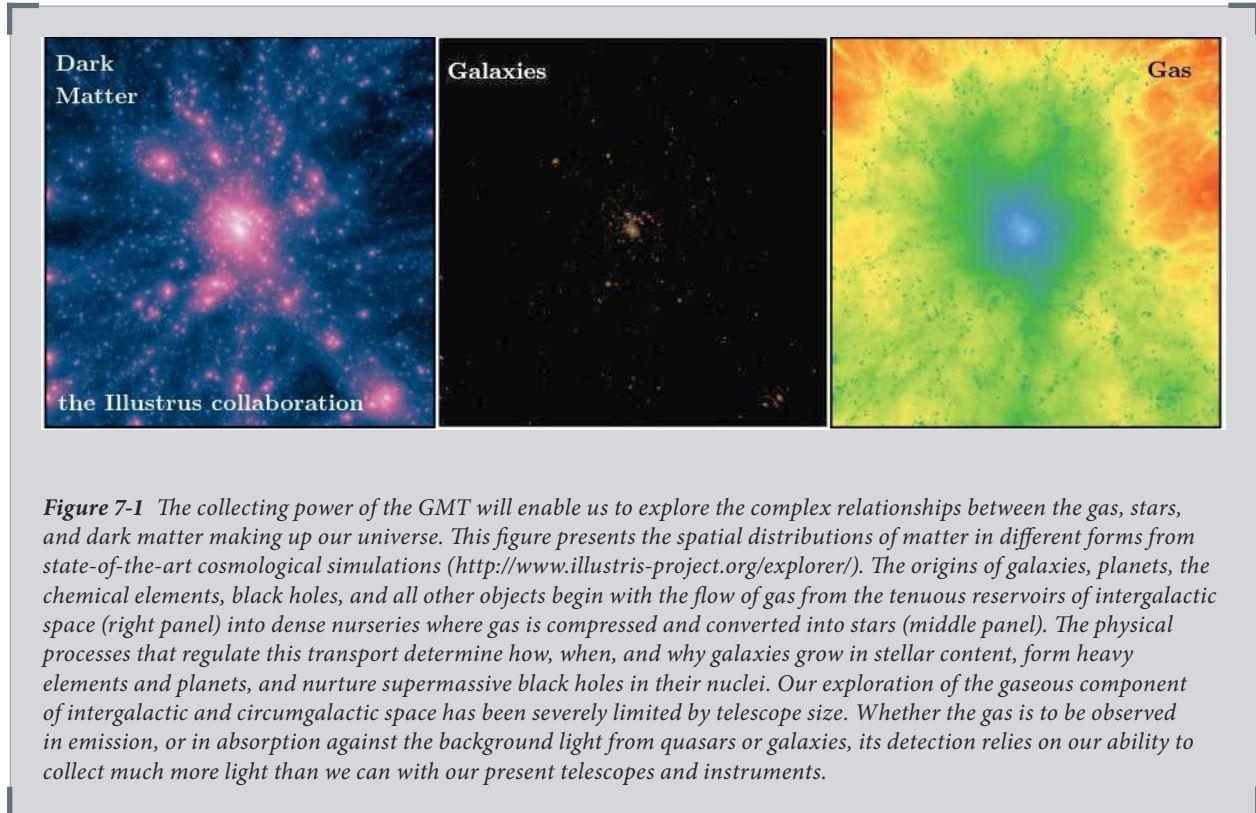
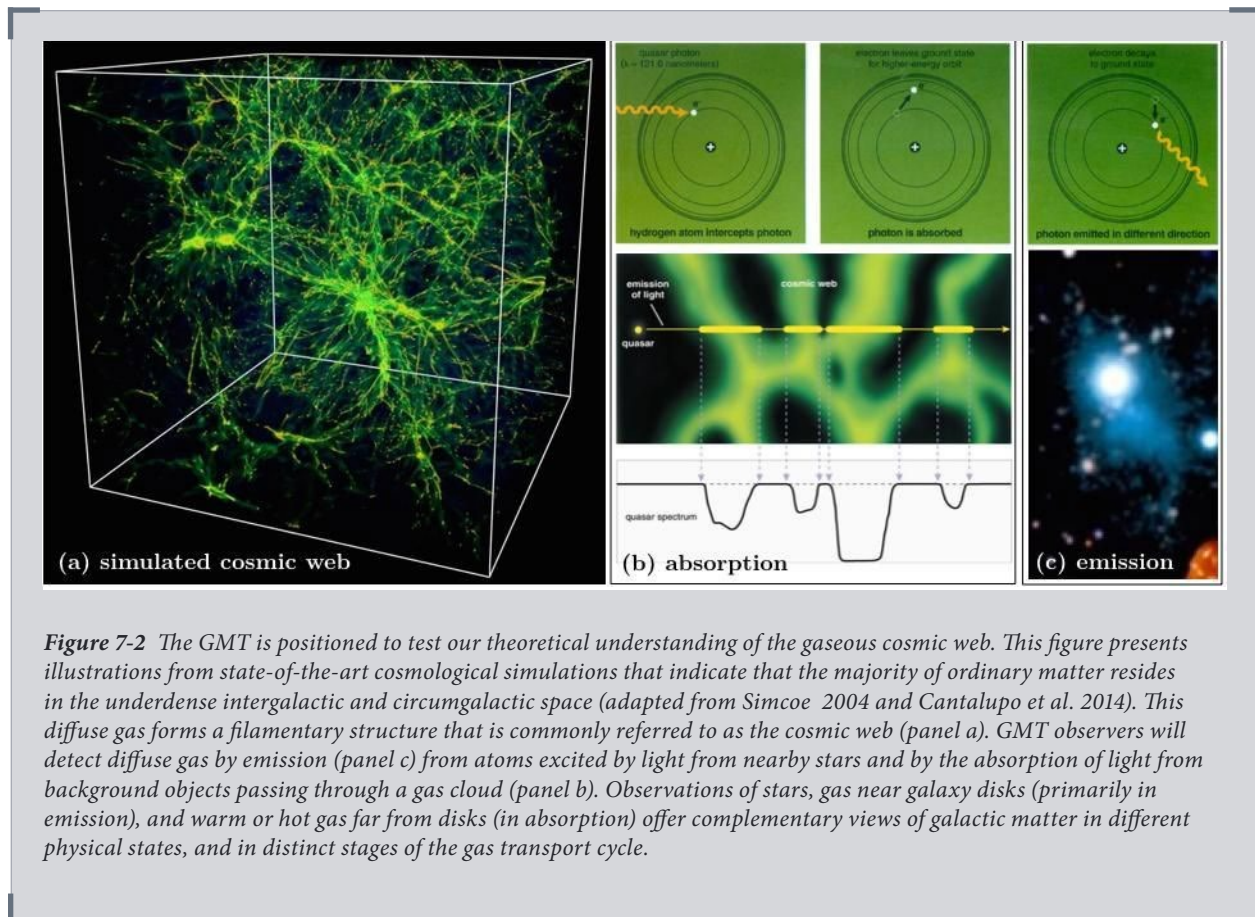


Figure 7-1 The collecting power of the GMT will enable us to explore the complex relationships between the gas, stars, and dark matter making up our universe. This figure presents the spatial distributions of matter in different forms from state-of-the-art cosmological simulations (<http://www.illustris-project.org/explorer/>). The origins of galaxies, planets, the chemical elements, black holes, and all other objects begin with the flow of gas from the tenuous reservoirs of intergalactic space (right panel) into dense nurseries where gas is compressed and converted into stars (middle panel). The physical processes that regulate this transport determine how, when, and why galaxies grow in stellar content, form heavy elements and planets, and nurture supermassive black holes in their nuclei. Our exploration of the gaseous component of intergalactic and circumgalactic space has been severely limited by telescope size. Whether the gas is to be observed in emission, or in absorption against the background light from quasars or galaxies, its detection relies on our ability to collect much more light than we can with our present telescopes and instruments.

limitations prevent fully realistic simulations. GMT's sensitivity and sharp images will allow us to probe the complex process of galaxy formation in fine detail, enabling observations of the full cycle of gas accretion, star formation, chemical enrichment, gas outflow, and recycling. These observations will in turn allow us to develop more faithful numerical simulations by illuminating the underlying physics.

This holistic approach combining the observation and simulation of galaxies and their gas envelopes would also inform our understanding of galaxies in the early universe. These distant and ancient objects are often too faint to detect directly in starlight. The gas processed by nascent galaxies and black holes will be observed with JWST and GMT in both atomic emission and absorption (**Figure 7-2**), connecting our comprehensive models of galaxies in the local universe with the exploratory data collected from the epoch of the earliest stars.

This chapter focuses on three selected areas where GMT is uniquely positioned to advance our understanding of the accretion—star-formation feedback cycle that meters the fuel for galaxy formation. We begin at the largest scales, where GMT's collecting area and large field of view allow us to map cosmological gas structures not yet bound to individual galaxies. Moving to the scale of galaxies, we outline programs to study the spatial distribution and dynamics of circumgalactic gas envelopes, using chemical enrichment from supernovae as a tracer of feedback. Finally, we zoom into the smallest scales, where the GMT's high resolution will



dramatically enhance our view of the nuclei of galaxies where black hole feedback couples to the surrounding medium.

7.1 Mapping Large-scale Cosmic Structures in Emission and in Absorption

Hydrogen is the most abundant element in the universe. Mapping the large-scale distribution of hydrogen therefore provides a high-fidelity view of the spatial distribution of matter in the cosmos. The bulk of this cosmic gas resides in very low density environments. Illuminated by the general background radiation, the low-density gas glows at an extremely faint level. Meanwhile, depending on the density, temperature, and ionization state of the gas, the interactions between hydrogen atoms and high-energy background photons are expected to generate varying degrees of absorption features against the background radiation (*Figure 7-2*). By capturing these emission and absorption features, we can construct a density map of the underlying matter distribution.

GMACS provides two ways to “see” the lower density gas around regular galaxies. The first approach is to use direct imaging of the faint glow of the cosmic gas, producing a clear map of the matter distribution in the cosmos. In addition, a 2D image shows how this gas is connected and interacting with galaxies where stars form. The brightness of this faint glow is determined by a combination of two factors: (1) the intensity of the ionizing radiation field and (2) gas density, and so higher density gas in the proximity of an ionizing source glows brighter. Recent efforts have shown that detecting this faint glow in modest density gas around luminous QSOs in the distant universe is within the reach of current world-class telescopes (*Figure 7-3a*), and stacks of millions of galaxy – galaxy spectrum pairs in the SDSS illustrates the presence of this gas in emission around galaxies in the nearby universe (Zhang et al. 2016).

The second approach relies on the absorption by the gas of the light from “background” quasars or faint galaxies. Absorption spectroscopy of background sources enables us to uncover tenuous gas that is otherwise invisible. Traditionally, this technique relies on the presence of distant luminous sources, which are, however, rare and can only facilitate pencil beam surveys along sparsely distributed individual lines of sight.

Combining moderate-to-high resolution spectrographs such as GMACS and G-CLEF with MANIFEST, the GMT will transform traditional absorption-line spectroscopy and provide a wide-field view of the cosmic web. The large collecting area of the GMT will enable us to use a large sample of faint background sources, such as starforming galaxies, to sample the diffuse gas around galaxies and build a 3D view of the cosmic web (*Figure 7-3b*). By directly measuring emission, the GMT will be able to trace the gas independent of any background sources. Combining these kinds of observations—measurements of the absorption and emission of the diffuse gas—we will be sensitive to gas at different densities. That will, in turn, allow us to understand the temperature of the gas and its density variations (“clumping factors”), which will let us connect physics to observations through models.

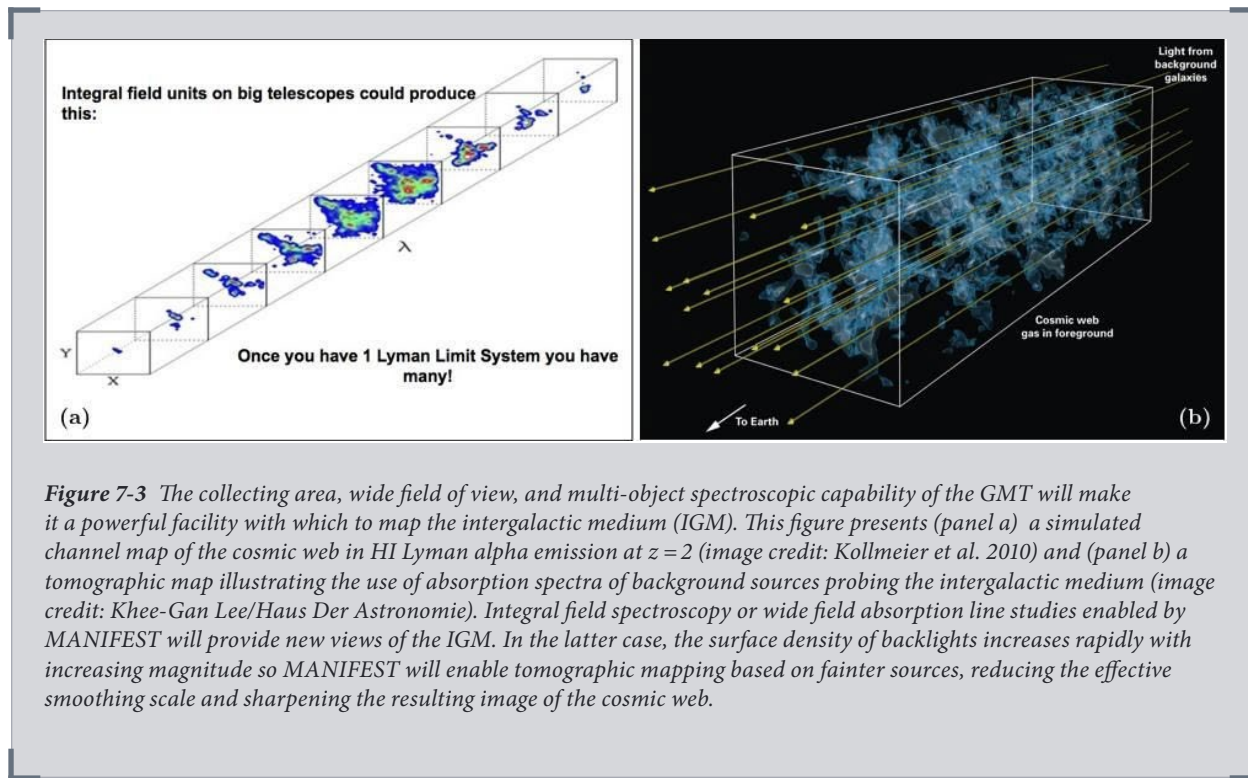


Figure 7-3 The collecting area, wide field of view, and multi-object spectroscopic capability of the GMT will make it a powerful facility with which to map the intergalactic medium (IGM). This figure presents (panel a) a simulated channel map of the cosmic web in HI Lyman alpha emission at $z = 2$ (image credit: Kollmeier et al. 2010) and (panel b) a tomographic map illustrating the use of absorption spectra of background sources probing the intergalactic medium (image credit: Khee-Gan Lee/Haus Der Astronomie). Integral field spectroscopy or wide field absorption line studies enabled by MANIFEST will provide new views of the IGM. In the latter case, the surface density of backlights increases rapidly with increasing magnitude so MANIFEST will enable tomographic mapping based on fainter sources, reducing the effective smoothing scale and sharpening the resulting image of the cosmic web.

7.2 Tracing the Movement of Gas in and out of Galaxies

As gas is processed through stars within a galaxy, it is enriched with heavy elements. The distribution and motions of chemically-enriched gas therefore provides unique clues about the process of star formation and its regulation within galaxies. Tracing the ejection of metal-enriched gas in galaxy scale outflows, and the re-accretion of some or all of that gas, offers critical constraints on our theories of galaxy formation and evolution. The presence of heavy elements also fundamentally alters the thermal and physical state of the gas, affecting subsequent star formation in recycled material.

GMACS+MANIFEST offer a unique opportunity to advance this research area by substantially expanding the parameter space of distant galaxies with measurements of their circumgalactic medium. These instruments can expand the statistical power of the data sets for L^* galaxies at $z \sim 2$, dramatically advancing our understanding of the CGM and gas flows for lower-mass galaxies, and galaxies in the more distant universe. Further, the GMT will allow for the mapping of the CGM of galaxies with multiple sightlines using background galaxies, allowing for tomographic studies of the gaseous halos of individual galaxies for the first time, as well as collecting wide-field tomographic data that will provide information on the large-scale environment of the galaxies. Collectively, these data will provide a comprehensive understanding of how gas properties depend on galaxy mass, environment, and cosmic age.

Metal Production in the Early Universe

The spectroscopic power of the GMT will play a key role in pushing the study of cosmic gas to the earliest epochs, where the transformation of the target pool from extremely rare luminous objects to more common backlights will dramatically improve our understanding. Heavy elements, fused in the first stars, and blown into the outer regions or ejected completely from galaxies through stellar winds and supernovae explosions, will be revealed by high-resolution spectroscopy with the GMT of the most distant quasars, measuring these heavy elements in both the intergalactic medium and the circumgalactic medium around galaxies.

GMT observations will provide a unique probe of the build-up of heavy elements through the first several billion years (e.g., Ryan-Weber et al. 2009, Becker et al. 2009, Simcoe et al. 2011, D’Odorico et al. 2013, Codoreanu et al. 2017). The chemical abundance ratios in quasar absorption systems provide insight into the yields from the first supernovae (e.g., Becker et al. 2012). The metals synthesized by Pop III stars will be strongly dependent on their IMF. If the IMF is weighted toward very massive stars, we would expect to see abundance patterns that are distinct from Pop II stars. Theoretical calculations predict that abundance measurements in $z \sim 7$ and 8 quasars will likely probe the era of “metal free” Pop III pollution (e.g., Kulkarni et al. 2014), potentially revealing carbon-enhanced abundance patterns such as those seen in some very metal poor damped-Lyman-alpha systems (DLAs) at $z \sim 2$ (Cooke et al. 2012) and in the Galactic halo (Frebel & Norris 2015).

Gas Flows Imaged Directly in Line Emission

Gas flowing in and out of star-forming regions can be directly imaged in line emission across a range of redshifts using GMACS+MANIFEST to sample a broad range of spatial scales—from an IFU mode on high redshift systems, through to many individual lines of sight from fibers scattered across the halos of nearby galaxies. The aim is to record the spectrum in as many locations around the target galaxy as possible to enable construction of 3D density and velocity fields by tracing line-emitting gas in both spatial and spectral directions.

Commonly seen emission features include the [OII], [OIII], and H-beta lines. Together, the relative strengths of these lines constrain the underlying gas density, relative motion, metallicity, and temperature (*Figure 7-5*). These 3D data cubes provide measures of mass flow rates in and out of galaxies, in addition to providing insight into the spatial variations in the chemical enrichment level and the ionizing radiation field. While detections of emission for circumgalactic hydrogen in averages of thousands of galaxies in the local universe exist (Zhang et al. 2016), these average detections do not allow for detailed analysis of the gas. The GMT will enable us to detect the same emission lines, but on a galaxy-by-galaxy basis — enabling us to connect the properties of the gas with those of the central galaxy.

High-Sensitivity Gas-Flow Mapping in Absorption

GMACS + MANIFEST will enable us to probe the rest-UV spectrum of individual galaxies in greater detail thanks to the combination of the GMT’s large aperture, high-sensitivity, and high-degree of multiplexing. Together these characteristics will allow for higher signal-to-noise spectroscopy of fainter background galaxies than has been possible before. This will open the study of cosmic gas flows to new populations of galaxies: massive galaxies with low star formation rates as well as intrinsically faint low-mass star-forming galaxies.



Synergy with WFIRST



Figure 7-4 The large collecting area and high resolution spectroscopic capabilities of the GMT through the near infrared will revolutionize the study of metal production in early galaxies by studying this gas in absorption against even more distant quasars. The next generation of space-based imaging surveys (Euclid, WFIRST) are expected to find many thousands of quasars (or photometric quasar candidates) at $z > 7$; the planned high latitude grism survey of WFIRST is alone projected to spectroscopically (i.e. cleanly) find and confirm $\sim 2,600$ quasars at $H < 26.5$ mag, with 20% of such systems at $z > 8$ (Spergel et al. 2015). While many of these quasars will be too faint for detailed spectroscopic study even with the GMT, almost none will be accessible as useful backlights to current telescopes. To measure robust gas column densities in absorption down to $\log(N_{\text{ion}}/\text{cm}) = 13.0$ requires continuum S/N ~ 50 or better, and at spectral resolutions of 30 km/s or better. This resolution is simply unavailable on JWST, and the S/N requirements restricts studies with ground based 8 m class telescopes — even with night-long total exposures — to the very few rarest brightest quasars at these redshifts, with $J < 19$ th magnitude. GMTNIRS or SuperFIRE will enable this work on the brightest sources with only hour-long exposures, while with longer integrations the GMT will study absorption in detail against the much larger populations of these most distant quasars down to $J \sim 21$, and thereby reveal the production of metals in the earliest galaxies. Image credit: European Space Agency/Hubble Space Telescope/NASA.

Complementary to direct imaging, absorption line techniques provide several unique opportunities to construct high-sensitivity maps of gas flows (**Figure 7-6**). These include (1) moderate resolution down-the-barrel spectroscopy of galaxies with a variety of physical properties to map the nature of galactic winds as a function of galaxy type and cosmic epoch, (2) combining these down-the-barrel spectra with densely-sampled background galaxy spectra to map the distribution of absorbing gas using multiple sightlines for single galaxies, and (3) using high S/N, high resolution, spatially resolved spectroscopy of background lensed galaxies to map absorbing gas surrounding foreground galaxies at unprecedentedly fine spatial scales.

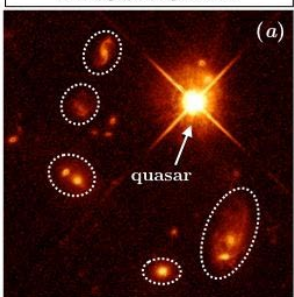
Early studies of the rest-UV of high-redshift galaxies found that nearly all high- z galaxies exhibit blue-shifted interstellar absorption lines and, when present, redshifted Ly α emission (Pettini et al. 2001, Shapley et al. 2003). These strong features are attributed to large-scale galactic winds which are thought to play a critical role in regulating star formation in L^* and sub- L^* galaxies. Continued observational effort has shown these UV signatures of winds to be persistent among star-forming galaxies at low ($z \sim 0.5$, Rubin et al. 2014), intermediate, ($z \sim 1.4$, Weiner et al. 2009, Kornei et al. 2013) and high redshifts (Jones et al. 2012), and recent results illustrate that galactic winds are remarkably similar across much of cosmic time (Rigby et al. 2018).



T

The Circumgalactic Medium in Emission

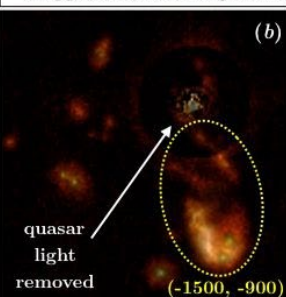
starlight in galaxies



(a)

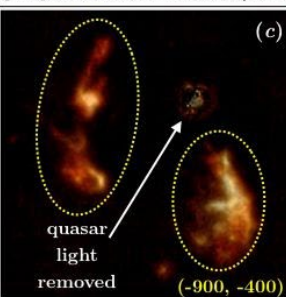
stripped interstellar gas at high speeds, from -1500 km/s to +100 km/s, from the quasar

quasar light removed



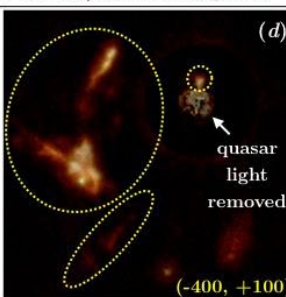
(-1500, -900)

quasar light removed



(-900, -400)

quasar light removed



(-400, +100)

Figure 7-5 Panel (a) shows a traditional broad-band image of the galactic environment of a luminous quasar. Panels (b-d) show narrow-band images taken with MUSE, a wide-field integral field unit (IFU) spectrograph recently commissioned on the VLT; these images show faint emission in H-beta, [OII], and [OIII] from diffuse gas moving at high speeds relative to the quasar, from -1,500 to +100 km/s. What appears in the broad-band image to be isolated galaxies is, in fact, a single, interconnected galaxy with gas being driven by violent interactions to distances ~ 10 times larger than the stellar disks. Some of the stripped gas is found to be moving at high speed into the luminous quasar. (Image Credit: Chen and Johnson.)

Equipped with a wide-field optical IFU (GMACS+MANIFEST), the GMT will be able to study the circumgalactic medium in emission around inactive galaxies where the ionizing flux is expected to be much lower than the vicinities of quasars. In addition, with a blue sensitive CCD, the GMT will enable such studies at $z \sim 2$ by targeting Lyman alpha emission. Because of the expected cosmological surface brightness dimming that follows $(1+z)^4$, the required sensitivity for detecting faint Lyman alpha flows drops rapidly with decreasing redshift. At $z \sim 2$, the virial radius of a typical star-forming galaxy is ~ 90 kpc, corresponding to an angular extent of 11 arcseconds, making an optical IFU spectrograph ideal for these studies.

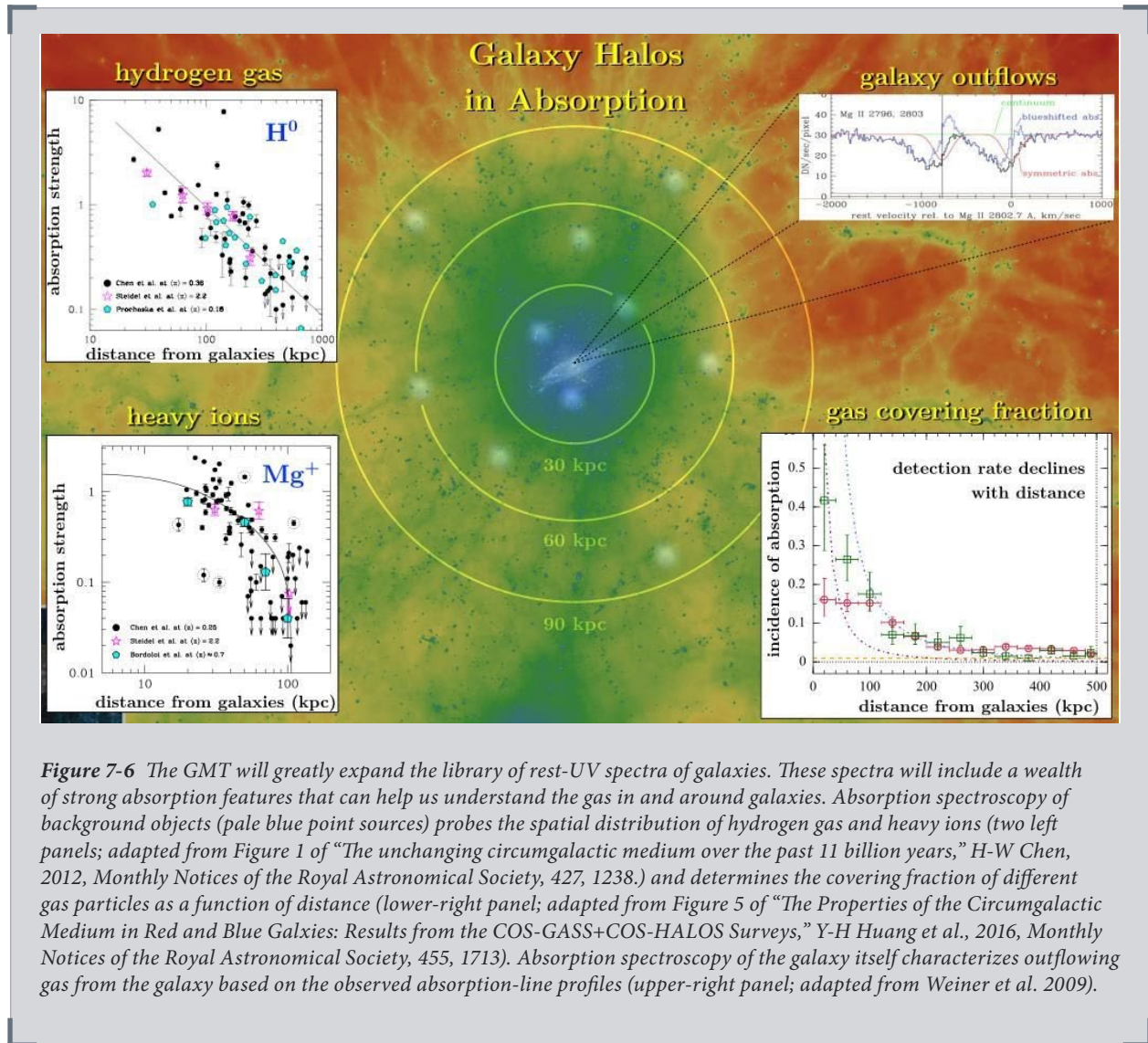


Figure 7-6 The GMT will greatly expand the library of rest-UV spectra of galaxies. These spectra will include a wealth of strong absorption features that can help us understand the gas in and around galaxies. Absorption spectroscopy of background objects (pale blue point sources) probes the spatial distribution of hydrogen gas and heavy ions (two left panels; adapted from Figure 1 of “The unchanging circumgalactic medium over the past 11 billion years,” H-W Chen, 2012, *Monthly Notices of the Royal Astronomical Society*, 427, 1238.) and determines the covering fraction of different gas particles as a function of distance (lower-right panel; adapted from Figure 5 of “The Properties of the Circumgalactic Medium in Red and Blue Galaxies: Results from the COS-GASS+COS-HALOS Surveys,” Y-H Huang et al., 2016, *Monthly Notices of the Royal Astronomical Society*, 455, 1713). Absorption spectroscopy of the galaxy itself characterizes outflowing gas from the galaxy based on the observed absorption-line profiles (upper-right panel; adapted from Weiner et al. 2009).

While outflows are known to be common, detailed studies of their properties in the distant universe are limited by the typically poor signal to noise and low resolution of the attainable spectra for most high-redshift galaxies. Because of this, the previous studies of gas flows within galaxies at redshifts beyond $z \sim 1$ have largely relied on stacked spectra of many hundreds of distant galaxies (e.g., Weiner et al. 2009; Steidel et al. 2010; Bordoloi et al. 2011; Jones et al. 2012; Trainor et al. 2015) or spectra of single lensed galaxies (Pettini et al. 2000, 2002; Quider et al. 2009, 2010; Dessauges-Zavadsky et al. 2011; Bayliss et al. 2014). High S/N, intermediate resolution rest-UV spectra of distant galaxies from the GMT will allow a more detailed view of gas flows at high redshift with high-quality spectra for a statistical sample of galaxies. With these data, we can map the outflow velocities and covering fractions of winds from individual galaxies as a function of their SFRs, masses, morphologies, environments, and other characteristics. Such a sample will also provide empirical understanding of the physical drivers of outflows and the manner in which cold ISM

is entrained, accelerated, or formed in outflows.

In particular, the GMT will enable us to probe the rest-UV spectrum of UV-faint galaxies in detail for the first time. This will open the study of cosmic gas flows to new populations of galaxies: those with SFRs placing them below the main sequence as well as intrinsically faint low-mass star-forming galaxies. This will provide a measurement of the degree to which the properties of the outflow (such as its maximum velocity) depend on mass or star formation rate. Using a sample with a wide range in SFR at fixed stellar mass, we can also understand the degree to which gas flows contribute to the down-turn in star formation. With these observations, we can understand what role galaxy-scale winds play in regulating star formation during the epoch when the majority of stars in the universe were formed.

Dense-sampling the gas surrounding distant galaxies

A highly-multiplexed spectroscopic galaxy survey with GMACS + MANIFEST will also allow for detailed study of the circumgalactic medium of galaxies in the volume, using background galaxies to probe the gas surrounding foreground systems in absorption. Steidel et al. (2010) used stacks of background galaxies in bins of impact parameter to map the average CGM of foreground galaxies. With GMACS + MANIFEST, galaxies with relatively close separations can be selected for observation. The inner 50–100 kpc (corresponding to angular separations of 6–12 arcseconds) are particularly interesting because there are only small samples of galaxies with background QSOs at these separations (see Rudie et al. 2012). To



A Sample Key Project: A Highly Multiplexed High-redshift Galaxy Survey

Figure 7-7 The GMT, utilizing the GMACS spectrograph fed by the MANIFEST fiber system, will provide high-quality absorption spectra for a statistical sample of galaxies. MANIFEST will use the Starbug positioning technology (as prototyped for the TAIPAN project, Kuehn et al. 2014) to access the full field of view of the GMT.

For absorption studies, the required resolution is ~ 100 km/s, with a minimum S/N of a few for large-scale tomographic work (e.g. Lee et al. 2014, 2017) and a minimum S/N of 20 needed for circumgalactic medium (CGM) properties of individual foreground galaxies. At $r \sim 26$, the GMT with GMACS and MANIFEST can reach the required S/N on all distant galaxies in a 20 arcminute MANIFEST field of view in less than 10 nights under typical conditions. This would provide a screen of background backlight galaxies with surface densities of ~ 4 per arcmin² with which to probe the CGM of foreground systems.



map the inner CGM of galaxies, these observations require spectroscopy of sources very close on the sky, providing motivation for improving the minimum possible spacing of MANIFEST fibers (set by the pitch). Otherwise, multiple observations of the same fields will be needed to collect sufficiently-close targets. Compared with the previous stacking analysis (Steidel et al. 2010), such a GMACS survey could provide high enough S/N that each background spectrum could be used to probe the foreground galaxies individually.

The surface density of UV color-selected targets at $z \sim 1.5-3$ roughly doubles as the limiting magnitude of the survey deepens by 0.5 magnitudes (Reddy et al. 2008), and so the density of available background sources is a strong function of the limiting magnitude of the survey at which spectroscopy of moderate S/N is possible. GMACS+MANIFEST will therefore allow for better data from individual sightlines and a higher density of background sources, giving us a higher-resolution mapping of the gas density field than has ever been possible before. Using such a technique, we will make the first detailed maps of the spatial distribution of gas surrounding a statistical sample of individual galaxies.

One clear way to achieve even-higher spatial sampling will be with integral field spectroscopy of background lensed sources. High spatial sampling of these

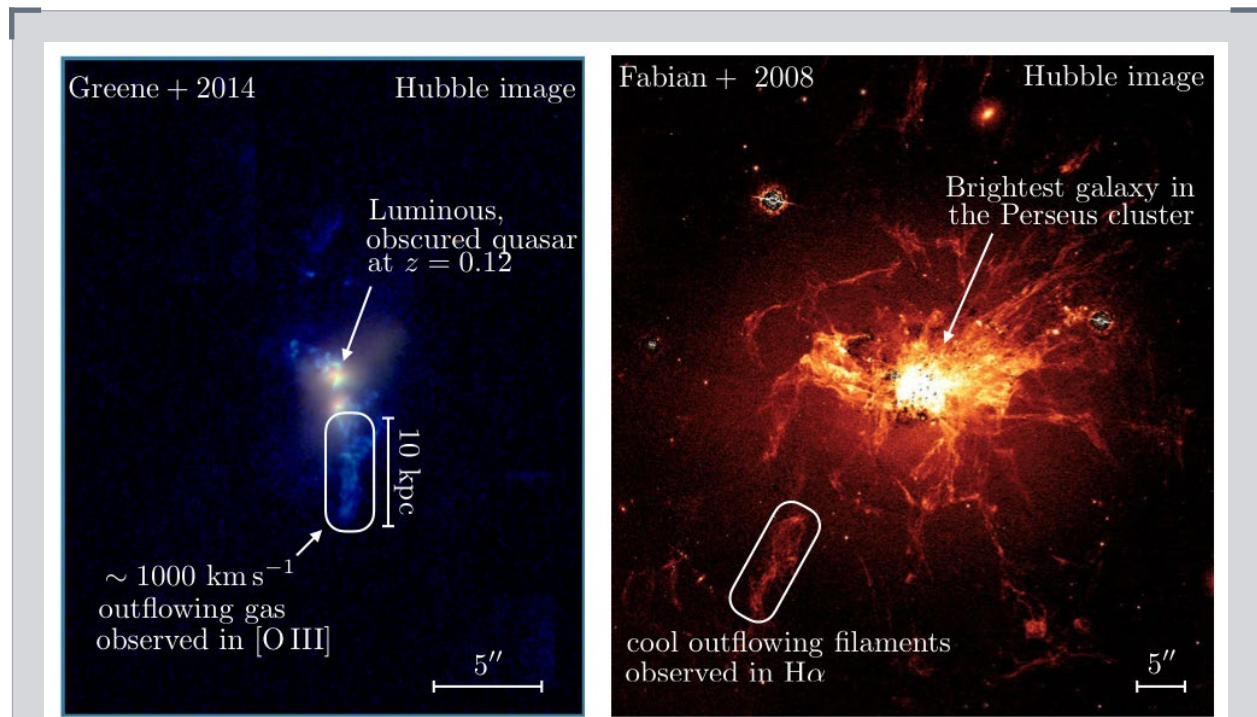


Figure 7-8 The GMT with a wide-field NIR integral field spectrograph will be able to trace outflowing gas from quasars at $z \sim 2$. This figure shows high-resolution, narrow-band images of quasar host environments at low redshifts that include 10 kiloparsec-sized (30 thousand light year) outflows around these energetic sources. The left panel displays fast-moving outflowing gas traced by [OIII] emission in the “blow-out” phase of an obscured quasar (Greene et al. 2014). The right panel shows the H-alpha cooling radiation of materials being lifted from the brightest cluster galaxy in Perseus (Fabian et al. 2008). The GMT will trace similar phenomenon at the epoch where the star formation rate peaks.

galaxies will allow them to be used as “light tables” against which any foreground gaseous structures can be mapped with spatial sampling limited only by the spatial resolution of the IFU and limitations imposed by seeing (or the GLAO system). For the brightest lensed galaxies, higher spectral resolution data would also be feasible, providing better velocity resolution in the mapping of the CGM, bridging the gap between low-resolution background galaxy and high-resolution background QSO observations (e.g., Lopez et al. 2018).

7.3 Revealing Black Hole Driven Winds from Small to Largest Scales

The GMT, with AO resolution and an integral field spectrograph, will provide an unprecedentedly detailed look at the powerful central engines of galaxies, especially the accreting supermassive black holes that are the brightest galaxy beacons — the quasars.

Quasars are the most powerful phenomena in the universe. These sources are powered by supermassive black holes and are routinely invoked in galaxy formation and evolution theories, acting to quench star formation and producing quiescent galaxies in massive halos. The powerful high resolution capability of the Hubble Space Telescope enabled the discovery of ubiquitous supermassive black holes at the centers of massive galaxies in the nearby universe (for a review, see Kormendy & Ho 2013). Even though the gravitational force from a black hole is only important on scales much smaller than the host galaxies themselves, their masses are strongly correlated with those of the host galaxy bulges. The observed relationship between galaxies and their central black holes can arise as the result of mergers of gas rich galaxies, which simultaneously drive gas to the nucleus to fuel black hole accretion in a quasar phase, transform the merging disks into a bulge, and fuel additional nuclear star formation. The nuclear starburst and quasar can then drive powerful outflows which couple to the surrounding gas and halt further cooling, accretion, and star formation. While this heuristic picture is compelling, developing an understanding of the physical processes that couple galaxy and black hole growth is one of the driving goals of extragalactic astrophysics.

Supermassive black holes accreting efficiently during a quasar phase release vast quantities of energy and momentum through radiative emission and jets which can unbind much of the host galaxy’s gas reservoir, at least in principle. In order for black holes and their host galaxies to co-evolve, this energy must effectively couple to the surrounding gas; however, the physical mechanisms that can bind the quasar energy/momentum to host galaxy gas supply remain largely unknown. Quasars can inject energy over a wide-range of scales, from less than a parsec to hundreds of kiloparsecs, making detailed simulations of quasar feedback impossible even with the world’s most powerful supercomputers. Consequently, our understanding of the quasars’ role in regulating galaxy growth must be guided by observations that connect small scale physics observed at high resolution with observations of the galactic scales needed for effective feedback.

The high resolution capability of the Hubble Space Telescope not only revealed the ubiquitous presence of supermassive black holes, but also provided detailed images of quasar feedback in-action in a few nearby galaxies (*Figure 7-8*). Hubble images combined with ground-based spectra identified large scale winds driven by a low-redshift quasar with gas reaching velocities of several hundred to a thousand km/s and distances of twenty kpc, well beyond the disk of the host galaxy. Moreover,

Hubble observations of nearby galaxy clusters show that subsequent accretion heats the surrounding gas, resulting in a buoyant wind that entrains denser gas observed as filaments in H-alpha images from Hubble. The fact that these filaments are several kpc long but only 70 pc in width indicate that magnetic fields play a critical role in stabilizing the dense gas, enabling massive dense gas reservoirs to accumulate without forming stars. Together these observations serve as a “proof-of-concept” demonstrating that quasars can produce powerful, extended outflows that halt star formation and that further black hole feedback can prevent subsequent star formation.

Detailed studies of quasar feedback in these low-redshift “prototypes” with Hubble has led to significant physical insights, but star formation and quasar activity were at their peak ten billion years ago in the $z=2-3$ universe. To understand the co-evolution of galaxies and their supermassive black holes, quasar feeding and feedback must be observed at work in this earlier epoch when today’s massive galaxies were still growing rapidly. At these redshifts, however, the necessary, ~ 40 pc resolution is beyond the capability of the largest current ground-based telescope as well as both Hubble and JWST.

GMT AO-assisted integral field spectroscopic observations will enable us to zoom in on the central nuclear region to capture quasar-driven outflows as these materials are being launched. Specifically, GMTIFS with a 6 mas spatial resolution provide a spatial sampling of 45 pc at $z\sim 3$, sufficient to resolve the nucleus from the quasar host galaxy. These observations will enable studies of the M - σ relation at $z=2$ with emission-line based velocity dispersions in massive galaxies without current AGN activity.

At the same time, a wide-field NIR integral field spectrograph will further enable searches for spatially extended line-emitting gas at distances 10 times larger than the optical disk of the host galaxy, and connect large-scale gas flows with quasar driven winds directly observed in the nuclear regions. These unique data will help establish a physical connection between nuclear activities and large-scale gas properties and provide the first empirical evidence for quasar feedback from small to large scales.

References

- Cantalupo et al, 2014, *Nature*, 50663–66
- Chen, H.-W. 2012, *MNRAS*, 427, 1238
- Fabian, A.C., Johnstone, R.M., Sanders, J.S., et al. 2008, *Nature*, 454, 968
- Greene, J.E., Pooley, D., Zakamska, N.L., Comerford, J.M., & Sun, A.L. 2014, *ApJ*, 788, 54
- Huang, Y.-H., Chen, H.-W., Johnson, S.D., & Weiner, B. J. (2016), *MNRAS*, 455, 1713
- Jones, T., Stark, D. P., & Ellis, R. S. 2012, *ApJ*, 751, 51
- Kollmeier, J.-A., Zheng, Z., Davé, R., et al. 2010, *ApJ*, 708, 1048
- Kornei, K. A., Shapley, A. E., Martin, C. L., Coil, A. L., Lotz, J. M., Schiminovich, D., Bundy, K., & Noeske, K. G. 2012, *ApJ*, 758, 135
- Kuehn K., et al., 2014, *Proc. SPIE*, 9147, 914710
- Lee, K.G., Hennawi, J.F., Stark, C., et al. 2014, *ApJ Letters*, 795, L12
- Lee, K.G., Krolewski, A., White, M., et al. 2017, *arXiv:1710.02894*
- Martin, C. L. 2005, *ApJ*, 621, 227
- Martin, C. L., Shapley, A. E., Coil, A. L., Kornei, K. A., Bundy, K., Weiner, B. J., Noeske, K. G., & Schiminovich, D. 2012, *ApJ*, 760, 127
- Pettini, M., Shapley, A. E., Steidel, C. C., Cuby, J., Dickinson, M., Moorwood, A. F. M., Adelberger, K. L., & Giavalisco, M. 2001, *ApJ*, 554, 981
- Pettini, M., Steidel, C. C., Adelberger, K. L., Dickinson, M., & Giavalisco, M. 2000, *ApJ*, 528, 96
- Quider, A. M., Pettini, M., Shapley, A. E., & Steidel, C. C. 2009, *MNRAS*, 398, 1263
- Quider, A. M., Shapley, A. E., Pettini, M., Steidel, C. C., & Stark, D. P. 2010, *MNRAS*, 402, 1467
- Reddy, N.A., Steidel, C.C., Pettini, M., et al. 2008, *ApJ Supplement*, 175, 48
- Rigby, J.R., Bayliss, M.B., Chisholm, J., et al. 2018, *ApJ*, 853, 87
- Rubin, K. H. R., Prochaska, J. X., Koo, D. C., & Phillips, A. C. 2012, *ApJ*, 747, L26
- Rubin, K. H. R., Prochaska, J. X., Koo, D. C., Phillips, A. C., Martin, C. L., & Winstrom, L. O. 2014, *ApJ*, 794, 156
- Rudie, G. C., Steidel, C. C., Shapley, A. E., & Pettini, M. 2013, *ApJ*, 769, 146
- Rudie, G. C., Steidel, C. C., Trainor, R. F., Rakic, O., Bogosavljevic, M., Pettini, M., Reddy, N., Shapley, A. E., Erb, D. K., & Law, D. R. 2012, *ApJ*, 750, 67
- Shapley, A. E., Steidel, C. C., Pettini, M., & Adelberger, K. L. 2003, *ApJ*, 588, 65
- Simcoe, R. A., Sargent, W. L. W., Rauch, M., & Becker, G. 2006, *ApJ*, 637, 648
- Spergel, D. et al. 2015, *arXiv:1503.03757*
- Steidel, C. C., Erb, D. K., Shapley, A. E., Pettini, M., Reddy, N., Bogosavljevic, M., Rudie, G. C., & Rakic, O. 2010, *ApJ*, 717, 289
- Trainor, R. F., Steidel, C. C., Strom, A. L., & Rudie, G. C. 2015, *ApJ*, 809, 89
- Weiner, B. J., Coil, A. L., Prochaska, J. X., Newman, J. A., Cooper, M. C., Bundy, K., Conselice, C. J., Dutton, A. A., Faber, S. M., Koo, D. C., Lotz, J. M., Rieke, G. H., & Rubin, K. H. R. 2009, *ApJ*, 692, 187
- Zhang, H., Zaritsky, D., Zhu, G., Menard, B., & Hogg, D.W. 2016, *ApJ*, 833, 276



*Hubble Space Telescope imaging of the strong gravitational lens SDSSJ2222+2745
(adapted from Sharon et al. 2017)*

Cosmology & The Dark Universe

How did the universe form and grow? The universe began in a hot Big Bang 13.8 billion years ago, and has been expanding and cooling ever since. After nearly a hundred years of study, we know that the universe is mostly made up of dark matter and dark energy, with normal matter—everything we can actually see—comprising just a small fraction of the universe’s mass and energy.

Our model for the Big Bang and the subsequent evolution of the universe is well supported by empirical evidence, but the nature of dark matter and dark energy remains unknown. Our understanding is framed by our bedrock theories of physics that have been directly tested over a limited range of conditions. Extreme environments in the cosmos—from the earliest moments of the Big Bang itself to the recently-discovered sources of gravitational waves—offer new opportunities to test these theories. The GMT will offer new ways to challenge and refine our understanding of the physical laws that govern the universe.

Chapter Authors

Eduardo Cypriano (University of São Paulo)

Alex Drlica-Wagner (Fermilab)

Wendy Freedman (University of Chicago)

Michael Gladders (University of Chicago)

Ting Li (Fermilab)

Dan Scolnic (University of Chicago)

8 Cosmology & The Dark Universe

Edwin Hubble's 1929 discovery that our universe is expanding profoundly changed astrophysical research and captured considerable public interest. In the 1930's Fritz Zwicky made the first attempt to weigh a collection of galaxies by measuring their orbital velocities. To his surprise, he found that the galaxies were much more massive than their collection of stars. The mysterious but dominant constituent of galaxies has still not been identified, although it now has a name: dark matter. In the late 1990s, two teams of scientists discovered that the expansion of the universe is accelerating, driven by an unknown energy source we call dark energy. The discovery of dark energy has fostered a further explosion of experimental, observational, and theoretical research. All three paradigm-shifting discoveries required extensive observations on the largest available telescopes. We have now come to understand that ordinary matter comprises a tiny fraction of the mass and energy content of the universe.

The GMT will enable cosmological tests and probes of fundamental physics that were previously impossible. In this chapter we explore some of those. One classic example is provided by the ever improving measurement of the local expansion rate of the universe as quantified by the Hubble Constant, H_0 . It is arguably the most important cosmological parameter to measure in the coming decade. Measurements of H_0 from the cosmic microwave background radiation emitted when the universe was 300,000 years old and local measurements don't agree precisely, hinting at new physics to be discovered. The GMT will measure the Hubble Constant with better than 1% accuracy using multiple independent probes.

The GMT's extraordinary spatial resolution will allow us to find the relatively faint standard candles, Cepheid variable stars, that Hubble used to discover the expanding universe, in more distant galaxies that have hosted much brighter standard candles: supernovae. The distance scale based on Cepheid variables can be used to calibrate the distance scale based on supernovae, vastly extending the reach of precision distance measurements. The extended distance scale can be checked with distance measurements based on gravitational lenses and on detection of gravity waves from merging neutron stars. In these cases, as well, the GMT's powerful instrument suite will allow a leap forward in precision distance measurements.

The evidence for dark matter comes from astronomical observations that detect dark matter over a vast range of scales from the smallest, faint galaxies to large clusters of galaxies. The only alternative to the existence of dark matter would be a modification to the law of gravity. Such a modification to the theory of gravity is becoming more and more untenable. Einstein's general relativity, our anchoring theory for gravity, has been tested many times and so far has passed each test. Recent detections of gravitational wave sources have further strengthened our confidence in general relativity.

The GMT's enormous aperture, extraordinary spatial resolution, and powerful instruments will enable potentially revolutionary investigations of the distribution of dark matter. Detailed studies of very low mass galaxies hold particular promise because dark matter completely dominates their contents. We anticipate that LSST will discover many extremely faint dwarf galaxies for GMT to examine with its powerful spectrographs. GMT observations will reveal the details of the stellar dynamics of these galaxies and the distribution of the dark matter they contain.

Astronomy observations have led to discoveries of new physics and an understanding of the structure and contents of our universe. Cosmology is intimately linked to

fundamental physics and astronomical observations show us convincingly that our present knowledge of physics incompletely describe our dark-matter and dark-energy dominated cosmos.

In this chapter we highlight the expected impact of the GMT on a few areas of cosmology. GMT observation could break our theoretical physics framework, resolve apparently discrepant measurements, and fill profound gaps in our understanding of the universe and the physical laws that describe its workings. In **Section 8.1** we discuss the GMT's expected impact on dark matter research. **Section 8.2** describes how the GMT will pin down the distance scale and the expansion history of the Universe.

8.1 Dark Matter and Ultra-Faint Dwarf Galaxies

The first detection of dark matter in galaxy clusters occurred in the 1930's when the *spectra* of member galaxies displayed velocities far in excess of what could be produced by the visible mass in those objects, and an abundance of data now indicates the presence of dark matter across a range of scales (Zwicky, 1933; Smith 1936). At present, dark matter is a key ingredient for a successful model of the universe, namely the consensus Λ CDM model, and it is needed to fit fundamental observations of the universe on large scales, such the distribution of galaxies and clusters and the anisotropies in the cosmic microwave background radiation.

The most successful models that are able to describe observations of the universe on large scales rely on the matter content being dominated by some elusive particle that interacts gravitationally but not electromagnetically (see Einasto 2009 for a review). Arguments from structure formation suggest such a particle must have been non-relativistic at early times (and hence massive) if thermally produced.

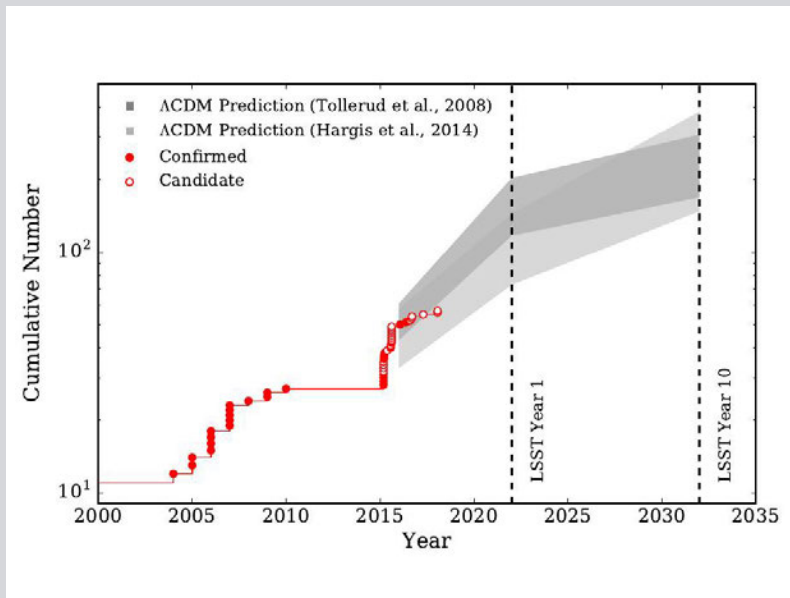
Despite decades of study, the fundamental nature of dark matter remains mysterious. Extensive micro-lensing observations have excluded most compact (baryonic) objects as the principle form of dark matter (Alcock et al. 2000; Tisserand et al. 2007). Primordial black holes are still a possibility (Carr, Kühnel, & Sandstad 2016), although not if their mass spectrum is monochromatic (Niikura et al. 2017). Observations of the CMB (e.g., Planck 2016) and Big Bang nucleosynthesis (e.g., Copi, Schramm & Turner 1995) also strongly constrain the total baryonic contribution to dark matter. From decades of research, we have (at best) only confined dark matter to an extensive range of theoretical possibilities (WIMPs, axions, sterile neutrinos, self-interacting dark matter, primordial black holes, strongly-interacting massive particles, etc.), among which the most popular candidate is some form of WIMP. While numerous direct-detection searches for such particles have been done, all have produced null results (apart from the still unexplained annual modulation of the DAMA experimental signal by Bernabei et al. 2013).

To make progress in understanding the fundamental nature of dark matter, we need new observational constraints, and dark matter halos around galaxies are an obvious target. The most appealing candidates for such work at present are dwarf galaxies, and in particular the ultra-faint dwarf galaxy satellites (UFDs) of the Milky Way. UFDs occupy a unique regime where they have just enough luminous matter to be observable, but too little to appreciably alter the structure of their dark matter halos; the least luminous UFDs have mass-to-light ratios in excess of 1000 times that of the Sun (e.g., Kirby et al. 2015, Kim et al. 2016). The structure and abundance of UFDs can thus be directly linked to the fundamental physics that governs the formation of dark matter halos. For example, the abundance of dwarf galaxies is sensitive to the

mass and temperature of dark matter particles, while the density of dark matter in these galaxies is sensitive to the dark matter self-interaction cross section.

Simulations of structure formation in the conventional Λ CDM model have long predicted an abundance of small dark matter subhalos that far exceeds the number of observed UFDs—this is the “missing satellites” problem. Resolving this discrepancy will require improvements in both simulations and observations. The proximity and large dark matter content of dwarf galaxies make ideal targets in which to detect the annihilation and/or decay of the proposed WIMPs using a combination of LSST imaging and GMT spectroscopy, as we discuss below.

Figure 8-1 LSST + GMT confront the “missing satellite” problem. The figure illustrates the recent rapid rise in the number of UFDs and the much larger rise that is expected between now and the end of the LSST nominal operating period. The LSST is expected to increase the number of Ultra Faint Dwarf candidates to more than 200 compared to the ~50 systems known to date. Resolving the missing satellite problem requires confirmation of the candidates and mass estimates to type the candidates as galaxies (dark matter dominated) or star clusters (absent dark matter). Spectroscopy with the GMT is required to do this work.

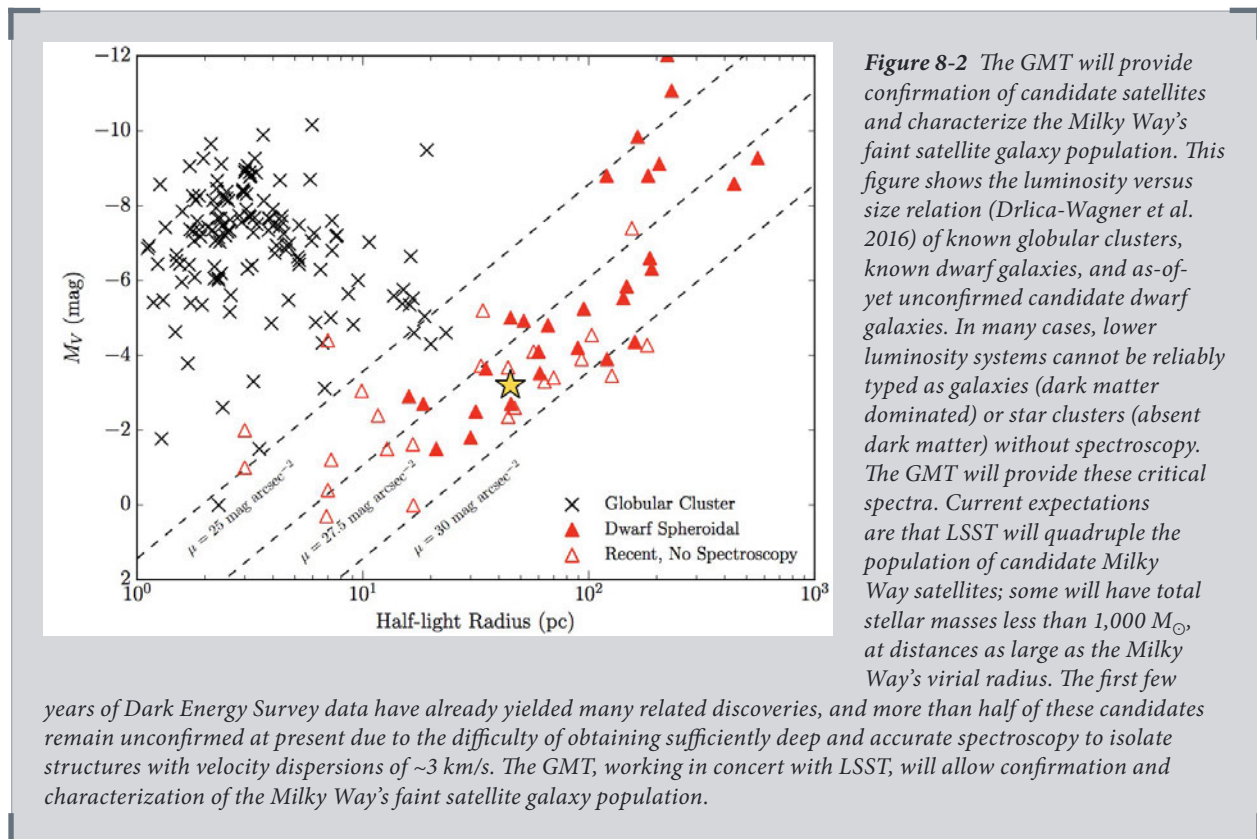


Are “Missing Satellites” a Problem?

On the scale of our galaxy, Λ CDM predicts the existence of numerous small dark matter halos. For the smallest of those halos, star formation is inefficient and fundamentally fragile, and hence galaxy formation models predict that only a fraction of those dark matter halos are inhabited by stars. Observationally, the Milky Way’s halo is richly populated by star clusters and dwarf galaxies, and many of each have been recently discovered in imaging surveys such as the Dark Energy Survey (DES; Bechtol et al. 2015; Koposov et al. 2015; Drlica-Wagner et al. 2015). Measuring the halo mass function on these scales provides fundamental constraints on the properties of dark matter, and the coming flood of deep imaging data from LSST will offer a powerful opportunity to do so when combined with GMT spectroscopy.

LSST data will be sufficiently deep to find UFDs to the virial radius of the Milky Way, giving an essentially complete census of candidate UFDs for the first time. But the dynamical nature of the candidates can only be determined with spectroscopy from telescopes like the GMT. The number of UFDs expected to be discovered in LSST is a factor of 4 times higher than all of those known to date (**Figure 8-1**), even when the predictions account for the inefficiency of star formation in small

halos. Many of these discoveries will be at greater distances than any known system with comparable intrinsic luminosity. At the same time, LSST data will reveal other stellar structures, such as the faintest most distant globular clusters, and, as is already apparent in DES data, the photometric boundary between the smallest galaxies (dark matter dominated) and largest star clusters (absent dark matter) is blurred at best, particularly when one considers the potential effects of tripping and tidal disruption over the lifetime of such objects. Spectroscopy is required to both confirm and classify these objects (**Figure 8-2**), which will be too faint to target with current telescopes. This is where the GMT becomes essential.



Confirmation and classification of existing candidates is already challenging; it requires spectroscopy of sufficient resolution and sensitivity to measure stellar velocities to a precision of ~ 1 km/s, since the velocity dispersions of these systems are typically less than 10 km/s. **Figure 8-3** shows a recently identified UFD candidate at an estimated distance of 250 kpc (Homma et al. 2018) found using the Subaru/Hyper Suprime-Cam, which is illustrative of the kind of discoveries we can expect from LSST. Only a handful of stars occupy the bright end of the giant branch and are amenable to spectroscopy with current telescopes. Most of the dwarf galaxies that will be discovered by LSST will be distant ($d > 200$ kpc) and/or faint (total absolute V magnitudes of -2 or fainter, with at most a few stars populating the giant branch). Current 6–10 m class telescopes can only measure absorption line velocities of the brightest candidate stars ($r < 22$ mag) in these dwarf galaxy candidates. Because the UFDs have so few stars, at most only a handful of members can possibly be followed

up spectroscopically with current facilities. Conversely, in two hours in median conditions, GMACS can reach to $r \sim 24.5$ at a resolution of 50 km/s at an average per-pixel S/N of 5, which is sufficient to establish individual stellar velocities to better than 2 km/s and sufficient to confirm and classify all expected LSST candidates. The GMT southern site gives full access to the LSST survey footprint. Only the GMT, working in synergy with LSST, can complete the census of dwarf galaxies of the Milky Way, measure their dark matter content, and finally provide the observational baseline against which we can ask if there are, in fact, missing satellites.

Annihilation Signals from Particle Dark Matter —Measuring Dark Matter Densities

One of the fundamental tests of the WIMP model for dark matter involves the properties of the particles themselves. If WIMPs were produced in the early universe and evolved thermally since, then the total WIMP content in the universe will depend upon the “velocity averaged annihilation cross section” of those particles, written as $\langle\sigma v\rangle$ (e.g., Steigman, Dasgupta & Beacom 2012). Particle physics also predicts that WIMPs will produce γ -ray emission through self-annihilation or decay. The WIMP dark matter model then suggests that γ -ray emission due to dark

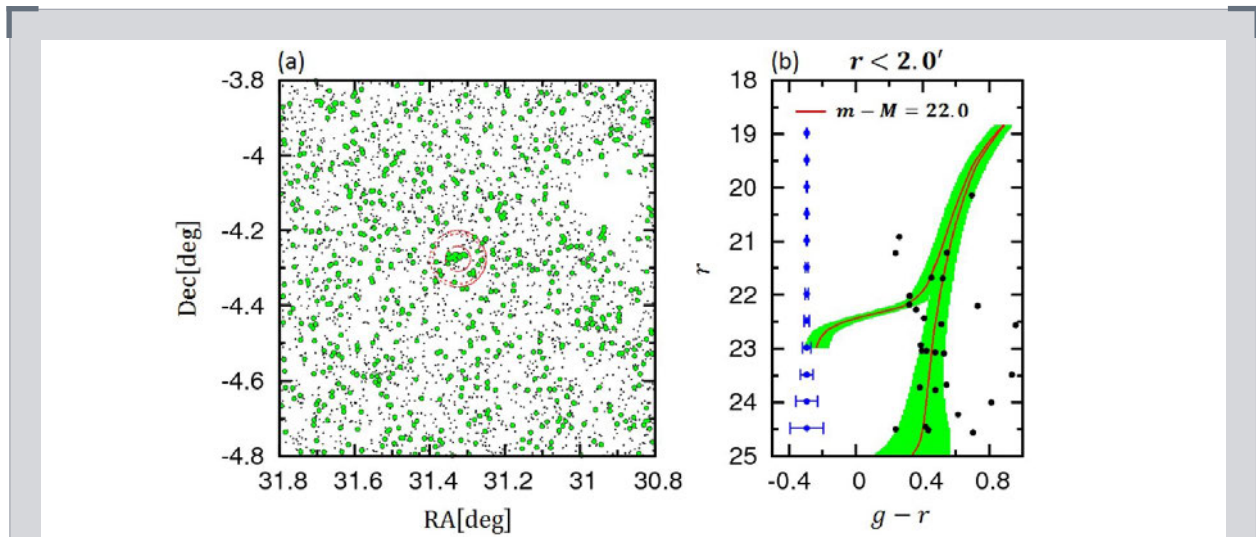


Figure 8-3 The challenge of confirming ultrafaint dwarfs (UFDs) will be met with GMACS, which is needed to confirm such discoveries, measure the dynamics of the galaxies’ stars, and determine which systems are in fact dark-matter dominated dwarf galaxies. This figure highlights the photometric data for the UFD galaxy candidate Cetus III as an example. The left panel presents the locations of stars in the field (image credit: Figure 5 of “Searches for New Milky Way Satellites from the First Two Years of Data of the Subaru/Hyper Suprime-Cam Survey: Discovery of Cetus-III,” D. Homma, et al., 2018 Publications of the Astronomical Society of Japan, 70, 18.) The green dots highlight stars that are consistent with a color-magnitude filter for distant UFD stellar populations. The dashed circle in the center shows the location of this recently suggested UFD from the detected overdensity of stars. The right panel presents the color-magnitude diagram of stars at this location, but only ~ 6 are bright enough for continuum spectroscopy using existing telescopes. Many similar systems will be discovered by LSST. With the current 6–10 m class telescopes, the spectroscopic limiting magnitude is $r \sim 22.5$ and only a handful of stars can be observed. The fainter (more distant) UFDs are entirely beyond the capabilities of existing telescopes.

matter decay should be detectable. Indeed, Fermi-LAT has detected an excess of ~ 10 GeV γ -rays in the region of the Galactic center that several groups interpret as a signature of dark matter annihilation (e.g., Gordon & Macias 2013; Abazajian et al. 2014; Calore et al. 2015; Daylan et al. 2016). However, the Galactic center is a complex environment, and the existence of numerous astrophysical backgrounds makes the interpretation of this signal difficult.

Nevertheless, this detection suggests a tantalizing self-consistency check between the Standard Model and the WIMP model of dark matter—the total density of dark matter in the universe and the observed annihilation cross section of the dark matter particles in nearby galaxy halos must be self-consistent if our understanding of dark matter is correct. If the γ -ray signal from more (and *simpler*) dark matter halos can be measured, and if the total dark matter content of those halos is known, then $\langle\sigma v\rangle$ can be inferred. That total dark matter content of the universe that is consistent with that number can then be compared to the empirical dark matter content of the universe as measured by astrophysical observations.

Compared to the Galactic center, Milky Way dwarf galaxy satellites have a high dark matter density, and lack astrophysical contaminants. This makes them some of the

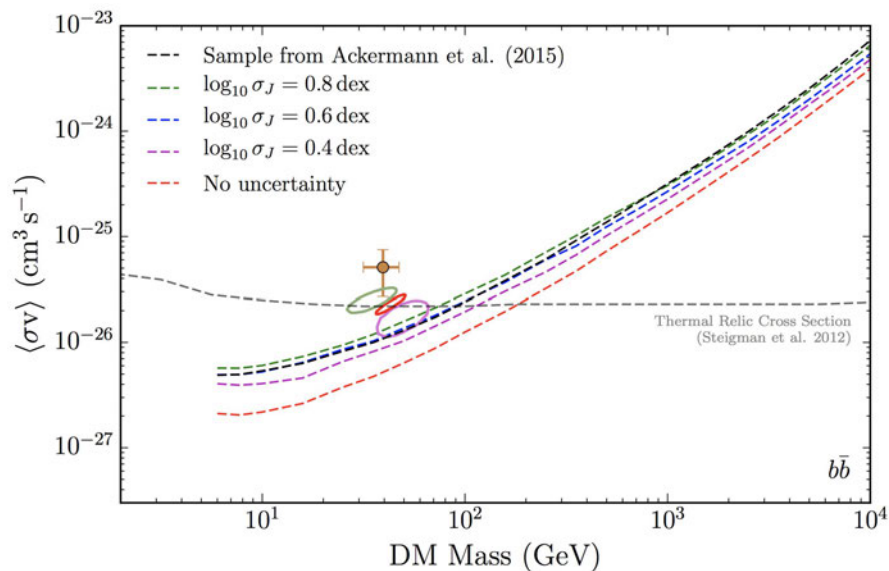


Figure 8-4 The GMT will greatly improve current constraints that are on the verge of ruling out WIMP decay as the source of gamma-ray emission from the Galactic center. This figure considers the dark matter cross section versus particle mass for the representative b/\bar{b} annihilation channel for WIMPS (from Albert et al. 2017). The near-horizontal dashed line shows the expected cross-section for dark matter WIMPS. Regions above the black dashed rising curve are already excluded by the lack of detection of γ -rays from UFDs. The three ellipses and the point with uncertainties represent four dark matter interpretations of the γ -ray excess in the Milky Way center. The figure illustrates that there is modest tension between the dark matter interpretation of that excess, and current limits from UFDs. The precision of J-factors changes the sensitivity of the constraints on the dark matter annihilation cross section (colored lines). Significant J-factor improvements can be readily achieved with the GMT. Even absent further UFD discoveries or γ -ray data, such work would exclude more of the potential WIMP cross-section/mass space, and effectively rule out a WIMP interpretation of the galactic center γ -ray excess.

most promising targets when searching for dark matter annihilation via γ -rays. Observations of multiple satellite galaxies can be combined in a joint-likelihood framework for increased sensitivity and reduced systematic uncertainties. In this way, the aggregate of Fermi-LAT observations of Milky Way satellite galaxies can provide a direct, independent test of dark matter models.

So far, γ -rays have not been detected from the dwarf galaxies near the Milky Way, and this non-detection already places strong constraints on dark matter models. But the interpretation of those non-detections is subject to accurate measurements of the dark matter density of the dwarfs; if the line-of-sight dark matter density integrated over the solid angle of those galaxies is not high enough, then detectable γ -ray emission would not be expected.

Synergy with LSST

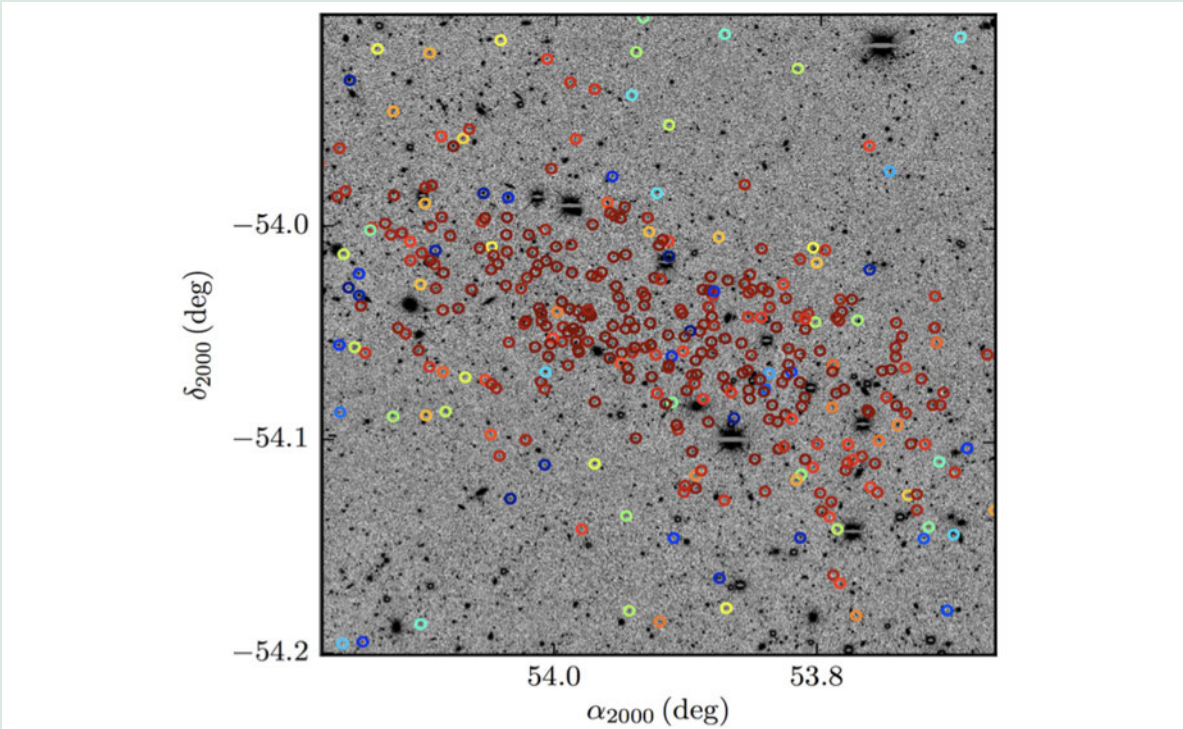


Figure 8-5 Stars that can be targeted for GMT spectroscopy in LSST-discovered UFDs to refine their J -factors. Here we show the photometric membership of Reticulum II in DES data (adapted from Bechtol et al. 2015), Reticulum II exemplifies the UFDs that we expect LSST to discover: relatively nearby, with extremely high mass-to-light ratio, total stellar mass less than $10^3 M_{\odot}$, and angular sizes of tens of arcminutes. These systems will be critical to improving the dark matter constraints from γ -ray measurements, as they will have some of the highest J -factors of the overall UFD population. Only GMACS+MANIFEST offers the combination of field-of-view and sensitivity necessary to acquire moderately-high-resolution spectroscopy of many faint stars in such systems. Smaller telescopes offer the field of view, but lack the collecting area to take spectra of faint stars; these dark matter halos have so few stars that it will be critical to reach stars fainter than the main sequence turnoff to measure J -factors.

In coordination with deep ground-based imaging surveys (such as LSST) and existing observations from γ -ray with Fermi-LAT (or future telescopes), the GMT will dramatically tighten the bounds of this analysis and offer deep insight into the dark matter puzzle. One of the key systematic uncertainties in predicting the expected flux of γ -rays from dark matter annihilation in dwarf galaxies comes from uncertainty regarding the dark matter density-content of these galaxies. These galaxies are dispersion-supported systems and the dark matter mass-density is determined by measuring the radial velocity distribution of individual stars populating the halo. In the coming decade, the GMT will be the premier facility for determining the dark matter properties of known ultra-faint dwarfs, as well as confirming and characterizing new UFDs in order to improve the accuracy of γ -ray analysis.



Refining the J-factors for Reticulum II – like UFDs

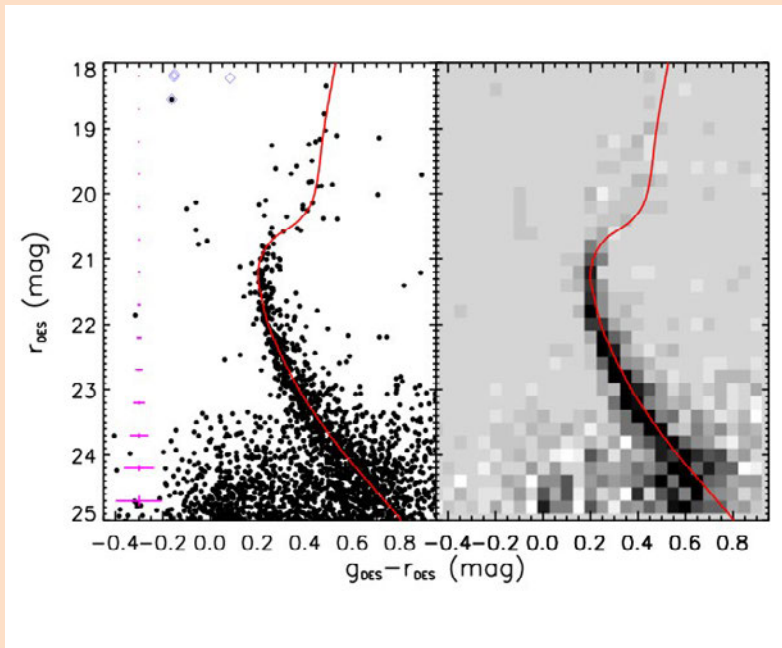


Figure 8-6 Color-Magnitude diagrams are shown for Ret II including stars within one half-light radius of its center. Magenta error bars show the color and magnitude uncertainties as a function of r -magnitude. Blue open diamonds are blue HB candidates within the field of view. Right: Same as left, but with background and foreground stars removed (adapted from Mutlu-Pakdil et al. 2018). Reticulum II is considered likely to have the highest J-factor of the known UFDs, and is the only UFD for which an apparent γ -ray excess has been reported, albeit at low significance (Geringer-Sameth et al. 2015) and subject to much debate (e.g., Zhao et al. 2018). Regardless, it is an excellent example for the properties of high-priority UFDs for which the refinement of J-factors will be a key observation by the GMT.

A fiducial goal of measuring 200 member stars to better than 2 km/s, sufficient to constrain the J-factor to 0.2 dex, would require a limiting magnitude of $i \sim 23$, given Reticulum II's total stellar mass of $\sim 2,600 M_{\odot}$ and a typical IMF. GMACS+MANIFEST can reach this limit in 2 hours under nominal observing conditions to obtain the S/N needed for reliable velocity measurements. The GMT's 20 arcmin field of view gives it a significant observational advantage in that the complete half-light radius of the UFD can be observed in a single pointing. Even with careful photometric selection, less than 50% of candidate stars selected will be members of the galaxy, so that several pointings will be needed to obtain 200 confirmed members in one UFD, making efficient multiplexing even more important. The GMT could thus provide the critical J-factor refinement for 10 UFDs in 10 nights of observing time. Such a data set would be sufficient to dramatically impact the current interpretation of dark matter annihilation γ -rays.

Accurate measurement of the “J-factor” — the line-of-sight dark matter density integrated over solid angle — of known or discovered UFDs directly improves the sensitivity of γ -ray searches for dark matter annihilation, because it improves the relative signal-weighting between UFDs. The limiting factor in determining the J-factor is the number of stars available for accurate velocity measurements from spectroscopy. Current 8–10 m class telescopes have been used to measure the velocities of the brightest stars (to $r \sim 22$ – 22.5 mag), and the J-factors of the most important systems are now nearly as refined as these telescopes permit. The GMT will measure velocities for stars 2 magnitudes fainter ($r \sim 24.5$ mag) to well past the main sequence turnoff, and hence increase the number of stars dramatically. As illustrated in **Figure 8-4**, this improves the sensitivity of the J-factor of known systems by a factor of 2 to 3, even absent additional γ -ray data or UFD discoveries.

Detailed calculations suggest that a reasonable target for the precision of J-factor measurements is ~ 0.2 dex, albeit many systems lack a J-factor measurement entirely. Wang et al. (2018) have considered detailed simulations of J-factor measurements in the recently discovered UFD Reticulum II (because this is a particularly nearby and well-characterized UFD and has a large J-factor, it is a key object to study); they find that observations of ~ 200 stars, with individual velocity precisions of ~ 2 km/s are necessary to reach 0.2 dex precision on the J-factor. Better velocity precision on individual spectra lowers the number of required stars, to perhaps ~ 150 for a precision of 0.5 km/s.

The nearby UFDs that are currently known have stellar masses of $\sim 10^3 M_{\odot}$ and lie at distances of tens of kpc. At 30 kpc, Reticulum II, for example, spans ~ 15 arcminutes. Spectroscopic observations to measure the velocities of member stars using 8–10 m class telescopes can only target stars with r-band magnitudes brighter than 22 mag, which is brighter than the main sequence turnoff for even such relatively nearby systems (e.g., Simon et al. 2015; Kim et al. 2016). As such, at most a few dozen RGB stars can be used to constrain the J-factor in current data for those galaxies (**Figure 8-6**). It will take the GMT, with the MANIFEST fiber system feeding the GMACS spectrograph, to confidently measure the stellar velocities of galaxies at similar and greater distances.

In addition to refining knowledge of the J-factor, there are two further ways to strengthen the constraints on dark matter. Trivially, ongoing observations with Fermi-LAT will continue to tighten constraints, though the mission is entering its 10th year, and so the tightening of non-detection limits will be slow, and the potential for the emergence of a detection is low. Conversely, the addition of further sources to the aggregate pool of high J-factor objects could improve constraints dramatically. The most promising targets for the detection of gamma-ray signals from dark matter annihilation are nearby UFDs. The LSST, in addition to finding distant systems, will expand our catalog and knowledge of nearby systems, at the low mass end where stellar populations are extraordinarily sparse. The GMT will be required to fully exploit those systems.

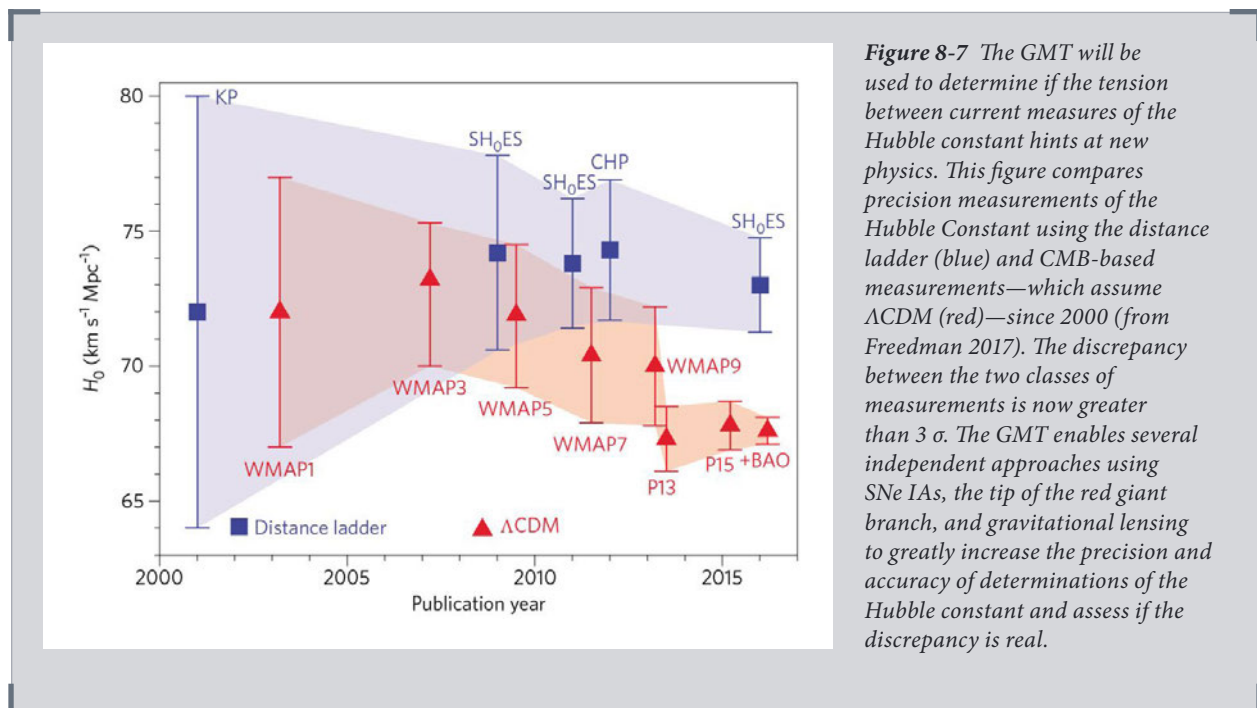
8.2 Measuring H_0

Recent determinations of the current expansion rate (**Figure 8-7**) based on CMB measurements from the Planck satellite—which assume Λ CDM—are now more than 3σ discordant with H_0 measurements based on the local distance ladder (e.g., Riess et al. 2016) and with H_0 measurements based on strong lensing time delays from multiply-imaged quasars (Bonvin et al. 2017). These latter two independent measurements of H_0 agree, and the CMB-derived value agrees with the H_0 value

derived from baryon acoustic oscillations (BAO) in combination with SNe Ia (Aubourg et al. 2015). Is this discrepancy due to systematic errors lurking in several of these methods, or does this tension point to new physics beyond the consensus model? If the answer is new physics, possible explanations would include cosmic acceleration of a more complicated nature than a cosmological constant, additional relativistic relics from the early universe, a decaying dark matter particle, or even a disruption of General Relativity.

The GMT offers opportunities to measure H_0 using multiple independent probes, *each* of which can constrain H_0 to better than 1%. If the current dissonance holds, the disagreements between different constraints on H_0 will *demand* a change to the current understanding of the universe and the Standard Model that describes it. Conversely, this comparison may unambiguously reveal systematic uncertainties and resolve the current tension, leaving precise and independent H_0 measures that can further refine the Λ CDM model.

When considered *within* the Λ CDM framework, multiple measurements of H_0 with percent-level accuracy will provide opportunities to probe cosmic acceleration and neutrino mass. As shown in **Figure 8-8**, a single measurement of H_0 with 1%



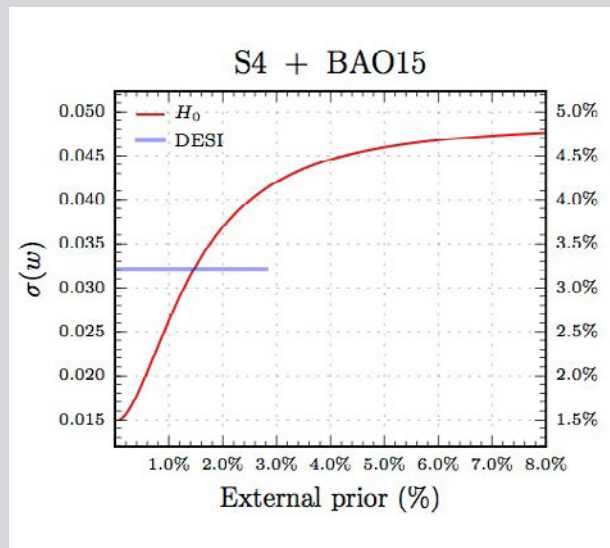
accuracy will improve the CMB+BAO constraint on the dark energy equation of state parameter, w , given current constraints by a factor of 2 compared to no H_0 prior, and by 50% compared to the best H_0 precision currently reported (2.4%, Riess et al. 2016). The sum of light neutrino masses can also be constrained 2.5 times better with a prior on H_0 that has 1% accuracy relative to no H_0 prior. Additionally, in conjunction with other probes, the absolute distance measurements that the GMT enables provide tight constraints on spatial curvature and the number of relativistic species N_{eff} . This is a rapidly evolving field, so improvements in the

external measurements are sure to come before GMT is operational. However, the critical aspect here is that GMT provides an independent test of these critical measurements at a competitive level of precision.

H_0 from Population I and II Distance Ladders

The Cepheid distance ladder to nearby galaxy hosts of SNe Ia has been refined to a precision of a few percent, with the dominant uncertainties now coming from the direct calibration of the Cepheid period-luminosity relation and the still-limited number of local SNe Ia hosts with modern photometry and Cepheid distances (e.g. Riess et al. 2016). A parallel, independent distance ladder is being developed based on Tip of the Red Giant Branch (TRGB) distances to SNe Ia host galaxies using GAIA parallaxes, which will provide a completely independent test of the zero-point of both methods within the next few years (Beaton et al. 2016). By the time the GMT sees first light, the Cepheid and TRGB distance scales will have been directly calibrated by GAIA to much better than 1%, and the limiting distance ladder uncertainty will be the number of SNe Ia host galaxies with distances from either method. Given other uncertainties in the distance ladder, achieving an H_0 constraint of 1% requires approximately 100 SNe Ia host-galaxy calibrators (Riess et al. 2016). Nearby SNe Ia are rare objects. Currently, the rate of discovery is only 1–2 per year within the volume where HST can provide complementary Cepheid or TRGB distances for the host galaxies. Current distance limits on Cepheid observations from HST (about 40 Mpc) are set by a combination of field crowding and faintness;

Figure 8-8 This figure from Manzotti, Dodelson & Park (2016) illustrates that the precision gained in the measurement of the Hubble constant using the GMT will lead to similar gains in our understanding of the dark energy equation-of-state parameter, w . The red line shows the predicted uncertainty in w from the next generation of CMB experiments (CMB-S4) and current BAO measurements as a function of the precision with which H_0 is known from independent (external) measurements. The Y-axes show the uncertainty as an absolute value (left) and a percentage (right). The X-axis shows the accuracy of the H_0 prior, which would be provided by GMT observations. The horizontal (blue) line corresponds to the precision obtained from the CMB S4 experiment + Planck Pol + DESI (see Manzotti, Dodelson & Park 2016). The accuracy with which w can be constrained improves significantly with precision in H_0 .



while variables are often discovered at optical wavelengths, where the amplitudes are larger, optimal measurements are made in the NIR. Because the diffraction limit scales with the wavelength, JWST's imaging resolution in the NIR is no better than HST's resolution at optical wavelengths, and JWST's significant overheads and limited observing flexibility make repeat monitoring programs expensive. Hence, it is critical to increase the volume out to which accurate Cepheid and TRGB distances can be measured if we want to increase the number of calibrating galaxies for SN

Ia. The GMT will offer NIR AO imaging with a NIR spatial resolution that exceeds JWST's by a factor of 4, allowing the clean measurement of Cepheids to distances greater than either HST or JWST.

The GMT's ability to image widely *and* deeply will additionally enable measurements of the TRGB in many SNe Ia host galaxies. For early-type galaxies not included in Cepheid-based samples, this is the only feasible way to measure their distances. TRGB stars have numerous advantages for measuring accurate distances to nearby galaxies. First, they are found in the outer halos of galaxies, where source crowding and blending is less than in the disk, and the gas and dust content is low. These objects are well-studied theoretically and mark the point of the He-flash for low-mass ($M < 1.8 M_{\odot}$; Salaris & Cassisi 2005) stars where the degeneracy of the helium core is lifted and stars rapidly descend from the high-luminosity (hydrogen shell-burning) TRGB onto the lower-luminosity (helium core-burning) Horizontal Branch. Second, the luminosity of a giant-branch star is directly related to its metallicity (e.g., Salaris & Cassisi 1998), which can be empirically and directly calibrated. Third, all galaxies contain an old, first generation of stars. Thus, it can be applied in galaxies of all morphological types. Finally, from an observational standpoint, the TRGB method offers the advantage of observing efficiency, since there is no need for a long time baseline to determine their periods.

TGRB distances can be measured using stars in galaxy halos from a *single* deep GMT image; depth *and* area are the keys to using this method efficiently. In contrast, Cepheid-distances require high spatial resolution to resolve field crowding and repeat observations over long periods of time to measure variability. In the natural seeing mode that will be available at first light, the GMT will reach to $i_{AB} = 28$ at 5σ under typical conditions in a half night. This will be sufficient to measure TGRB distances to ~ 30 Mpc. Ultimately, ground layer AO will improve this distance limit to ~ 50 Mpc, for night-long integration times.

Across all host galaxy types, the GMT will be able to quickly calibrate new nearby SNe Ia discoveries from ongoing surveys (e.g., ASAS-SN, KAIT, etc.) at distances greater than will be accessible to either HST or JWST, and in some cases using both Population I and II distance ladders. Within the current volume accessed by HST, there are only 19 galaxies hosting well-measured SNe Ia (Riess et al. 2016) that have robust distances. Pushing that sample to the ~ 100 systems needed for a 1% H_0 measurement will be possible with the GMT, limited only by the nearby SNe Ia discovery rate.

Measuring H_0 with Time Delays and the GMT

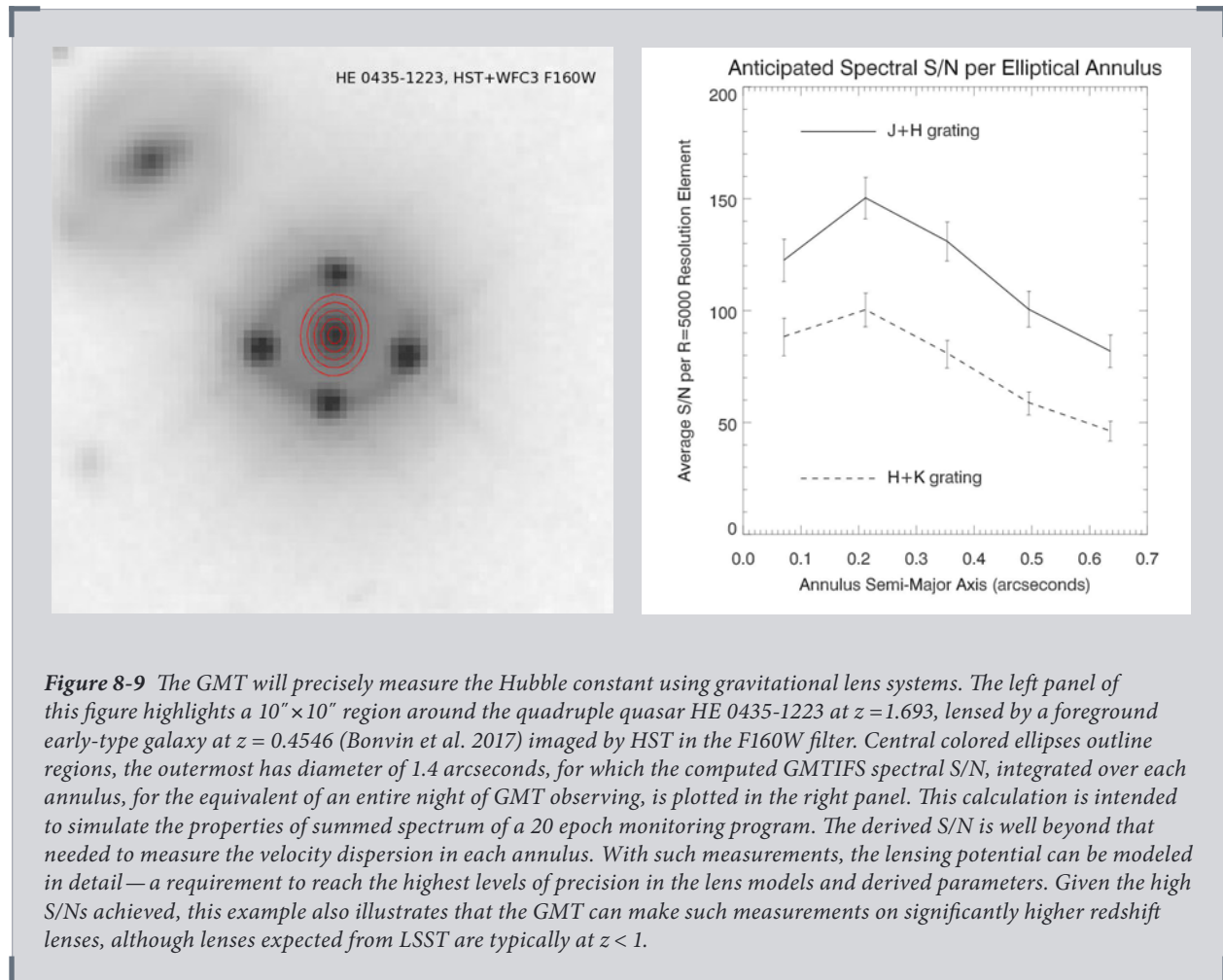
Strong-lensing time delay measurements involve measurements of light from a background variable source multiply-imaged by an intervening lens and rely on two affects: a geometric time delay from the varied length of the two light paths from source to lens to observer, and a gravitational time delay from the photons' passage through the gravitational potential of the lens two different impact parameters. An H_0 value derived from the relative distances between observer, lens, and source is independent of approaches that rely on the local distance ladder or CMB data. To extract a precise and accurate measurement of H_0 from a multiply-imaged lens system, three basic elements are needed: (1) a well-measured time delay, (2) knowledge of any other intervening mass along the light of sight, and (3) the redshift of both the lens and the source, all of which enable the reconstruction of a reliable mass model for the lens together with an estimate of H_0 .

Recent work on well-studied systems shows the dramatic impact of such analyses, with an H_0 value reported to 3.8% precision from a *single* strong lens (Bonvin et al. 2017) and a prior regarding the dimensionless distance scale. Currently, multiply-imaged quasars are the variable source of choice for such work, but multiply-imaged supernovae, particularly Type Ia SNe, offer extraordinary opportunities in the coming years. The first such system found was iPTF16geu, which was recognized early enough for space-based images, ground based spectroscopy, and ground-based AO-assisted images to be taken (SN 2016geu; Goobar et al. 2017).

The GMT will make powerful contributions in this area, particularly in coordination with LSST, which will discover many hundreds of new galaxy-scale strong lens systems with variable sources. GMTIFS will provide high-resolution dynamical observations of the lens galaxies that will be more sensitive and at higher resolution than any data currently available. GMTIFS and GMACS will probe the line-of-sight with imaging and spectroscopy to reveal other intervening or adjacent mass structures that may affect the model and cosmological solution, again to a sensitivity far beyond currently available data.

The best quasar lens systems for cosmological analyses include lensed images of the quasar host galaxy, as these offer significant additional constraints to the lens mass model, independent of the quasar images. Work is ongoing to develop accurate mass models and techniques for deriving them, but accurate observations of both the lensed source and the lens itself are critical. In particular, a well-measured velocity dispersion for the lensing galaxy is key to obtaining accurate constraint on H_0 (e.g., Sonnenfeld 2018; Bonvin et al. 2017). GMTIFS spectroscopy of the entire strong-lensing region will capture both the extended source and the lens galaxy and allow a reconstruction of the velocity dispersion field to several effective radii for typical systems (**Figure 8-9**). The ability of GMTIFS to image the lensed quasar at a resolution 10x sharper than HST's in the NIR will allow a more robust exploration of the source galaxy and immediate environment (e.g., Chen et al. 2016; Ostrovski et al. 2018) than currently possible (e.g., Suyu et al. 2014), and hence a tighter constraint on H_0 .

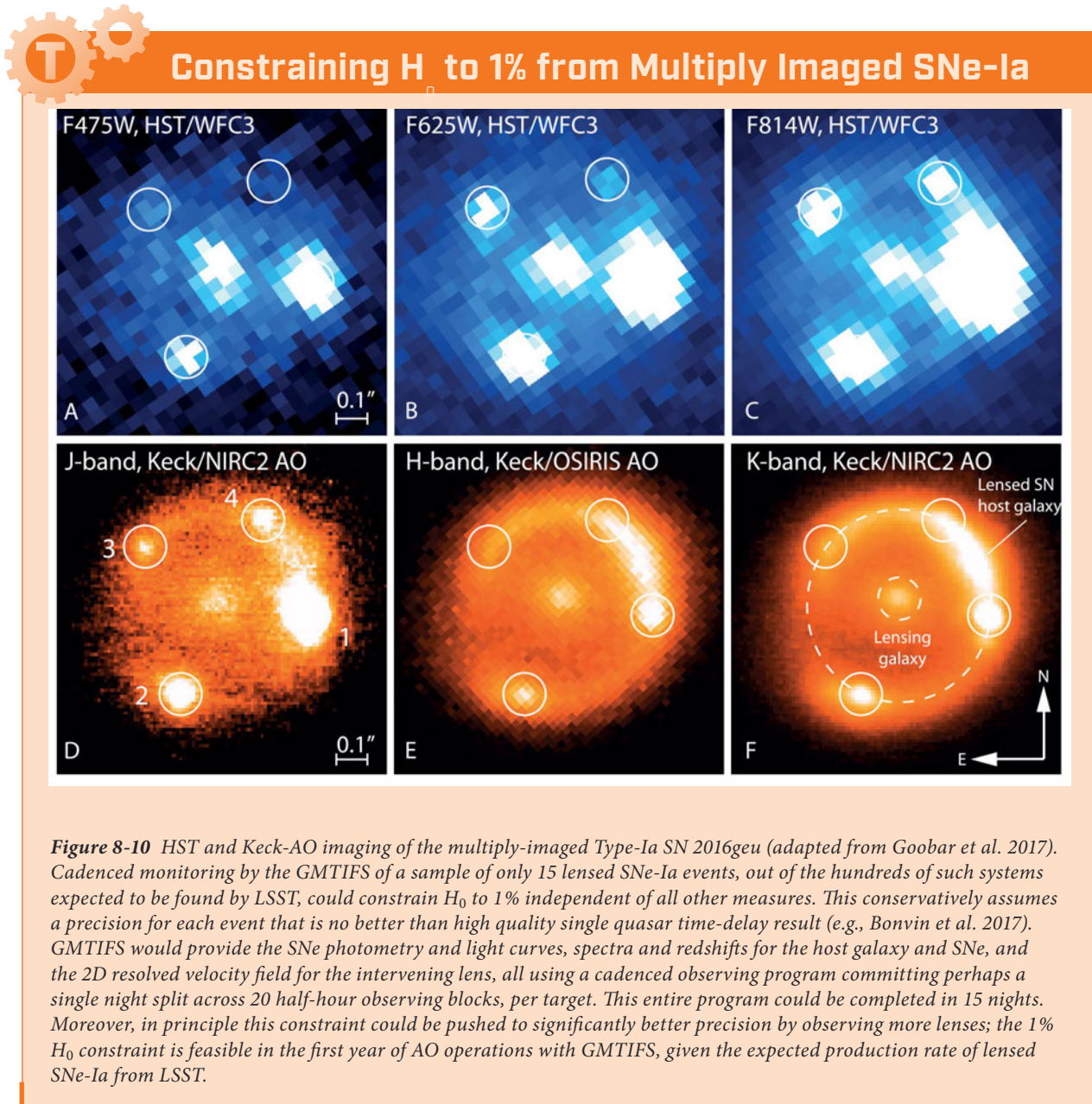
It has proven challenging to extract time delays for the small numbers of lensed quasar systems for which time delays are now well-measured, even with large, dedicated ground-based follow-up programs. The successful COSMOGRAIL collaboration has published robust time delays for a handful of systems (e.g., Rantha Kumar et al. 2013; Tewes et al. 2013; Eulaers et al. 2013; Courbin et al. 2011) typically after 7 or more years of monitoring to obtain ~400 to ~700 epochs of observations per system. The Bonvin et al. result shown in **Figure 8-9** relies on 13 years of monitoring data. Recent studies of *nightly* monitoring suggests that this high cadence may be as effective as long durations (Courbin et al. 2018). LSST will likely be game-changing for this work, with hundreds of well-measured time delays expected over the lifetime of the LSST program. Forward-looking “time delay challenge” studies have been completed that illustrate LSST's potential to harvest ~400 well-measured time delays across the southern sky (Dobler et al. 2013; Liao et al. 2015).



A recent prediction for the number of Type Ia SNe that LSST will find with multiple lensed images is 50 systems per year using a photometric method that does not require spatially-resolving the individual images (Goldstein & Nugent 2017; see **Figure 8-10**). Even a strategy requiring individual detection of each lensed image is predicted to yield 4–5 multiply-imaged Type Ia SNe per year (Oguri & Marshall 2010). This is still a potential bonanza for time delay cosmography, given that Type Ia SNe uniquely offer an absolute magnification constraint on the model. Moreover, measuring time delays using lensed SNe Ia require months rather than years of monitoring, provided one can effectively measure the peak of the SNe light curve for each image, because the variation is so evident and understood. The measurement requires at most tens of epochs, with a signal-to-noise ratio of only 10 to 20 in each SN image per epoch (e.g., Scolnic et al. 2017); SNe Ia have a known spectral energy distribution (SED), have light curves drawn from a constrained family, and so time delays can be robustly characterized with a modest amount of data compared to the stochastic ongoing flickering of lensed quasars.

Additionally, lensed SNe Ia are achromatic to microlensing for the first few weeks of the event, making wide band observations, spectroscopic or otherwise, particularly powerful for time-delay measurements (Goldstein et al. 2018). Moreover, SNe Ia are

significantly better standard candles when observed in the rest J-band (e.g., Dhawan, Jha & Leibundgut 2018) and hence naturally matched to the GMT's powerful capabilities with GMTIFS. Finally, compared to multiply-imaged quasars, lensed SNe are relatively rapid events, and timely response and monitoring of numerous events by the GMT is likely much more feasible than space-based follow-up using WFIRST or JWST. Cadenced GMTIFS observations of such events, spanning their months-long duration, can provide the entirety of the required follow-up data. The time series of data cubes will yield times delays, and the stacked data cube will yield detailed dynamical data on the lens and detailed spectroscopic and imaging information on the SNe host galaxy. Both will allow precise refinement of the mass model that will be more than sufficient to reveal the underlying cosmological signal.



8.3 Cosmology on the Frontier: Gravitational Wave Standard Sirens

Chapter 4 discusses the impact GMT on our understanding of the physics associated with merging neutron stars pairs (kilonovae) and merging black hole–neutron star mergers; current telescopes lack the collecting area to observe those events as they evolve and at the range of distances we expect to see them. It is worth re-emphasizing that kilonovae associated with gravitational wave (GW) events were expected to be faint—about two orders of magnitude fainter than a typical Type Ia SN—and that the first observed source, GW170817, conformed to that expectation. Over much of the time they shine, many kilonovae to be discovered by LIGO will require 30 m class telescopes for follow-up. The general agreement between theoretical predictions for kilonovae and the observed properties of GW170817 should be considered a triumph, but a multitude of questions remain. As emphasized in Chapter 4, the diversity of these events is unknown and will only be revealed by extensive further observations.

Another extraordinary way in which these transient events are important is as cosmological probes. Kilonovae can be used as “standard sirens”—their GW signal can be analyzed to produce a direct distance measure. This is an entirely new tool for quantifying the expansion history of the cosmos. Analyses of GW170817 produced an H_0 measurement with an uncertainty of 10–20% (Abbott et al. 2017; Guidorzi et al. 2017). Each such measurement will be independent, so that sufficiently large numbers of events will provide an H_0 value with the precision similar to what can be obtained using the methods described above. This first event was (luckily) unusually close and within the reach of current facilities across a broad swath of wavelengths, but the greater sensitivity of the GMT will be needed to make use of more distant events.

In principle, standard sirens should be simple; the GW signal yields a distance measure, with the orbital inclination of the merging pair relative to the line of sight being the dominant uncertainty. The necessary redshift comes from a spectrum of the host galaxy. The role of the GMT here is not to provide redshifts; if most future LIGO events occur unambiguously in luminous galaxies, then current telescopes will be sufficient to secure redshifts of the hosts. Rather, the long term critical impact of the GMT will be in assessing the physics of the events in cases with associated kilonovae, and confirming that the simple theory of standard sirens is consistent with the observed reality for any given event. After all, while supernovae in general (Zwicky 1938, Wilson 1939) and Type Ia supernovae in particular (Kowal 1968) were long suggested as cosmological probes, and while the basic theory describing the explosion mechanism was well established (Hoyle & Fowler 1960), it did take decades to observationally differentiate the majority population of “normal” SN Type Ia’s and establish second-parameter measurements (e.g., Phillips 1993) that transformed these events into the key cosmological probe that they are today. The history of cosmology and astrophysics abundantly suggests that complexity will emerge as GW source numbers increase. Unraveling and exploiting that complexity to make the best possible cosmological measurements will undoubtedly require the imaging and spectroscopic capabilities of the GMT.

References

- Abbott, B.P., Abbott, R., Abbott, T.D., et al. 2017, *Nature*, 551, 85
- Ackermann, M., Albert, A., Anderson, B. et al. 2015, *PhRvL*, 115 1301
- Albert, A., Anderson, B., Bechtol, K., et al. 2017, *ApJ*, 834, 110
- Alcock, C., Allsman, R.A., Alves, D.R., et al. 2000, *ApJ*, 542, 281
- Aubourg, E. et al. *Phys. Rev. D* 2015, 92, 123516
- Azabajian, K., Canac, N., Horiuchi, S., & Kaplinghat, M. 2014, *PhRvD*, 90, 3526
- Beaton, R.L., Freedman, W.L., Madore, B.F., et al. 2016, *ApJ*, 832, 210
- Bechtol, K., Drlica-Wagner, A., Balbinot, E., et al. 2015, *ApJ*, 807, 50
- Bernabei, R., Belli, P., Cappella, F., et al. 2013, *European Physical Journal C*, 73, 2648
- Blumenthal, G.,R., Faber, S.M., Primack, J.R., Rees, M. J. 1984, *Nature*, 311, 517
- Bonvin, V., Courbin, F., Suyu, S. H., et al. 2017, *MNRAS*, 465, 4914
- Calore, F., Cholis, I., & Weniger, C. 2015, *JCAP*, 3, 38
- Carr, B., K[“u]hnel, F., & Sandstad, M. 2016, *Ph. Rev. D*, 94, 083504
- Chen, G.C.-F., Suyu, S.H., Wong, K.C., et al. 2016, *MNRAS*, 462, 3457
- Copi, C.J., Schramm, D.N., & Turner, M.S. 1995, *Science*, 267, 192
- Courbin, F., Bonvin, V., Buckley-Geer, E., et al. 2018, *A&A*, 609, 71
- Courbin, F., Chantry, V., Revaz, Y., et al. 2011, *A&A*, 536, A53
- Davis, M., Frenk, C.S., Efstathiou, G., & White, S.D.M. 1985, *ApJ*, 292, 371
- Daylan, T., Finkbeiner, D.P., Hooper, D., et al. 2016, *Physics of the Dark Universe*, 12, 1
- Dhawan, S., Jha, S.W., & Leibundgut, B. 2018, *A&A*, 609, A72
- Dobler, G., Fassnacht, C., Treu, T., et al. 2013, *arXiv:1310.4830*
- Drlica-Wagner, A., Bechtol, K., Allam, S., et al. 2016, *ApJL*, 833, L5
- Drlica-Wagner, A., Bechtol, K., Rykoff, E.S., et al. 2015, *ApJ*, 813, 109
- Einasto, J. 2009, *arXiv:0901.0632*
- Eulaers, E., Tewes, M., Magain, P., et al. 2013, *A&A*, 553, A121
- Freedman, W. 2017, *NatAs*, 1, 121
- Geringer-Sameth, A., Walker, M.G., Koushiappas, S.M., et al. 2015, *Physical Review Letters*, 115, 081101
- Goldstein, D.A., & Nugent, P.E. 2017, *ApJL*, 834, L5
- Goldstein, D.A., et al. 2018, *ApJ*, 855, 22
- Goobar, A., Amanullah, R., Kulkarni, S.R., et al. 2017, *Science*, 356, 291
- Gordon, C., & Macias, O. 2013, *PhRvD*, 88, 3521
- Guidorzi, C., Margutti, R., Brout, D., et al. 2017, *ApJ Letters*, 851, 36
- Hargis, J.R., Willman, B., & Peter, A.H.G. 2014, *ApJ Letters*, 795, 13
- Hatt, D., Beaton, R.L., Freedman, W.L. et al. 2017, *arXiv:1703.06468*
- Homma, D., Chiba, M., Okamoto, S. et al. 2018, *PASJ*, 70, 18
- Hoyle, F. & Fowler, W. A. 1960, *ApJ*, 132, 565
- Hubble, E. 1929, *PNAS*, 15, 168
- Jang, I.S., & Lee, M.G. 2017, *ApJ*, 836, 74
- Kirby, E.N., Cohen, J.G., Simon, J.D., & Guhathakurta, P. 2015, *ApJL*, 814, L7
- Kim, D., Jerjen, H., Geha, M., et al. 2016, *ApJ*, 833, 16
- Koposov, S.E., Belokurov, V., Torrealba, G., & Evans, N.W. 2015, *ApJ*, 805, 130
- Kowal, C.T., 1968, *AJ*, 73, 1021
- Kowal, C.T. 1968, *AJ*, 73, 1021
- Liao, K., Treu, T., Marshall, P., et al. 2015, *ApJ*, 800, 11
- Liu, J., Chen, X., & Ji, X. 2017, *Nature Physics*, 13, 212
- Lundmark, K., 1930, *Meddelanden fran Lunds Astronomiska Observatorium Series I*, 125, 1
- Manzotti, Dodelson & Park 2016
- Mutlu-Pakdil, B., Sand, D.J., Carlin, J.L., Spekkens, K., Caldwell, N., Crnojević, D., Hughes, A.K., Willman, B., Zaritsky, D., *arXiv:1804.08627*
- Niikura, H. et al. 2017, *arXiv:1701.02151*
- Oguri, M., & Marshall, P.J. 2010, *MNRAS*, 405, 2579
- Ostrovski, F., Lemon, C.A., Auger, M.W., et al. 2018, *MNRAS*, 473, L116
- Phillips, M.M., 1993, *ApJ Letters*, 413, 105
- Randall, S.W., Markevitch, M., Clowe, D., et al. 2008, *ApJ*, 679, 1173
- Rathna Kumar, S., Tewes, M., Stalin, C.S., et al. 2013, *A&A*, 557, A44
- Riess, A. G. et al. 2016, *Astrophysical Journal*, 826, 56
- Salaris, M., & Cassisi, S. 1998, *MNRAS*, 298, 166
- Salaris, M., & Cassisi, S. 2005, *Evolution of Stars and Stellar Populations*, by Maurizio Salaris, Santi Cassisi, pp. 400. ISBN 0-470-09220-3. Wiley-VCH , December 2005., 400
- Scolnic , D.M. et al. 2017, *arXiv:1710.00845*
- Simon, J.D., Drlica-Wagner, A., Li, T.S., et al. 2015, *ApJ*, 808, 95
- Sharon, K., Bayliss, M.B., Dahle, H., et al. 2017, *ApJ*, 835, 5
- Smith, S. 1936, *ApJ*, 83, 23
- Sonnenfeld, A., 2018, *MNRAS*, 474, 4648
- Steigman, G., Dasgupta, B., & Beacom, J.F. 2012, *Ph. Rev. D*, 86, 023506
- Strigari, L.E., Bullock, J.S., Kaplinghat, M., et al. 2008, *Nature*, 454, 1096
- Suyu, S.H., Treu, T., Hilbert, S., et al. 2014, *ApJL*, 788, L35
- Tewes, M., Courbin, F., Meylan, G., et al. 2013, *A&A*, 556, A22
- Tisserand, P., Le Guillou, L., Afonso, C., et al. 2007, *A&A*, 469, 387
- Tollerud, E., Bullock, J.S., Strigari, L.E. & Willman, B. 2008, *ApJ*, 688, 277
- Wilson, O.C. 1939, *ApJ*, 90,634
- Zhao, Y., Bi, X.-J., Yin, P.-F., & Zhang, X. 2018, *Chinese Physics C*, 42, 025102
- Zwicky, F. 1933, *Helvetica Physica Acta*, 6, 110
- Zwicky, F. 1938, *Phys. Rev.* 55, 726



Image credit: D. Jemison. Cosmic web simulation courtesy Phil Mansfield (U Chicago) and Benedikt Diemer (ITC, Harvard).



First Light & Reionization

What were the first sources of light and how did they transform the universe? We know that the primordial hydrogen and helium gas created in the Big Bang gave rise to the objects that became the luminous galaxies, stars, and planets that we see today. However, we do not yet understand how these first objects formed and how their radiation changed the early universe.

GMT will enable detailed spectroscopy of these sources for the first time. In doing so, and working in concert with the next generation of space observatories and radio telescopes, the GMT will help us understand how the first sources of light formed and how they influenced the early Universe.

Chapter Authors

Dan Stark (University of Arizona)

Casey Papovich (Texas A&M University)

Steven Finkelstein (The University of Texas at Austin)

Eduardo Bañados (Carnegie Institution for Science, The Observatories)

Rob Simcoe (Massachusetts Institute of Technology)

Emma Ryan-Weber (Swinburne University of Technology)

Juna Kollmeier (Carnegie Institution for Science, The Observatories)

Hsaio-Wen Chen (University of Chicago)



9 First Light & Reionization

The first stars, galaxies, and black holes formed a few hundred million years after the Big Bang. The light from these early objects ionized the matter between galaxies, rendering the universe transparent, ending the “dark ages”. Our curiosity about the “dark ages” and their end is matched with little direct knowledge. The first stars were possibly hundreds of times more massive than our Sun and as much as one million times more luminous. Stellar explosions marking the death of these stars seeded the universe with the first heavy elements, which became part of future stars and planets. The first black holes likely formed from these massive stellar remnants. Some of these black holes grow into the supermassive black holes (masses of a million to a billion Suns) found at the centers of galaxies only a few hundred million years later. This narrative is an informed guess based on a few glimpses with today’s state-of-the-art facilities (combined with insight from theory and numerical simulations). The GMT, working with other next-generation facilities from the ground and space, will directly probe the “dark ages” for the first time.

Our goal is to assemble a seamless timeline of cosmic history from its beginning to the current epoch. Our first glimpse is the map of the cosmic microwave background from 400,000 years after the Big Bang. This period marks the start of the cosmic dark ages when the universe is permeated by neutral hydrogen and helium before the birth of the first stars (see *Figure 9-1*). Our next glimpse of the universe, hundreds of millions of years later, is provided by deep near-infrared images from the Hubble Space Telescope. These Hubble images reveal a completely different landscape with abundant galaxies that contain as much as ten billion solar masses

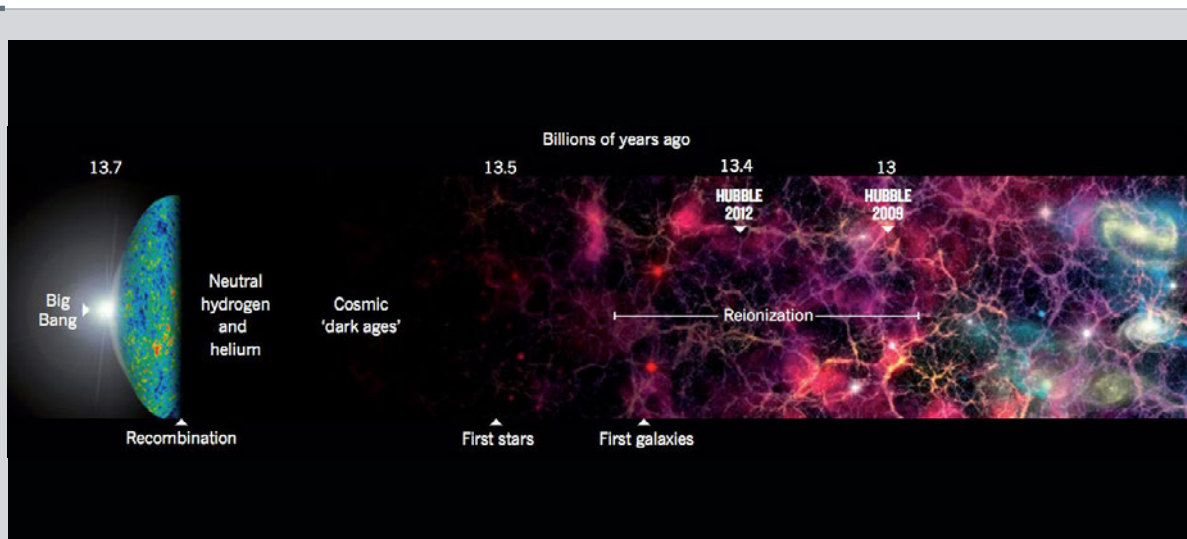


Figure 9-1 The GMT will track the formation of the first stars and galaxies and their impact on the evolution of the universe. We know little about galaxies and their formation during the “Dark Ages,” that time between recombination (the formation of neutral gas) and the birth of the first stars and galaxies. The figure graphically outlines key events in the early history of the universe in a sequential fashion from left to right (adapted from Cowen 2013). In addition to labels that highlight the epochs of particular relevance to this chapter, two labels indicate the observational reach of current telescopes (exemplified by the Hubble Space Telescope) back in time, all the way to the epoch of reionization. Such observations are, however, at the extreme of what is currently possible. The GMT will explore this epoch in unprecedented detail and be a key facility in our quest to understand this era. Illustration: Nik Spencer; Source: NASA/WMAP Science Team; R. Ellis (Caltech).

in stars. Heavy elements, the products of stellar evolution, are found in the galaxies and the material between galaxies. Some galaxies have formed supermassive black holes powering luminous quasars. Deep quasar spectra show that the intergalactic hydrogen is highly ionized by one billion years after the Big Bang.

Over the last few decades, observers and theorists have been working to understand these widely separated periods of cosmic history. Theory, supported by some recent observations (Bowman et al. 2018), suggests that the cosmic dark ages end as the first generation of stars form at $z \sim 20-30$ (see Bromm & Yoshida 2011). These first stars, formed from primordial hydrogen and helium (so called “Population III” [Pop III] stars) bring the cosmic dark ages to a close, and begin the formation of heavier elements. The physical characteristics and evolution of the first stars remains contentious as we lack observational constraints. Much early theoretical work suggested that primordial stars had to be very massive to allow gravitational collapse, where more recent simulations question this conclusion (Stacy & Bromm 2014). Only by observing the properties of these first stars will we begin to understand them.

We theorize that the first luminous galaxies form in dark matter halos containing gas processed by these earlier generations of stars and form stars with low (but non-zero) quantities of heavy elements. These galaxies are expected to form stars rapidly as the gas in these halos will be very dense and unstable to gravitational collapse. Ultraviolet light emitted by these massive stars ionizes the hydrogen gas surrounding these galaxies. Bubbles of ionized hydrogen emerge. Eventually these bubbles overlap, and the hydrogen gas between galaxies becomes fully reionized.

First light research is poised for rapid progress. Deep IR imaging from future space-based observatories including the James Webb Space Telescope (JWST), the Euclid mission, and the Wide Field Infrared Survey Telescope (WFIRST) will identify large numbers of candidates for early galaxies. The GMT’s huge collecting area, unprecedented angular resolution, and powerful spectrographs will allow us for the first time to study the astrophysical nature of these first stars, galaxies, and black holes in the universe.

In **Section 9.1** we describe how GMT observations will enable the study of the first generations of stars and galaxies and the first heavy elements. In **Section 9.2** we discuss GMT observations that will reveal how radiation from the first stars and galaxies ends the dark ages. In **Section 9.3** we describe GMT observations that will allow us to detect the seeds of the first supermassive black holes and to understand their growth.

9.1 Probing the First Stars and Galaxies

The Physics of the First Stars and Galaxies from Integrated GMT Spectroscopy

Spectroscopy from the GMT will enable the astrophysical study of the earliest and most distant galaxies to be discovered in the next decade from future space missions. Starting in 2020, JWST will find the first large samples of faint galaxies at $z \sim 10-20$. While JWST will be very efficient at detecting early star forming galaxies, its field of view is small. Deep surveys over these relatively small areas ($<10-100$ arcmin²) will uncover large numbers of faint galaxies in the reionization era. By the mid 2020s, WFIRST will start to deliver large samples over wider areas, both through the High Latitude Survey (HLS; $\sim 2,000$ deg² to 26.5th magnitude) and

the Guest Observer program ($\sim 1 \text{ deg}^2$ to 28th or 29th magnitude, see **Figure 9-2**). The GMT will provide the contemporaneous spectroscopy to enable science from these new galaxy samples.

The near-IR window that we have available from the ground (0.9–2.5 micron) probes the rest-frame UV of reionization-era systems, providing access to a number of important nebular emission lines that are sensitive to the stellar populations and gas properties. Lyman- α is generally the strongest line in the far-UV, but it is potentially strongly attenuated by neutral hydrogen in the IGM at $z > 7$ (Stark et al. 2010, Finkelstein et al. 2013, Schenker et al. 2014, Tilvi et al. 2014, de Barros et al. 2017; see **Section 9.2**).

The GMT will determine the accurate physical nature of the stars in galaxies in the reionization era by measuring spectral lines other than Ly α . The first such (weak) detections have emerged in the last several years. Deep spectra of a small number of $z \sim 6-8$ galaxies have revealed faint emission lines from metallic species (NV $\lambda 1240$, CIV $\lambda 1548, 1551$, OIII] $\lambda 1660, 1666$, [CIII] CIII] $\lambda 1907, 1909$), demonstrating that

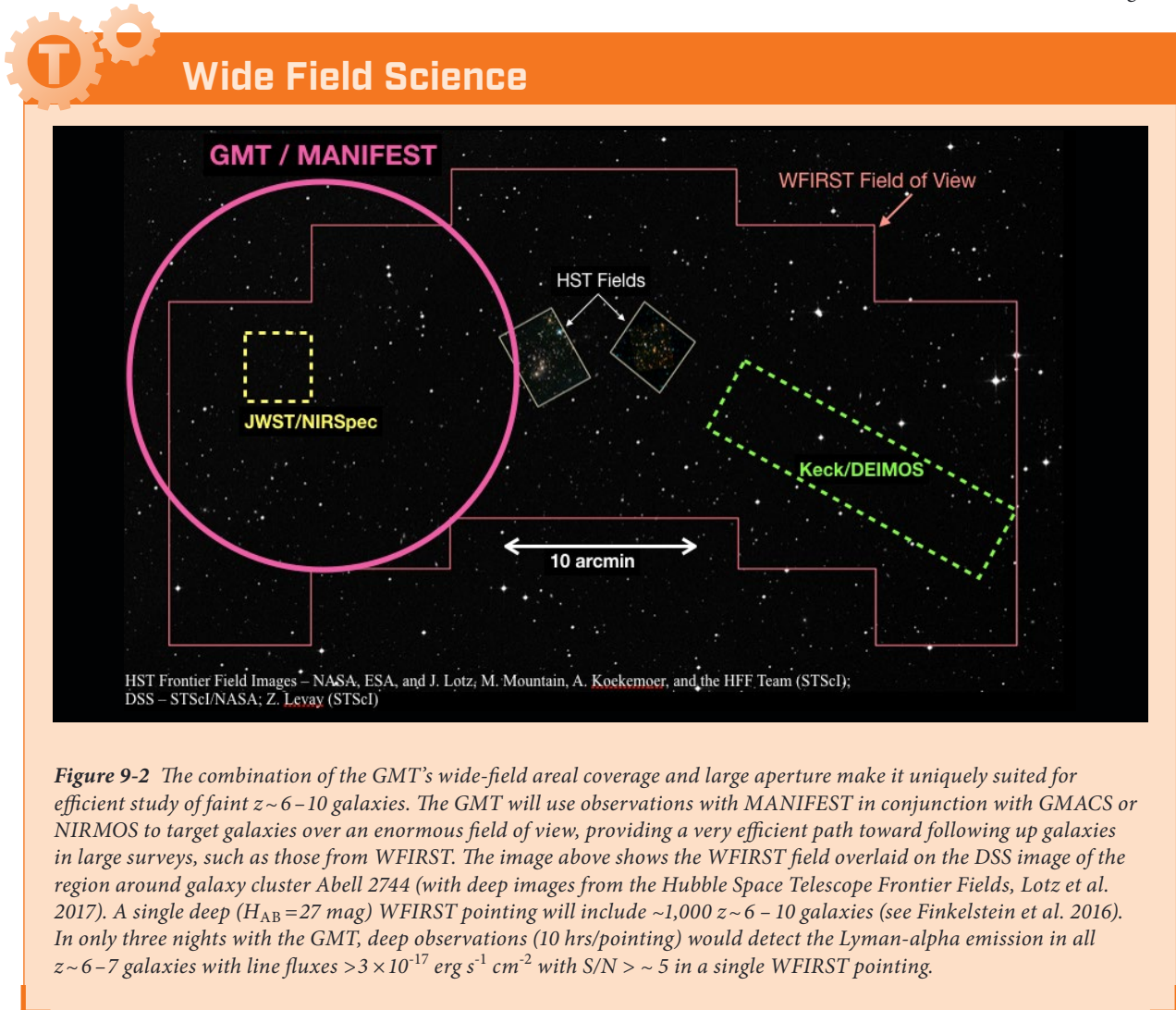
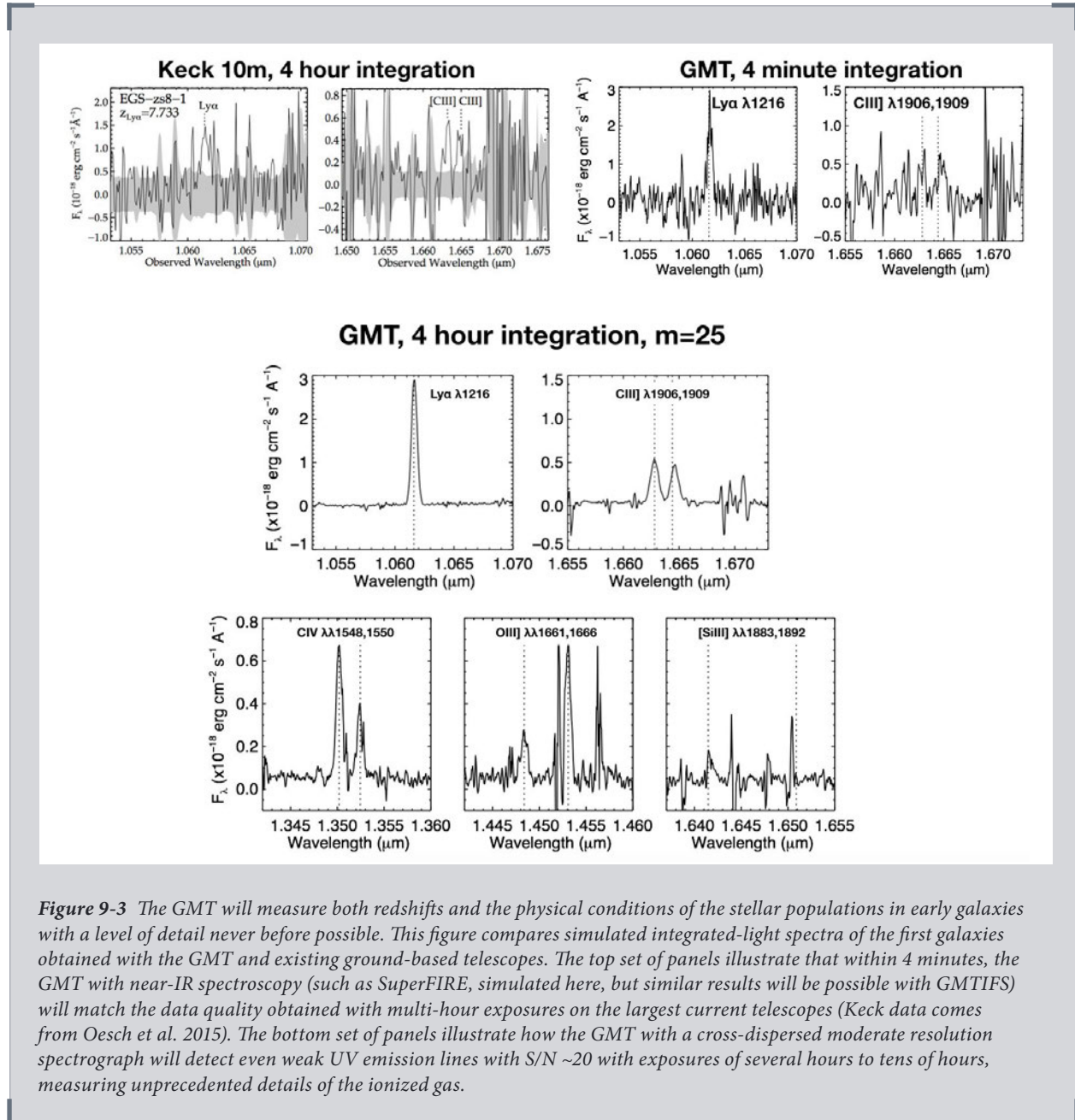


Figure 9-2 The combination of the GMT’s wide-field areal coverage and large aperture make it uniquely suited for efficient study of faint $z \sim 6-10$ galaxies. The GMT will use observations with MANIFEST in conjunction with GMACS or NIRMOS to target galaxies over an enormous field of view, providing a very efficient path toward following up galaxies in large surveys, such as those from WFIRST. The image above shows the WFIRST field overlaid on the DSS image of the region around galaxy cluster Abell 2744 (with deep images from the Hubble Space Telescope Frontier Fields, Lotz et al. 2017). A single deep ($H_{AB} = 27 \text{ mag}$) WFIRST pointing will include $\sim 1,000$ $z \sim 6-10$ galaxies (see Finkelstein et al. 2016). In only three nights with the GMT, deep observations (10 hrs/pointing) would detect the Lyman-alpha emission in all $z \sim 6-7$ galaxies with line fluxes $> 3 \times 10^{-17} \text{ erg s}^{-1} \text{ cm}^{-2}$ with $S/N > \sim 5$ in a single WFIRST pointing.

the ISM of these early galaxies has already been seeded with carbon and oxygen (Stark et al. 2015a,b, 2017, Tilvi et al. 2016, Mainali et al. 2017). Surprisingly, the intensity of the metal emission lines is an order of magnitude larger than was predicted from observations of galaxies at lower redshifts, suggesting that the nature of reionization-era galaxies may be very different from what is common at $z \sim 3$. The presence of nebular CIV and NV emission is even more unexpected, indicating that a significant component of interstellar metals is extremely ionized. This requires a supply of very energetic radiation that is typically only seen in galaxies that host



AGN or very metal-poor stellar populations.

GMT spectroscopy will probe these weaker emission lines with the accuracies necessary to measure the physical conditions in the galaxies. Current 8–10 m telescopes are only able to detect line emission from metals in the very brightest ($H \sim 25$ AB mag) galaxies. Because such sources are very rare on the sky at $z \sim 7$ (1 per 100 arcmin²), we only know of a handful of galaxies that are bright enough for spectroscopic study. Current samples are too small to understand the distribution of

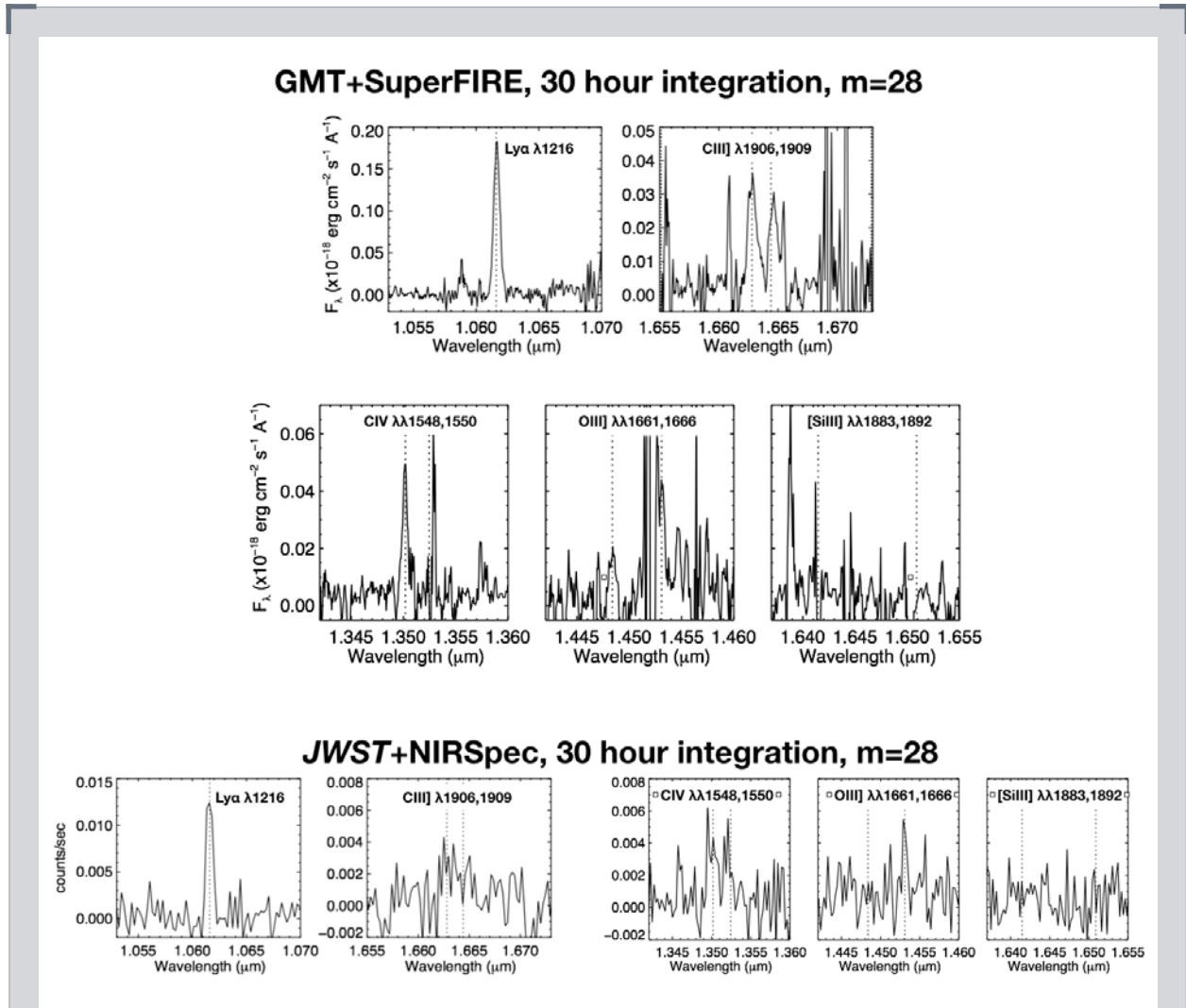


Figure 9-4 The GMT is so capable for near-IR spectroscopy that it even outperforms the forthcoming JWST+NIRSpec. The top set of panels shows that a 30-hour simulated GMT spectrum (with a cross-dispersed echellette such as SuperFIRE) detects weak UV emission lines even in faint ($m = 28^{\text{th}}$ AB mag) objects at $z = 8$ at high significance. In comparison, the bottom panels show the corresponding exposure with JWST + NIRSpec. The capability will enable GMT observers to study the ionization conditions and physical properties of the gas in these distant galaxies.

emission line properties of the galaxy population. Even in the brightest sources, the sensitivity of our spectrographs is unable to detect more than a 1–2 emission lines, and those have signal-to-noise (S/N) of 5 or less even with up to ~10 hour exposures from 10 m class telescopes (e.g., Mainali et al. 2017, Stark et al. 2017). The GMT will provide higher-significance detections of multiple metal emission lines, which are sensitive to the physical processes and ionizing sources in the galaxies (i.e., AGN, hot stars, X-ray binaries).

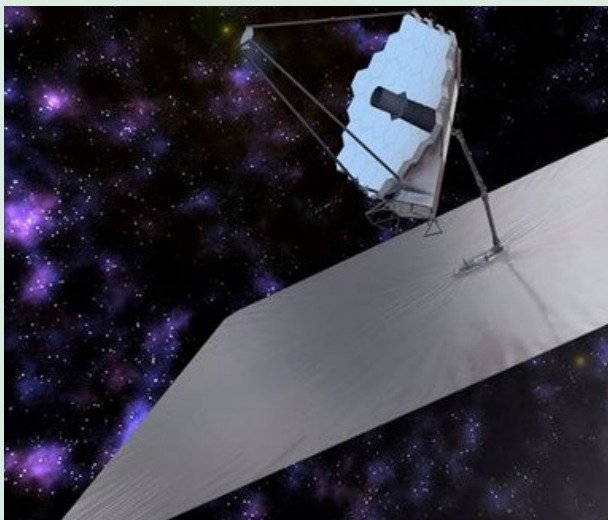
Near-IR spectrographs on the GMT will enable for the first time the efficient study of the rest frame UV emission in these galaxies. The efficiency gains of near-IR spectroscopy by the GMT (with GMTIFS or a cross-dispersed echellette such as



Synergy with Optical/Near-IR Telescopes



Figure 9-5 The GMT will play a major role in confirming and measuring the physical properties of galaxies during the epoch of reionization. In the next decades, the ground-based 8 m Large Synoptic Survey Telescope (LSST, **Figure 4-6**), located at the same latitude as the GMT, will survey the Southern sky extremely deeply through optical wavelengths. In addition, space-based telescopes (such as NASA's WFIRST (**Figure 7-4**) and ESA's Euclid mission (top) will survey the night sky in optical and near-IR light. These telescopes will image billions of galaxies (including many with HST-like image quality from WFIRST), ushering in a new era of galaxy-survey science. Deep surveys with WFIRST over one-square-degree fields would produce hundreds (or thousands) of candidates for galaxies at redshifts 6 to 10, during reionization. Wide-field spectroscopy from MANIFEST will confirm these galaxies and enable the study of their physical properties.



The GMT will also be a key telescope to study the astrophysical properties for all future space-based optical/near-IR missions such as NASA's LUVOIR concept mission (bottom). The concept for LUVOIR includes a space-based telescope with an 8 to 18 meter-diameter mirror. It will be a NASA Flagship mission designed to study the Universe at UV, optical, and near-IR wavelengths. The powerful GMT spectrographs will study the astrophysical details of the objects found with these new space telescopes. Image credits: ESA/C. Carreau, NASA/Luvoir.

SuperFIRE) are apparent in *Figure 9-3* and *Figure 9-4*, which show the ability of the GMT to study $z \sim 6 - 10$ galaxies. For the brightest galaxies ($H \sim 25$ AB mag), the GMT will require only a few minutes to detect emission lines with similar equivalent widths to what has been observed with current facilities. A host of fainter emission lines will become apparent in moderate GMT exposures ($\sim 1 - 4$ hrs), enabling characterization of origin of emission lines (e.g., nature of hot stars and/or AGN), and the metal content and ionization (e.g., Mainali et al. 2017). Whereas we are currently very limited in the number of $H \sim 25$ AB mag galaxies known at these high redshifts, by the time the GMT is in operation, WFIRST will be in the process of uncovering large samples, providing the GMT with a slew of bright targets for IR spectroscopy. Longer exposures ($\sim 10 - 30$ hrs) with GMTIFS or a SuperFIRE-like instrument would enable emission line studies to be extended to even fainter ($H \sim 28$ AB mag) galaxies, providing insight into how the physical characteristics of ionization and metal fraction depend on galaxy luminosity/mass, and informing us about the properties of the more representative population of low mass galaxies. Probing to fainter galaxies (or gravitationally lensed systems) will enable studies to be extended to the very highest redshifts ($z > 10$) where typical systems are likely to be very faint.

The GMT's combination of wide-field areal coverage, high multiplexing, and large aperture provide enormous efficiency gains in the study of faint $z \sim 6 - 10$ objects. These galaxies have higher surface densities (~ 1 per arcmin² at $H \sim 27^{\text{th}}$ magnitude [AB]; Finkelstein 2016). Multi-object optical and near-IR spectrographs on the GMT such as GMACS and NIRMOS take advantage of the full observable field of view of the GMT (powered by MANIFEST). This is illustrated in *Figure 9-2* (see also *Figure 9-5*). The GMT will then be able to target galaxies over a $20 \text{ arcmin} \times 20 \text{ arcmin}$ patrol area (covering a physical area of $7 \text{ Mpc} \times 7 \text{ Mpc}$), providing a very efficient path toward following up $z > 6$ galaxies identified in the large areas surveyed by WFIRST. The GMT spectroscopic survey speed is a huge advantage for this science, compared to JWST or other ground-based telescopes given their much smaller fields of view (see Newman et al. 2015). Present estimates of the luminosity function predict that there will be ~ 300 $z = 6 - 10$ galaxies in the MANIFEST patrol area to the WFIRST/HLS depth. This number increases by a factor of 10 at the 29^{th} magnitude limit that is expected over $\sim 1 \text{ deg}^2$ from GO programs with WFIRST. The GMT requires only ~ 10 different pointings to cover the full square degree. Other ELTs have too small a field of view (requiring over 500 pointings), and current $8 - 10 \text{ m}$ class telescopes are not sensitive enough to detect faint emission lines from $26^{\text{th}} - 29^{\text{th}}$ magnitude galaxies in the reionization era.

A large GMT near-IR spectroscopic campaign targeting galaxies at $z \sim 6 - 10$ could discover the first known galaxies with “metal-free” stars. Such galaxies would show strong emission from hydrogen and helium (i.e., He II $\lambda 1640$) with no UV lines from other heavier elements (see *Figure 9-2*). This discovery would be transformative in that it would provide the first glimpse of how metal-free stars behave. Such a survey with the GMT would enable many other exciting science cases. While galaxy formation is well underway by this epoch, the metal enrichment provided by star formation is a local and gradual process, leaving chemically-pristine gas in large volumes at relatively low redshifts. Theoretical investigations using both semi-analytic models and numerical simulations predict that Pop III stars can still form in under-dense regions at $z \sim 6$, one billion years after the Big Bang (e.g., Scannapieco et al. 2003, Trenti et al. 2009, Xu et al. 2016). If the Pop III initial mass function (IMF) is weighted toward very high mass stars, the strong EUV radiation field will power strong nebular He II $\lambda 1640$ emission, while the absence of metals

will result in very weak emission from the carbon and oxygen emission lines we have described above (e.g., Schaerer 2002). Near-IR spectrographs on the GMT will be able to characterize the strength of He II and metal lines in galaxies at redshifts $z \sim 6-14$. Because the Pop III phase is expected to be very short (~ 10 Myr), these objects are rare and challenging to find. By observing thousands of $z > 6$ galaxies over a $\sim 1 \text{ deg}^2$ field of view, a multi-object near-IR spectrograph like NIRMOS will be effective at finding rare objects in the under-dense regions where Pop III galaxies are expected to reside. Deep spectroscopic follow-up of Pop III galaxy candidates (which can be recognized by their He II 1640 emission in the absence of other UV metal lines) will offer precious insight into metal free stellar populations.

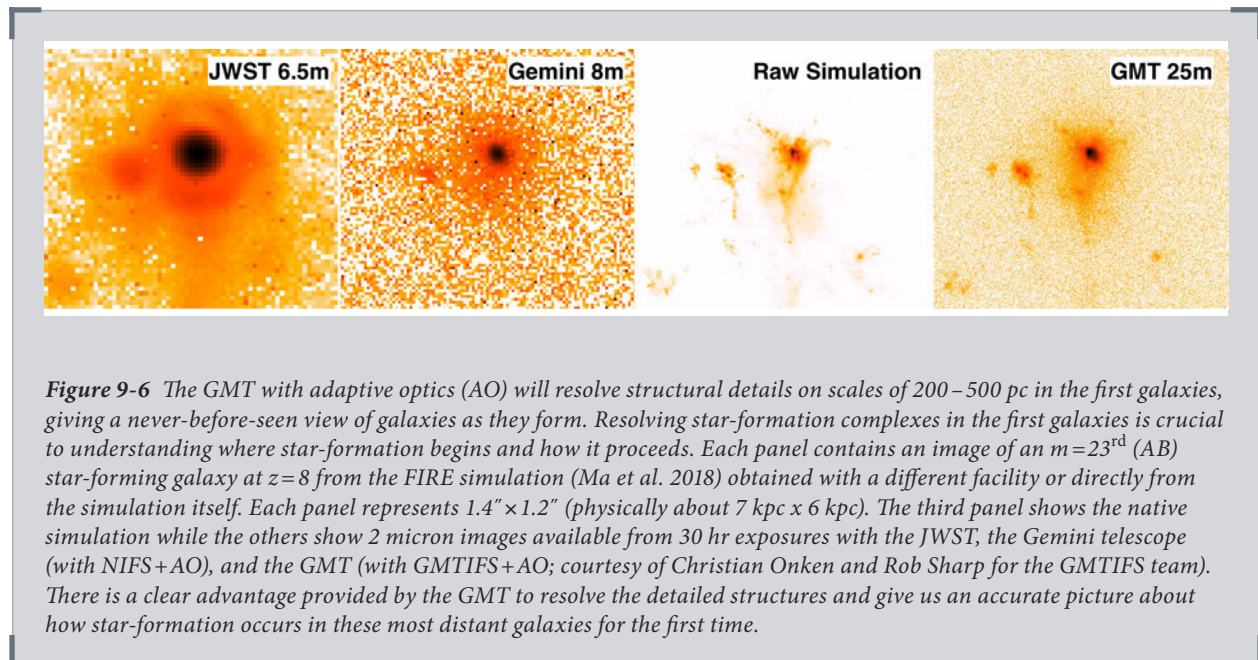


Figure 9-6 The GMT with adaptive optics (AO) will resolve structural details on scales of 200–500 pc in the first galaxies, giving a never-before-seen view of galaxies as they form. Resolving star-formation complexes in the first galaxies is crucial to understanding where star-formation begins and how it proceeds. Each panel contains an image of an $m=23^{\text{rd}}$ (AB) star-forming galaxy at $z=8$ from the FIRE simulation (Ma et al. 2018) obtained with a different facility or directly from the simulation itself. Each panel represents $1.4'' \times 1.2''$ (physically about 7 kpc \times 6 kpc). The third panel shows the native simulation while the others show 2 micron images available from 30 hr exposures with the JWST, the Gemini telescope (with NIFS+AO), and the GMT (with GMTIFS+AO; courtesy of Christian Onken and Rob Sharp for the GMTIFS team). There is a clear advantage provided by the GMT to resolve the detailed structures and give us an accurate picture about how star-formation occurs in these most distant galaxies for the first time.

The Assembly of the First Galaxies from Spatially Resolved Spectra from the GMT

With AO, the GMT will allow us to witness galaxy formation in action, resolving the structure of galaxies from kpc scale to few hundred parsec scale (size-scale GMCs, etc) in the highest redshift galaxies for the first time. Galaxies at $6 < z < 10$ have median effective radii of 200–500 pc, corresponding to 50–100 mas on the sky. This is well matched to the GMT resolution with the adaptive optics system (diffraction limit of 10–20 mas at 1–2 microns), which will provide an unprecedented resolved view of the most distant known galaxies. The GMT combined with AO will measure the size, growth, and kinematic evolution of galaxies throughout the epoch of reionization. In contrast, while JWST will be efficient at locating these very high redshift galaxies, its resolution is lower by a factor of 4 (~ 80 mas at 2 microns) so that it may not resolve the relevant structures.

Imaging with the GMTIFS instrument, an AO-fed near-infrared IFU, will characterize the size of star forming regions within $z > 6$ galaxies, providing a unique probe of galaxy assembly in the reionization era. **Figure 9-6** shows a reconstructed image of a star forming galaxy at $z=8$ simulated from the FIRE survey (Ma et al. 2017).

The figure shows that ultra-deep exposures with GMTIFS observations will provide constraints on the internal structure, allowing direct comparisons between theoretical models and observations. Spectra taken with GMTIFS will detect the spatially resolved Lyman- α emission and nebular emission lines from the metallic species described above (e.g., CIII], CIV), opening the door for a variety of new investigations. (These studies may identify (so-called) Pop III star-forming complexes that lack metal lines, see above). Comparison of the spatial distribution of the UV continuum and nebular emission regions will constrain the covering fraction of the ionized nebular gas and potentially offer insight into the escape of ionizing radiation (see additional discussion in [Section 9.2](#)).

The GMT will also constrain the dynamical state of the ionized gas by spatially resolving the emission lines. Currently it is not known when ordered disk-like rotation appears in galaxies. Spiral arms have been seen in galaxies at redshifts as high as $z=2$ (Law et al. 2012), but the sensitivity and resolution of current telescopes is not sufficient to make similar measurements at $z>6$. By mapping the centroid of a strong non-resonant line such as CIII], the GMT will be able to study the kinematics of reionization-era systems in detail, revealing whether ordered motions are in place at $z>6$.

9.2 Cosmic Reionization

How and when reionization occurs depends on the nature of the first-light objects. We still know very little about this important process. Measurement of the optical depth of electron scattering of CMB photons suggests that the process is underway by $z\sim 9$ (Planck Collaboration et al. 2016). Quasar absorption spectra tell us that reionization is largely complete by $z\sim 6$ (e.g., McGreer et al. 2015). Starting in the 2020s, the SKA and the GMT will work together to build on this basic knowledge base (see [Figure 9-6](#)), transforming our understanding of reionization at $6<z<9$ and of the role galaxies and AGN played in driving that transition.

The GMT, with its larger collecting area and advanced instrumentation, will provide the data to break the degeneracies in these effects and shed light on the nature of reionization of the IGM. The physics of reionization is complicated and depends on the evolution of the production of UV photons by galaxies, the evolution of the galaxy luminosity distribution (the UV luminosity function), and the number of photons that escape galaxies to ionize intergalactic gas.

The Role of Galaxies: Photon Production and Escape

GMT spectroscopy will be a key tool to assess how, where, and when reionization of the intergalactic medium occurs. Star-forming galaxies have long been thought to be the primary agents responsible for reionization of intergalactic hydrogen. The UV luminosity density of galaxies, $\rho_{1,500}$, is derived by integrating the $z>6$ luminosity function to a low-luminosity limit below which galaxy formation is assumed to be very inefficient. The cosmic ionization rate from galaxies, n_{ion} , can then be calculated from the UV luminosity density as follows: $n_{\text{ion}} = f_{\text{esc}} \xi_{\text{ion}} \rho_{1,500}$, where f_{esc} is the fraction of hydrogen ionizing photons that escape galaxies and ξ_{ion} is the number of hydrogen ionizing photons produced per second divided by the emergent far UV luminosity at 1,500 Å. Applying this method to recent results using the Hubble Space Telescope suggest that the ionizing radiation produced by galaxies is capable of completing reionization by $z\sim 6$ (e.g., Finkelstein et al. 2015). It is becoming increasingly clear that there is a problem in these studies. For galaxies to drive reionization, they must leak 20% of their ionizing radiation into the IGM (e.g., Robertson et al. 2015), roughly an order of magnitude larger than what is typically seen at $z\sim 2-3$ (e.g., Mostardi et al. 2015).

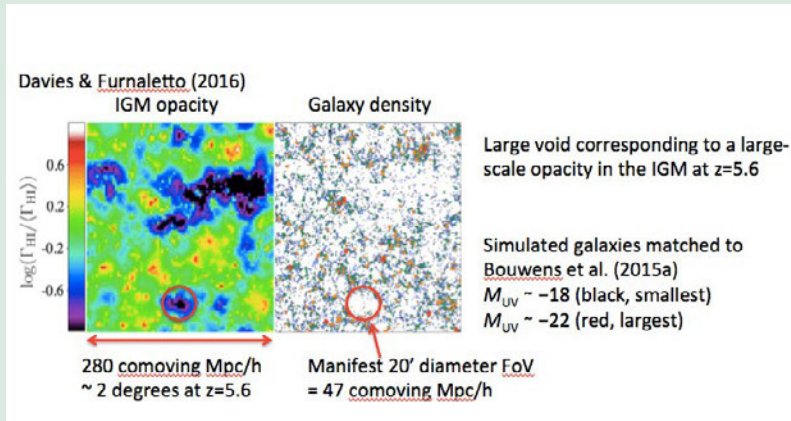


Synergy with the Square Kilometer Array [SKA]



Figure 9-7 The GMT will play a major role in identifying galaxies during the epoch of reionization (marked by $6 < z < 9$), and in measuring their location in space and distance. During reionization, the intense UV emission from these galaxies will blow ionized bubbles of gas in the intergalactic medium (IGM). The distribution of ionized and neutral gas will be measurable by studying the distribution of the (redshifted) 21 cm emission from neutral hydrogen in the IGM by the next generation of dedicated radio telescopes, such as the Square

Kilometer Array (SKA, top), planned to be built in Australia, New Zealand, and South Africa. SKA will begin operating in the 2020s, and will be completed in the 2030s. Image credit: SKA Organization.



The bottom figure shows a simulation of the IGM opacity and galaxy density from Figure 4 of “Large fluctuations in the hydrogen-ionizing background and mean free path following the epoch of reionization,” Davies & Furlaetto, 2016, *Monthly Notices of the Royal Astronomical Society*, Vol 460, Issue 2. The GMT spectrographs, combined with the MANIFEST positioner, will provide the wide-field spectroscopy that is required to measure galaxy redshifts over large areas (tens of arcminutes) in order to correlate them with the IGM opacity bubbles measured by SKA. The GMT will measure the location of the galaxies and their UV emission. The GMT will work with telescopes such as the SKA to build on this basic knowledge, transforming our understanding of how reionization happened during the epoch of reionization.

The GMT will explore whether escape fractions are larger for high redshift galaxies. These efforts must focus on indirect indicators of the leakage of Lyman Continuum (LyC) photons (i.e., photons at wavelengths $< 916 \text{ \AA}$ in the rest-frame), since the IGM is optically thick to LyC photons at $z > 4$. One test is the covering fraction of the ISM in galaxies: as this relates to the covering fraction of neutral hydrogen around the hot stars that produce ionizing radiation. Galaxies with LyC leakage likely have a porous ISM resulting in lower than average covering fractions. The strength of low ionization metal absorption lines in $z > 4$ galaxies (i.e., Si II $\lambda 1260$, OI $\lambda 1302, \lambda 1260$, CII $\lambda 1334$, Si II $\lambda 1526$) offers a sensitive probe of the neutral gas covering fraction. Currently, because the galaxies are faint, most knowledge of absorption line measurements been acquired through stacking analyses of low signal to noise ratio $z \sim 4-5$ galaxy spectra and a small number of highly-magnified gravitationally-

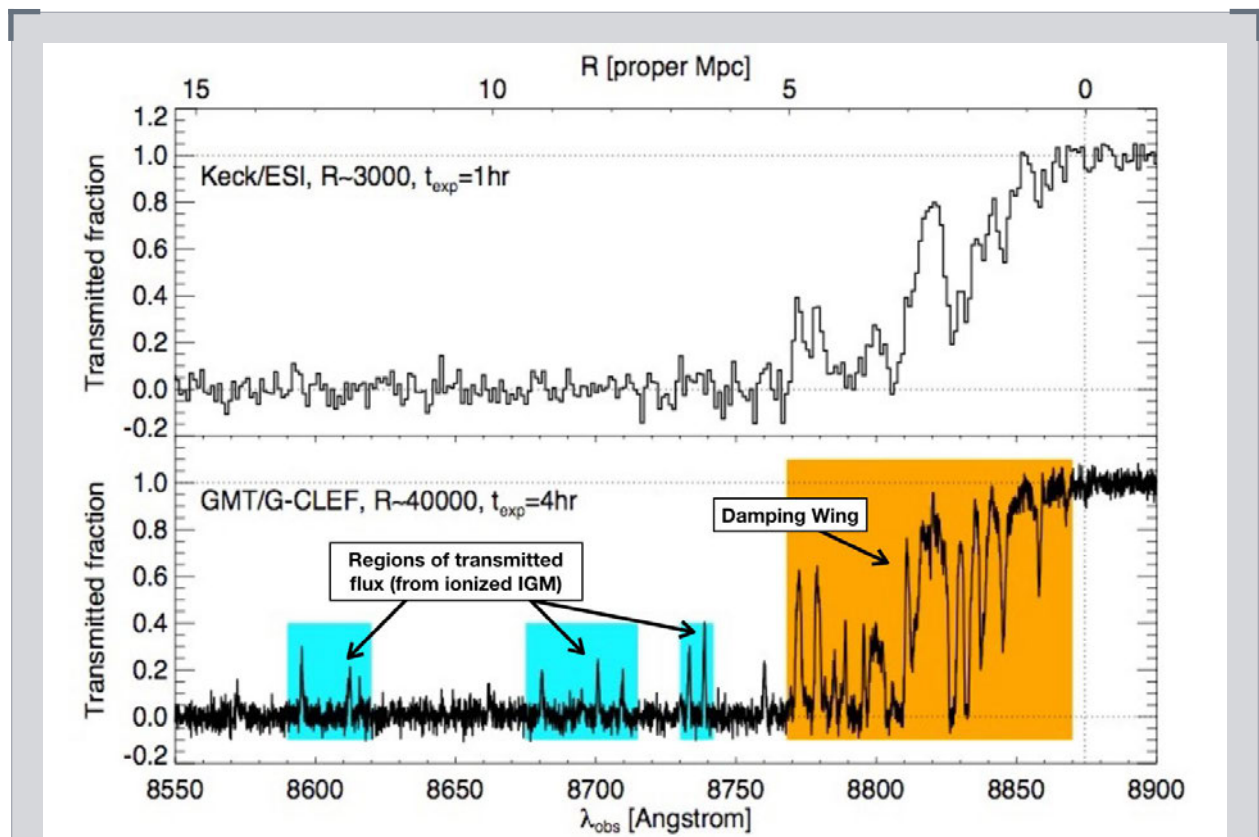


Figure 9-8 The GMT will be able to obtain the high quality spectra of diffuse gas around galaxies and quasars needed to understand the evolution of gas in the early universe during the epoch of reionization. The lower panel shows the simulated spectrum of a bright $z \sim 6$ quasar ($z_{AB} = 20^{\text{th}}$ mag) observed at a high spectral resolution ($\sim 40,000$) with G-CLEF, which reaches S/N ~ 27 in four hours. High quality spectra like the one shown are required to measure narrow transmission peaks in the Gunn-Peterson trough (cyan shading) resulting from patches of the intergalactic medium that are highly ionized. The shape of the “damping wing” (orange-shaded region) provides additional constraints on the HI column density, but G-CLEF sensitivity and resolution are needed to determine if the absorption is from an extended cloud or multiple collapsed systems in the quasar “near zone.” For reference, the upper panel shows the same quasar with noise and resolution characteristics similar to data obtainable today (e.g. with Keck/ESI) for the brightest known quasars ($z_{AB} \sim 20$) at $z \sim 6$ with an exposure time of one hour, which is binned (to $R \sim 3,000$) to reach S/N $\sim 20/\text{pixel}$.

lensed galaxies (Jones et al. 2013; Leethochowalt et al. 2016). These results suggest that the strength of low ionization absorption lines may indeed decrease at higher redshifts, potentially indicating reduced cold-gas covering fractions, allowing higher escape fractions of ionizing LyC photons. But because of the limited sensitivity of current telescopes, these studies have not sampled a representative population at $z \sim 4$ and $z \sim 5$ (focusing instead on only stacked [average] samples or rare lensed systems). A more definitive investigation will require larger samples and extension to higher redshift.

GMT spectroscopy will excel at measuring the ISM covering fraction at very high redshift. In particular, the large field of view, multiplex, and sensitivity of GMACS will make it very effective at building large samples of high quality ultraviolet spectra of $z \sim 5 - 6$ galaxies. Deep, multi-hour integrations targeting $z \sim 5 - 6$ galaxies will constrain absorption line profiles of a variety of species that are sensitive to the neutral gas covering fraction (see **Figure 9-7**). The source density of $z \sim 5 - 6$ galaxies is $\sim 2 \text{ arcmin}^{-2}$ at a magnitude of 26.5 [AB] (Finkelstein 2016), so as many as 100 (600) sources should exist within the GMACS (or GMACS + MANIFEST) areal coverage. For the brightest sources (brighter than 25th magnitude), the spectra will be of high enough quality to extract covering fractions *in individual systems* and indirectly infer escape fractions. For the more abundant population with magnitudes in the range $25 < m(\text{AB}) < 27.5$, composite spectra will extend the analysis to $z \sim 6$ for the first time, while increasing the number of $z \sim 5$ galaxies included in the stack by two orders of magnitude. These studies will reveal whether galaxies at the end of reionization have the conditions that are conducive to levels of LyC leakage necessary for galaxies to drive reionization.

The GMT will also constrain the astrophysical properties of high redshift galaxies, which lead to indirect constraints on the value of ξ_{ion} as this depends sensitively on the properties of the population of massive stars (age, metallicity, binary fractions, IMF). Many of these effects manifest in the rest-frame UV, which is shifted to the red optical and near-IR bands. For example, for a $z \sim 5$ galaxy, the Si IV and C IV stellar wind features are located at 8,000 – 9,000 Å, well situated for deep spectroscopy with GMACS. Deep (10 hr) exposures by the GMT with GMACS (see again **Figure 9-7**) will also constrain the Lyman continuum production efficiency, constrain the metallicities of the nebular gas and hot stars in the galaxies, and test for the effects from stellar binaries (and the binary fraction) and the shape of the IMF (Steidel et al. 2016).

Probing the Timescale of Reionization with Quasars

The improvement in sensitivity provided by the GMT, combined with high resolution optical spectroscopy (e.g., with G-CLEF) of $z \sim 5 - 7$ quasars, will provide one of the key observational probes of the cosmic dawn and epoch of reionization. Deep high-resolution spectroscopy is necessary to resolve the distribution and sizes of neutral gas clouds in the “near zone” of quasars during reionization (see **Figure 9-8**). In these regions, the light from the quasar is blocked by neutral gas clouds, while regions already ionized are transparent to the light from the quasar. Existing spectra of the brightest known quasars ($z_{\text{AB}} \sim 20$ th magnitude) are limited to about $z \sim 6$, and typically have moderate resolution ($R \sim 3,000 - 6,000$) and/or signal-to-noise ($S/N \sim 20$), even when using the largest of the current generation of optical telescopes. This exacerbates cosmic variance uncertainties arising from the inhomogeneous nature of the IGM density and ionization state, and lends the existing data limited power for distinguishing between differing reionization histories (Mesinger 2010). A handful of high resolution spectra ($R \sim 40,000$) at $z > 6$

have been attained at moderate signal-to-noise ($S/N \sim 10 - 20$) for the very brightest quasars, although these typically require exposure times in excess of 8 hours with an 8–10 m class telescope (Becker, Bolton, & Lidz 2015).

The high-resolution G-CLEF spectrograph will allow for analyses of the size and shape of the Lyman- α transmission in the highly ionized near-zone of high-redshift. **Figure 9-8** displays a simulation of a spectrum of a $z=6.30$ quasar from G-CLEF that covers this region. The greater wealth of information available at high spectral resolution enables detailed insight into reionization the physical state of the IGM, facilitating tighter constraints on the ionization state and temperature. Furthermore, larger data sets will also be possible with access (at lower S/N) to high resolution data for fainter background quasars ($z_{AB} > 21^{\text{st}}$ magnitude, e.g. Willott et al. 2010), resulting in a commensurate improvement in the statistical power of the data. This aspect is vital for probing reionization in detail, because it is an inherently spatially and temporally inhomogeneous process. Crucially, higher resolution data can resolve these transmission peaks on small scales and place tighter constraints on the

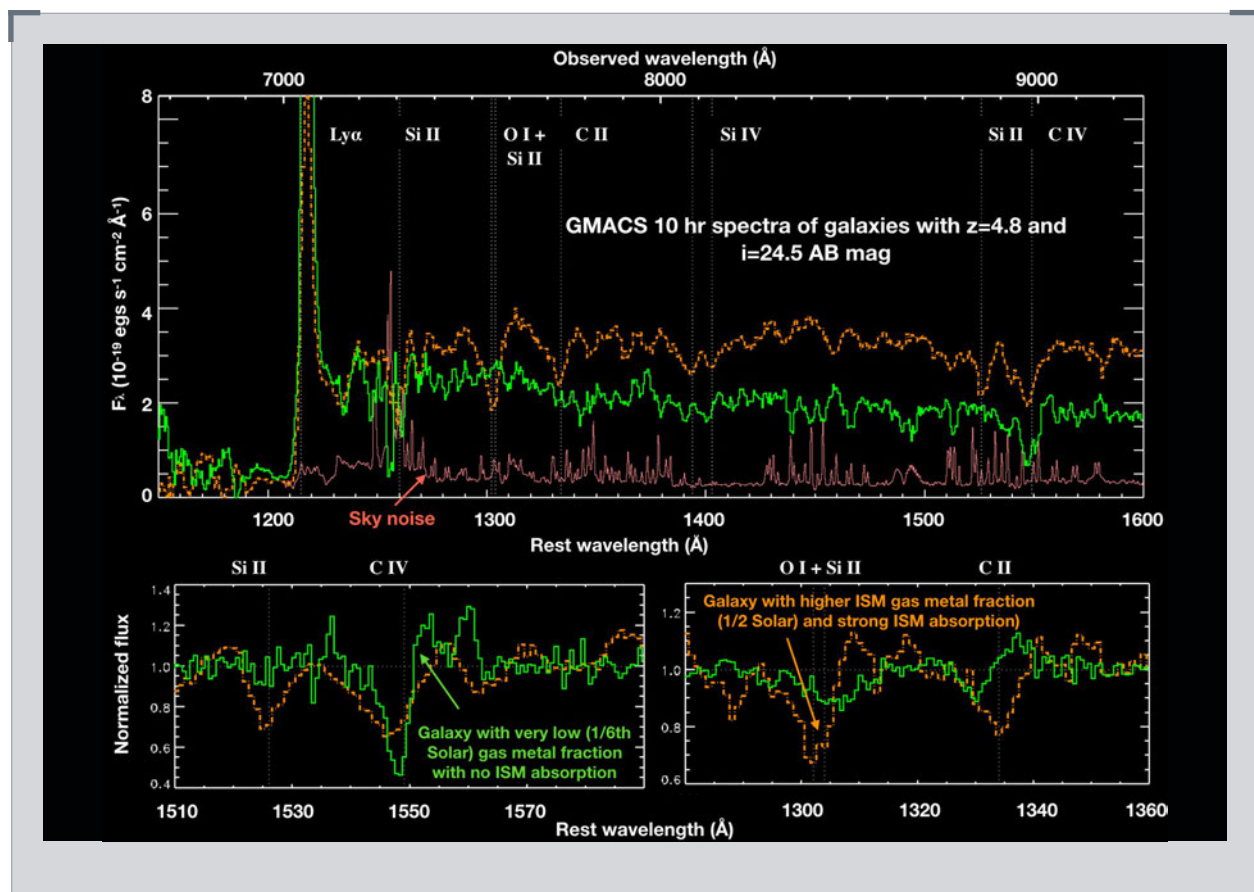


Figure 9-9 Deep spectroscopy with the GMT will measure the physical properties of distant galaxies. This figure presents simulated GMACS observations of star-forming galaxies with $i = 24.5$ AB mag at $z = 4.8$ in 10 hrs ($S/N \sim 17$ per 3.73 \AA resolution element). This particular example illustrates how the GMT can be used to differentiate between galaxies with high metallicities with high ISM covering fraction (orange, dot-dashed spectrum; Shapley et al. 2003) and with low ($1/6^{\text{th}}$ Solar) metallicities and negligible ISM absorption (green, solid spectrum; Erb et al. 2010). The bottom panels expand the view around critical ISM and stellar features.

HI fraction. G-CLEF will make such measurements feasible for the first time. To measure the average effect, several tens of near zone determinations are required to average over the large scatter in individual line-of-sight measurements arising from cosmic variance, and high resolution, high signal-to-noise data increases the reliability of the measurement (Bolton & Haehnelt 2007).

In addition, G-CLEF spectroscopy of quasars will identify any neutral gas along quasar sight lines, which contains information about neutral gas in the immediate vicinity of the quasar. This affects the overall shape of the Lyman- α transmission in the quasar near-zone, and contains important information. **Figure 9-8** shows that G-CLEF spectra will resolve this at high resolution and signal-to-noise. In this figure, the quasar has a large column of neutral gas in the immediate vicinity. This produces the large absorption feature (Gunn-Peterson trough) with a characteristic “damping” from the Lorentzian wing that extends to the red side of the Ly α line. The shape of this “damping wing” provides additional constraints on the HI column density. The ability to distinguish between the shape of a damping wing caused by an extended neutral medium (which declines as $[\lambda_{\text{obs}}/\Delta\lambda_{\text{obs}}]$) or by a multiple discrete collapsed system (which decline as $[\lambda_{\text{obs}}\Delta\lambda_{\text{obs}}]^2$ see McQuinn et al. 2008) depends on the ability to resolve the relatively narrow thermal widths of these lines. This requires high resolution ($R\sim 40,000$) spectroscopy. The GMT will provide these high resolution, high signal-to-noise spectra with G-CLEF.

High-resolution GMT spectroscopy will measure the intrinsic widths of Lyman- α absorption features in the quasar near-zone (**Figure 9-9**) enables the direct measurement of the temperature of the gas in the near zones. Intergalactic hydrogen is predominantly photo-heated by ultraviolet radiation and is thus sensitive to prior photo-heating by sources of ionizing photons. Because the cooling time-scale in the low-density IGM is long, information on the reionization history and any subsequent heating by the quasar is encoded in the thermal widths of these absorption lines. Furthermore, the amount of photo-heating is dependent on the ionizing spectrum: a hard ionizing spectrum (e.g. metal-free stars) will result in a larger IGM temperature immediately following the reionization of hydrogen.

Probing Reionization with Lyman- α emission from Galaxies

The GMT will test theoretical models of the evolution of the neutral fraction of the IGM by observing the Lyman- α emission in galaxies during the epoch of reionization. Because Lyman- α photons are resonantly scattered by neutral hydrogen, they will be spatially diffused to extremely low surface brightness levels as they pass through the neutral IGM. Detecting this line at a given redshift places constraints on the average neutral fraction in the IGM at that epoch.

The GMT will play a key role by allowing the efficient study of the evolution of Lyman- α emission using enormous numbers of galaxies during the epoch of reionization. The fraction of continuum-selected galaxies with detected Lyman- α emission rises from $\sim 30\%$ at $z=3$ to $60-80\%$ at $z=6$ (e.g., Stark et al. 2011). This increase is likely due to decreasing dust attenuation (Finkelstein et al. 2012; Bouwens et al. 2014), which should continue to higher redshifts, thus Lyman- α should be nearly ubiquitous amongst star-forming galaxies at $z>6$. An observed drop in the fraction of galaxies exhibiting Lyman- α emission (typically parameterized by comparing the equivalent width [EW] distributions at the two redshifts) may signal a rapidly evolving IGM neutral fraction. This test is powerful as it relies on a known sample of robustly selected galaxies, and even non-detections are very constraining as one can model upper limits in the data and thus study the non-detections on a galaxy-by-galaxy basis (Treu et al. 2013, Tilvi et al. 2014).

Current instrumentation on 8–10 m class telescopes provides only upper limits on the evolution. Studies with MOSFIRE and Keck have targeted large samples of $z=6-9$ galaxy candidates selected from deep imaging by HST but have failed to measure redshifts or Lyman- α emission except in only a small fraction of this population (Finkelstein et al. 2013, Pentericci et al. 2014). This is primarily due to the limited spectroscopic sensitivity of 8–10 m class telescopes for such distant galaxies, as low equivalent width ($EW < 20 \text{ \AA}$) Lyman- α emission is only accessible for extremely bright galaxies ($< 26^{\text{th}}$ magnitude AB). Consequently, out of the now > 1000 distant galaxy candidates known, robust ($S/N > 5$) spectroscopic Lyman- α detections exist only a dozen galaxies at $z > 7$. This implies a non-zero neutral fraction in the IGM at $z = 6-8$, with some inferences on the IGM neutral fraction being as high as 60% (but this number is highly uncertain; e.g., Pentericci et al. 2014; Treu et al. 2013; Tilvi et al. 2014; Stark et al. 2017).

The GMT will measure even weak Lyman- α emission in galaxies, which can be used to trace reionization. Results (primarily from the Keck telescope) demonstrate that Lyman- α is observable in fewer galaxies than expected ($< 20\%$), implying a non-zero neutral fraction in the IGM at $z = 6-8$, with some inferring an IGM neutral fraction as high as 60% (see Tilvi et al. 2014). Near-IR spectrographs on the GMT (GMTIFS or SuperFIRE) will provide a tremendous leap in our spectroscopic sensitivity, allowing the measurement of Lyman- α emission to fainter line-flux levels, needed for this science. In addition, GMTIFS will allow the spatial distribution of Lyman- α to be studied for the brightest galaxies (*Figure 9-5*). A highly multiplex near-IR spectrograph (such as NIRMOS, fed by the MANIFEST fiber system) will provide multiplicative gains in observing efficiency.

The GMT can probe both Lyman-alpha and CIII] to faint flux levels (see *Figure 9-2*), providing measurement of both the Lyman- α EW and the velocity offset of the line from the systemic redshift (the latter quantity determined from CIII]). The two measurements together provide very powerful constraints. The velocity offset between Lyman- α and the systemic velocity is one of the dominant systematics in determining the neutral hydrogen fraction from the Lyman- α fraction (Mason et al. 2018). Observations at both low and high-redshift (e.g., Stark et al. 2017) show that Lyman- α is redshifted between 50 and 400 km/s from the systemic redshift. If reionization-era galaxies typically have small velocity offsets, then most Lyman- α photons escape close to resonance, and will be easily scattered by even a small IGM neutral fraction. On the other hand, if the offsets from systemic are large, Lyman- α may be readily observable through even a modest IGM neutral fraction. The GMT will not only deliver Lyman- α EW distributions at $z > 6$, but it will also produce the distribution of velocity offsets, providing the information necessary to robustly extract constraints on the neutral hydrogen fraction of the IGM.

Connecting Galaxies and Gas during the Epoch of Reionization

The clear advantage of the GMT for this Lyman- α experiment is its large field of view, unmatched by any other 10–30 m telescope. By the year 2030 the completed Square Kilometer Array (SKA) will be online (see *Figure 9-7*). Through combination of GMT measurements of the clustering of Lyman- α emitting galaxies and SKA 21 cm observations, it will be possible to map of the neutral and ionized gas at a given redshift, allowing extremely detailed studies into the state of the IGM during the epoch of reionization. A conservative assumption is that SKA observations will resolve neutral regions on linear scales of ~ 10 arcminutes, corresponding to

a physical size of ~ 3 Mpc at $z=8$, comparable to the expected size of both ionized bubbles in the early universe (e.g., Furlanetto 2006, **Figure 9-7**) and the deepest HST survey fields (e.g., GOODS, CANDELS). To measure how the large-scale spatial distribution of galaxies relates to the ionized bubbles in the IGM requires the very large field of view only provided by the GMT (combined with wide-field spectroscopy fed by MANIFEST). Thus, to obtain a statistical sample of ionized and neutral regions, a much wider survey is needed. The large area surveying capability of WFIRST will be ideal to identify the candidate galaxies possibly associated with the IGM ionization bubbles, for which spectroscopic redshifts from the GMT will be required for this science case. The WFIRST Guest Observer program should enable faint (29^{th} magnitude in the H-band) $z > 7$ galaxies to be identified over large 1 deg^2 areas (see **Figure 9-2**).

The GMT, combined with the wide-field patrol area enabled by MANIFEST and NIRMOS will be the clear choice to spectroscopically follow-up these galaxies, necessary both to confirm their redshifts, but also to obtain measurements of the Lyman- α emission strength to provide the counter-image to SKA's neutral hydrogen maps.

The large 20 arcminute field patrolled by MANIFEST allows a single WFIRST field to be observed with only 3 different pointings (**Figure 9-2**), and the GMT could observe a full square with only ~ 10 different pointings (compared to an untenable > 500 pointings with the small field-of-view near-IR spectrographs planned for the other large telescopes), and allow astronomers to map the relation between the distribution of galaxies and ionized IGM gas (see **Figure 9-7**). Observing Lyman- α emission to extremely faint flux levels over such a large field will allow the first direct probes of the IGM ionization state over the scales where we expect to see several ionized and neutral bubbles. A map of Lyman- α detections will directly trace these ionized bubbles, providing the first such map of the spatial distribution of reionization (making this map over several redshift slices from $z=6-10$, will probe the temporal evolution as well), and will be highly complementary to the neutral gas traced by the SKA (see **Figure 9-6**). These maps will then provide targets for future large space-based telescopes, such as NASA's LUVOIR concept (see **Figure 9-5**), to perform a full census of galaxies in both ionized and neutral regions.

9.3 Observing the Formation of Supermassive Black Holes

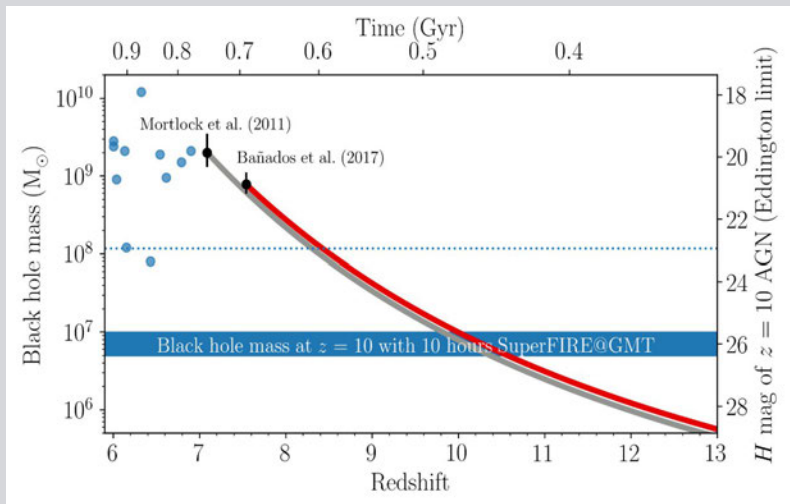
The GMT will measure the masses of the supermassive black holes in quasars through the epoch of reionization, as high as $z \sim 10$. As matter accretes onto supermassive black holes, it fuels exponential growth, rapidly building their masses. This accretion powers the high luminosities of quasars, which have been identified at redshifts greater than 6, and as far as redshift $z=7.5$ (Mortlock et al. 2011, Venemans et al. 2015, Wu et al. 2015, Bañados et al. 2016, 2018). The supermassive black holes in these quasars require masses of (and exceeding) one billion Solar masses. It is a challenge for models to grow black holes with these masses in less than one billion years (Volonteri et al. 2012) as it requires hyper-maximal growth (super-Eddington accretion), and depends strongly on the initial “seed” mass of the originally formed nascent black hole (see Volonteri & Belovary 2012). The origin of these seed black holes remains a mystery, and models span the gamut from remnant black holes from the first stars (seed masses of hundreds of Solar masses, Pezzuli et al. 2016), to the runaway collapse of star clusters (thousands of Solar masses, Stone et al. 2017), and to direct collapse of massive gas clouds (tens

of thousands of Solar masses, Smith et al. 2017).

GMT spectroscopy can measure the masses of supermassive black holes at $z > 6$ and deduce the rate of growth (either rapid or slow) which informs models of galaxy seeds and their growth histories. Masses of the supermassive black holes in quasars by measuring the rest UV continuum luminosity and the shape and luminosity of the CIV and MgII broad emission lines (Vestergard & Osmer 2009, Coatman et al. 2017). At redshifts $6.0 < z < 7.6$ the CIV and MgII lines are accessible in the near-infrared J- and K-band observing windows, respectively. At redshifts $z > 8.3$, only the C IV line is available from the ground, as it moves into the H-band observing window. Current 8–10 m class telescopes can only characterize and measure black-hole masses for the most extreme and luminous quasars.

GMT near-IR spectroscopy (with instruments like GMTNIRS, GMTIFS, or a

Figure 9-10 The GMT will identify the progenitors of supermassive black holes. Such measurements address questions about the start of the process of supermassive black hole formation and the growth rate of the black hole. The data in the figure show the measured black hole masses of known redshift $z \sim 6-7$ quasars. The two most distant quasars currently known are shown in black: at $z=7.09$ (Mortlock et al. 2011) and $z=7.54$ (Bañados et al. 2018). The red and grey curves show how the black hole masses would have needed to grow if the black holes accreted at the Eddington limit for their entire life up to that time with an efficiency of 10%. Therefore, the expected black hole masses for the progenitors of the observed quasars at $z \sim 7$ are of the order of $10^7 M_{\odot}$ at $z \sim 10$. The right axis shows the observed H-band AB magnitude for an AGN at $z=10$ with a black hole mass indicated in the left axis. The GMT will measure the masses of the parent population of the $z=6-7$ luminous quasars to $z \sim 10$, thereby tracing this anticipated evolution. For reference, the dotted line shows the limit with a 10 hr exposure on a 8–10 m class telescope.

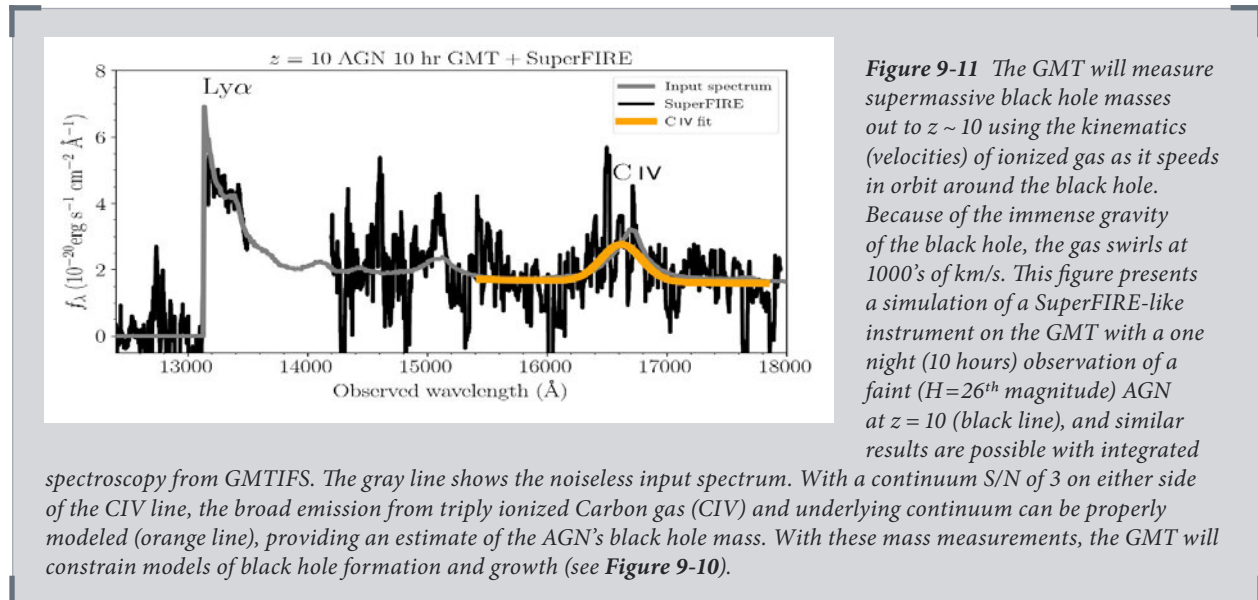


SuperFIRE-like instrument) can measure black hole masses of quasars out to $z \sim 10$. **Figure 9-10** shows a compilation of known quasar black hole masses at $z > 6$, highlighting the two most distant quasars currently known at $z=7.09$ (Mortlock et al. 2011) and $z=7.54$ (Bañados et al. 2018). Assuming that all the growth in these quasars occurs at the Eddington limit ($L_{\text{Edd}}=L_{\text{Bol}}$), their progenitors would be AGN with black hole masses of $\sim 10^7 M_{\odot}$ by $z \sim 10$. This implies that their observed H-band magnitude would be $H \sim 26$. The S/N required to detect the continuum and properly model the emission lines of such a faint object is far beyond the capabilities of an 8 m class telescope with reasonable exposure times. **Figure 9-11** shows the capabilities of GMT near-IR spectroscopy for observing a $z=10$ AGN, $H=26$ quasar. In a 10-hour exposure near-IR spectroscopy with the GMT reaches a continuum S/N of 3

near the CIV line, allowing recovery of the black hole mass by modeling the CIV emission line. Quasars with sub-Eddington growth would have even higher mass progenitors (and be brighter) at earlier times. Therefore, we will be able to track the growth of supermassive black holes. The rate of growth informs our understanding of the “seeds” from which the quasars began.

Although most contemporary work favors faint star-forming galaxies as the main sources responsible for reionization, the role of AGN is certainly non-zero and at present a topic of much debate (e.g., Giallongo et al. 2015, Parsa et al. 2018). The GMT will be fundamental to determine accurately the faint end of the AGN luminosity function during the epoch of reionization and it will finally reveal the exact contribution of AGN to the reionization of the universe (see also the previous section on “Probing the Timescale of Reionization with Quasars,” above).

The spectroscopic study of quasars—especially those associated with lower-mass, growing supermassive black holes—requires a synergy with surveys that will be



operating contemporaneously with the GMT. Future facilities such as the LSST (ground-based optical), Euclid and WFIRST (space based OIR), and eRosita (X-ray, see Figure 9-12) will be ideally suited as they provide the area, depth, and multi-wavelength information required to identify and select the most promising candidates. By the time the GMT is online there will be thousands of faint AGN candidates at $z > 6$ selected by these telescopes. The GMT is the telescope that will convert these candidates into confirmations and provide the data with which to characterize their astrophysical nature. Additional future X-ray facilities, such as Lynx and Athena (Figure 9-12), would provide additional sensitivity and angular resolution necessary to complement GMT studies of the most distant supermassive black holes. Such data would probe simultaneously the accretion disk physics (winds, accretion disk structure with high spatial resolution) combined with the information from the UV continua and broad-line regions that could aid to the understanding of how these supermassive black holes came into existence.

Synergy with eRosita, ATHENA, and the Lynx X-ray Surveyor

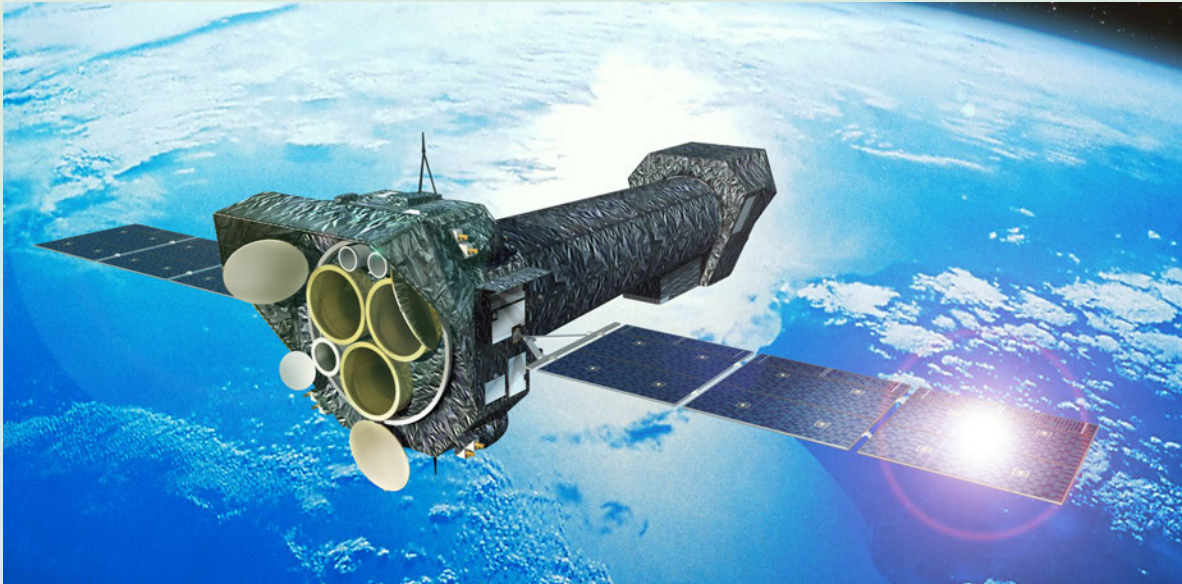
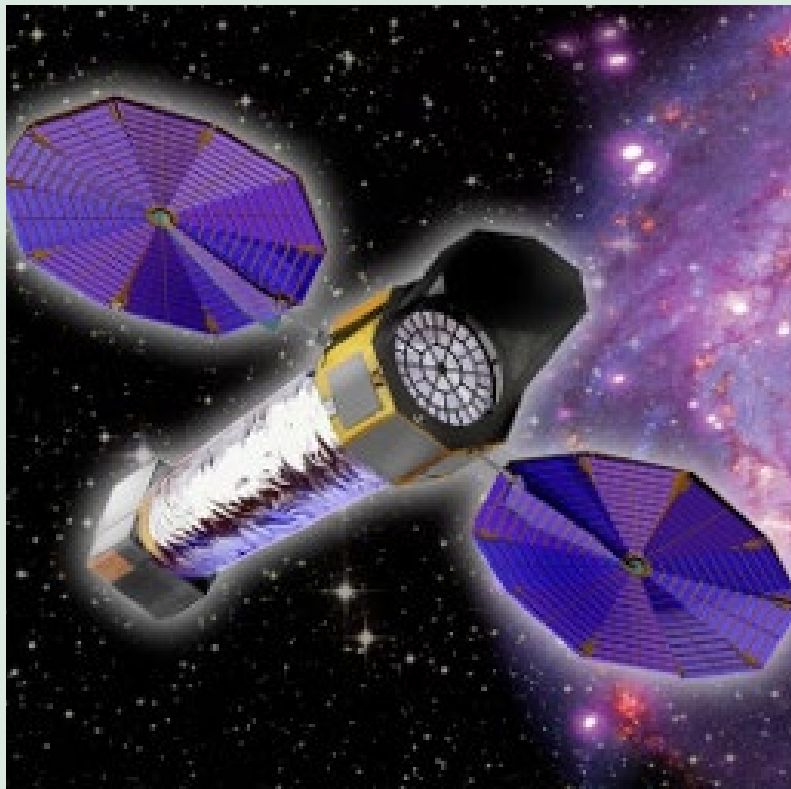


Figure 9-12 The GMT will play a major role in measuring the properties and masses of the most distant supermassive black holes (SMBHs). The candidates for these SMBHs are rare and require selection from imaging surveys (such as the LSST, WFIRST, or Euclid, see above). In addition, X-ray surveys, such the future eRosita (top), the Lynx X-ray Surveyor (right) and ATHENA (not shown) missions will identify distant SMBHs from their X-ray emission. The SMBHs grow by accreting gas. As the gas swirls near the black hole, it heats up and glows brightly in the X-ray bands. The new X-ray telescopes are tuned to identify this emission and find the SMBHs, but to measure the masses will require spectroscopy of their optical and IR light. This requires deep integrations with the GMT. Image credit: ESA, NASA.



References

- Bañados et al. 2016, ApJS, 227, 11
- Bañados et al. 2018, Nature, 553, 473
- Becker, Bolton, & Lidz 2015, PASA, 32, 45
- Bolton & Haehnelt 2007, MNRAS, 381, L35
- Bouwens et al. 2014, ApJ, 793, 115
- Bowman et al. 2018, Nature, 555, 67
- Bromm & Yoshida 2011, ARAA 49, 373
- Coatman et al. 2017, MNRAS, 465, 2120
- Cowen 2013, Nature, 430, 554
- de Barros et al. 2017, A&A, 608, 123
- Davies & Furlanetto 2016, MNRAS, 460, 1328
- Erb et al. 2010, ApJ, 719, 1168
- Giallongo et al. 2015, A&A, 578, 83
- Finkelstein et al. 2013, Nature, 502, 524
- Finkelstein et al. 2015, ApJ, 803, 34
- Finkelstein et al. 2016, PASA, 33, e037
- Furlanetto 2006, New Astronomy, 50, 157
- Giallongo et al. 2015, A&A, 578, 83
- Jones et al. 2013, ApJ, 779, 52
- Law et al. 2012, Nature, 487, 338
- Leethochawalit et al. 2016, ApJ, 831, 152
- Lotz et al. 2017, ApJ, 837, 97
- Ma et al. 2018, MNRAS, 477, 219
- Mainali et al. 2017, ApJL, 836, 14
- Mason et al. 2018, ApJ, 856, 2
- McGreer et al. 2015, MNRAS, 447, 499
- McQuinn et al. 2008, MNRAS, 388, 1101
- Mesinger 2010, MNRAS, 407, 1328
- Mortlock et al. 2011, Nature, 474, 616
- Mostardi et al. 2015, ApJ, 810, 107
- Newman et al. 2015, APh, 63, 81
- Oesch, P.A. et al. 2015, ApJL, 804, 30
- Parsa et al. 2018, MNRAS, 474, 2094
- Pentericci et al. 2014, ApJ, 793, 113
- Pezzuli et al. 2016, MNRAS, 458, 3047
- Planck Collaboration et al. 2016, A&A, 594, 13
- Robertson et al. 2015, ApJL, 802, 19
- Scannapieco et al. 2003, ApJL, 753, 31
- Schaerer 2002, A&A, 382, 28
- Schenker et al. 2014, ApJ, 795, 20
- Shapley et al. 2003, ApJ, 588, 65
- Smith et al. 2017, MNRAS, 472, 205
- Stacy & Bromm 2014, ApJ, 785, 73
- Stark et al. 2010, MNRAS, 408, 1628
- Stark et al. 2011, ApJL, 728, 2
- Stark et al. 2015a, MNRAS, 450, 1846
- Stark et al. 2015b, MNRAS, 454, 1393
- Stark et al. 2017, MNRAS, 464, 469
- Steidel et al. 2016, ApJ, 826, 159
- Stone et al. 2017, MNRAS 467, 4180
- Tilvi et al. 2014, ApJ, 794, 5
- Tilvi et al. 2016, ApJL, 827, 14
- Trenti et al. 2009, ApJ, 700, 1672
- Treu et al. 2013, ApJL, 775, 29
- Venemans et al. 2015, ApJL, 801, 11
- Vestergard & Osmer 2009, ApJ, 599, 800
- Volonteri & Belovary 2012, Reports on Progress in Physics, 75, 124901
- Volonteri et al. 2012, Science, 337, 544
- Willott et al. 2010, AJ, 139, 906
- Wu et al. 2015, Nature, 518, 512
- Xu et al. 2016, ApJ, 833, 84

